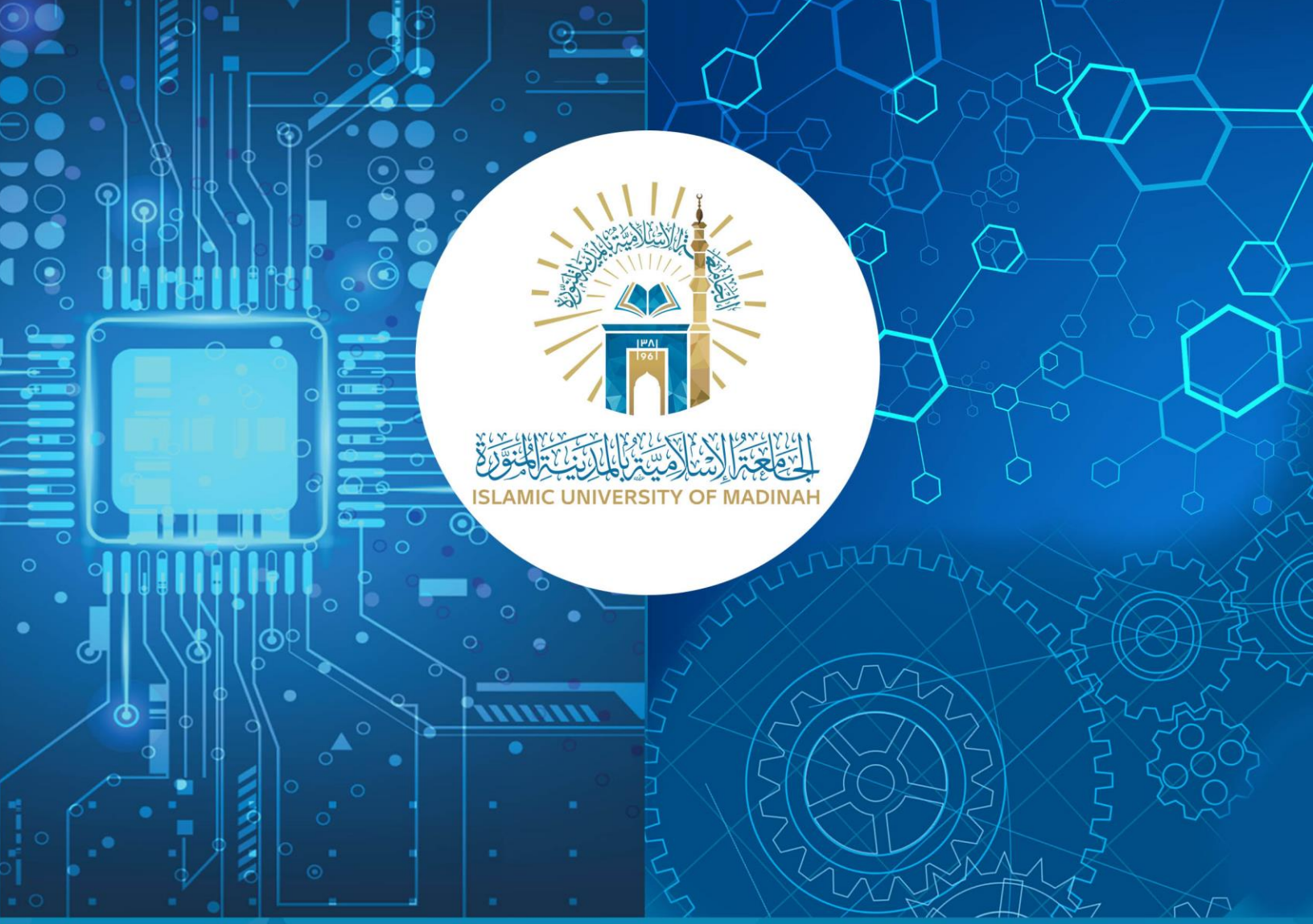

The Islamic University

Journal of Applied Sciences (JESC)

Volume: V **Issue: I** Year: 2023


بسم الله الرحمن الرحيم

Paper version

Filed at the King Fahd National Library No. 8742/1439 on 17/09/1439
AHInternational serial number of periodicals (ISSN) 1658-7936

Online version

Filed at the King Fahd National Library No. 8742/1439 on 17/09/1439
AHInternational Serial Number of Periodicals (e-ISSN) 1658-7944

The Journal's Website

https://jesc.iu.edu.sa

The papers are sent in the name of the Editor-in-Chief of the Journal tothisE-mail address

jesc@iu.edu.sa

Publication Rules at the Journal (*)

❖ General rules:

- Report original scientific research (the main results and conclusions must nothave been published or submitted elsewhere).
- Fit with the topics of the journal.
- Report novel results, innovative work and show a new scientific contribution.
- Not to bear similarity of more than 25% of a previously published work ofthe same author(s).
- Follow the rules, regulation and authentic research methodologies.
- Fulfill the required items and the format of the journal provided in appendix below related to the guide for author.
- Opinions expressed in published articles commit the authors themselves onlyand not necessarily the opinion of the journal.

❖ For all articles:

- The exclusive right to publish and distribute and article, and to grant rights toothers, including commercial purposes.
- For open access articles, IU will apply the relevant third-party user licensewhere IU publishes the article on its online platforms.
- The right to provide the article in all forms and media so the article can beused on the latest technology even after publication.
- The authority to enforce the rights in the article, on behalf of an author,against third parties, for example in the case of plagiarism or copyright infringement.

The Editorial Board

The Advisory Board

The Islamic University Journal of Applied Sciences

Issued By

Islamic University of Madinah, Madinah, Saudi Arabia

Table of Contents

Power generation by using Photovoltaic systems for Yanbu and Rabigh regions in Saudi Arabia: a cost-effective study

Abdulaziz F. Shendi [1], Ahmad M. Nahhas [2,*]
1 Department of Electrical Engineering, Student at Umm Al Qura University, Makkah, Saudi Arabia.
2 Department of Electrical Engineering, Professor at Umm Al Qura University, Makkah, Saudi Arabia.
* Corresponding author: amnahhas@uqu.edu.sa

Abstract: Saudi Arabia's power producing capacity will need to be expanded to meet anticipated increases in energy consumption. The expansion of solar energy consumption in Saudi Arabia has a promising future, owing to the availability of strong solar radiation, a huge rain-free territory, and lengthy sunshine. The Kingdom intends to enhance solar energy generation in order to fulfill a significant portion of the nation's future energy requirements. To accomplish its solar energy aims, the monarchy is now undertaking a variety of installations and research projects. As a result, the most current improvements to the country's solar business are critical for advancing Research and Development (R&D). The area of Yanbu and Rabigh was previously studied by the student Qasim Alabdali in 2021. In this research, the student Abdulaziz Shendi will continue the previous research by studying the two areas in addition to drawing using the SketchUp program and a feasibility study of total costs for the project. Current situation of the Saudi Arabian solar sector and its prospective possibilities.

Additionally, the study initiative intends to conduct a comprehensive research study of the Yanbu and Rabigh areas of the Kingdom. For the Yanbu and Rabigh area, a feasibility study will be done in order to determine if solar energy can be produced there and whether there are acceptable locations and amounts of energy produced. As well as securing the top high-efficiency solar panel manufacturers and incorporating their products into the PVsyst program for use in our studies. First, select the appropriate sort of solar cells for Yanbu and Rabigh areas. Then, calculate the project's total cost in Saudi riyals for the On-Grid system. Besides, using SketchUp program, create a 2D or 3D model of an integrated On-Grid system. Finally, select the study region on the map and use PVsyst program to compute the area.

Keywords: Energy, Solar, Power, Electricity, Photovoltaic, Saudi Arabia.

توليد الطاقة باستخدام الأنظمة الكهروضوئية لمنطقتي ينبع ورابغ في المملكة العربية السعودية: دراسة فعالة من حيث التكلفة

الملخص: ستحتاج المملكة العربية السعودية إلى توسيع قدرة إنتاج الطاقة لمواجهة الزيادات المتوقعة في استهلاك الطاقة. إن التوسع في استهلاك الطاقة الشمسية في المملكة العربية السعودية له مستقبل واعد ، نظرًا لتوفر إشعاع شمسي قوي ، ومنطقة شاسعة خالية من الأمطار ، وضوء الشمس الطويل. تعتزم المملكة تعزيز توليد الطاقة الشمسية من أجل تلبية جزء كبير من متطلبات الطاقة المستقبلية للأمة. لتحقيق أهداف الطاقة الشمسية ، يقوم النظام الملكي الآن بمجموعة متنوعة من المنشآت والمشاريع البحثية. نتيجة لذلك ، تعد أحدث التحسينات في أعمال الطاقة الشمسية في البلاد بالغة الأهمية لتعزيز البحث والتطوير .(R & D) سبق للطالب قاسم العبدلي أن درس منطقة ينبع ورابغ عام 2021. وفي هذا البحث سيواصل الطالب عبدالعزيز شندي البحث السابق بدراسة المجالين بالإضافة إلى الرسم باستخدام برنامج SketchUp ودراسة جدوى التكاليف الإجمالية. للمشروع. الوضع الحالي لقطاع الطاقة الشمسية في المملكة العربية السعودية وإمكانياته المستقبلية.

تهدف المبادرة الدراسية إلى إجراء دراسة بحثية شاملة لمنطقتي ينبع ورابغ بالمملكة. بالنسبة لمنطقة ينبع ورابغ ، سيتم إجراء دراسة جدوى لتحديد ما إذا كان يمكن إنتاج الطاقة الشمسية هناك وما إذا كانت هناك مواقع وكميات مقبولة من الطاقة المنتجة. بالإضافة إلى تأمين أفضل مصنعي الألواح الشمسية عالية الكفاءة ودمج منتجاتهم في برنامج PVsyst لاستخدامها في دراساتنا. أولاً ، حدد نوع الخلايا الشمسية المناسب لمنطقتي ينبع ورابغ. ثم احسب التكلفة الإجمالية للمشروع بالريال السعودي لنظام .On-Grid بالإضافة إلى ذلك ، باستخدام برنامج SketchUp ، قم بإنشاء نموذج ثنائي الأبعاد أو ثلاثي الأبعاد لنظام مدمج على الشبكة. أخيرًا ، حدد منطقة الدراسة على الخريطة واستخدم برنامج PVsyst لحساب المنطقة.

1. Introduction

The Kingdom of Saudi Arabia (KSA) recognizes the necessity of a diverse energy mix, as well as the spread of renewable energy technology, for its long-term socioeconomic success. As a result, the country's National Renewable Energy Program (NREP) and National Transformation Program (NTP), administered by the Ministry of Energy, Industry, and Mineral Resources, have devised a roadmap for the promotion and deployment of RETs in order to meet KSA's future energy demand. On April 25, 2016, KSA made public for the first time the contents of Vision 2030, with an initial objective of 50 percent renewable power [1]. On June 7, 2016, the Ministry of Energy, Industry, and Mineral Resources revealed that the Kingdom of Saudi Arabia changed Vision 2030 to reduce the renewable energy deployment objective to 10% of power production from renewables in its energy mix, down from 50% before. The updated objectives for 2020 and 2023 were 3.45 GW and 9.5 GW, respectively [2]. In order to meet the increased objective of 3.45 GW in 2020, the KSA Renewable Energy Project Development Office (REPDO) submitted a request for proposal (RFP) in 2018 for a 300 MW grid-connected solar power plant in Sakaka [3] and a 400 MW wind power plant in Dumat Al-Jandal [4]. The Saudi Renewable Energy Project Development Office (REPDO) amended the Vision 2030 goals for the second time in January 2019. The updated plans include a significant increase in RE targets, from 9.5 GW to 27.3 GW in 2023, with an overall target of 58.7 GW in 2030. As indicated in Figure 1, of this 58.7 GW, 40 GW will be solar PV, 16 GW will be wind, and 2.7 GW will be other RE sources by 2030 [5], as shown in Figure 1.

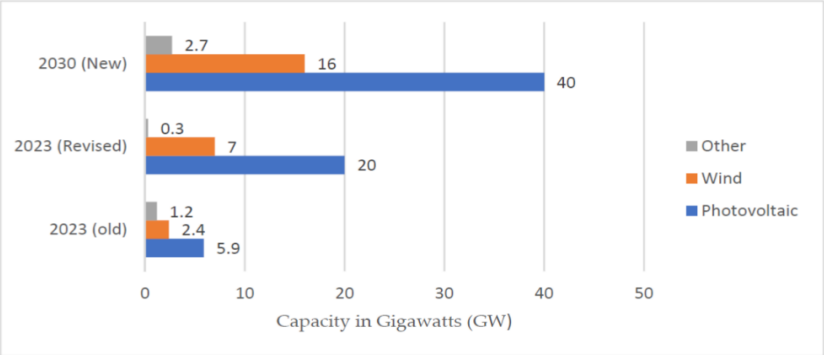

Figure 1. Revised renewable targets of KSA's Vision 2030.

1.2 Electricity

Saudi Arabia produced the most electricity in the Middle East, with an estimated 362 terawatt hours in 2019, almost the same as in 2018 [6]. After expanding at a 6% annual pace between 2000 and 2015, power generation growth has slowed dramatically as population growth has slowed, GDP growth has slowed, energy efficiency and demand-side control measures have been introduced, and electricity costs have risen between 2016 and 2018 [7].

According to statistics from the BP Statistical Review of World Energy 2021, power production fell by 1% in 2020 because of the contraction caused by the COVID-19 pandemic [8]. Residential power usage increased as a result of COVID-19-related lockdowns and limitations, whereas business and government energy sales declined [9].

In 2020, Saudi Arabia powered virtually all of its electricity production with natural gas (61%) and crude oil (39%), however the Saudi government intends to diversify fuels used for electricity generation in order to boost accessible crude oil for export and minimize carbon emissions (Figure 2).

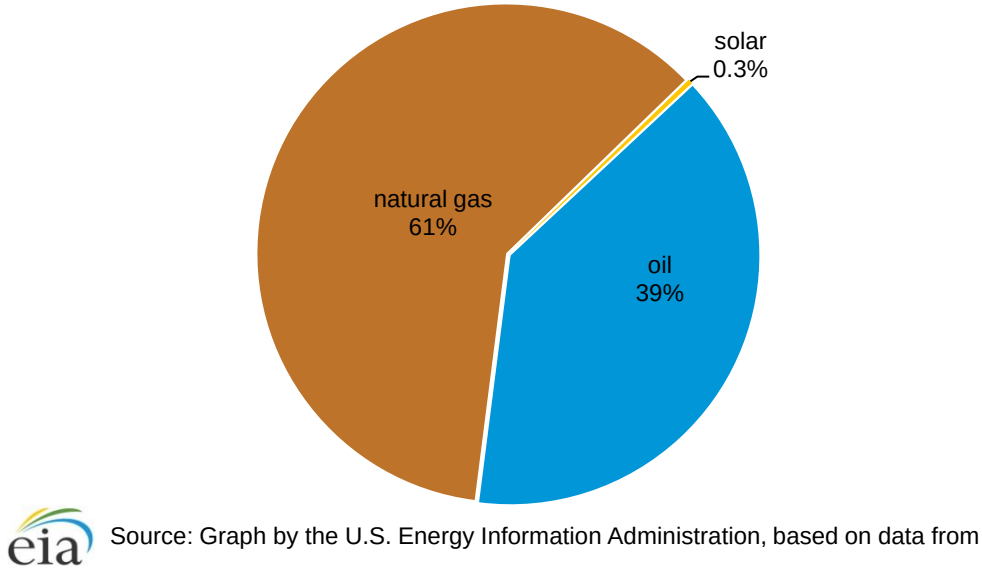

Figure 2. Saudi Arabia's electric power generation by fuel, 2020

1.3 Research Problem

Unpolluted air is a fundamental need for human health, yet air pollution continues to be a global hazard to public health. The traditional electricity-generation business is a major source of hazardous gases that pollute the environment. Low-quality fuels and typical Saudi Arabian generating techniques (such as crude oil with high sulfur content in power plants with little emission controls) produce a range of pollutants that contribute to public health concerns [10].

Conventional power plants release greenhouse gases such as CO_2, NOx, and SO_2) all of which have been linked to global warming. The Kingdom of Saudi Arabia was identified as a major CO_2 emitter, accounting for about 1.8 percent of world emissions in 2017 [11]. As shown in Figure 3, the country's yearly CO_2 emissions were estimated to reach 559.6 million tons in 2019, a significant rise from 394.68 million tons in 2007 [11].

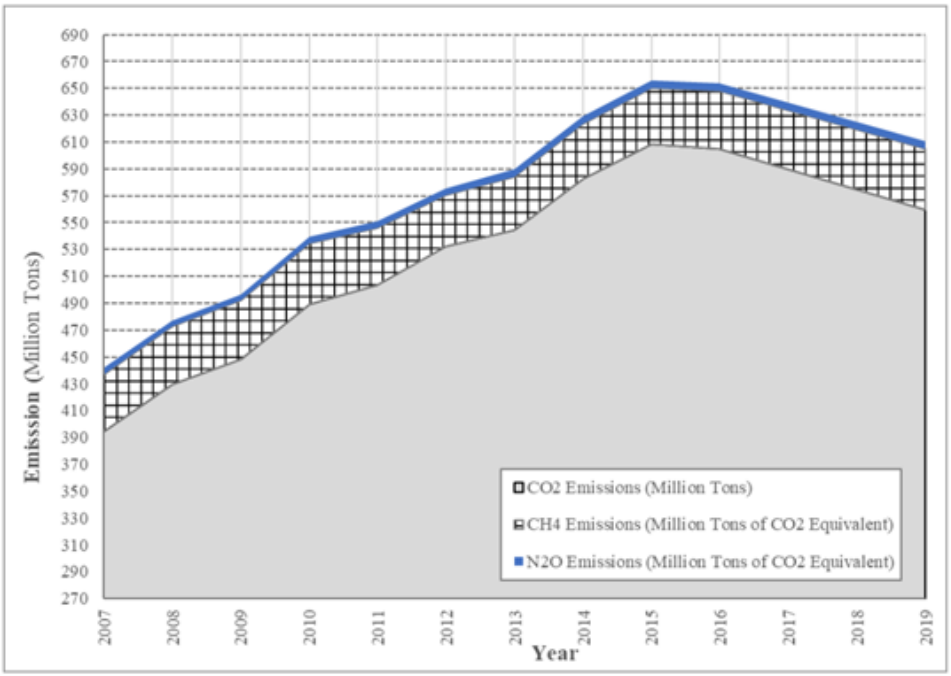

Figure 3. GHG emissions from the energy sector of Saudi Arabia [11].

CO_2 emissions have climbed by about 11% in the previous 10 years. A similar pattern has been seen for CH4 and NOx emissions. From 41.88 million tons of CO_2 equivalents (CO_2e) in 2007 to 44.97 million tons CO_2e in 2019, CH4 emissions have grown. Overall emissions of CO_2 from the electrical field are the greatest contribution to total GHG emissions in the nation, which have climbed by 22% between 2012 and 2017 becouse of consistent expansion in practically all sectors. In 2017, the primary fields of CO_2 emissions were industry (38%), power, heating, and others (38%), transportation of road (23%), and home, agriculture, and services (1%). According to prior data, power generating is one of Saudi Arabia's major CO_2 and CH4 emitting industries. As a result, in accordance with Saudi Vision 2030, the Kingdom has been attempting to cut GHG emissions by gradually eliminating subsidies for fossil fuels. It has previously said that it intends to reduce its annual carbon dioxide emissions by up to 130 metric tons by 2030 [12].

The demand for electricity in Saudi Arabia rises at a 5.8 percent annual rate [13] due to a variety of factors such as the rapid rise of economies, population growth, cheap electricity costs, and neglect of energy preservation [14]. In 2008, the nation used 35 GW and could not supply all demand for peak-time applications, causing a lack of energy in certain areas; this volume is anticipated to increase to 70 GW 11 by the year 2023[15]. The population growth and development prosperity in Saudi Arabia are driving up the country's power needs. Continuously increasing loads need enough power generation.

This undoubtedly leads to the running out of fossil fuels, raising environmental worries. Nonetheless, it is recognized as the principal source of environmental pollution and the adverse health effects of conventional fossil fuels caused by polluting gases such as nitric oxide, nitrogen dioxide, nitrous oxide, and carbon oxides.

Consequently, there is a great patriotic need for alternate sources of energy that are ecologically friendly and can readily provide the nation's energy needs in the post-oil era. In Saudi Arabia, an alternative plan to boost existing conventional Saudi generations and safeguards human health and the environment must be developed. This necessitates the development of new techniques for transacting with increasing numbers.

In the 1970s, modest dispersed operations around the Kingdom proved the effectiveness and operational efficiency of the usage of PV systems in collecting power, demonstrating the suitability for domestic conditions. Solar energy is an infinitely renewable source of power production. It was demonstrated to have several features and enormous economic avails, and also to be promising for prospective usage. Saudi Arabia's energy consumption is exacerbated by yearly population expansion, guaranteeing that the sector of residential, which utilizes over half of the nation's yearly energy production, is the dominant user of local energy [16].

Because solar energy is a significant renewable energy source, many organizations and governments have invested in solar energy as a viable alternative to burning fossil fuels.

1.4 Aim and Objective

This research investigates the existing situation in Saudi Arabia as well as the future potential of the solar sector. In addition, the study effort intends to conduct an integrated research study on several places around the Kingdom. A feasibility study will be done to determine the optimum locations for producing solar energy in Saudi Arabia, as well as the sites and amount of energy production. On the map, choose the study region and use the PVsyst application to calculate the area. Then, create a 2D or 3D model of an integrated On-Grid system in SketchUp. In addition to this, research the sunshine tracking system and its installation for solar panels, as well as the possibilities of enhancing energy output with this technology. Furthermore, determine, using diagrams, how to link the solar energy system to the electrical grid. Also, determine and compute the CO_2 emissions saved from projected Saudi Arabian locations by

using a PV system.

1.5 Reducing Emissions in Saudi Arabia

Saudi Arabia would need to reduce its emissions to below 389 Mt CO_2e by 2030 and to below 263 $MtCO_2e$ by 2050 to be within its emissions allowances under a fair-share range compatible with global 1.5°C.

Figure 4. Reducing Emissions in Saudi Arabia 2017 – 2050 [17]

Saudi Arabia does not utilize coal to generate energy; yet, the electrical industry remains heavily reliant on fossil fuels (65 percent natural gas, 35 percent oil). Renewable energy is becoming more important, although it is still insignificant. To be consistent with a 1.5°C trajectory, the percentage of renewables must expand dramatically and quickly [17].

Study photovoltaic energy production in Saudi Arabia

2.1 Simulation and Analysis

2.1.1 A feasibility assessment for the installation of PV systems on the Rabigh region

This section will cover the installation of PV systems for two locations near Saudi Electricity Company's power plants, making it simple to connect PV systems directly to the grid and with short distribution line distances. That sites located in Rabigh and Yanbu. All computations and simulations were carried out using the PVsyst 7.2.12 software, the GLOBAL SOLAR ATLAS, the NOAA SOLAR Calculator, Latlong.net, and Google Earth. Also the reason of this study is calculate how much the CO_2 emissions will decrease. Comparison between Rabigh and Yanbu, which one is better for the solar cell system.

Each site's power generating capacity is anticipated to be 200 MWp. The first site in this study is Rabigh, the Coordinates are (Latitude 22.68°N, Longitude, 39.06°E). The steps as follow:

1: Find Latitude by using Pvsyst program or https://www.latlong.net/

2: Find PV power output by using Pvsyst program or https://gml.noaa.gov/grad/solcalc/

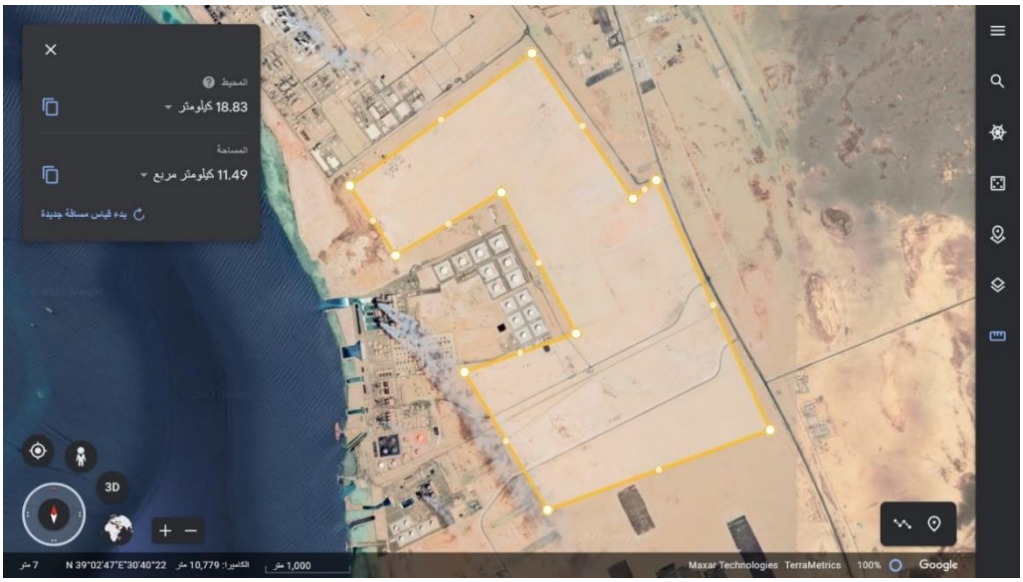

Figure 5. Location of Rabigh project on the map by using Google Earth

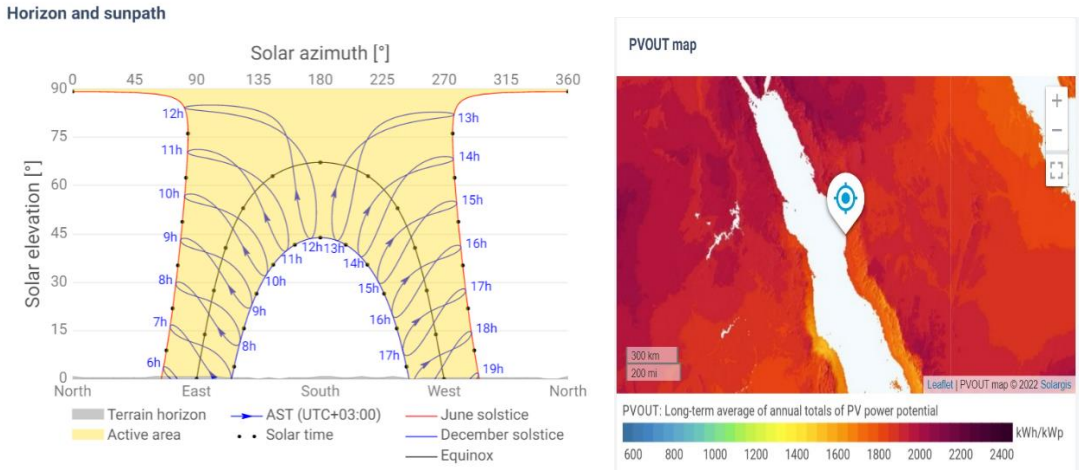

Figure 6. Solar path at Rabigh from January to December & PVOUT by using globalsolaratlas.

Figure 6 (left) relationship between solar elevation , solar azimuth according to sun path to obatin the best solar azimuth for the plant.

Figure 6 (Right) the right map to display the specific producation of the pv plant in Rabigh region measured in KWh/KWp /year

SITE INFO

Map data Per year

Specific photovoltaic power output	PVOUT specific	**1860.2**	kWh/kWp
Direct normal irradiation	DNI	**2056.5**	kWh/m²
Global horizontal irradiation	GHI	**2251.4**	kWh/m²
Diffuse horizontal irradiation	DIF	**832.4**	kWh/m²
Global tilted irradiation at optimum angle	GTI opta	**2411.0**	kWh/m²
Optimum tilt of PV modules	OPTA	**24 / 180**	°
Air temperature	TEMP	**28.5**	°C
Terrain elevation	ELE	**2**	m

Figure 7. PV power output by using globalsolaratlas

Figure 7 shows general information an summry about the side project like that:

Plant capacity, DNI (direct normal irradiation), DIF (Diffuse horizontal irradiation), GHI (Global horizontal irradiation 2251.4= 832.4 + 2056.6 cos()), tilt angle (24), Azumith angle (180) and nominal temperature (28.5).

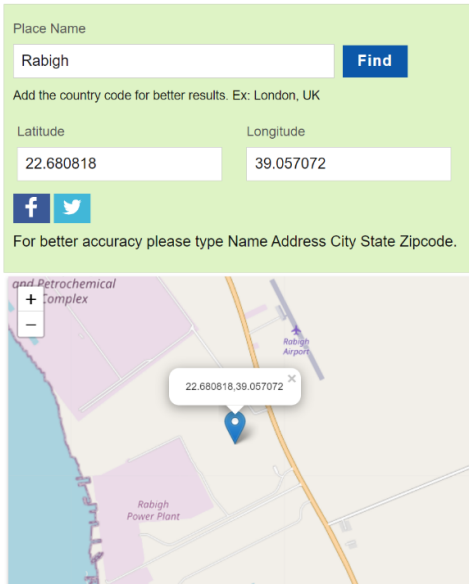

Figure 8. Latitude of Rabigh by using latlong website
Figure 8 shows the latitude which equals 22.680818 degree and longitude which equals 39.057072 for the plant location

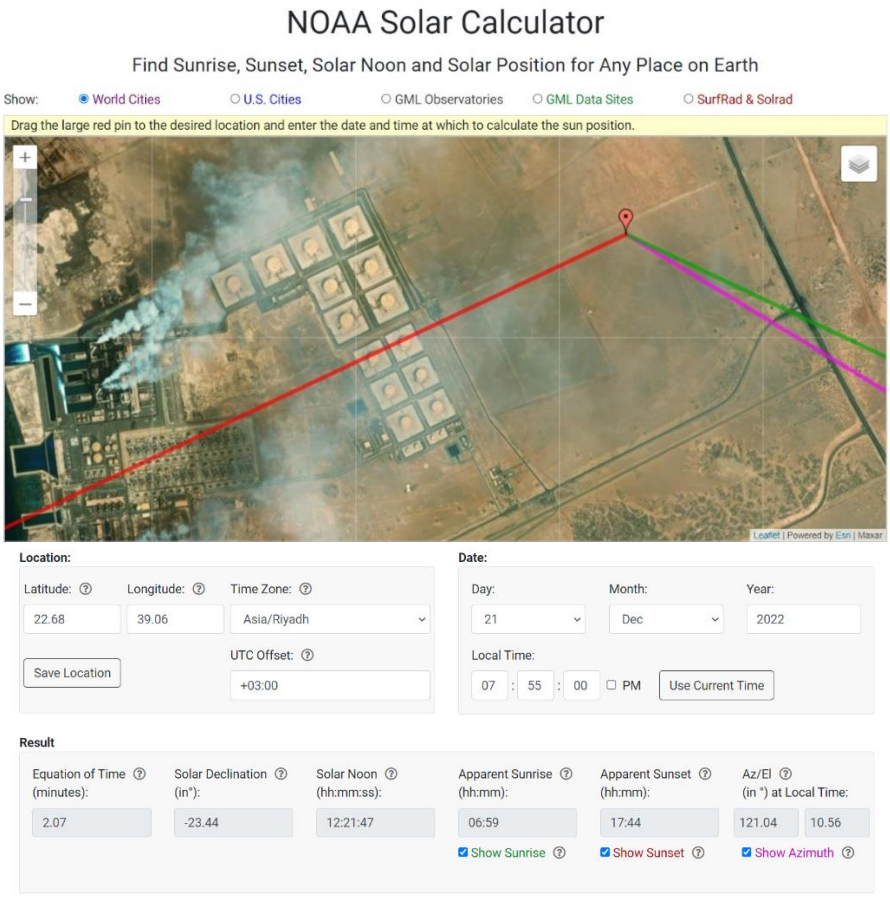

Figure 9. Find Sunrise, Sunset, Azimuth of Rabigh by using NOAA Solar Calculator.

Figure 9 shows the maximum shading time in year and although obtain sunrise, Sunset and solar noon acording to location details (longatude, latitude and time zone)

3: Select type solar panel

4: Calucalte how to installation solar panels and shadow angle

5: calculate Panel tilt: For all year performance panel tilt should be equal Latitude.

- In summer panel Tilt = Latitude – 15

- In winter Panel Tilt = Latitude + 15

2.1.2 Impact of Shading in Rabigh region

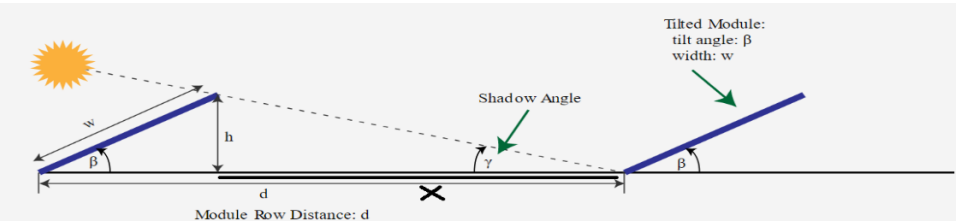

Figure 10. Shadow angle of solar module [18]

To calculate shadow angle should be to know W , h and B

type of solar module type we selected in this research is Jinko solar(JKM540M-72HL4-TV)

Equation of h= sin (latitude angle) x solar panel width (m)

$$\text{Equation of X=} \frac{h}{\tan(\text{shadow angle})}$$

The width of the solar panel in this research is 2.274m and Latitude is 25 , to calculate

h= sin(25)x 2.274= 0.96

Where h is height the solar panel on the surface

To find shadow angle from NOAA website, on December 21 at local time (7:55 AM) we have Y angle= 10.56

Now tan10.56= $\frac{h}{X}$

X= $\frac{h}{\tan(10.56)}$, where h = 0.96

X= 5.15 m This distance is between the end of the first solar panel and the beginning of the second solar panel, Thus there is no shadow between the solar panels if we leave a distance of 5.15 meters.

So will leave a distance of about 12 meters because to put two solar panels on top of each other. And therefore, there is no shadow between rows of solar modules.

Figure shows below the optimal Azimuth angle and tilt for the Rabigh area; the optimal tilt angle for PV panels is 25 degrees with an azimuth of zero degrees.

The sun path statistics are gathered from the Meteonorm software, which offers an unrivaled mix of accurate data and powerful mathematical materials. This data may be used to get accurate history and information for any period of year.

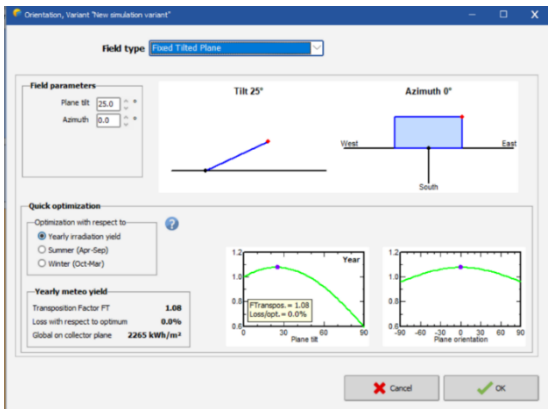

Figure 11. Tilt and Azimuth angle for Rabigh site by using PVSYST

Figure 11 shows the optimum tilt angle and azimuth according to the plant location with optimization with respect to yearly irradiation yield and the loses of the plant with respect to the optimum. In this system, roughly (366,984) PV modules with unit nominal power (540wp) will be used to produce 200MWp, and the modules connection design will be (13592 strings)*(27 series)

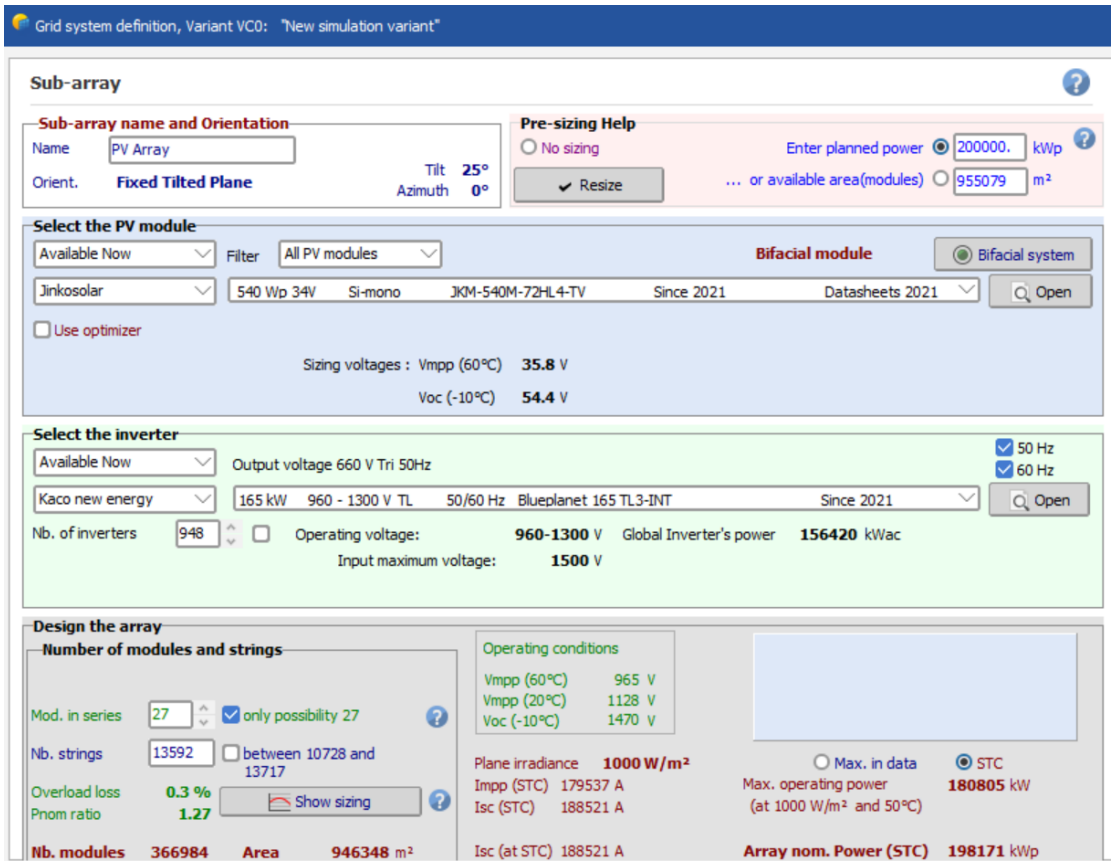

Figure 12. shows the distribution number of modules and PV strings.

Figure 12 shows the orientation of the plant, the plant capacity and area, the used PV module, the used inverter, its number, operating voltage and the design of the array which contain 13592 strings each string have 27 modules, with over sizing ratio 127%

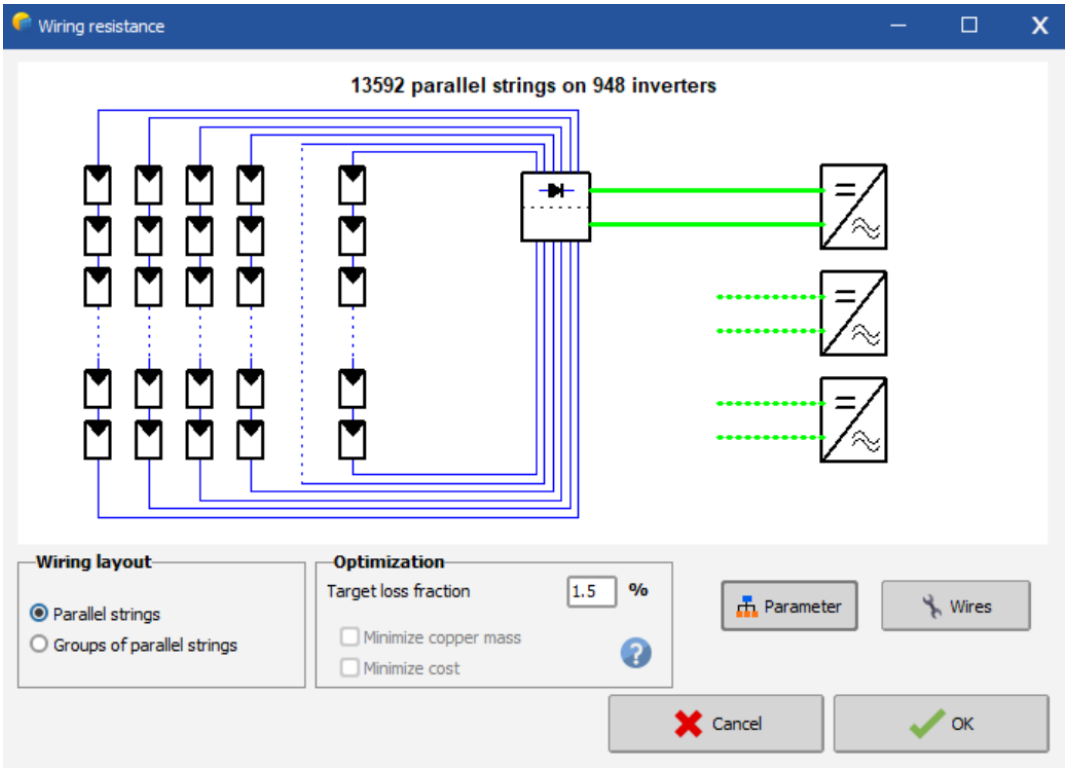

Figure 13. Connecting solar panels strings with inverter

Figure 13 shows single line diagram of the plant (strings to inverters)

Loss fraction is the ratio between Ohmic losses and output AC power

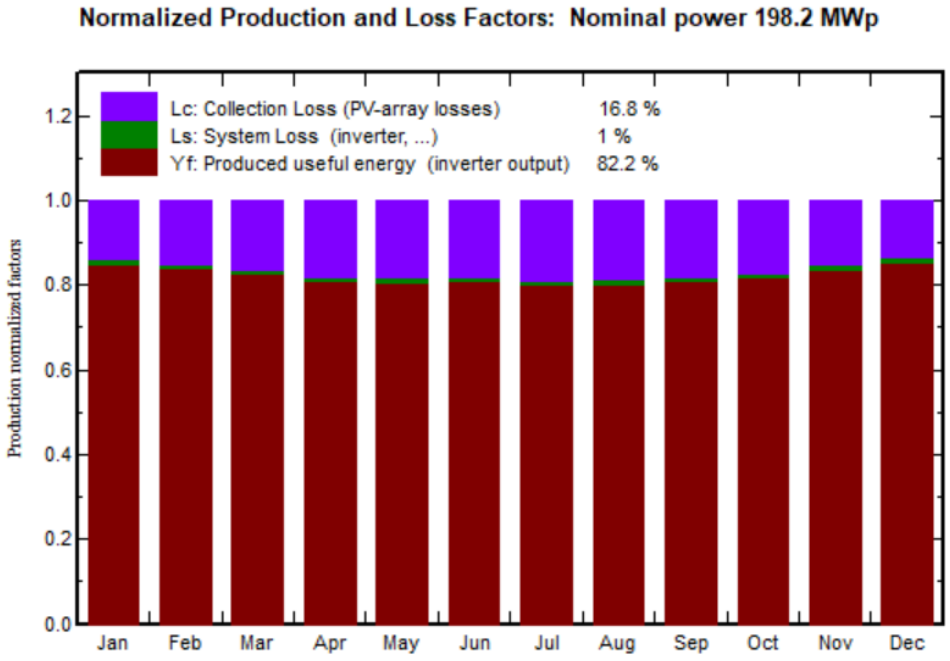

Figure 14. Normalized production and loss factors of Rabigh Site

Diagram 14 displays produced energy from the plant (82.2% * 198.2 MWp= 162.9 MWp) , systems losses (1% * 198.2 MWp = 1.92 MWp) and collection losses (16.8% * 198.2 MWp= 33.279MWp). Note that: the plant supposed to generate 198.2 MWp, but due to collection and system losses we get only 162.9 MWp.

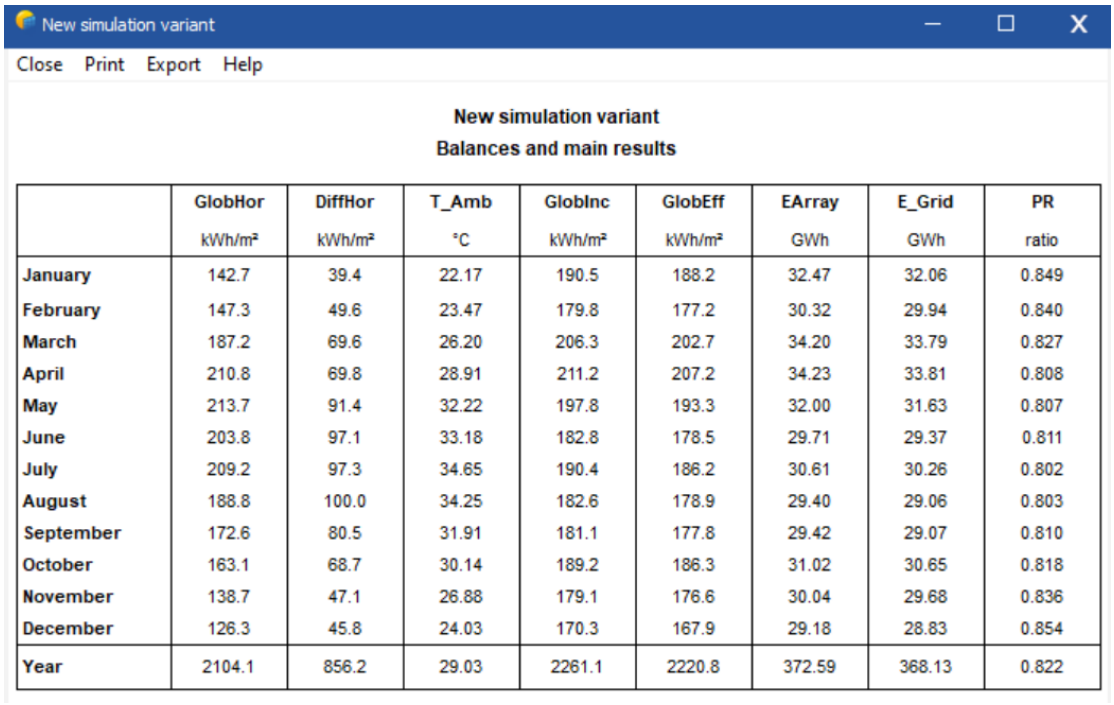

	GlobHor kWh/m²	DiffHor kWh/m²	T_Amb °C	GlobInc kWh/m²	GlobEff kWh/m²	EArray GWh	E_Grid GWh	PR ratio
January	142.7	39.4	22.17	190.5	188.2	32.47	32.06	0.849
February	147.3	49.6	23.47	179.8	177.2	30.32	29.94	0.840
March	187.2	69.6	26.20	206.3	202.7	34.20	33.79	0.827
April	210.8	69.8	28.91	211.2	207.2	34.23	33.81	0.808
May	213.7	91.4	32.22	197.8	193.3	32.00	31.63	0.807
June	203.8	97.1	33.18	182.8	178.5	29.71	29.37	0.811
July	209.2	97.3	34.65	190.4	186.2	30.61	30.26	0.802
August	188.8	100.0	34.25	182.6	178.9	29.40	29.06	0.803
September	172.6	80.5	31.91	181.1	177.8	29.42	29.07	0.810
October	163.1	68.7	30.14	189.2	186.3	31.02	30.65	0.818
November	138.7	47.1	26.88	179.1	176.6	30.04	29.68	0.836
December	126.3	45.8	24.03	170.3	167.9	29.18	28.83	0.854
Year	2104.1	856.2	29.03	2261.1	2220.8	372.59	368.13	0.822

Table 1. The total power generation of Rabigh site

Table 1 shows monthly for total power generation of Rabigh site where (DiffHor is Horizontal diffuse irradiation, GlobHor is Global horizontal irradiation, GlobInc Global is incident in coll. Plane, T_Amb is Ambient Temperature, GlobEff Effective Global, corr for IAM and shadings, EArray is Effective energy at the output of the array, E_Grid is Energy injected into grid, PR is Performance Ratio. Finally, the plant will injected in to grid 368.13 GWh energy).

PR is the performance ratio that measure the quality of the PV plant that is independent of location and also describes as the quality factor on the plant, ranging from 80 to 100 percent. PR= Actual reading of plant output in KWh/ nominl plant output in KWh

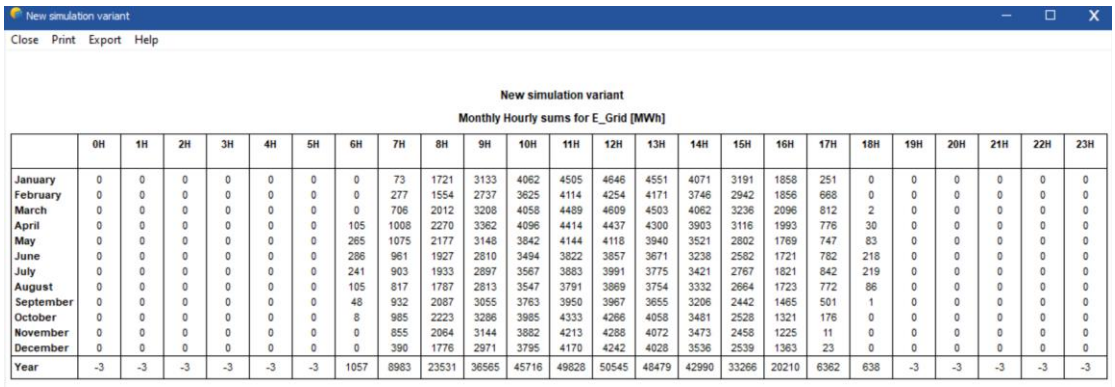

	0H	1H	2H	3H	4H	5H	6H	7H	8H	9H	10H	11H	12H	13H	14H	15H	16H	17H	18H	19H	20H	21H	22H	23H
January	0	0	0	0	0	0	0	73	1721	3133	4062	4505	4646	4551	4071	3191	1858	251	0	0	0	0	0	0
February	0	0	0	0	0	0	0	277	1554	2737	3625	4114	4254	4171	3746	2942	1856	668	0	0	0	0	0	0
March	0	0	0	0	0	0	0	706	2012	3208	4058	4489	4609	4503	4062	3236	2096	812	2	0	0	0	0	0
April	0	0	0	0	0	0	105	1008	2270	3362	4096	4414	4437	4300	3903	3116	1993	776	30	0	0	0	0	0
May	0	0	0	0	0	0	265	1075	2177	3148	3842	4144	4118	3940	3521	2802	1769	747	83	0	0	0	0	0
June	0	0	0	0	0	0	286	961	1927	2810	3494	3822	3857	3671	3238	2582	1721	782	218	0	0	0	0	0
July	0	0	0	0	0	0	241	903	1933	2897	3567	3883	3991	3775	3421	2767	1821	842	219	0	0	0	0	0
August	0	0	0	0	0	0	105	817	1787	2813	3547	3791	3869	3754	3332	2664	1723	772	86	0	0	0	0	0
September	0	0	0	0	0	0	48	932	2087	3055	3763	3950	3967	3655	3206	2442	1465	501	1	0	0	0	0	0
October	0	0	0	0	0	0	8	985	2223	3286	3985	4333	4266	4058	3481	2528	1321	176	0	0	0	0	0	0
November	0	0	0	0	0	0	0	855	2064	3144	3882	4213	4288	4072	3473	2458	1225	11	0	0	0	0	0	0
December	0	0	0	0	0	0	0	390	1776	2971	3795	4170	4242	4028	3536	2539	1363	23	0	0	0	0	0	0
Year	-3	-3	-3	-3	-3	-3	1057	8983	23531	36565	45716	49828	50545	48479	42990	33266	20210	6362	638	-3	-3	-3	-3	-3

Table 2. Monthly Hourly sums for E-Grid [MWh]

Table 2 shows the hourly-monthly energy generated for 24 hours note that we will find the plant is generating energy from April to September from 6:00AM to 6:00 PM, So the plant will generate energy for 12 hours for 6 months per year. With absence the sun, the inverters consume energy as self-consumption.

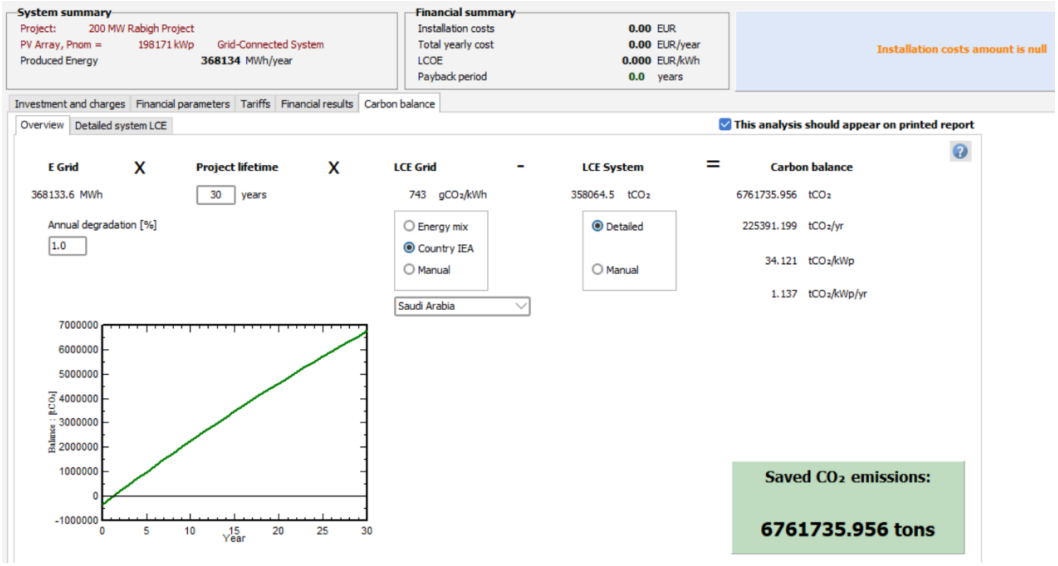

Figure 15. CO_2 emissions saved at Rabigh site

Figure 15 shows the quantity of CO_2 emissions saved by building the plant in Rabigh region for 30 years, the plant will saved 6761735.956 tons of CO_2 emissions.

2.3 A feasibility assessment for the installation of PV systems on the Yanbu region

This section will cover the installation of PV systems for two locations near Saudi Electricity Company's power plants, making it simple to connect PV systems directly to the grid and with short distribution line distances. That sites located in Rabigh and Yanbu. All computations and simulations were carried out using the PVsyst 7.2.12 software, the GLOBAL SOLAR ATLAS. Also, the reason of this study is calculating how much the CO_2 emissions will decrease. Comparison between Rabigh and Yanbu, which one is better for the solar cell system. Each site's power generating capacity is anticipated to be 200 MWp. • The second site in this study is Yanbu, the Coordinates are (Latitude 23.91°N, Longitude, 38.33°E). The steps as follow: First: Find Latitude by using Pvsyst program or https://www.latlong.net/. Second: Find PV power output by using Pvsyst program or https://gml.noaa.gov/grad/solcalc/

Figure 16. Location of Yanbu project on the map by using Google Earth

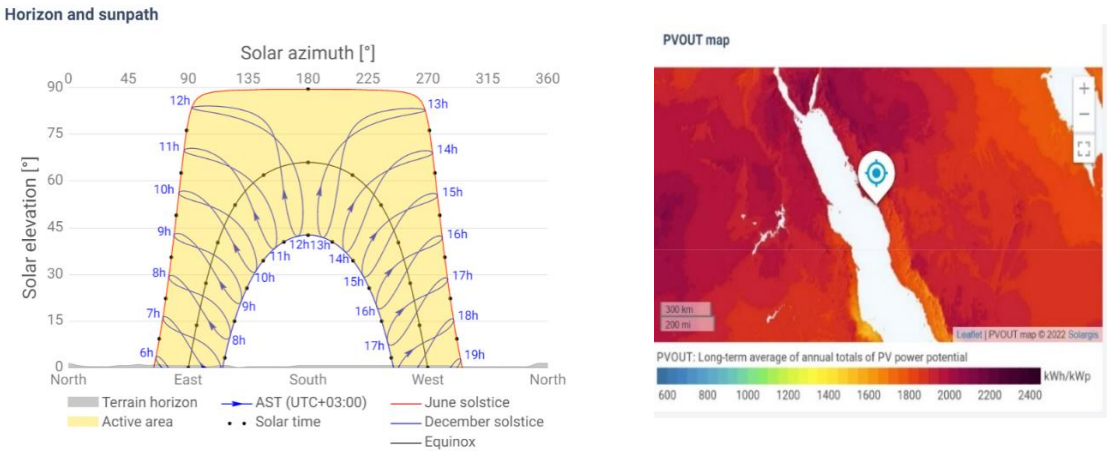

Figure 17. Solar path at Yanbu from January to December & PVOUT by using globalsolaratlas.

Figure 17 (left) shows the relationship between solar elevation , solar azimuth according to sun path to obatin the best solar azimuth for the plant.

Figure 17 (Right) shows the right map to display the specific producation of the pv plant in Rabigh region measured in KWh/KWp /year

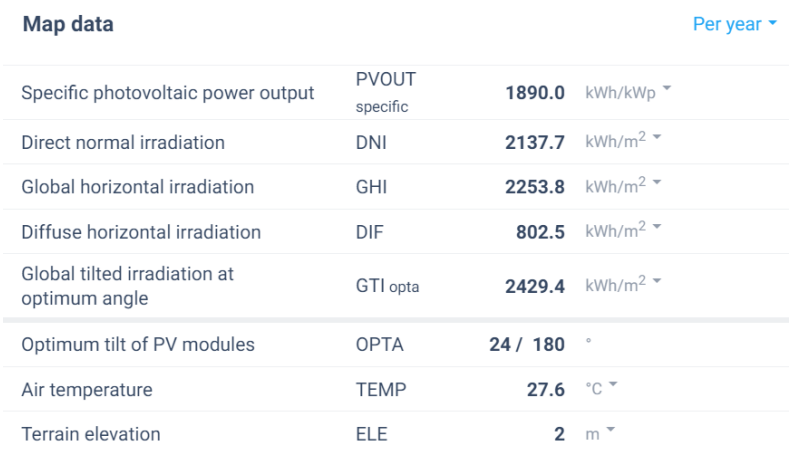

Map data			Per year
Specific photovoltaic power output	PVOUT specific	1890.0	kWh/kWp
Direct normal irradiation	DNI	2137.7	kWh/m²
Global horizontal irradiation	GHI	2253.8	kWh/m²
Diffuse horizontal irradiation	DIF	802.5	kWh/m²
Global tilted irradiation at optimum angle	GTI opta	2429.4	kWh/m²
Optimum tilt of PV modules	OPTA	24 / 180	°
Air temperature	TEMP	27.6	°C
Terrain elevation	ELE	2	m

Figure 18. Find PV power output of Yanbu by using globalsolaratlas.

Figure 18 shows general information an summry about the side project like that:
Plant capacity, DNI (direct normal irradiation = 2137.7 kWh/m²), DIF (Diffuse horizontal irradiation is 802.5 kWh/m²), GHI (Global horizontal irradiation is 2253.8 kWh/m²), tilt angle (24°), Azumith angle (180°) and nominal temperature (27.6 °C).

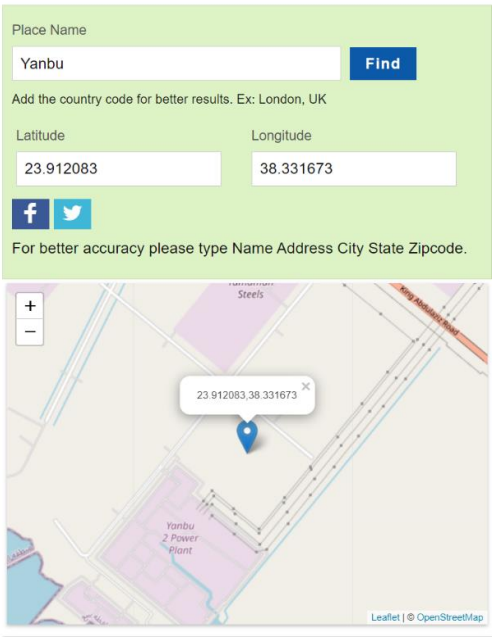

Figure 19. Latitude of Yanbu by using latlong website

Figure 19 shows the latitude which equals 23.912083 degree and longitude which equals 38.331673 for the plant location

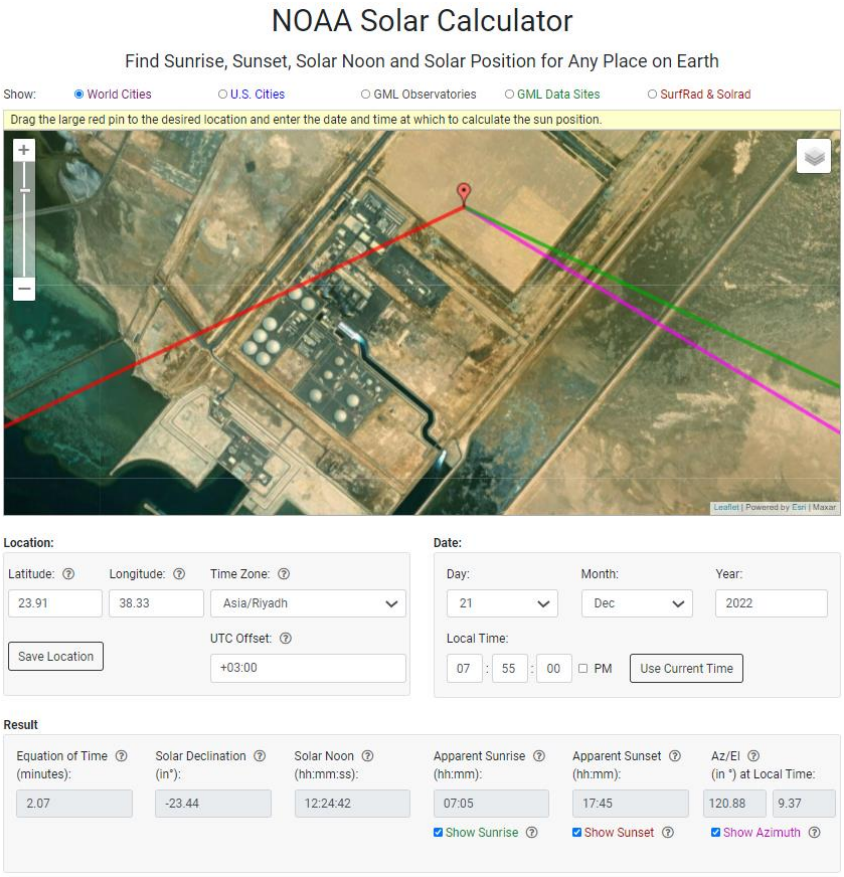

Figure 20. Sunrise, Sunset, Azimuth of Yanbu by using NOAA Solar Calculator.

Figure 20 shows the maximum shading time in year and although obtain sunrise, Sunset and solar noon acording to location details (longatude, latitude and time zone)

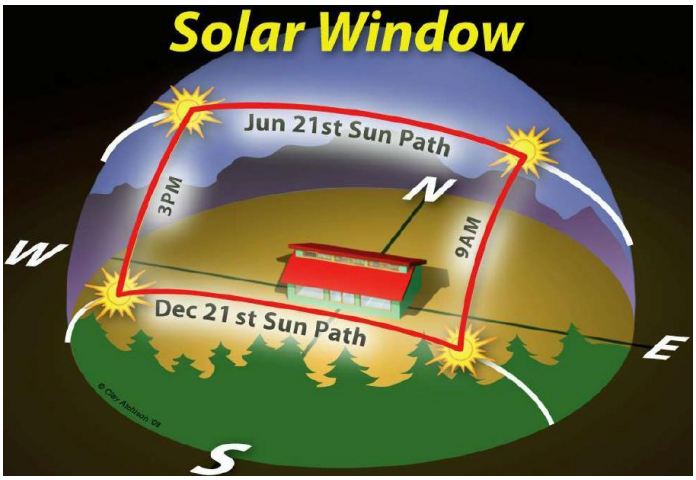

Figure 21. The sun on June 21 and December 21 [19] [20]

Figure 21 shows the path of the sun in summer and winter according to peak sun hour (9AM to 3PM). On June 21 of every year, the sun is as high as possible and there are no shadows during that day, while on December 21 of every year the sun is the lowest possible and the shadows are as high as possible and based on this day we calculate how we can install the panels and leave a distance between them to avoid shadows.

2.3.1 Impact of Shading in Yanbu region

As shown below to calculate shadow angle should be to know W , h and B

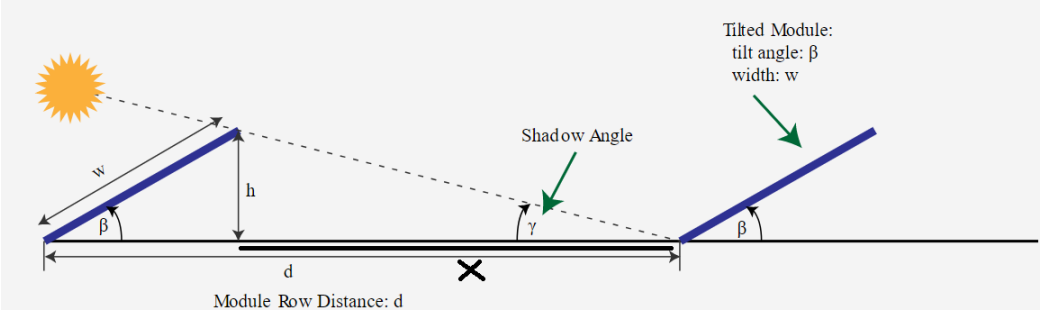

Figure 22. Shadow angle of solar module [17]

Type of solar module type we selected in this research is Jinko solar(JKM540M-72HL4-TV)

Equation of h= sin (latitude angle) x solar panel width (m)

Equation of X= $\frac{h}{\tan(\text{shadow angle})}$

The width of the solar panel in this research is 2.274m and Latitude is 25 , to calculate

Where h is height the solar panel on the surface.

h= sin(25)x 2.274= 0.96

To find shadow angle from NOAA website, on December 21 at local time (7:55 AM) we have Y angle= 9.37

Now tan9.37=h÷x

X= $\frac{h}{\tan(9.37)}$, where h = 0.96

X= 5.82 m This distance is between the end of the first solar panel and the beginning of the second solar panel, Thus there is no shadow between the solar panels if we leave a distance of 5.82 meters.

So will leave a distance of about 12 meters because to put two solar panels on top of each other. And therefore, there is no shadow between rows of solar modules.

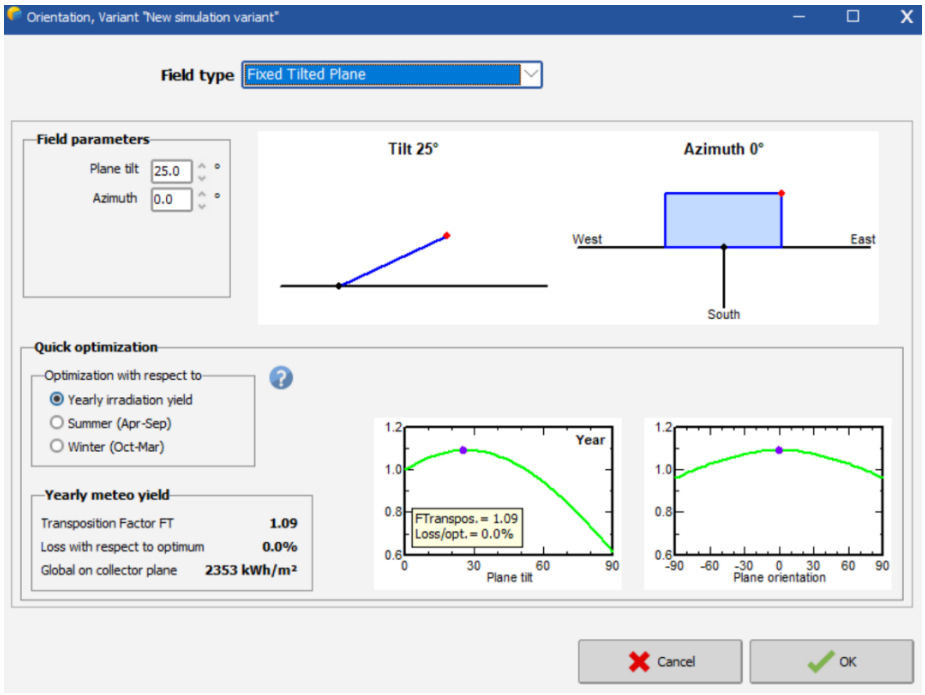

Figure 23. Tilt and Azimuth angle for Yanbu site

Figure 23 displays the optimal Azimuth angle and tilt for the Yanbu area; the optimal tilt angle for PV panels is 25 degrees with an azimuth of zero degrees. The sun path statistics are gathered from the Meteonorm software, which offers an unrivaled mix of accurate data and powerful mathematical materials. This data may be used to get accurate history and information for any period of year. In this system, roughly (366,984) PV modules with unit nominal power (540wp) will be used to produce 200MWp, and the modules connection design will be (13592 strings)*(27 series).

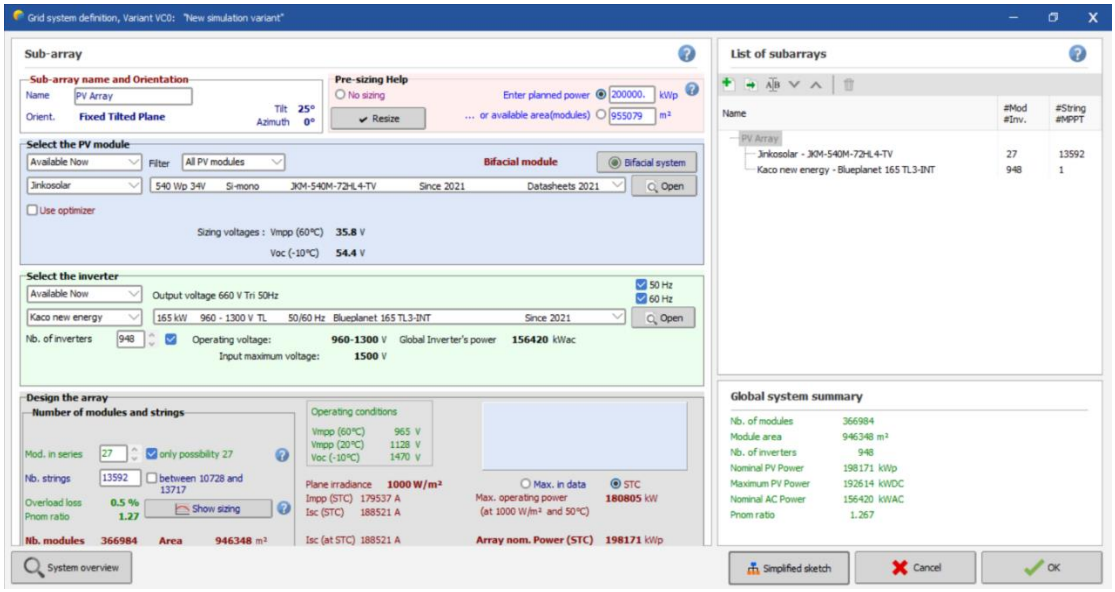

Figure 24. shows the distribution number of modules and PV strings.

Figure 24 shows the orientation of the plant, the plant capacity and area, the used PV module, the used inverter, its number, operating voltage and the design of the array which contain 13592 strings each string have 27 modules, with over sizing ratio 127%

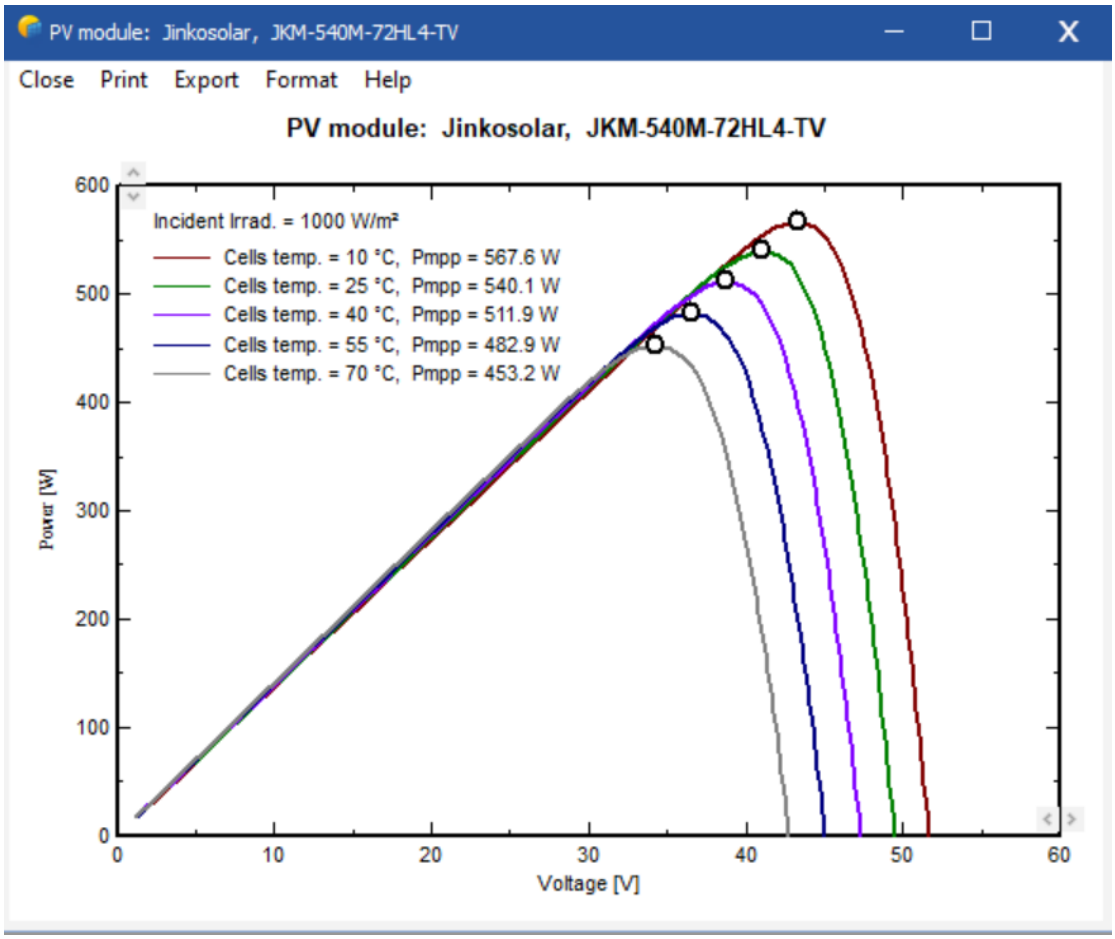

Figure 25. The relationship between voltage and power

figure 25 shows the relationship between the power of the module and its voltage
Note that if the cell temperture increces, the voltage and power of the module decreas.
For example: at temperature 25 degree, the module generate 540 W but at 55 degree the module generate 482.9 W. all of that at the constant radaition equal to 1000 W/m²

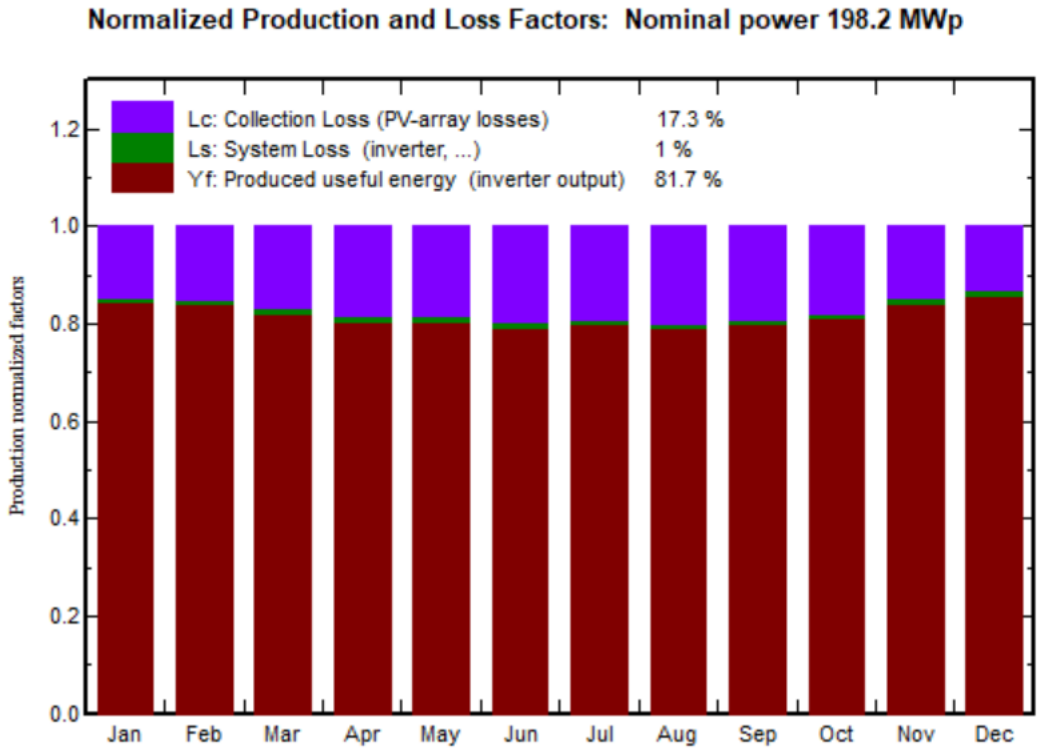

Figure 26. Normalized production and loss factors of Yanbu Site.

Diagram 26 displays produced energy from the plant (81.7% * 198.2 MWp= 162 MWp) , systems losses (1% * 198.2 MWp = 1.92 MWp) and collection losses (17.3% * 198.2 MWp= 34.2 MWp). Note that: the plant supposed to generate 198.2 MWp, but due to collection and system losses we get only 162 MWp.

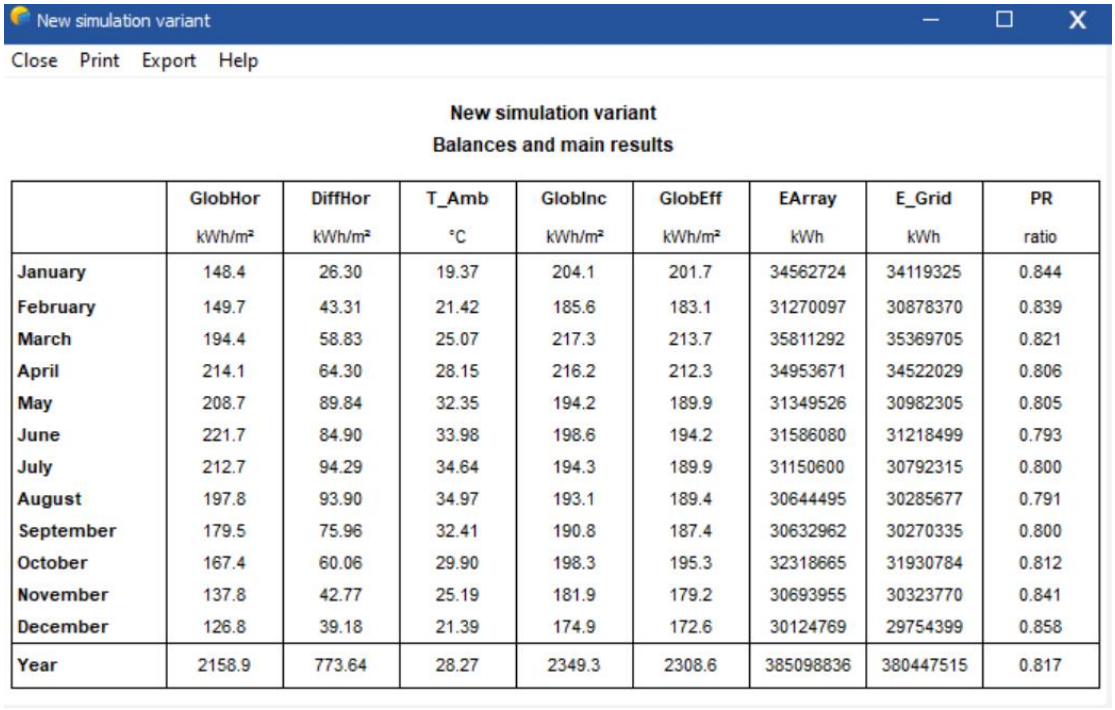

New simulation variant

Close Print Export Help

New simulation variant

Balances and main results

	GlobHor kWh/m²	DiffHor kWh/m²	T_Amb °C	GlobInc kWh/m²	GlobEff kWh/m²	EArray kWh	E_Grid kWh	PR ratio
January	148.4	26.30	19.37	204.1	201.7	34562724	34119325	0.844
February	149.7	43.31	21.42	185.6	183.1	31270097	30878370	0.839
March	194.4	58.83	25.07	217.3	213.7	35811292	35369705	0.821
April	214.1	64.30	28.15	216.2	212.3	34953671	34522029	0.806
May	208.7	89.84	32.35	194.2	189.9	31349526	30982305	0.805
June	221.7	84.90	33.98	198.6	194.2	31586080	31218499	0.793
July	212.7	94.29	34.64	194.3	189.9	31150600	30792315	0.800
August	197.8	93.90	34.97	193.1	189.4	30644495	30285677	0.791
September	179.5	75.96	32.41	190.8	187.4	30632962	30270335	0.800
October	167.4	60.06	29.90	198.3	195.3	32318665	31930784	0.812
November	137.8	42.77	25.19	181.9	179.2	30693955	30323770	0.841
December	126.8	39.18	21.39	174.9	172.6	30124769	29754399	0.858
Year	2158.9	773.64	28.27	2349.3	2308.6	385098836	380447515	0.817

Table 3. The total power generation of Yanbu site

Table 3 shows monthly for total power generation of Yanbu site where (GlobHor is Global horizontal irradiation, DiffHor is Horizontal diffuse irradiation, T_Amb is Ambient Temperature, GlobInc Global is incident in coll. plane, GlobEff Effective Global, corr for IAM and shadings, EArray is Effective energy at the output of the array, E_Grid is Energy injected into grid, PR is Performance Ratio).

Finally, the plant will be injected in to grid 380447515 kWh or 380.45 GWh energy. PR is the performance ratio that measure the quality of the PV plant that is independent of location and also describes as the quality factor on the plant, ranging from 80 to 100 percent. PR= Actual reading of plant output in KWh/ nominl plant output in KWh.

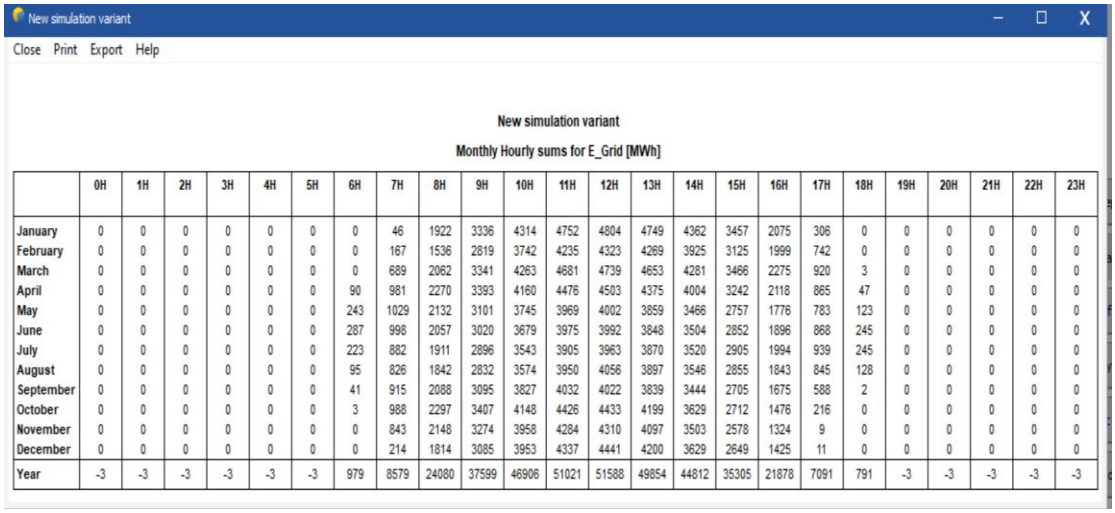

New simulation variant

Close Print Export Help

New simulation variant

Monthly Hourly sums for E_Grid [MWh]

	0H	1H	2H	3H	4H	5H	6H	7H	8H	9H	10H	11H	12H	13H	14H	15H	16H	17H	18H	19H	20H	21H	22H	23H
January	0	0	0	0	0	0	0	46	1922	3336	4314	4752	4804	4749	4362	3457	2075	306	0	0	0	0	0	0
February	0	0	0	0	0	0	0	167	1536	2819	3742	4235	4323	4269	3925	3125	1999	742	0	0	0	0	0	0
March	0	0	0	0	0	0	0	689	2062	3341	4263	4681	4739	4653	4281	3466	2275	920	3	0	0	0	0	0
April	0	0	0	0	0	0	90	981	2270	3393	4160	4476	4503	4375	4004	3242	2118	865	47	0	0	0	0	0
May	0	0	0	0	0	0	243	1029	2132	3101	3745	3969	4002	3859	3466	2757	1776	783	123	0	0	0	0	0
June	0	0	0	0	0	0	287	998	2057	3020	3679	3975	3992	3848	3504	2852	1896	868	245	0	0	0	0	0
July	0	0	0	0	0	0	223	882	1911	2896	3543	3905	3963	3870	3520	2905	1994	939	245	0	0	0	0	0
August	0	0	0	0	0	0	95	826	1842	2832	3574	3950	4056	3897	3546	2855	1843	845	128	0	0	0	0	0
September	0	0	0	0	0	0	41	915	2088	3095	3827	4032	4022	3839	3444	2705	1675	588	2	0	0	0	0	0
October	0	0	0	0	0	0	3	988	2297	3407	4148	4426	4433	4199	3629	2712	1476	216	0	0	0	0	0	0
November	0	0	0	0	0	0	0	843	2148	3274	3958	4284	4310	4097	3503	2578	1324	9	0	0	0	0	0	0
December	0	0	0	0	0	0	0	214	1814	3085	3953	4337	4441	4200	3629	2649	1425	11	0	0	0	0	0	0
Year	-3	-3	-3	-3	-3	-3	979	8579	24080	37599	46906	51021	51588	49854	44812	35305	21878	7091	791	-3	-3	-3	-3	-3

Table 4. Monthly Hourly sums for E-Grid [MWh].

Table 4 shows the hourly-monthly energy generated for 24 hours note that we will find the plant is generating energy from April to September from 6:00AM to 6:00 PM, So the plant will generate energy for 12 hours for 6 months per year.

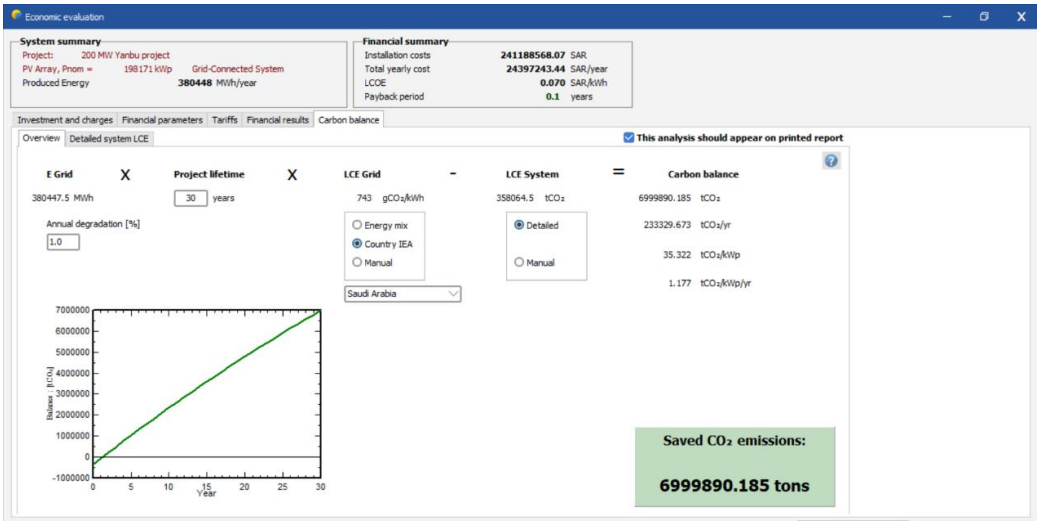

Figure 27. CO_2 emissions saved at Yanbu site.

Figure 27 shows the quantity of CO_2 emissions saved by building the plant in Yanbu region for 30 years, the plant will saved 6999890.185 tons of CO_2 emissions.

2.4 Drawing By using SketchUp

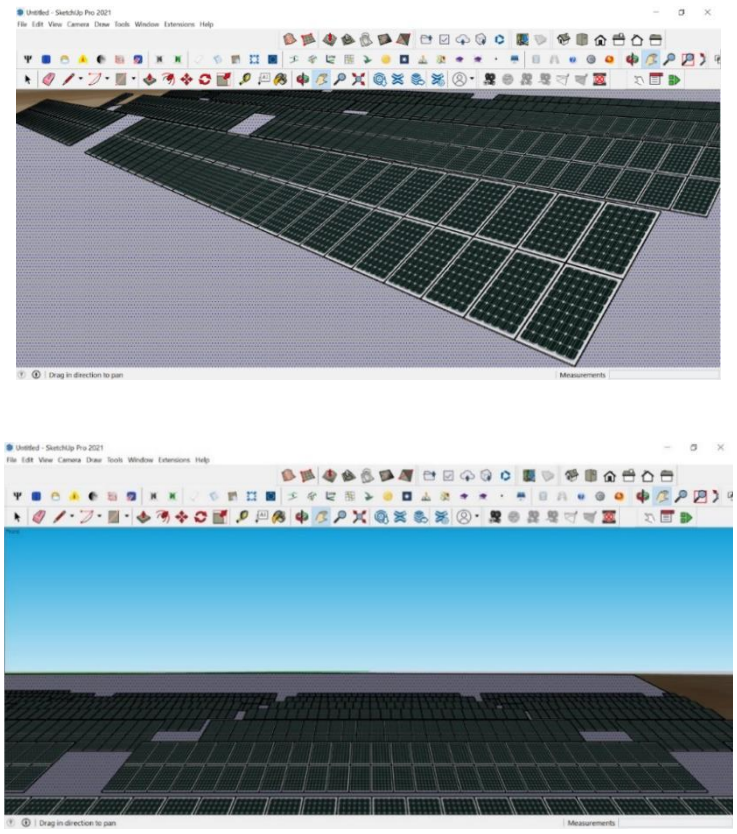

Figure 28. Sketch solar panels by using Sketchup program

Figure 28 shows the distribution of the solar panel in ground. the PV plant is

consisting of tables each table consider as two string each table consisting of two portrait module.

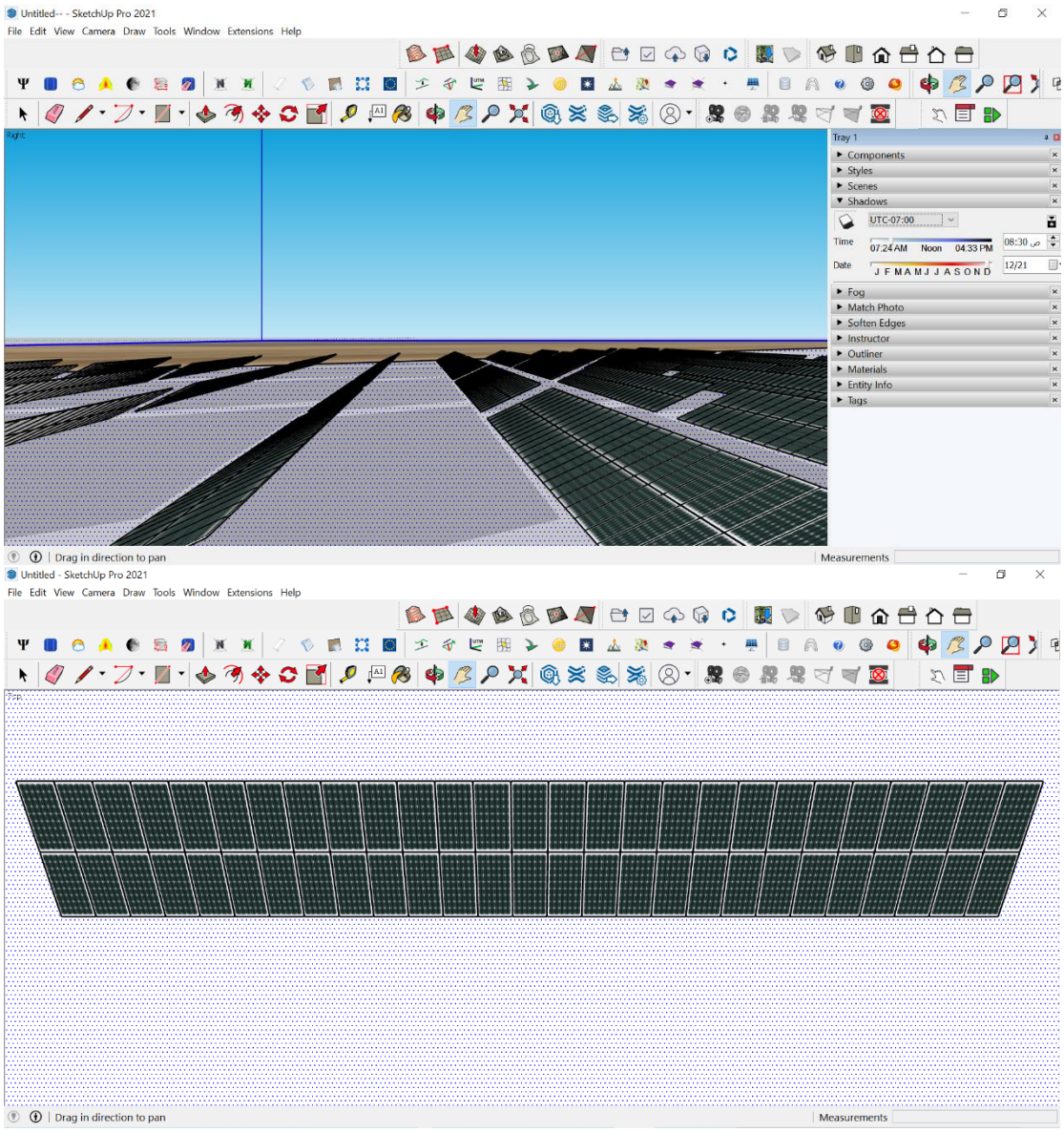

Figure 29. Impact of Shading in SketchUp program

Figure 29 shows the shading analysis of the plant at December 21, 8:30 AM

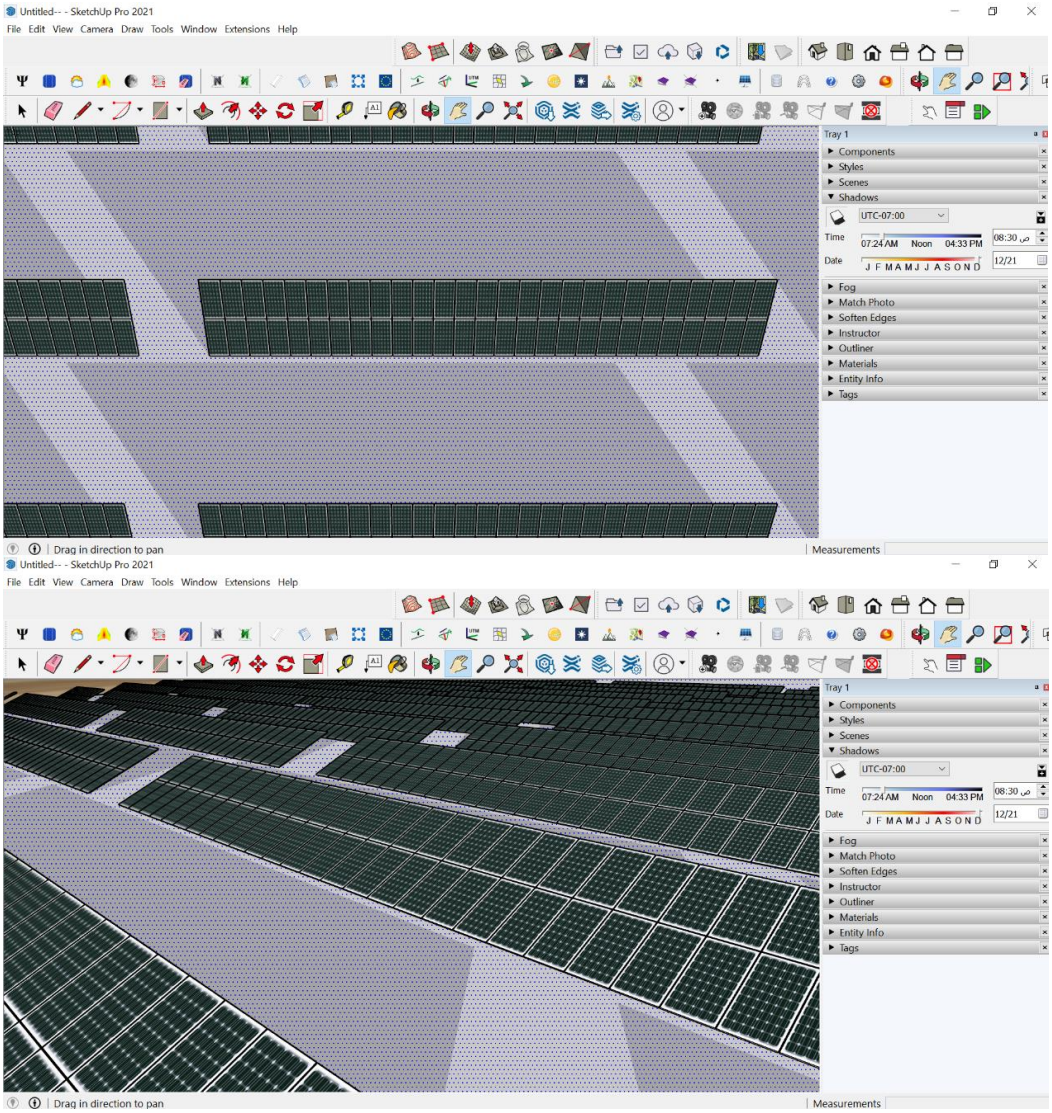

Figure 30. Impact of Shading on December 21 at 8:30AM

Figure 30 shows a distance of 12 meters has been left between the solar panels to avoid the effect of shadow

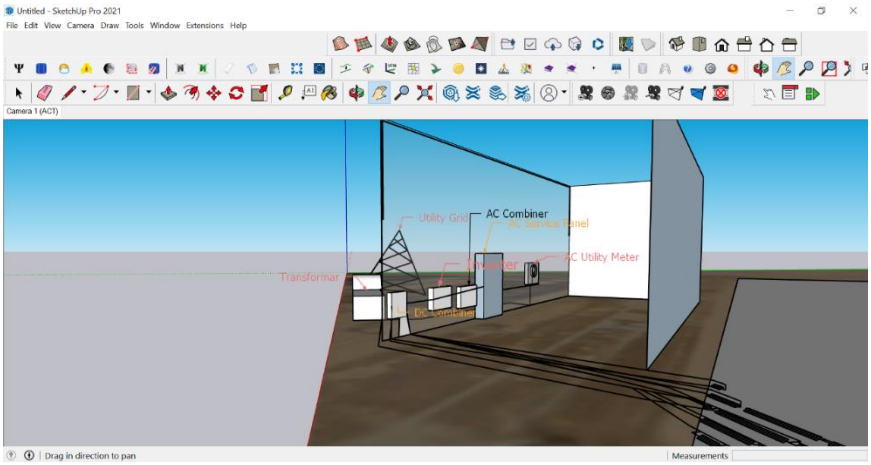

Figure 31. Sketch solar panels connected to the on-grid by using SketchUp program.

Figure 31 shows the room that contain inverters combiner boxes main distributed board and the connection between the transformer and the grid.

2.5 Project's total cost in Saudi Riyals

200 MW Ongrid system Bill of material

Total price SAR	Unit Price SAR	QTY	Description	Vendor	ref.
SAR 193,217,076.00	SAR 526.50	366,984	540 Watt solar panel	Jinko solar	1
SAR 23,700,000.00	SAR 25,000.00	948	165KW ongrid inverter with Combiner DC	Kako New energy	2
SAR 15,000,000.00	SAR 15,000,000.00	1	Fixation frame	Chint	3
SAR 2,114,229.00	SAR 3.00	704,743	DC Cable 6mm	El sewedy	4
SAR 17,839.50	SAR 1.31	13,592	MC4 Connector	Sun tech	5
SAR 127,425.00	SAR 9.38	13,592	Cable Connector 6mm	ABB	6
SAR 924,489.60	SAR 12.19	75,840	60mm Ac cable	El Swedey	7
SAR 1,023.84	SAR 0.18	5,688	Cable Lug	ABB	8
SAR 3,555,000.00	SAR 15,000.00	237	AC Combiners	ABB	9
SAR 200,000.00	SAR 50,000.00	4	AC Cabinets	ABB	10
SAR 238,857,082.34	Total before Installation				11
SAR 23,885,708.184	10% of total cost		Installation		12
SAR 262,742,790.02	Total				13

Table 5. The cost of the on-grid connected solar panel system project [21].

Table 5 shows the detail Bill of quantities of the plant including prices with SAR and All technical data: There are 366,984 Jinko solar panels, the capacity of one panel is 540 watts, and the price of one panel is 526.5 Saudi riyals, and the total panels = 193,217,076.00 SAR. We have 948 Kako New energy inverters, each with a power of 165 kilowatts, and the price of one inverter is 25,000 SAR. The total cost of inverters = 23,700,000.00 SAR. In addition to the aluminum frame of the Chint type, on which solar panels are installed, and its price is 15,000,000 SAR, and we also need DC Cable 6mm of the El sewedy type, and in this project we need 704,743 and the cable is 3.00 Saudi riyals per meter, and the total of the cable is 2,114,229.00 SAR and we have an MC4 Connector of the Sun type tech, and we need 13,592 MC4 Connector to connect the solar panels with each other. The price of one MC4 Connector is 1.31 Saudi riyals. The total MC4 Connector is 17,839.50. Also need to 13,592 Cable Connector 6mm of type ABB the price of Cable Connector 6mm is 9.38 SAR, and the total cost of Cables Connector 6mm is 127,425.00 SAR. And we need a 60mm Ac cable of the El Swedey type to connect the inverters to the AC panel box, and in this project, we need 75,840 (60mm) Ac cable, and the cable price is 12.19 Saudi riyals, with a total cost of 924,489,60 SAR.

We also need ABB Cable Lug to connect the solar panels side by side. We need 5,688. The Cable Lug price is 0.18 SAR.

The total cost Cable Lug is 1,023.84 SAR. Also need to ABB AC Combiners to connect every 4 inverters to the AC Combiner. The price of the AC Combiner is 15,000.00 SAR and the total cost of AC combiners are 3,555,000 SAR, and we have AC Cabinets so that AC Cabinets are connected to the transformer and to the grid, and we need AC Cabinets to connect 237 inverters AC Cabinet, and the price of the AC cabinet is 50,000.00 SAR, and the total cost of AC Cabinets are 200,000.00 SAR, and the installation and manpower fees are 10% of the project cost, which is 23,885,708.184 SAR. The total project cost = 262,742,790.02 SAR

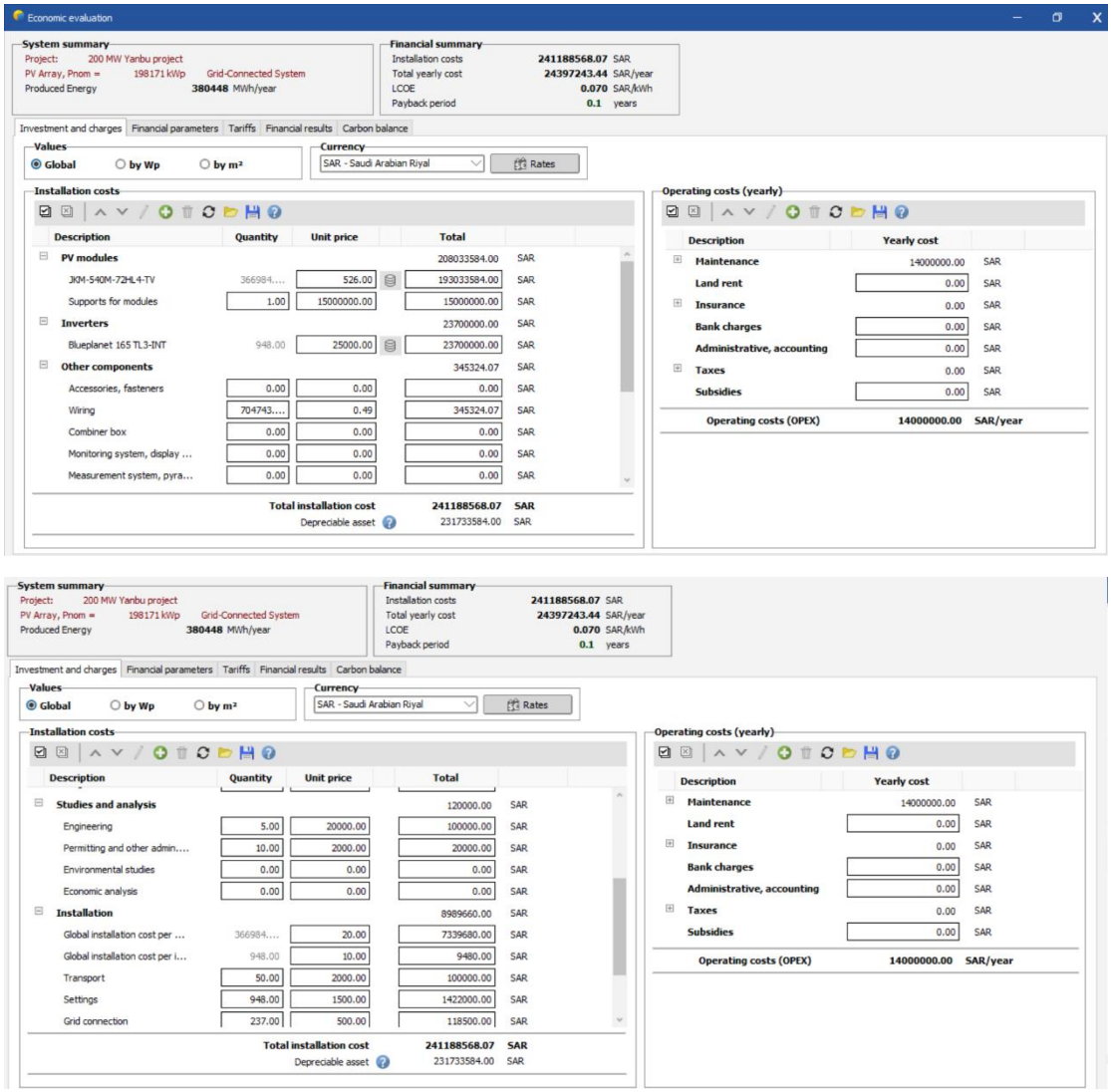

Figure 32. Investment & charges of economic evaluation solar project

Figure 32 shows a detialed in econmic analysis for the plants including CAPEX and OPEX. CAPEX consisting of hard cost (PV modules, Inverters, mounting structure, MDBs,

Transformer, Cabales, combiner box, and installation), and soft cost(Engineering, Permitting fees).
OPEX including all operitional cost like that(Team Salaries, Rapairs, and Cleaning).

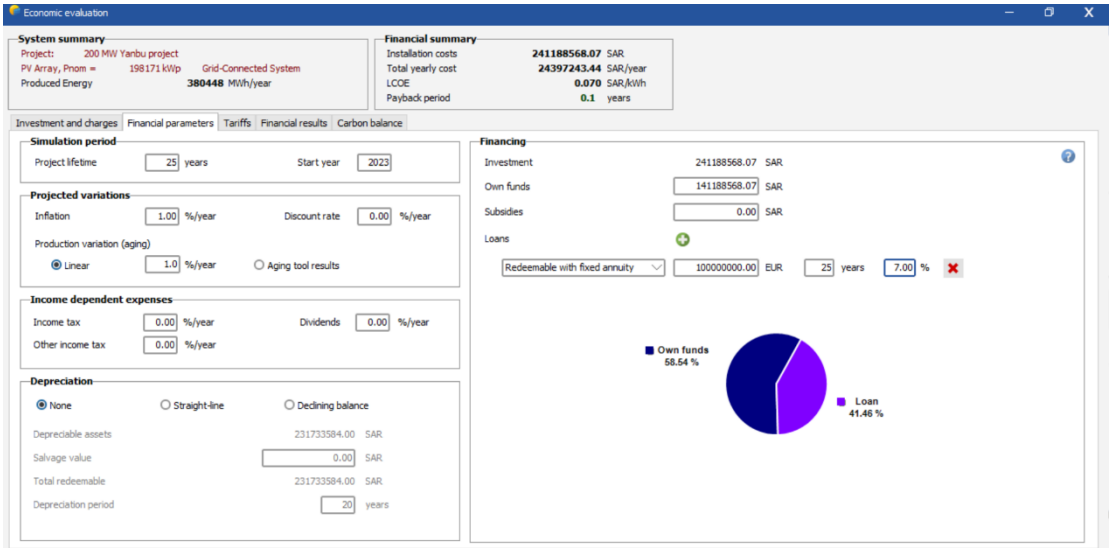

Figure 33. financial Parameters for solar project

Figure 33 shows the financial parameters: Simulation period which started at 2023 and last for 25 years, So the simulation period will end at 2048. Projected variations which include the inflation(which considered to be 1% per year), and the production variations due to aging(which considered to be 1% per year due to annual degradation of PV modules).financing and investment which include: the total investment for the project is dividing into own funds with 58.54% which equals 141,188,568.07 SAR and a loan with 41.46% which equals 100,000,000.00 SAR for a payment plan for 25 years with fixed interest 7%.

As shown below, there is the financial analysis of the solar energy project, as the project starts in 2023 until 2048, and the project cost starts from 261 million. In 2023, revenues were recorded at about one billion and 738 million and 670 thousand Saudis, and then in 2024, the revenues were recorded at one billion and 898 million and 744 thousand. And the cumulative profit for the year 2024 (one billion and 738 million and 670 thousand + one billion and 898 million and 744 thousand) is the total = 3 billion and 637 million and 414 thousand.

Where the cumulative profit from 2023 to 2048 (46 billion and 714 million and 757 thousand Saudi riyals)

Financial analysis

Detailed economic results (kSAR)

	Electricity sale	Loan principal	Loan interest	Run. costs	Deprec. allow.	Taxable income	Taxes	After-tax profit	Cumul. profit	% amorti.
2023	1902440	1581	7000	14000	0	1881440	0	1879859	1738670	780.1%
2024	1921464	1692	6889	14140	0	1900435	0	1898743	3637414	1568.0%
2025	1940489	1810	6771	14281	0	1919436	0	1917626	5555040	2363.8%
2026	1959513	1937	6644	14424	0	1938445	0	1936508	7491548	3167.5%
2027	1978538	2072	6509	14568	0	1957460	0	1955388	9446936	3979.1%
2028	1997562	2218	6364	14714	0	1976484	0	1974267	11421203	4798.6%
2029	2016586	2373	6208	14861	0	1995517	0	1993144	13414347	5626.0%
2030	2035611	2539	6042	15010	0	2014559	0	2012020	15426366	6461.2%
2031	2054635	2717	5865	15160	0	2033611	0	2030894	17457261	7304.4%
2032	2073660	2907	5674	15312	0	2052674	0	2049767	19507027	8155.5%
2033	2092684	3110	5471	15465	0	2071748	0	2068638	21575666	9014.4%
2034	2111708	3328	5253	15619	0	2090836	0	2087508	23663174	9881.3%
2035	2130733	3561	5020	15776	0	2109937	0	2106376	25769550	10756.1%
2036	2149757	3810	4771	15933	0	2129053	0	2125243	27894793	11638.9%
2037	2168782	4077	4504	16093	0	2148185	0	2144108	30038900	12529.5%
2038	2187806	4362	4219	16254	0	2167334	0	2162971	32201872	13428.1%
2039	2206830	4668	3914	16416	0	2186501	0	2181833	34383705	14334.7%
2040	2225855	4994	3587	16580	0	2205688	0	2200693	36584398	15249.2%
2041	2244879	5344	3237	16746	0	2224896	0	2219552	38803950	16171.7%
2042	2263904	5718	2863	16914	0	2244127	0	2238409	41042359	17102.1%
2043	1141464	6118	2463	17083	0	1121918	0	1115800	42158160	17567.3%
2044	1150976	6546	2035	17253	0	1131688	0	1125142	43283301	18036.5%
2045	1160488	7005	1576	17426	0	1141486	0	1134481	44417783	18509.8%
2046	1170001	7495	1086	17600	0	1151314	0	1143819	45561602	18987.1%
2047	1179513	8020	561	17776	0	1161175	0	1153155	46714757	19468.6%
Total	**47465877**	**100000**	**114526**	**395405**	**0**	**46955946**	**0**	**46855946**	**46714757**	**19468.6%**

Table 6. Financial analysis (kSAR) of solar project

Table 6 shows a detail financial and economic analysis for the period 25 years regirding to : Electricity sale, loan principal, loan interest, run costs, taxable income, after-tax profit, cumulative profit in kSAR for the first year of the investment (2023) Electricity sale will be 1902440 kSAR, Loan principal 1581 kSAR, loan interest 7000kSAR, run costs 2450 kSAR, taxable income 1892990 kSAR, after-tax profit 1879859 kSAR, cumulative profit 1738670 kSAR, and cumulative profit 46714757 kSAR.

As shown below, there is the yearly cashflow & Financial results of the project from 2023 to 2048

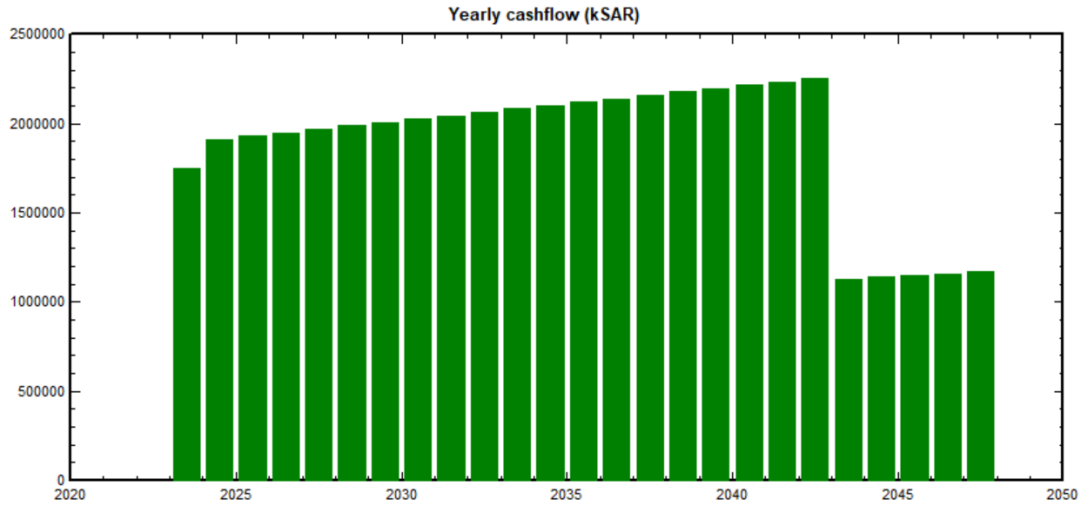

Figure 34. Yearly cashflow of the project (kSAR), 2023 to 2048

Figure 34 shows the yearly net cashflow earn due to plan production for example: 2025 the net cash flow is equals 1917626 kSAR

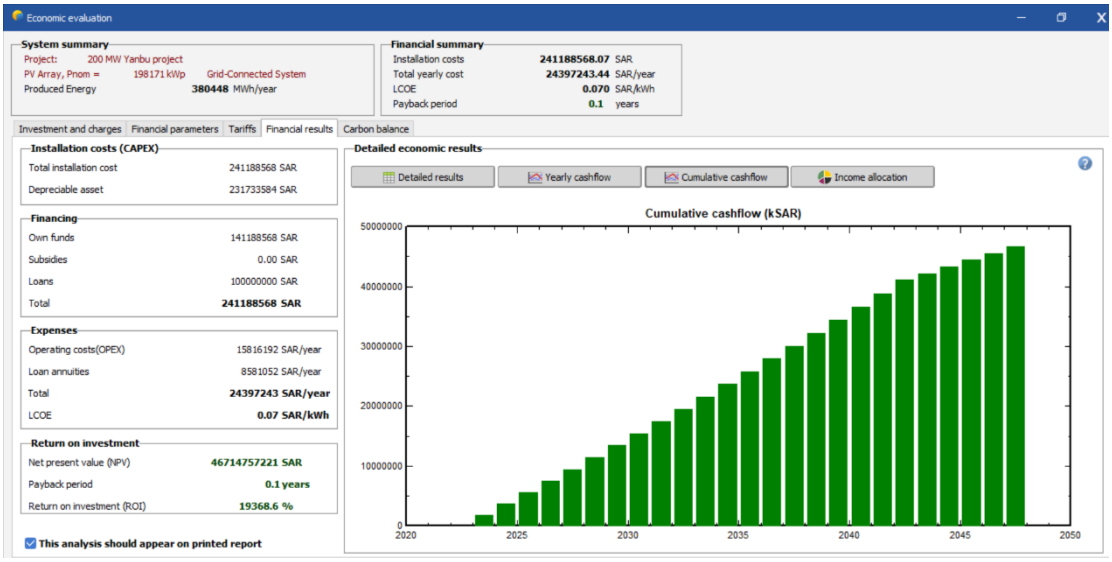

Figure 35. Financial results of the project from 2023 to 2048

Figure 35 shows the cumulative cashflow of the project starts with 1738670 kSAR and ends with 46714757 kSAR

Conclusion

3.1 Conclusion

Saudi Arabia has significant natural solar energy potential as well as an economic opportunity to expand renewable energy to fulfill local energy demand. Solar energy technology, in particular, has advanced at a dizzying pace in recent years, and so represents the most potential alternative to conventional energy systems. While experimental initiatives to expand solar energy production were initiated in the 1980s, Saudi Arabia has chosen a much more aggressive approach to solar energy production. This research project presents the results of an analytical study that was conducted on the use of PV systems in two locations within Saudi Arabia.A feasibility study for a project to establish a solar power plant with a capacity of 200 megawatts in the regions of Yanbu and Rabigh The study includes the design of a photovoltaic system using PVsyst and SketchUp programs and a feasibility work on quantities for all components required and total costs for the construction of the station.

4.References:

[1] Alharthi, Y.Z.; Siddiki, M.K.; Chaudhry, G.M. The New Vision and the Contribution of Solar Power in the Kingdom of Saudi Arabia Electricity Production. In Proceedings of the 2017 Ninth Annual IEEE Green Technologies Conference (GreenTech), Denver, CO, USA, 29–31 March 2017; pp. 83–88.

[2] Barber, J. 3 MA. Available online: https://www.acwapower.com (accessed on 20 May2021).

[3] Ivan Shumkov Saudi Auction for 400 MW of Wind Attracts 4 Bids. Available online: https://renewablesnow.com (accessed on 20 May 2021).

[4] National Transformation Program Vision 2030. Available online: https://vision2030.gov.sa/en (accessed on 7 January 2021).

[5] Alnatheer, Othman, 2005a. The potential contribution of renewable energy to electricity supply in Saudi Arabia. Energy Policy 33, 2298–2312.

[6] U.S. Energy Information Administration, International Energy Statistics.

[7] Arab Petroleum Investment Corporation (APICORP), MENA Power Investment Outlook 2019-2023, July 2019, page 8.

[8] BP Statistical Review of World Energy 2021.

[9] Saudi Electricity Company, Annual Report 2020, page 91.

[10] S. Fleming. (Jun. 7, 2019). Chart of the day: These countries create most of the world's CO2 emissions. World Economic Forum. Accessed: Oct. 24, 2020. [Online]. Available: https://www. weforum.org/agenda/2019/06/chart-of-the-day-these-countries-createmost-of-the-world-s-co2-emissions/

[11] ClimateWatch. (2021). Climate Change Country Profile of Saudi Arabia. Accessed: Feb. 22, 2021. [Online]. Available: https://www. climatewatchdata.org/countries/SAU

[12] Climate Action Tracker. (2021). Emissions in Saudi Arabia. Accessed: Feb. 24, 2021. [Online]. Available: https://climateactiontracker.org/countries/saudi-arabia/

[13] Ministry of Water and Electricity, Office of the Deputy Minister Information & Statistic Centre. Electricity: Growth and Development in the Kingdom of Saudi Arabia, 2007.

[14] Al-Saleh YM. A glimpse into the status and prospect of renewables in oil-producing countries; with a special reference to the Saudi Arabia of Saudi Arabia. Geopolitics of Energy vol. 29(11): pp. 2–13, 2007.

[15] Al-Saleh, Yasser M., and Hanan M. Taleb. "The Economic Viability of Solar Photovoltaics within the Saudi Residential Sector." In Conference On Technology & Sustainability in the Built Environment, pp. 747-758. 2010.

[16] Chukwuka, C., Folly, K.A. Overview of concentrated photovoltaic (CPV) cells. J. Power Energy Eng. Vol. 2, pp. 1–8, 2014.

[17] CLIMATE TRANSPARENCY REPORT COMPARING G20 CLIMATE ACTION AND RESPONSES TO THE COVID-19 CRISIS https://www.climate-transparency.org/media/saudi-arabia-country-profile-2020

[18] Solar Photovoltaics | Impact of shading - Green Rhino Energy http://www.greenrhinoenergy.com/solar/performance/shading.php

[19] Ravindra Krishnamurthy. October 23, 2015. Charting The Sun's Motion https://www.permaculturenews.org/2015/10/23/charting-the-suns-motion-in-relation-to-your-home-and-permaculture-site/

[20] The solar window. Image credit: Clay Atchison, www.solarschoolhouse.org

[21] Solar Land Energy, Saudi Arabia, Jeddah https://sle.sa/

List of Abbreviations

Abbreviation	Meaning
R&D	Research and Development
RETs	renewable energy technologies
PV	photovoltaic
NREP	National Renewable Energy Program
NTP	National Transformation Program
REPDO	Renewable Energy Project Development Office
RFP	request for proposal
CO_2	Carbon Dioxide
SO_2	sulphur dioxide
NO_2	Nitrogen dioxide
CH_4	*Methane* is a chemical compound
GHG	Greenhouse gas
OPEC's	Organization of the Petroleum Exporting Countries
GDP	Is the total monetary or market value of all the finished goods and services produced within a country's borders in a specific time period
EIA	*Energy Information Administration - EIA* - Official Energy Statistics from the U.S. Government.
JODI	The Joint Organisations Data Initiative (JODI) is a concrete outcome of the producer-consumer dialogue and aims to improve gas and oil data transparency.
Tcf	The term trillion cubic feet refers to a volume measurement of natural gas used by the U.S. oil and gas industry. The measurement is usually abbreviated as Tcf.
Bcf	Billion cubic feet (Bcf)
$MtCO_2$/Year	Metric tons of carbon dioxide equivalent per year
DNI	Direct normal irradiance
GHI	Global horizontal irradiance
DHI	Diffuse horizontal irradiance
Solar PV IPP	An independent power producer (IPP) is an entity that is not a public utility but owns facilities to generate electric power for sale to utilities and end users.
KACST	King Abdulaziz City for Science and Technology
KAPSARC	King Abdullah Petroleum Studies and Research Center
NOAA	The National Oceanic and Atmospheric Administration (NOAA) is an American scientific and regulatory agency within the United States Department of Commerce works to understand and predict changes in climate, weather, oceans, and coasts.

Tetra(4-aminophenyl) porphyrin-based Covalent Organic Frameworks

Maher Fathalla*

* Department of Chemistry, Faculty of Science, Islamic University of Madinah, Madinah 42351, SA

Email: maherfathalla@iu.edu.sa

Abstract: Covalent Organic Frameworks (COFs) are robust crystalline porous materials with unique properties and have promising applications in many fields such as gas adsorption, sensing and catalysis. COFs properties can be tailored by the judicious choice of their building units. Stemming from its unique properties, rigid structure and synthetic accessibility, tetra(4-aminophenyl)porphyrin (TAPP) has been employed as a building unit to construct various COF materials. This review highlights the different synthetic approaches that were exploited by researchers to assemble COF materials based on TAPP.

Keywords: Porphyrins; Covalent Organic Frameworks; Porous Organic Polymers; Imide; Imine.

الهياكل العضوية التساهمية (COFs) القائمة على (4-أمينوفينيل) بورفيرين

الملخص: الهياكل العضوية التساهمية (COFs) عبارة عن مواد بلورية مسامية قوية ذات خصائص فريدة ولها تطبيقات واعدة في العديد من المجالات مثل ادمصاص الغاز والاستشعار والحفز. يمكن تصميم خصائص COFs من خلال الاختيار الحكيم لوحدات البناء الخاصة بهم. وقد تم استخدام (4-أمينوفينيل) بورفيرين (TAPP) كوحدة بناء لبناء العديد من مواد COFs ، وذلك نظرًا لخصائصه الفريدة وهيكله الصلب وسهولة تحضيره. هذا البحث يسلط الضوء على الأساليب التركيبية المختلفة التي استغلها الباحثون لتحضير مواد COFs بناءً علىTAPP.

1. Introduction.

Covalent Organic Frameworks (COFs) are emerging class of crystalline porous organic materials that have attracted the interest of researchers worldwide owing to their potential applications in a large variety of domains, such as gas adsorption and separation, chemosensors, heterogeneous catalysis, energy storage and optoelectronics [1–8]. Based on reticular chemistry, COFs are constructed by the integration of organic building blocks by strong covalent bonds to make highly porous materials with predictable structures. The pore dimensions as well as the skeletons of COFs can be tailored by the judicious predesign of the knots and linkers whose symmetries determine the COFs shape and whose dimensions dictate COFs pore sizes [9–14]. Owing to their excellent thermal and chemical stabilities as well as synthetic accessibility, COFs are considered an attractive alternative to MOFs (Metal Organic Frameworks) [15]. Various organic molecules have been applied as building units to construct wide range of COFs. Among these molecules, porphyrin macrocycles are considered attractive building units for making COFs owing to their rigid structures, synthetic accessibility, as well as broad-ranging optoelectronic and catalytic properties that could be tuned by substituent effects and incorporation of various metals in porphyrin macrocycle. Consequently, various porphyrin derivatives have been applied as building block to make a wide-range of porphyrin-based COFs [16–21] among which tetra(4-aminophenyl)porphyrin (TAPP) has been one of the most used building unit to construct COFs since the pioneering work by Yaghi's group [22]. This review summarizes the common approaches the were employed by researchers to construct COFs by using tetra(4-aminophenyl)porphyrin (TAPP) as a building unit. As shown in scheme 1, the four amino groups of TAPP have been harnessed to construct various COFs through two main synthetic strategies, namely, formation of imine- or imide-bonds.

2. Synthesis of TAPP-based COFs.

2.1. Imine-linked porphyrin COFs.

The reversible condensation between amines and aldehydes is one of the oldest reactions in organic chemistry. The dynamic nature of this reaction allows "error checking" and "proof-reading" of the resulting materials. Yaghi's group harnessed the condensation between TAPP and terephthaldehyde to construct imine-linked porphyrin COFs known as COF-366 by solvothermal reactions. As shown in scheme 1, COF-366 has square channels with porphyrin moieties located at the nodes of the square skeletons and are linked by the imine-bonds [23].

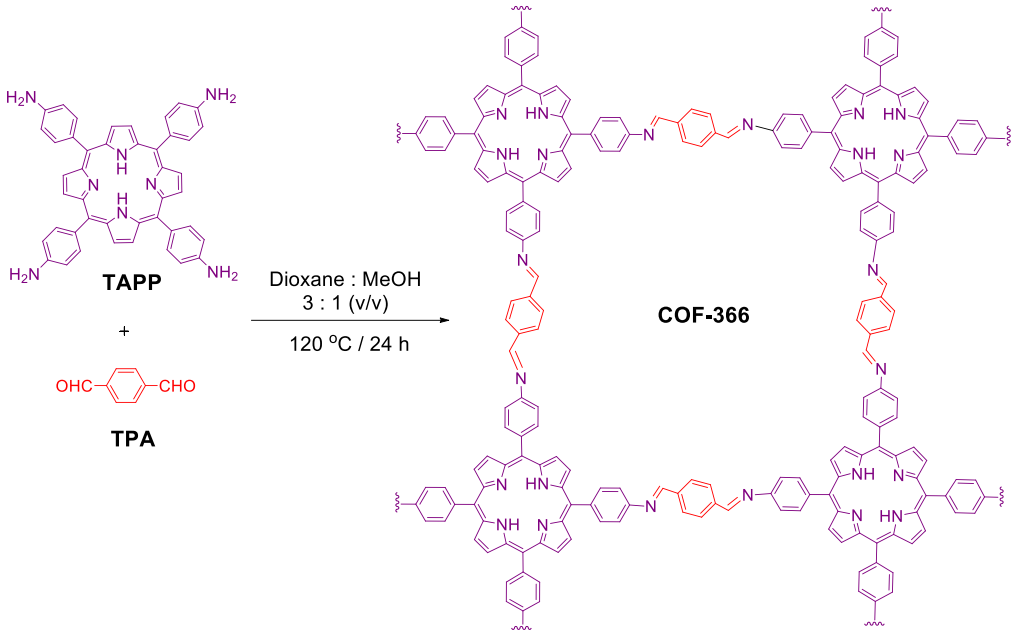

Scheme 1. The synthesis of COF-366 via the reaction of TAPP and TPA.

Later on, the effect of incorporating hydrogen bonding on the stability of the resulting imine-linked COFs was investigated through the synthesis of DmaTph and DhaTph via the condensation of TAPP with either 2,5-dimethoxyterephthaldehyde or 2,5-dihydroxyterephthaldehyde, respectively [24]. It was concluded that, DhaTph exhibits higher thermal, water, and acid stability than DmaTph owing to the OH….N=C intramolecular hydrogen bonding within the DhaTph structure (scheme 2).

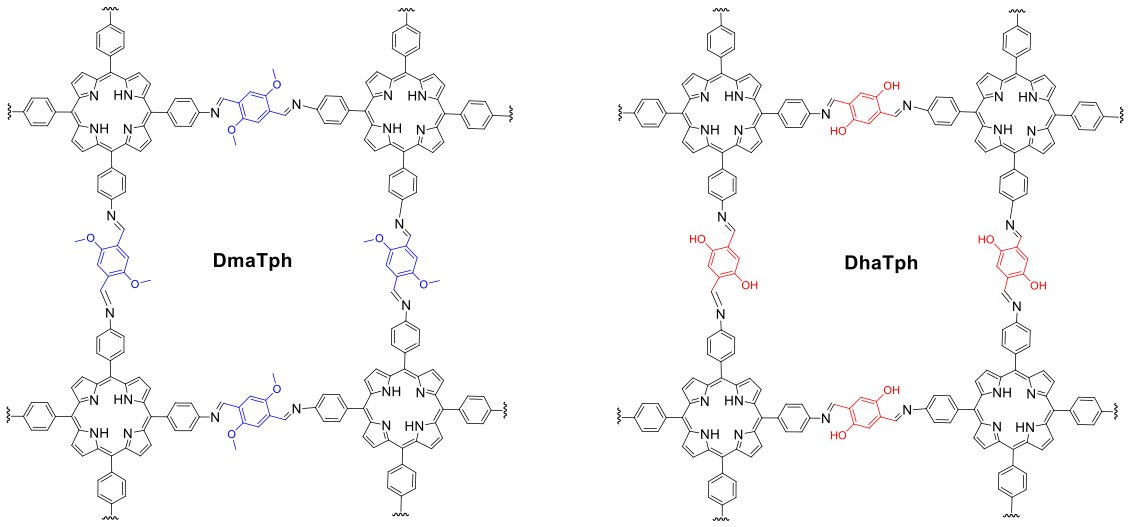

Scheme 2. Structures of imine-linked DmaTph and DhaTph porphyrin COFs via the reaction of TAPP with either 2,5-dimethoxyterephthaldehyde or 2,5-dihydroxyterephthaldehyde, respectively.

In another report, Beuerle et al. exploited the condensation between TAPP and a diketopyrrolopyrrole (DPP) to assemble a novel imine-linked porphyrin COFs (DPP-TAPP-COF) with an enhanced absorption capability up to 800 nm [25]. Furthermore, the resulting COF self-assembles into a hollow microtubular with outer and inner tube diameters of around 300 and 90 nm, respectively (scheme 3).

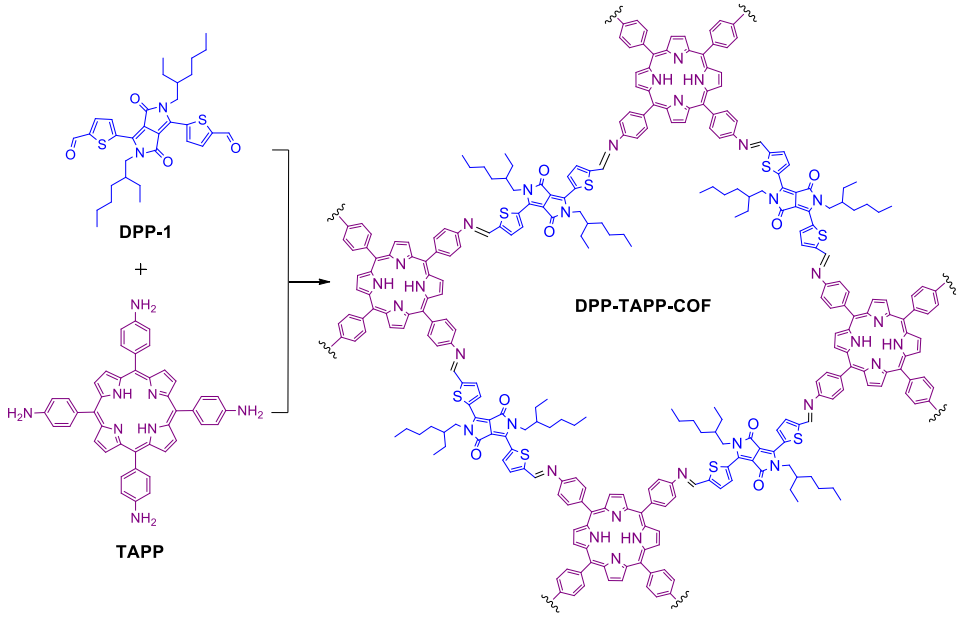

Scheme 3. Synthesis of DPP-TAPP-COF via the condensation between TAPP and a diketopyrrolopyrrole (DPP).

Huang et al. reported the synthesis of another imine-linked porphyrin COF (TAPP-TFPP-COF) through the condensation between TAPP and tetra(4-formylphenyl)porphyrin TFPP under typical solvothermal conditions (scheme 4) [26]. The resulting COF has a tetragonal micropores at a size of 1.8 nm and exhibited high crystallinity, excellent stability, and good porosity. In addition, the conductivity of TAPP-TFPP-COF can be greatly enhanced after doping with iodine.

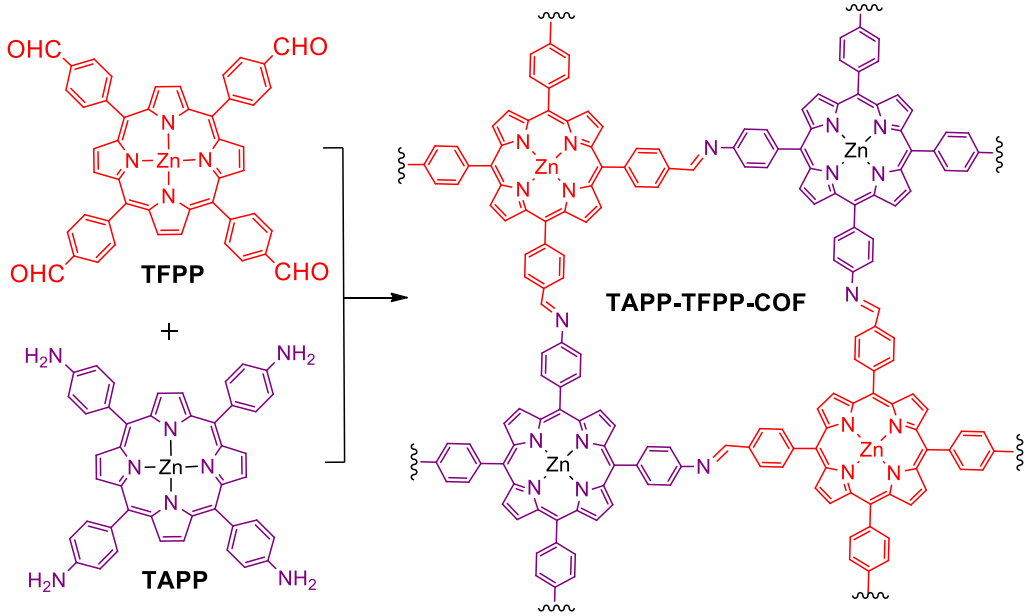

Scheme 4. Synthesis of TAPP-TFPP-COF via the reaction of TAPP and tetra(4-formylphenyl)porphyrin TFPP.

Recently, Gao et al. reported the synthesis of another imine-linked porphyrin COF, termed Co(II)@TA-TF COF by the solvothermal reaction of cobalt(II) TAPP and 1,3,6,8-tetrakis(4-formylphenyl)pyrene (TFPPy) (scheme 5) [27]. The resulting Co(II)@TA-TF COF possesses micropores suitable for CO_2 adsorption owing to the alternate stacking of the building units, and was equipped with cobalt(II) porphyrin units as catalytic sites into the vertices of the layered tetragonal networks that enable the conversion of CO_2 into cyclic carbonates under mild conditions.

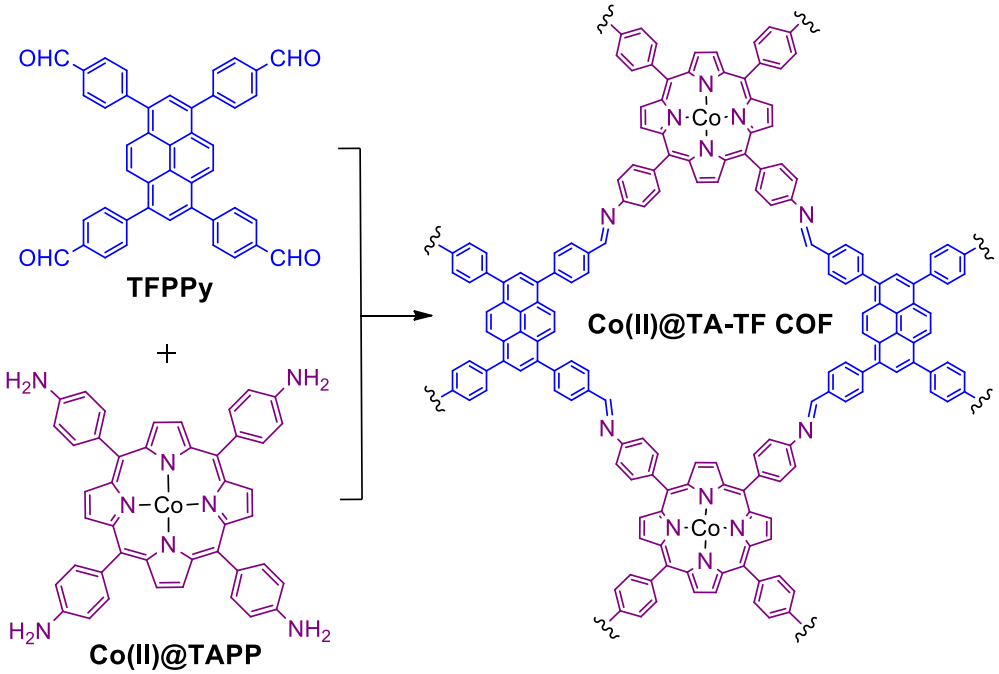

Scheme 5. Synthesis of Co(II)@TA-TF COF via the reaction of cobalt(II) TAPP and 1,3,6,8-tetrakis(4-formylphenyl)pyrene (TFPPy).

Chen et al. reported a recent imine-linked porphyrin COF, termed TPE-Por-4, by the condensation of TAPP and 4,4',4",4"'-(ethene-1,1,2,2-tetrayl)tetrabenzaldehyde (D_{2h}-symmetric) [28]. The expected route for the [4+4] condensation was not observed based on a series of structure characterization of TPE-Por-4 (scheme 6). The resulting COF suspension shows unique fluorescent properties originated from its building units and displays an apparent response to pH fluctuation ranging from 2 to 4, rendering it suitable for spectroscopic monitoring of medium pH value.

In another approach, Gu et al. constructed a novel imine-linked porphyrin COF, termed PPOP-1(Pd), first, via imine condensation of TAPP and acenaphthalenequinone followed by refluxing with $PdCl_2$ to afford PPOP-1(Pd) (scheme 7) [29]. The resulting COF contains two catalytic sites, namely, Pd(II)-porphyrin and Pd(II)-α-diimine moieties rendering it efficient for tandem catalytic reactions.

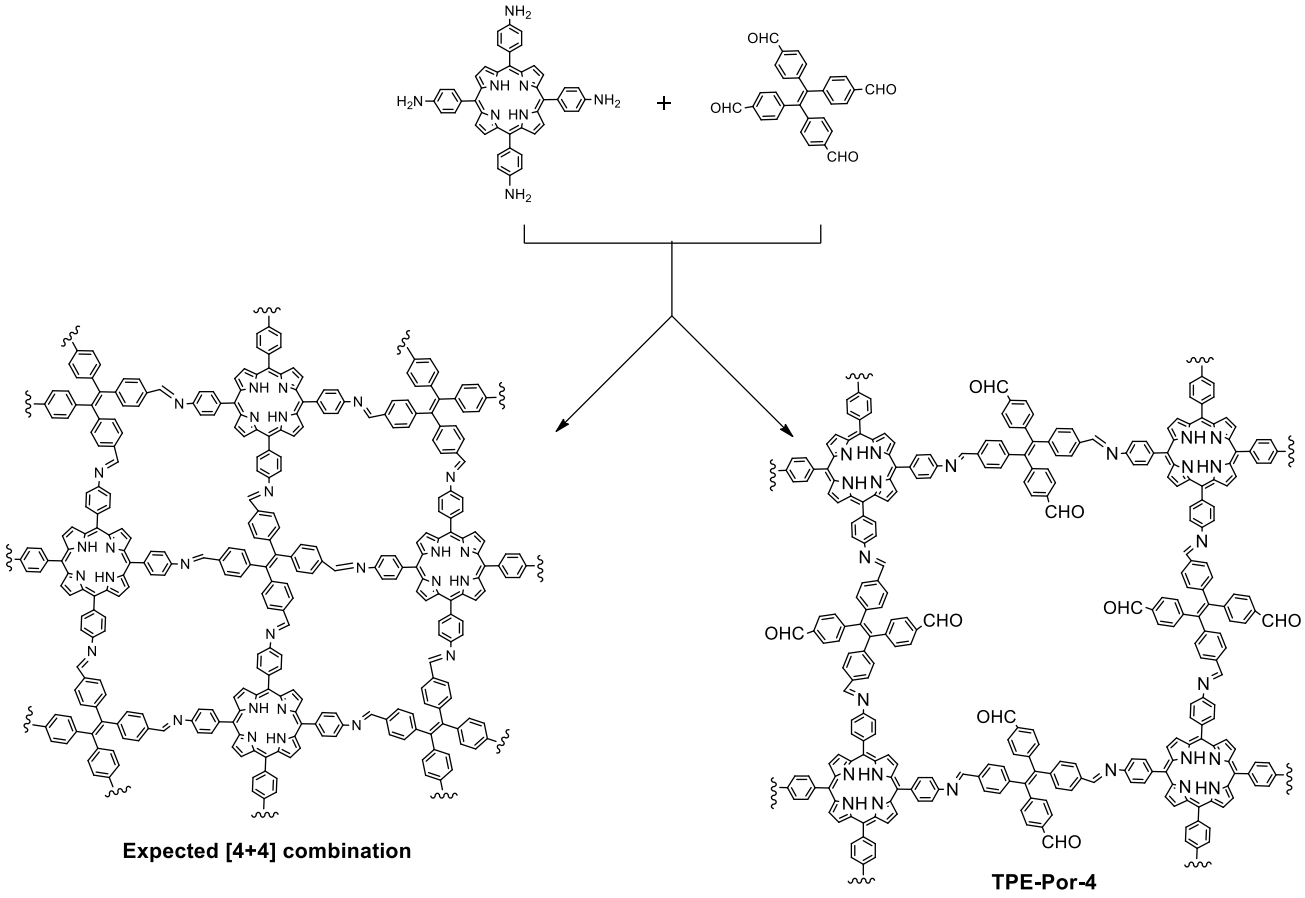

Scheme 6. Synthesis of TPE-Por-4 condensation of TAPP and 4,4',4",4"'-(ethene-1,1,2,2-tetrayl)tetrabenzaldehyde.

2.2. Imide-linked porphyrin COFs.

Polyimide (PI) polymers are known for their excellent chemical and thermal stabilities. Typically, imidization reaction involves the condensation of an amine and an anhydride. The imidization reaction has been exploited to construct various porphyrin COFs in which TAPP (amine monomer) was employed as a node and the anhydride monomer as a linker. For instance, Echegoyen et al. reported the synthesis of a polyimide porphyrin COF via the condensation of Cu (II)-TAPP and naphthalene tetracarboxylic dianhydride in m-cresol/isoquinoline mixture (scheme 8) [30]. The resulting polyimide porphyrin COF exhibited adsorption capacity of 3.5 wt% for CO_2, 0.32 wt% for CH_4 at 273K, 1bar, and 0.4 wt% for H_2 at 77 K/1 bar.

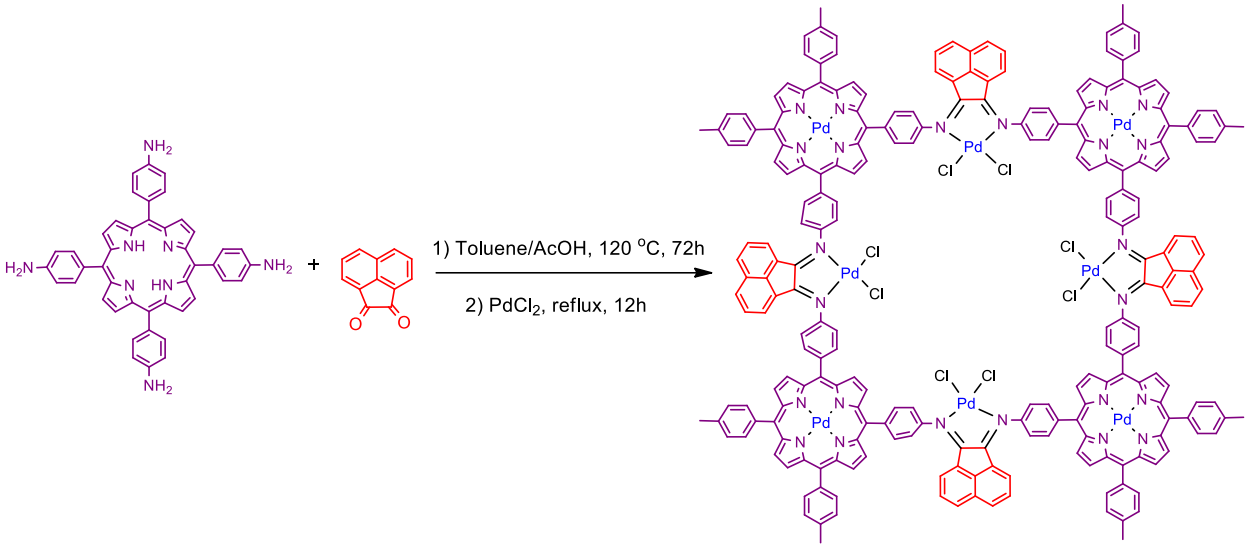

Scheme 7. Synthesis of PPOP-1(Pd) via imine condensation of TAPP and acenaphthalenequinone followed by refluxing with $PdCl_2$.

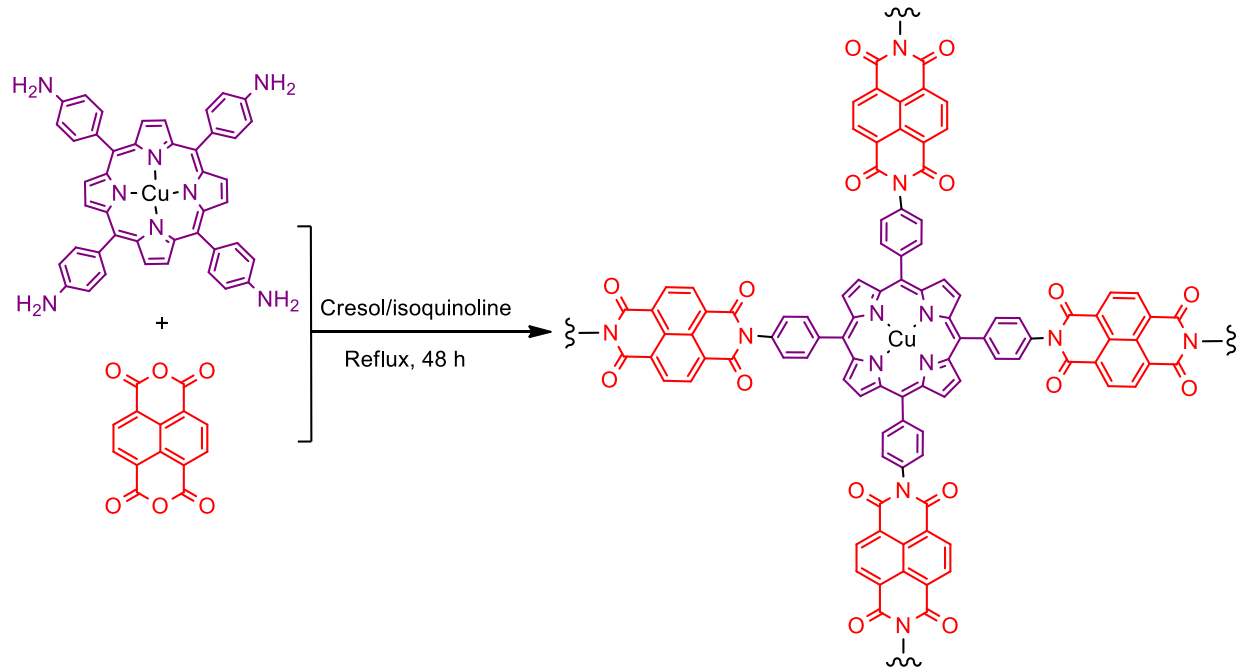

Scheme 8. Synthesis of Cu(II)-TAPP and naphthalene tetracarboxylic dianhydride based COF via the condensation of Cu (II)-TAPP and naphthalene tetracarboxylic dianhydride.

Another polyimide porphyrin COF, termed PI-COF, was constructed by Xian et al. via the imidization reaction of TAPP and perylenetetracarboxylic dianhydride (PTCA) (scheme 9) [31]. The resulting PI-COF possesses porous crystalline and excellent thermal stability. Furthermore, it exhibits a strong fluorescence which was attributed to the existence of a p-n heterojunction between TAPP and PTCA building units. The fluorescence was enhanced upon the exfoliation of PI-COF to few layered PI covalent

organic nanosheets (PI-CONs). The latter was employed as a fluorescent probe to detect TNP with high sensitivity and selectivity.

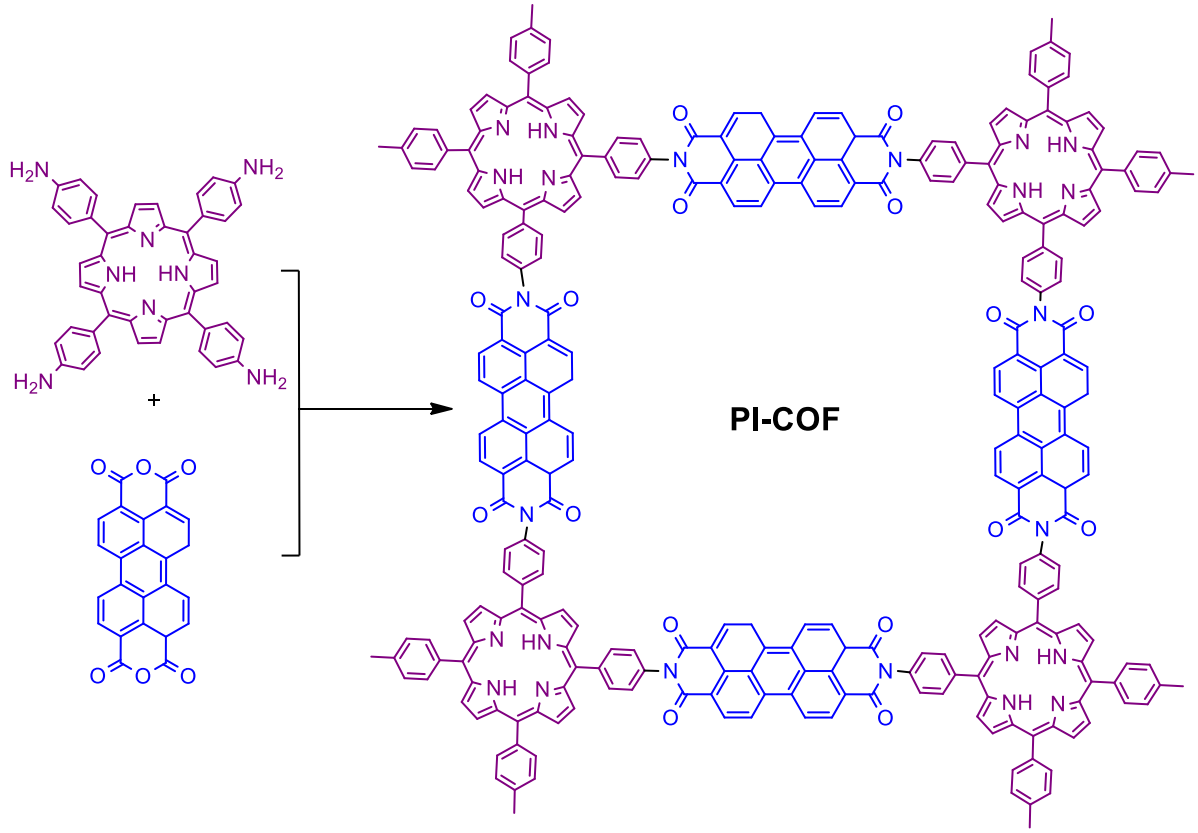

Scheme 9. The synthesis of PI-COF via the reaction of TAPP and perylenetetracarboxylic dianhydride (PTCA).

Recently, Fathalla reported the synthesis of new porphyrin COFs through the condensation between TAPP and pyromellitic dianhydride (scheme 10) [32]. Furthermore, the post-synthetic metallation of the free-base porphyrin macrocycles of the resulting COF with either Zn or Mn metals afforded the metallo-porphyrin COF analogues in excellent yields. The metalated analogues showed higher CO_2 uptake capabilities compared to the free-base COF. In addition, Mn^{III}-COF was found to be an effective catalyst for the selective epoxidation of styrene to the corresponding epoxide.

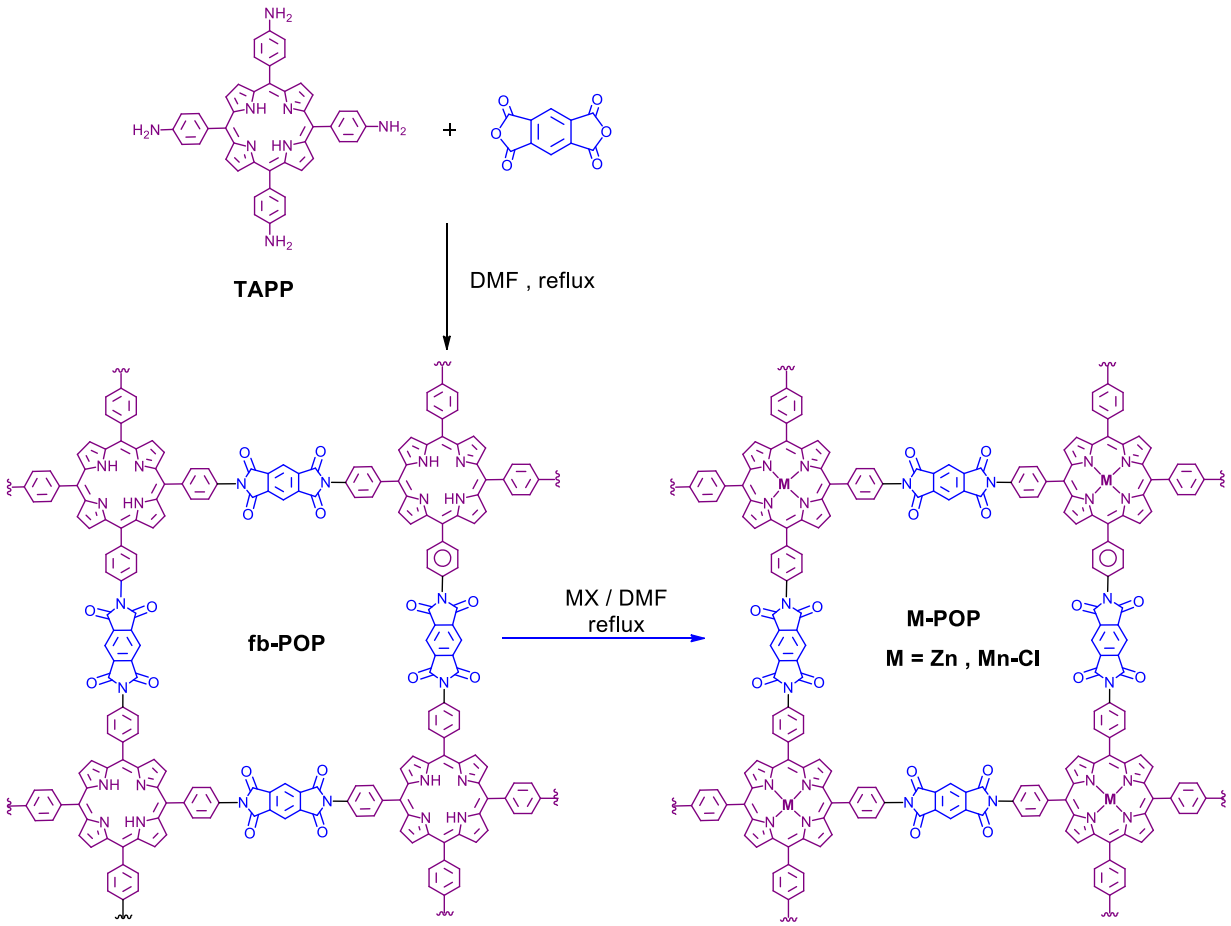

Scheme 10. Synthesis of TAPP and pyromellitic dianhydride based COFs the condensation between TAPP and pyromellitic dianhydride.

2.3. Miscellaneous TAPP based COFs.

Even though the imine and imide bond formation are the most common synthetic approaches to construct TAPP-based COFs. There have been other synthetic strategies that were employed to assemble COFs using TAPP building units. For instance, Jiang et al. harnessed squaraine chemistry to assemble a novel COF (CuP-SQ-COF) through the condensation between Cu-TAPP and squaric acid (scheme 11) [33]. The reported COF are highly stable in solvents and has a zigzagged conformation which prevents the side slippage of the layered structure. In addition, it exhibits a very broad range of light absorption.

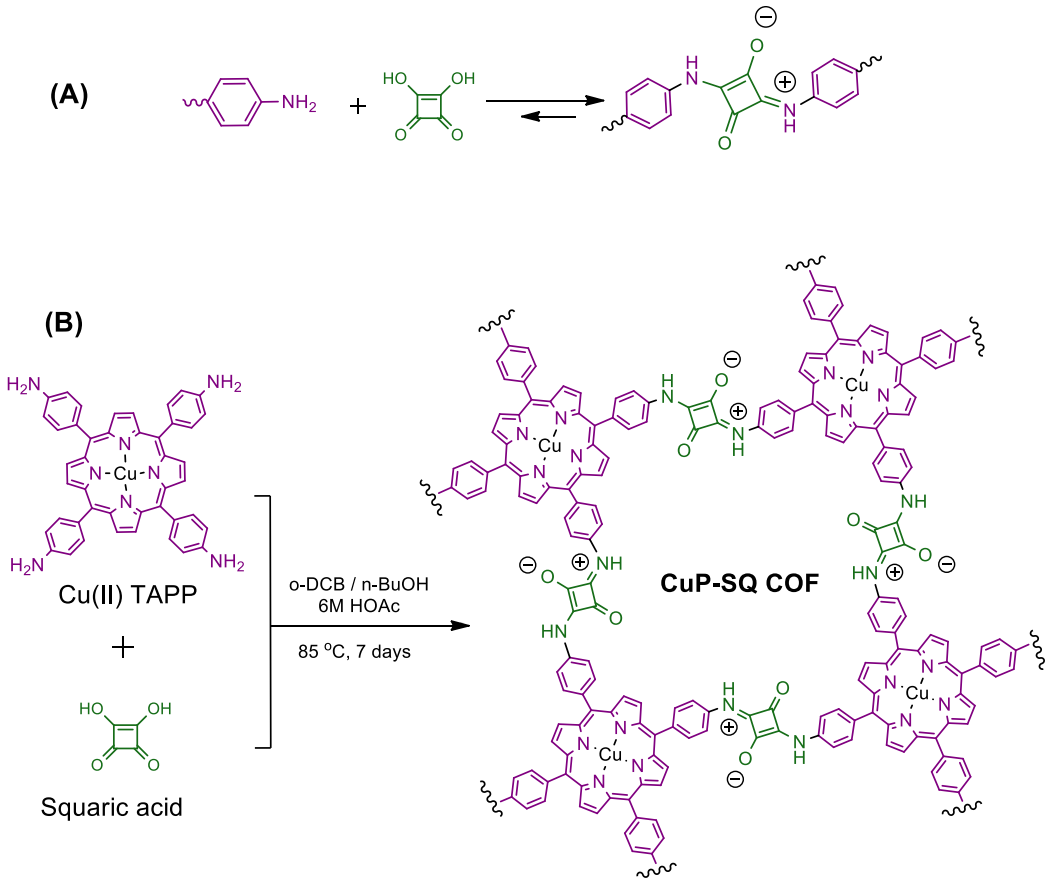

Scheme 10. Synthesis of CuP-SQ COF via the condensation between Cu-TAPP and squaric acid.

3.Conclusion.

Owing to its potential applications in many fields as well as predictable structures and pore functionality, COFs have gained considerable attention over the past decade. Porphyrin-containing COFs have been relatively well-explored and proven to be attractive materials in terms of stability and promising applications. Specifically, tetra(4-aminophenyl)porphyrin (TAPP) has been one of the most used building units in constructing various COFs. This review summarized the synthetic approaches employed so far to assemble COFs based on TAPP. The amino groups of TAPP rendering it an attractive building unit for the formation of imine- and imide-linked COFs. Various carbonyl containing buildings units in conjunction with TAPP have been employed to construct a wide range of porphyrin-based COFs with potential applications in many fields such as gas adsorption sensing and catalysis.

3.References

[1] R. Liu, K. T. Tan,Y. Gong, Y. Chen, Z. Li, S. Xie, T. He, Z. Lu, H. Yanga and D. Jiang. Covalent organic frameworks: an ideal platform for designing ordered materials and advanced applications. Chem. Soc. Rev., 50 (2021) 120-242.

[2] D. Jiang. Covalent Organic Frameworks: An Amazing Chemistry Platform for Designing Polymers. Chem., 6 (2020) 2461-2483.

[3] K. Geng, T. He, R. Liu, S. Dalapati, K. T. Tan, Z. Li, S. Tao, Y. Gong, Q. Jiang, and D. Jiang. Covalent Organic Frameworks: Design, Synthesis, and Functions. Chem. Rev., 120 (2020) 8814–8933.

[4] H. Wang, H. Wang, Z. Wang, L. Tang, G. Zeng, P. Xu, M. Chen, T. Xiong, C. Zhou and X. Li. Covalent organic framework photocatalysts: structures and applications, Chem. Soc. Rev., 49 (2020) 4135-4165.

[5] J. Wang and S. Zhuang, Covalent organic frameworks (COFs) for environmental applications, Coord. Chem. Rev., 400 (2019) 213046.

[6] Z. Wang, S. Zhang, Y. Chen, Z. Zhang and S. Ma, Covalent organic frameworks for separation applications, Chem. Soc. Rev., 49 (2020) 708-735.

[7] Y. Yusran, H. Li, X. Guan, Q. Fang and S. Qiu, Covalent organic frameworks for catalysis, EnergyChem, 2 (2020) 100035.

[8] X. Zhao, P. Pachfule and A. Thomas, Covalent organic frameworks (COFs) for electrochemical applications, Chem. Soc. Rev., 50 (2021) 6871-6913.

[9] S.-Y. Ding and W. Wang, Covalent organic frameworks (COFs): from design to applications, Chem. Soc. Rev., 42 (2013) 548-568.

[10] X. Feng, X. Ding, D. Jiang, Covalent organic frameworks, Chem. Soc. Rev., 41 (2012) 6010-6022.

[11] K. Geng, T. He, R. Liu, S. Dalapati, K.T. Tan, Z. Li, S. Tao, Y. Gong, Q. Jiang and D. Jiang, Covalent organic frameworks: design, synthesis, and functions, Chem. Rev., 120 (2020) 8814-8933.

[12] X. Guan, F. Chen, Q. Fang and S. Qiu, Design and applications of three dimensional covalent organic frameworks, Chem. Soc. Rev., 49 (2020) 1357-1384.

[13] Y. Li, W. Chen, G. Xing, D. Jiang and L. Chen, New synthetic strategies toward covalent organic frameworks, Chem. Soc. Rev., 49 (2020) 2852-2868.

[14] M.S. Lohse and T. Bein, Covalent organic frameworks: structures, synthesis, and applications, Adv. Funct. Mater., 28 (2018) 1705553.

[15] H. Furukawakyle, C. O'keeffeand and O. M. Yaghi. The Chemistry and Applications of Metal-Organic Frameworks. Science, 341 (2013) 6149.

[16] Q.-Y. Liu, J.-F. Li and J.-W. Wang. Research of covalent organic frame materials based on porphyrin units. J Incl Phenom Macrocycl Chem., 95 (2019) 1–15.

[17] X. Wu, X. Zhang, Y. Li, B. Wang, Y. Li and L. Chen. A porphyrin-based covalent organic framework with pH-dependent fluorescence. J. Mater. Sci., 56 (2021) 2717–2724.

[18] H. Shan, D. Cai, X. Zhang, Q. Zhu, P. Qin and J. Baeyens. Donor-acceptor type two-dimensional porphyrin-based covalent organic framework for visible-light-driven heterogeneous photocatalysis. Chem. Eng. J., 432 (2022) 134288.

[19] J. Chen, Y. Zhu and S. Kaskel. Porphyrin-Based Metal–Organic Frameworks for Biomedical Applications. Angew. Chem. Int. Ed., 60 (2021) 5010-5035.

[20] C. Zhao, L. Zhang, Q. Wang, L. Zhang, P. Zhu, J. Yu, and Y. Zhang. Porphyrin-Based Covalent Organic Framework Thin Films as Cathodic Materials for "On–Off–On" Photoelectrochemical Sensing of Lead Ions. ACS Appl. Mater. Interfaces., 13 (2021) 20397–20404

[21] H. Huang, F. Li, Y. Zhang and Y. Chen. Two-dimensional graphdiyne analogue Co-coordinated porphyrin covalent organic framework nanosheets as a stable electrocatalyst for the oxygen evolution reaction. J. Mater. Chem. A., 7 (2019) 5575-5582

[22] A.P. Côté, I. A. Benin, N. W. Ockwig, M. O'Keeffe, A. J. Matzger and O. M. Yaghi. Porous, crystalline, covalent organic frameworks. Science, 310 (2005) 1166–1170.

[23] S. Wan, F. Gándara, A. Asano, H. Furukawa, A. Saeki, S.K. Dey, L. Liao, W.W. Ambrogio, Y.Y. Botros, X. Duan, S. Seki, J.F. Stoddart and O.M. Yaghi. Covalent organic frameworks with high charge carrier mobility, Chem. Mater., 23 (2011) 4094–4097.

[24] S. Kandambeth, D.B. Shinde, M.K. Panda, B. Lukose, T. Heine and R. Banerjee. Enhancement of chemical stability and crystallinity in porphyrin containing covalent organic frameworks by intramolecular hydrogen bonds. Angew. Chem. Int. Ed., 52 (2013) 13052–13056.

[25] B. Gole, V. Stepanenko, S. Rager, M. Grüne, D.D. Medina, T. Bein, F. Würthner and F. Beuerle. Microtubular self-assembly of covalent organic frameworks. Angew. Chem. Int. Ed., 57 (2018) 846–850.

[26] X. Xu, S. Wang, Y. Yue, and N. Huang. Semiconductive Porphyrin-Based Covalent Organic Frameworks for Sensitive Near-Infrared Detection. ACS Appl. Mater. Interfaces, 12 (2020) 37427–37434.

[27] Y. Li , J. Zhang, K. Zuo, Z. Li, Y. Wang, H. Hu, C. Zeng, H. Xu, B. Wang and Y. Gao. Covalent Organic Frameworks for Simultaneous CO_2 Capture and Selective Catalytic Transformation. Catalysts, 11 (2021) 1133.

[28] X. Wu1, X. Zhang, Y. Li, B. Wang, Y. Li and L. Chen. A porphyrin-based covalent organic framework with pH-dependent fluorescence. J. Mater. Sci., 56 (2021) 2717–2724.

[29] R. Shen, W. Zhu, X. Yan, Ta. Li, Yo. Liu, Y. Li, S. Daia and Z.-G. Gu. A porphyrin porous organic polymer with bicatalytic sites for highly efficient one-pot tandem catalysis. Chem. Commun., 55 (2019) 822-825.

[30] V. S. P. K. Neti, J. Wang, S. Deng, and L. Echegoyen. Synthesis of a Polyimide Porous Porphyrin Polymer for Selective CO_2 Capture. J. Chem., (2015) Article ID 281616: http://dx.doi.org/10.1155/2015/281616.

[31] C. Zhang, S. Zhang, Y. Yan, F. Xia, A. Huang, and Y. Xian. Highly Fluorescent Polyimide Covalent Organic Nanosheets as Sensing Probes for the Detection of 2,4,6-Trinitrophenol. ACS Appl. Mater. Interfaces, 19 (2017) 13415–13421.

[32] M. Fathalla. Synthesis, CO_2 Adsorption and Catalytic Properties of Porphyrin-Pyromellitic Dianhydride Based Porous Polymers. Macromol. Res., 29 (2021) 321–326.

[33] A. Nagai, X. Chen, X. Feng, X. Ding, Z. Guo, and D. Jiang. A Squaraine-Linked Mesoporous Covalent Organic Framework. Angew. Chem., 125 (2013) 3858 –3862.

Physicochemical Analysis and Potential Uses of Oil Extracted from Terminalia catappa Seeds

Dahiru Abdulmalik Kona[1*], Aminu Dikko Mahmud[1*] , Gazali Tanimu [2*], Muktar Abdulazeez Abdullahi[1*], Nuhu Umar Hussaini[1] *,

[1] Chemical Engineering Department, Ahmadu Bello University, Nigeria

[2] Center for Refining and Advanced Chemicals, King Fahd University of Petroleum and Minerals, Saudi Arabia

*Corresponding authors: abdulmaleekkona@gmail.com, admahmud@abu.edu.ng, **gtu4ever@yahoo.com,** abdulazeezbinmuktar@gmail.com, umarhussayn@gmail.com

Abstract: Terminalia catappa is a widely planted ornamental tree in the Samaru campus of Ahmadu Bello University, Zaria. Although its seeds are known to be edible, there is limited research on their potential uses in the food and industrial sectors. This study aimed to extract oil from Terminalia catappa seeds using n-Hexane, Petroleum ether, and Ethanol solvents and analyze its physicochemical properties. The extraction was carried out using the Soxhlet apparatus, and the physicochemical properties determination was done using standard methods of analysis. The percentage oil yields were 51.80 %, 49.77 %, and 43.08 % for n-Hexane, Petroleum ether, and Ethanol extracts, respectively. The acid values (mg KOH/g), saponification values (mg KOH/g), iodine values ($gI_2/100g$), and peroxide values (meq/kg) were determined to be 4.488, 3.366, and 15.147; 211.78, 166.898, and 123.42; 6.091, 6.345, and 6.345; and 8.75, 9.00, and 10.00 for n-Hexane, Petroleum ether, and Ethanol extracts, respectively. The highest oil yield was achieved using n-Hexane, and petroleum ether extract was most suitable for edible purposes. All three extracts could be used for soap making, but the n-Hexane extract was the most suitable. However, the three extracts were considered non-drying oil based on iodine values and not suitable for ink and paint production. Based on peroxide values, they were stable to oxidative rancidity.

Keywords: Terminalia catappa, oil extraction, physicochemical analysis, n-Hexane, petroleum ether, ethanol solvent

التحليل الفيزيائي والكيميائي والاستخدامات المحتملة للزيت المستخرج من بذور الكاباس

الملخص: تعتبر Terminalia catappa من أشجار الزينة المزروعة على نطاق واسع في حرم جامعة Samaru بجامعة Ahmadu Bello ، Zaria. على الرغم من أن بذورها معروفة بأنها صالحة للأكل ، إلا أن هناك أبحاثًا محدودة حول استخداماتها المحتملة في قطاعي الأغذية والصناعة. هدفت هذه الدراسة إلى استخلاص الزيت من بذور نباتات كاتابا باستخدام n-Hexane و Petroleum etherو Ethanol Solvents وتحليل خواصه الفيزيائية والكيميائية. تم الاستخراج باستخدام جهاز Soxhlet ، وتم تحديد الخصائص الفيزيائية والكيميائية باستخدام طرق التحليل القياسية. كانت النسبة المئوية لإنتاج الزيت 51.80٪ و 49.77٪ و 43.08٪ لمستخلصات n-Hexane و Petroleum etherو Ethanol على التوالي. تم تحديد قيم الحمض (mg KOH / g) وقيم التصبن (mg KOH / g) وقيم اليود (gI2 / 100g) وقيم البيروكسيد (meq / kg) لتكون 4.488 و 3.366 و 15.147 ؛ 211.78 و 166.898 و 123.42 ؛ 6.091 و 6.345 و 6.345 ؛ و 8.75 و 9.00 و 10.00 لمستخلصات n-Hexane و Petroleum ether و Ethanol على التوالي. تم تحقيق أعلى إنتاجية للزيت باستخدام n-Hexane ، وكان مستخلص الإيثر البترولي هو الأنسب للأغراض الصالحة للأكل. يمكن استخدام المقتطفات الثلاثة لصنع الصابون ، لكن مستخلص-n Hexaneكان الأنسب. ومع ذلك ، اعتبرت المستخلصات الثلاثة زيتًا غير جاف بناءً على قيم اليود وغير مناسبة لإنتاج الحبر والطلاء. بناءً على قيم البيروكسيد ، كانت مستقرة للنتانة التأكسدية.

1. Introduction

Vegetable oils, as an essential component of the human diet, provide energy, fat-soluble vitamins, and essential fatty acids. They play a vital role in maintaining healthy bones, protecting the liver, boosting the immune system, and providing structural integrity to cells (FAO, 2009). Vegetable oils are obtained by extracting oil from seeds, kernels, and nuts of various plants using mechanical pressure or solvents. These oils are primarily composed of triacylglycerol (Gunstone, 2011). The global demand for vegetable and seed oils is increasing due to their various applications in domestic, industrial, pharmaceutical, and cosmetic industries. Therefore, there is a need to search for high-quality vegetable and seed oils to meet the growing demand.

However, obtaining large quantities of oil is only possible through the extraction of available nuts and oil seeds (Okene & Evbuomwan, 2014). Almost 80% of the global vegetable oil production is consumed by humans, while the remaining 20% is used for chemicals and animal industries. The availability, ease of processing technology, production rate, and utilization potential define the potential of an oil seed as a feedstock for industries (Aremu *et al.,* 2015). While soybean, groundnut, castor, coconut, palm, and jatropha are the sources of most oils, there are many underutilized potential sources of oil (Ogala *et al.,* 2018). Terminalia catappa seeds oil is one such source of nutritional oil (Agunbiade & Olanlokun, 2006).

Terminalia catappa, also known as the umbrella tree or tropical almond, is a member of a group of nuts that possess hard-shelled seeds which enclosed a single edible kernel. However, the crop is underutilized. The small size of the seeds and their difficulty in extraction may have contributed to their limited usage in many areas (Adu *et al.,* 2013). The Terminalia catappa tree is mostly planted in the tropics, particularly along sandy seashores, as a source of edible fruits, for shade, and ornamental purposes. It tolerates salt spray, relatively high salinity in the root zone, and strong winds (Lex & Barry, 2006).

The oil extracted from the dried nuts of Terminalia catappa is edible and used for cooking in parts of South America (Adu *et al.,* 2013). However, there is a lack of in-depth information on the nutritional potential of Terminalia catappa, resulting in the underutilization of the seeds.

Therefore, this research aims to extract oil from Terminalia catappa seeds using the solvent extraction method with different solvents and to characterize the oil extracted from the seeds using physical and chemical analysis. Furthermore, this study compares the effects of different solvents for Terminalia catappa oil extraction.

2.0 Materials and Methods

2.1 Collection, identification, and drying of the seeds

The Terminalia catappa seeds were sourced under some of the Terminalia catappa trees in the Samaru campus of Ahmadu Bello University Zaria. Moreover, the seeds were deshelled and dried for five days. In preparation for extraction, a pestle and mortar were used to ground the deshelled seeds.

2.2 Extraction procedure

Three samples each of 65g of the grounded Terminalia catappa seeds were wrapped in a filter paper and subjected to the extraction process using n-Hexane, Petroleum

Ether, and Ethanol respectively for 3 hours in a Soxhlet extractor. To recover some of the solvents in the extracted oil, a rotary evaporator was employed, and the remaining oil-solvent mixture was heated to the boiling points of the solvents to remove the residual solvent.

2.3 Determination of physicochemical properties of the oil

2.3.1 Color

The oil's colors were determined by visual inspection

2.3.2 Oil yield (%)

The % yield of the oil samples was determined using equation 2.1.

$$\text{Oil yield (\%)} = \frac{\text{Weight of the oil}}{\text{Weight of the seed}} \times 100 \qquad (2.1)$$

2.3.3 Oil recovery (%)

The oil recoveries were determined using equation 2.2

$$\text{Oil recovery (\%)} = \frac{\text{Weight of oil}}{\text{X} \times \text{weight of the seed}} \times 100 \qquad (2.2)$$

Where X is the oil content of the seed = 60%

2.3.4 Specific gravity

The specific gravities of the oils were determined using a 2 ml syringe. A 2ml capacity dry and clean syringe was weighed and recorded as W_0, it was then filled with each oil sample and reweighed and recorded as W_1. The syringe was then washed and dried and then filled with distilled water to give W_2.

The specific gravities were calculated using equation 2.3;

$$\text{Specific gravity} = \frac{W_1 - W_0}{W_2 - W_0} \qquad (2.3)$$

Where,

W_0 = empty dry syringe weight;

W_1 = syringe + oil weight;

W_2 = syringe + distilled water weight

2.3.5 Acid value

25 ml alcohol (propanol) and 2 drops of phenolphthalein indicator were mixed and were then neutralized using 0.1M KOH. 1g of the oil sample was added to the neutralized solvent and titrated with aqueous 0.1M KOH and vigorously agitated to a pink color, which marked the endpoint. The volume of the 0.1M KOH consumed was recorded. Equation (2.4) was used to calculate the acid value:

$$\text{Acid value} = \frac{56.1 \times V \times M}{w} \qquad (2.4)$$

Where,

V = KOH used Volume;

M = KOH molarity and

w = weight of the sample.

2.3.6 Iodine value

1g of the oil sample was placed in a 250 ml conical flask, and 20 ml of Wiji's solution was added. The flask was stoppered, then shaken. The mixture was allowed for 30 minutes in the dark. This was followed by adding 20 mL of 10 % potassium iodide solution and then shaking. The resulting mixture was then titrated against 0.1 M Sodium thiosulfate ($Na_2S_2O_3$) with 3 drops of starch solution as an indicator. The volume of $Na_2S_2O_3$ was recorded at the endpoint. Further, a blank titration was carried out. Equation (2.5) was used to calculate the Iodine value (I.V).

$$\text{I.V.} = \frac{(b-a)\times N\times 12.69}{\text{Weight of the sample}} \quad (2.5)$$

Where;
b = Blank titre
a = Sample titre
N = Normality of $Na_2S_2O_3$ used

2.3.7 Determination of Saponification Value

25 ml of 4% ethanolic potassium hydroxide solution was placed into a 250 ml conical flask and 2.0g of sample oil was added to it. The mixture was heated in a water bath for 30min. After it has cooled, 2 drops of phenolphthalein were dissolved in it and then titrated against 0.5M Hydrochloric acid solution with vigorous agitation to the disappearance of the purple color. Further, as a control, a blank titration was carried out. Equation (2.6) was used to calculate the saponification value.

$$\text{SV} = \frac{(b-a)\times M\times 56.1}{\text{Weight of the sample}} \quad (2.6)$$

Where;
b = Blank titre
a = Sample titre
M = HCl Molarity

2.3.8 Peroxide value

1 g of the oil sample was placed into a 250 ml capacity conical flask. 20 ml of solvent mixture (glacial acetic acid/chloroform, 3/2 by volume) and 1.0 g of potassium iodide were added and the mixture was boiled for one minute. Further, the hot solution was transferred into a flask containing 20 ml of 5% KI. Consequently, three drops of the starch solution were added to the mixture and titrated with 0.025 N standardized $Na_2S_2O_3$. Equation (.27) was used to calculate the peroxide value.

$$P.V = \frac{V\times N\times 100}{\text{Weight of the sample}} \quad (2.7)$$

Where;
V =] $Na_2S_2O_3$ Volume;
N = $Na_2S_2O_3$ Normality

2.3.9 Ester value

The ester value was calculated using equation (2.8) by the procedure described by Pearson (1991).

$$\text{Ester value} = \text{Saponification value} - \text{Acid value} \quad (2.8)$$

3.0 Results and Discussion

Table 3.1: Percentage of oil yield and oil recovery assuming 60 % oil content in the seed

S/no	Parameters/Solvents	n-Hexane	Petroleum Ether	Ethanol
1	Oil yield (%)	51.80	49.77	43.08
2	Oil recovery (%)	86.4	82.95	71.80

Table 3.2: Summary of physical properties of the extracted oil with the three different solvents

S/no	Properties/Solvents	n-Hexane	Petroleum Ether	Ethanol
1	Color	Pale brown	Medium brown	Dark Brown
2	Specific gravity	0.892	0.892	0.921
3	Odor	Smell of groundnut	Smell of groundnut	Smell of groundnut
4	State at room temperature	Liquid	Liquid	Liquid

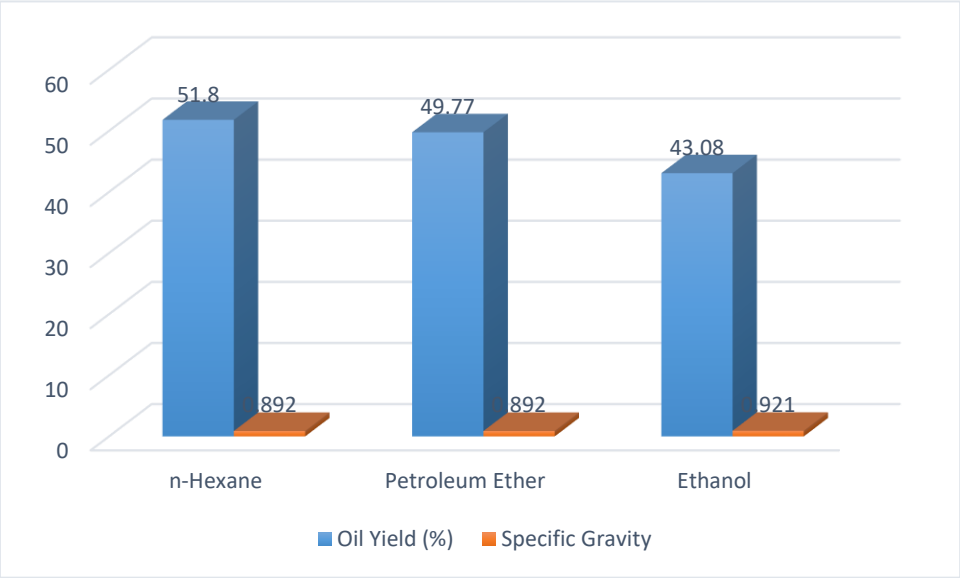

Figure 3.1: Oil yield and specific gravities of the three oil samples

Table 3.3: Summary of chemical properties of the extracted oil with the three different solvents

S/no	Properties/Solvents	n-Hexane	Petroleum Ether	Ethanol
1	Acid Value (mg KOH/g)	4.488	3.366	15.147
2	Saponification Value (mg KOH/g)	211.780	166.898	123.420
3	Iodine Value (gI_2/100g)	6.091	6.345	6.345
4	Peroxide Value (meq/kg)	8.750	9.000	10.000
5	Ester Value (mg KOH/g)	207.292	163.532	108.273

3.2 Discussion of Results

3.2.1 Oil yield

The percentage oil yield using n-Hexane, Petroleum ether, and Ethanol solvents were 51.80%, 49.77%, and 43.08% respectively as shown in Table 4.1. These values are greater than 38.00% for Terminalia mentalis using Petroleum ether as the extraction solvent (Kayode, 2015) and 10.34% for Zobo seeds (Theodora & Cosmas, 2017). However, the values are closer to 47.08% and 49.34% for Sesame and Cashew seeds (Saeed & Shola, 2015). The study shows that the highest amount of oil extraction was achieved with n-Hexane, followed by Petroleum ether, then Ethanol. Moreover, these oil yields can be considered economical for commercial production since they are within the standard range of≥ 32% (AOAC, 1990)

3.2.2 Specific gravity

The oils obtained using n-Hexane, Petroleum ether, and Ethanol recorded specific gravities of 0.892, 0.892, and 0.921 respectively as shown in Table 4.2 and Figure 4.1. The values obtained for n-Hexane and Petroleum ether are comparable to 0.85 for ackeed seed oil (Omosuli, 2013), and that of the Ethanol is comparable to 0.90 for Zobo seed oil (Theodora & Cosmas, 2017). However, the values are all greater than 0.500 and 0.512 for Cashew nut and Cashew shell liquid oil (Idah *et al.,* 2014). The result obtained in this study shows that water is denser than the three oil samples. Moreover, the extracted oil using Ethanol solvent is denser than those extracted using n-Hexane and Petroleum Ether. Perhaps, Ethanol extracts not just oil but also some pigments in the seed.

3.2.3 Chemical properties

3.2.3.1 Acid value

The free fatty acid present or the degree of hydrolysis of oil determines the acid value of oil. The Acid value for an oil that is suitable for edible purposes should be less than or equal to 4 mg/g (Janporn et *al.,* 2014). Acid value depends on the degree of rancidity which is used as a measure of oil freshness (Ochigbo & Paiko, 2011). The acid values obtained using n-Hexane, Petroleum Ether and Ethanol were 4.488, 3.366, and 15.147 mg KOH/g respectively as shown in Table 4.3. Kayode (Kayode, 2015), reported a lesser value of 0.052 mg KOH/g for Terminalia mentalis using Petroleum ether as the extraction solvent. Also, Olatidoye et al. (Olatidoye *et al.,* 2011), reported a lesser value of 1.3 mgKOH/g for Terminalia catappa using Petroleum ether as the extraction solvent. However, the values obtained in this study for n-Hexane and Petroleum ether are similar to the reported values of 4.77 mg KOH/g for white cultivars of melon seed and 5.99 mg KOH/g for ground nut oil by Olaofe et al. (Olaofe *et al.,* 2012). The acid value obtained in this study using Petroleum ether as the extraction solvent is within the recommended limit. Hence, it is suitable for edible purposes. However, those obtained using n-Hexane and Ethanol

need to be refined properly before consumption because they exceeded the required value for edible oils. The results also suggested that the obtained oil using Petroleum ether is most stable for a long period and resistant to rancidity and peroxidation.

3.2.3.2 Saponification value

The measure of oils' oxidation on storage and their deterioration is defined by their saponification value. The presence of a higher number of carbon atoms fatty acids indicates a high saponification value (Ardabili *et al.,* 2011). The saponification value recorded in this study for n-Hexane, Petroleum ether, and Ethanol were 211.78, 166.898, and 123.42 mg KOH/g respectively as shown in Table 4.3. The value obtained for the oil extracted using Petroleum ether is greater than 140.275 mg KOH/g obtained for Terminalia mentalis (Kayode, 2015), and 128.0 mg KOH/g recorded for Terminalia catappa (Olatidoye *et al*., 2011). However, the saponification values obtained for the extracted oils using n-Hexane and Petroleum ether are quite higher than 159.33 mg KOH/g for Dennettia tripatala fruit oil (pepper fruit) reported by Nwinuka et al. (Nwinuka *et al.,* 2009) and 143.76 for African pear oil (Ikhuoria & Maliki, 2007).

The saponification values of the oils fall within the range of these oils, therefore they could also be used for soap making. Higher saponification value determines the usage of fat or oil for soap making, therefore, the oil extracted using n-Hexane would be most suitable for soap making among the three extracts. Moreover, the oil extracted using Ethanol is higher than 93.0 mg KOH/g of bese wax (Mabrouk, 2015). Hence, it can also be used for soap making but finds the least application among the three oils.

3.2.3.3 Iodine value

The degree of unsaturation in oil is determined by its iodine value, which determines the number of double bonds present in the oil which defines its proneness to oxidation (Bello *et al.,* 2011). Oils with less than 100 $gI_2/100g$ iodine value are classified as non-drying oils, more than 100 $gI_2/100g$ but less than 130 $gI_2/100g$ are semi-drying, while oils with iodine value above 130 $gI_2/100g$ are classified as drying oils (Aremu et al., 2006). The iodine values obtained are 6.091, 6.345, and 6.345 $gI_2/100g$ using n-Hexane, Petroleum ether, and Ethanol respectively as shown in Table 4.3. These values are less than 54.567 $gI_2/100g$ for Terminalia mentalis oil extracted using Petroleum ether (Kayode, 2015), and 65.0 $gI_2/100g$ for Terminalia catappa extracted using Petroleum ether (Olatidoye *et al.,* 2011). However, the values are closer to the 9.4 $gI_2/100g$ for coconut seed oil extracted using Isopropyl alcohol solvent and 9.3 $gI_2/100g$ for the same oil extracted using Petroleum ether (Okene & Evbuomwan, 2014). In this study, the oils obtained using the three solvents can be classified as non-drying oils. Hence, not applicable for paint and ink production, owing to their non-drying properties. However, could be used in soap manufacturing.

3.2.3.4 Peroxide value

The rate of lipid oxidation, which causes rancidity is determined by peroxide value. Normally, oils are said to be rancid when their peroxide value is between 20.0 meq/kg to 40.0 meq/kg (Babalola, 2011). The maximum limit for nuts and seed oils as marked by the Codex Alimentarius Commission is 10 meq/kg (SON, 2000). The values obtained in this study for n-Hexane, Petroleum ether, and Ethanol are 8.75 meq/kg, 9.00 meq/kg, and 10.00 meq/kg respectively as presented in Table 4.3. These values are greater than 2.600 meq/kg for Terminalia mentalis extracted using Petroleum ether as the extraction solvent (Kayode, 2015) and 2.8 meq/kg for

Terminalia catappa oil extracted using Petroleum ether (Olatidoye *et al.,* 2011). However, these values are less than 13.80 meq/kg and 10.80 meq/kg for Moringa oil and Ground nut oil respectively (Afolayan *et al.*, 2014).

The peroxide values obtained using Petroleum ether and n-Hexane as the extraction solvents were less than the maximum limit while that obtained using Ethanol was equal to the maximum. Therefore the oils are not prone to oxidative rancidity.

4. Conclusion

This study successfully extracted oil from the seeds of Terminalia catappa using three distinct solvents: n-Hexane, Petroleum ether, and Ethanol via the soxhlet apparatus. The results showed that n-Hexane achieved the highest oil yield of 51.80%, followed by Petroleum ether at 49.77% and Ethanol at 43.08%. Physicochemical analysis revealed that the Petroleum ether extract is suitable for edible purposes without undergoing refining, while the other two extracts require refining to be considered edible. Additionally, all three extracts can be used in soap making, with n-Hexane being the most suitable based on their saponification values. However, none of the extracts are suitable for ink and paint production since they were classified as non-drying oils. The peroxide values of the three samples were less than the maximum allowable limit of 10 meq/kg, indicating that they will be stable to oxidative rancidity. Terminalia catappa seed is a potential source of oil that can meet the ever-growing demand for quality oil that could be used in industries and other domestic purposes.

5. References

[1] O. B. Adu, M. Omojufehinsi, M. O. Esanboro, D. A. Abe, A. O. Shofolahan, E. Uzodinma, and O. Martins, “Effect of processing on the quality, composition, and antioxidant properties of Terminalia catappa (Indian almond) seed oil,” African Journal of Food, Agriculture, Nutrition and Development, vol. 13, no. 3, pp. 64–76, 2013.

[2] M. Afolayan, F. Akanji, and D. Idowu, “Extraction and physicochemical analysis of some selected seed oils,” International Journal of Advanced Chemistry, 2014.

[3] S. O. Agunbiade and J. O. Olanlokun, “Evaluation of some nutritional characteristics of Indian almond nut,” Pakistan Journal of Nutrition, vol. 5, no. 4, pp. 316–318, 2006.

[4] G. A. Ardabili, R. Farhoosh, and M. H. Haddad-Khodaparast, “Chemical composition and physicochemical properties of pumpkin seeds (Cucurbita pepo subsp. pepo Var. Styriaka) grown in Iran,” Journal of Agricultural Science and Technology, vol. 13, pp. 1053–1063, 2011.

[5] M. O. Aremu, H. Ibrahim, and T. O. Bamidele, “Physicochemical characteristics of the oils extracted from some Nigerian plants foods. (A review),” Chemical and Engineering Research, vol. 32, pp. 36–52, 2015.

[6] M. O. Aremu, A. Olonisakin, D. A. Bako, and P. C. Madu, “Compositional studies and physicochemical characteristics of cashew nut (Anarcadium occidentale) flour,” Pakistan Journal of Nutrition, vol. 5, no. 4, 2006.

[7] T. O. Babalola and D. F. Apata, "Chemical and quality evaluation of some alternative lipid sources for aqua feed production," Agric. Biol. J. N., vol. 2, pp. 935–943, 2011.

[8] M. O. Bello, T. L. Akindele, D. O. Adeoye, and O. A. Oladimeji, "Physicochemical properties and fatty acids profile of seed oil of Telfairia occidentalis (Hook, F)," Int. J. Basic Appl. Sci., vol. 11, no. 6, pp. 9–14, 2011.

[9] Food and Agriculture Organization of the United Nations, Food Composition Table for the Near East Nuts and Seeds. Rome, Italy: FAO Food and Nutrition Paper, 2009.

[10] F. D. Gunstone, Vegetable Oils in Food Technology: Composition, Properties and Uses, 2nd ed. Chichester, UK: John Wiley & Sons, 2011, pp. 97–101

[11] P. A. Idah, M. I. Simeon and M. A. Mohammed, "Extraction and Characterization of Cashew Nut (Anacardium Occidentale) Oil and Cashew Shell Liquid Oil," Department of Agricultural and Bioresources Engineering, Federal University of Technology, Minna, NIGERIA, 2014.

[12] E. U. Ikhuoria, and M. Maliki, "Characterization of avocado pear (Persea americana) and African pear (Dacryodes edulis) extracts," African Journal of Biotechnology, 6(7), 2007.

[13] S. Janporn et al., "Physicochemical properties of Terminalia catappa seed oil as a novel dietary lipid source," Journal of Food and Drug Analysis, 2014. doi 10.1016/j.jfda.2014.06.007

[14] E. S. Kayode, "Extraction and Physicochemical Characterisation of the Oil Extract from the Seed of Umbrella Tree (Terminalia Mentalis)," International Journal of Scientific & Engineering Research, vol. 6, no. 10, pp. 1612-1616, Oct. 2015. ISSN 2229-5518.

[15] T. J. Lex and E. Barry, "Terminalia catappa (tropical almond), ver. 2.2," in Species Profiles for Pacific Island Agroforestry, C. R. Elevitch, Ed. Permanent Agriculture Resources (PAR), Hōlualoa, Hawai'i, 2006.

[16] S. T. Mabrouk, "Making Useable, Quality Opaque or Transparent Soap," Journal of Chemical Education, vol. 82, no. 10, pp. 1534 - 1537, 2015.

[17] N. M. Nwinuka, and B. I. Nwiloh, "Physicochemical properties and fatty acid composition of Dennettia tripetala fruit oil (pepper fruit)," Nigerian Journal of Biochemistry and Molecular Biology, 24(1), 42-46. 2009.

[18] S. S. Ochigbo and Y. B. Paiko, "Effects of solvent blending on the characteristics of oils extracted from the seeds of Chrysophyllum albidium," Int. J. Sci. Nature, vol. 2, no. 2, pp. 352–358, 2011.

[19] "Official method of analysis 13th ed.," W. Horwitz, Ed., Association of Official Analytical Chemists, Washington, DC, 1990, pp. 56–132.

[20] H. Ogala, C. M. Elinge, I. G. Wawata, A. Adegoke, A. Muhammad, and A. Ige, "Extraction and physicochemical analysis of desert date (Balanite aegyptiaca) seed oil," J. Food Res., vol. 7, no. 4, pp. 115–123, 2018.

[21] O. Olaofe, H. N. Ogungbenle, B. E. Akhadelor, A. O. Idris, O. V. Omojola, O. T. Omotehinse, and O. A. Ogunbodede, "Physicochemical and fatty acids composition of oils from some legume seeds," Int. J. Biol. Pharm. Allied Sci., vol. 1, no. 3, pp. 355–363, 2012.

[22] O. P. Olatidoye, S. S. Sobowale, J. V. Akinlotan, and O. O. Olorode, "Chemical composition and physicochemical characteristics of tropical almond nuts (Terminalia catappa L) cultivated in South West Nigeria," J. Med. Appl. Biosci., vol. 3, no. 1, pp. 5–9, 2011.

[23] E. O. Okene and B. O. Evbuomwan, "Solvent extraction and characterization of oil from coconut seed using alternative solvents," Int. J. Eng. Tech. Res., vol. 2, no. 11, pp. 180–184, 2014.

[24] S. V. Omosuli, "Physicochemical properties and fatty acid composition of oil extracted from akee apple (Blighia sapida) seeds," Res. Rev. J. Food Dairy Technol., vol. 2, no. 1, pp. 5–8, 2013.

[25] M. D. Saeed and Shola, E. A. Shola "Extraction and physico chemical properties of some edible seed oils sampled in Kano metropolis, Kano state," Bayero Journal of Pure and applied Sciences, 8(2), 239-244, 2015.

[26] SON, "Standards for edible refined palm oil and its processed form," Standard Organization of Nigeria, pp. 2-5, 2000.

[27] I. E. Theodora and E. A. Cosmas, "Extraction and physicochemical characterization of oil from Zobo seeds (Hibiscus sabdariffa L.) for its nutritional and industrial application," International Journal of Scientific Research in Knowledge, vol. 5, no. 2, pp. 057-060, 2017.

Development and performance evaluation of a bricklaying gantry-based parallel robot manipulator

Musa Hassan Ibrahim[1], Umar Ali Umar[1, *], Matthew Afolayan Olatunde[1], Ayodeji Nathaniel Oyedeji[1]

[1]Department of Mechanical Engineering, Ahmadu Bello University, Zaria, 810107, Nigeria

[*]Corresponding Author: Umar Ali Umar. Email: umaraliumar@yahoo.co.uk

Abstract: Gantry robots are still used in wide application areas, especially pick and place applications. However, there is a gap in the utility of these robots in the building sector, particularly for the pick-and-place application of building blocks from and to a predefined location. The Gantry-based robot is considered a parallel manipulator because, unlike serial manipulators, the load is divided among its multiple links/legs or arms; this is just so because it is made up of more than one link. Hence, this research presents a study in the field of linear and nonlinear model fit system identification on the aforementioned robot through an attempt to provide a better design to take care of the limitations of parallel manipulators, small workspace problems and robot mobility problems. In this study, Arduino Mega was used for the control system. Other materials included bipolar nema17 stepper motors, MG996R servo motor, A4988 driver, sprocket and chain, belt, pulley and buggy wheels, while SolidWorks was used for the system's design and simulation. Aluminium (Al alloy 6061) was used for the robot construction due to its excellent properties and suitability. Actuators and parts were analyzed and modelled to gain knowledge of the kinematic behaviour, and the analyses established the linear and nonlinear identification of model fitness. This study used a compact model fit system and a two-method validation identification procedure. The results show that the system model can be successfully identified and validated from the measured data and provide a near-accurate estimate between hypothetical and measured data. Two experimental validations gave 94% using the first setup and 97% using the second setup. This provides a 0.8% progress increment from previous studies.

Keywords: Gantry robot, Robot manipulator, Simulation, Validation, Linear and nonlinear model, Model fit.

التطوير وتقييم الأداء لمناور روبوت متوازي قائم على جسر من الطوب

الملخص: لا تزال الروبوتات العملاقة مستخدمة في مجالات التطبيق الواسعة ، وخاصة تطبيقات الالتقاط والمكان. ومع ذلك ، هناك فجوة في فائدة هذه الروبوتات في قطاع البناء ، لا سيما لتطبيق الانتقاء والمكان لبنات البناء من وإلى موقع محدد مسبقًا. يعتبر الروبوت القائم على جسر الرافعة من المناور المتوازي لأنه ، على عكس المتلاعبين التسلسليين ، يتم تقسيم الحمل بين الوصلات / الأرجل أو الأذرع المتعددة ؛ هذا فقط لأنه يتكون من أكثر من ارتباط واحد. ومن ثم ، يقدم هذا البحث دراسة في مجال تحديد النظام الملائم للنموذج الخطي وغير الخطي على الروبوت المذكور أعلاه من خلال محاولة تقديم تصميم أفضل للعناية بحدود المعالجات المتوازية ، ومشاكل مساحة العمل الصغيرة ومشاكل حركة الروبوت. في هذه الدراسة ، تم استخدام Arduino Mega لنظام التحكم. وشملت المواد الأخرى محركات السائر ثنائية القطب nema17 ومحرك مؤازر MG996R وسائق A4988 وعجلة مسننة وسلسلة وحزام وبكرة وعجلات عربات التي تجرها الدواب ، بينما تم استخدام SolidWorks لتصميم النظام والمحاكاة. تم استخدام الألومنيوم (سبيكة 6061) لبناء الروبوت نظرًا لخصائصه الممتازة ومدى ملاءمته. تم تحليل المحركات والأجزاء ونمذجتها لاكتساب المعرفة بالسلوك الحركي ، وأثبتت التحليلات التحديد الخطي وغير الخطي لملاءمة النموذج. استخدمت هذه الدراسة نظامًا ملائمًا للنموذج المضغوط وإجراء تحديد التحقق من الصحة بطريقتين. تظهر النتائج أنه يمكن تحديد نموذج النظام والتحقق من صحته بنجاح من البيانات المقاسة وتقديم تقدير شبه دقيق بين البيانات الافتراضية والبيانات المقاسة. أعطت عمليتا تحقق تجريبيتان 94٪ باستخدام الإعداد الأول و 97٪ باستخدام الإعداد الثاني. يوفر هذا زيادة تقدم بنسبة 0.8 ٪ من الدراسات السابقة.

1. Introduction

In this century, the development and success of a country are highly dependent on its technological level and that its industries are using for construction. Robots are the top building equipment, and robotic arms have become widely used and economical in manufacturing, medicine and other industries [1]. Specifically, contour crafting (similar to 3D printing) is applied in construction, but its principle is unlike bricklaying; rather, it's like choking of mortar [2]. The manual bricklaying process has been linked with significant health hazards or problems due to the use of human labour and the slow rate of construction activities [3]. Furthermore, Semi-Automated Mason (SAM) bricklayer is also applied, but being a serial robot, it has the following demerits; less payload, less accuracy and less dynamic performance [4]. Generally, gantry robots used for bricklaying applications in construction are usually mounted and fixed in one place and equipped with parallel manipulators with small workspaces [5].

Parallel manipulators are seen as a new kind of robot other than serial manipulator [6]; it has the following merits: higher stiffness, strong bearing capacity, a small error, high precision, small weight-load ratio, very good dynamic performance, easy-to-control, etc. [7]. However, parallel manipulators have small workspace areas compared to serial manipulators. The serial manipulator has a larger workspace area, is less rigid, has a large weight-load ratio and is slower than the parallel manipulator [8]. To put this into context, the construction industry heavily relies on technological advancements and robots, particularly robotic arms. However, traditional bricklaying processes involving manual labour are associated with health hazards, slow construction rates, and limited efficiency. This study aims to address the limitations of existing gantry robots by proposing the development and performance evaluation of a novel bricklaying gantry-based parallel robot manipulator that offers enhanced flexibility, mobility, and dexterity. Specifically, the research objective includes designing a gantry-based parallel robot manipulator through the simulation of the system and the implementation of its control algorithm and evaluating the performance of the proposed robot manipulator in terms of speed, accuracy, and payload capacity to determine its effectiveness in replacing manual labour and enhancing construction rates.

The goal of this study was built on the literature review to consider some of the limitations of gantry robots, particularly regarding the lack of mobility and adequate workspace and the need to compare to footprint and the utilization of manual labour. Reviewing previous studies on robot manipulators included the study of Afolayan *et al.* [9], who developed a biomorphic carbon-filled natural rubber hyper-redundant joint mechanism robot. The researcher modelled a fish of *teleost* species (a 394.1cm Mackerel) using the biomorphic hyper-redundant joint developed. The study's control algorithm uses built-in motion patterns, and the path planning algorithm is sensor-based, and both were hosted within a single PIC18F4520 microcontroller. Furthermore, three Futaba 3003 servo motors were used to drive the joints under the control of the microcontroller control algorithm.

Karam *et al.* [10] also presented a study on the design, implementation and automation of a multi-robotic processing station. Two robot manipulators, serial and parallel robot manipulators of multi-degree of freedom, were presented. The design was to develop and test an integrated PRM and SRM system for capping plastic bottles in a scale processing line. Panda *et al.* [11] developed a gantry material handling robot for use in the bottling industry in food plants.

The design was to replace manual labour with an automated system to increase these plants' accuracy, safety and production rate. The design was also analyzed from various angles like material selection, cost and simplest and best selection of configuration. Also, Gunnar [12] developed the dynamical analysis and system identification of a Gantry-Tau parallel robot manipulator. The design was to determine the maximum stiffness of the Gantry robot manipulator. The study intended to determine the maximum in the z-direction, accomplished at the end of the research.

Also, Toby [13] proposed a robotic gantry with an end-effector for product lifting. The researcher developed a method that permits the selection of varying portions of a stack of products with the end-effector and protects the selected portions of products using a movable floor. Ye *et al.* [14] developed a variable-scale modular 3D printing robot for building interior walls. The design was to improve the efficiency of construction. The modular robot consisted of a mobile lifting module and a beam printing module. The robot can fully print complex curved interior walls under different working conditions.

From the literature review, it was observed that gantry robots are mostly mounted fixed at a place. Also, parallel manipulators have a common small workspace to footprint problem, which has got great attention and needs to be taken care of. However, this work thus considers a solution to the gap of mobility and workspace regarding current parallel manipulator designs and manual labour replacement by introducing a different gantry design with greater flexibility, mobility and dexterity. Furthermore, this study is a modification to previous studies by Gunnar [12], who considered dynamical analysis and system identification of a gantry-tau parallel manipulator, and the study of Panda *et al.* [11], who considered a gantry material handling robot for use in the bottling industry.

2. MATERIALS AND METHODS

2.1 Operation Principle of the Gantry Robot

The robot's structure, as seen in Figure 1, is a four-frame/stands figured device with dimensions of 550 x 450 x 300 mm. Each leg of the mobile robot platform is considered a serial kinematic chain (KC) made of four-link joints. The y-axis mobile platform is linked to the body frame through a sliding rail situated under; the mobile platform is driven to and fro along the y-axis by a stepper motor fixed/mounted under at both sides of the y-axis. The x-axis mobile platform is directly linked to the y-axis with the help of 2 rails situated at the 2 opposite sides of the y-axis; the platform slides horizontally along the 2 rails horizontally. The gripper is connected to the x-axis mobile platform and manipulated via the manipulator guide's aid. The end-effector guide ascends and descends along the x-axis mobile platform through the help of a toothed sprocket and chain drive.

The chain drive is driven by a toothed sprocket, driven by a stepper motor drive at the 2 adjacent sides of the x-axis mobile platform. The whole structure is movable by four 85 mm-long wheels located at the lower end of the four legs.

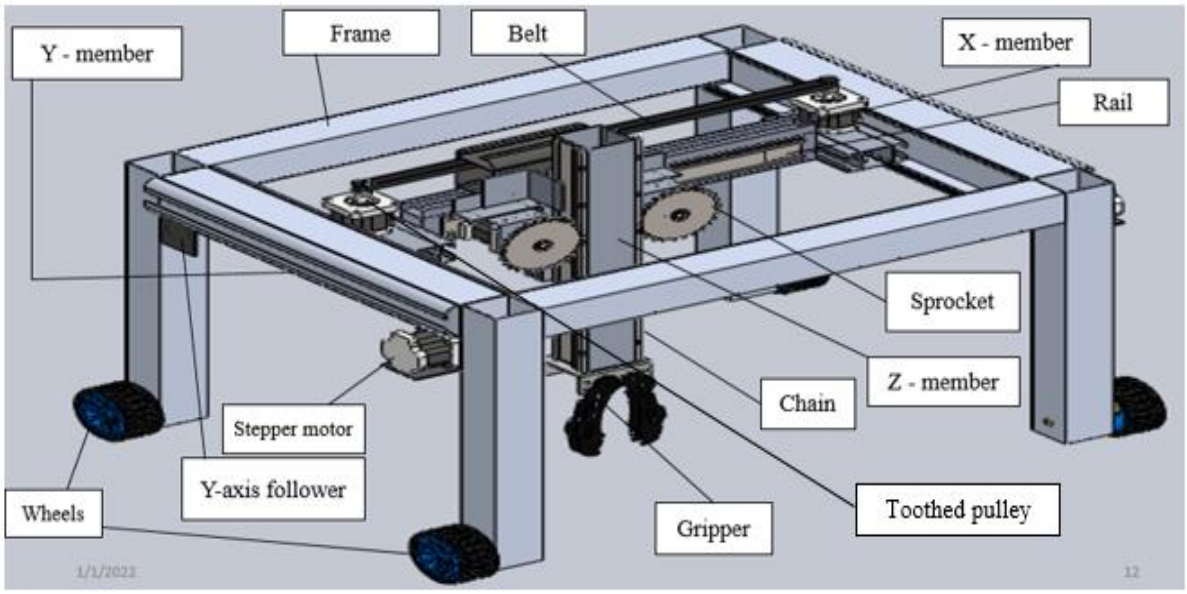

Figure 1: Gantry–based parallel robot manipulator (isometric view)

The operational user guide is shown in Figure 2 as a flowchart. It consists of switching on the device, feeding design data, defining the pick/drop spot, and going to the next working area when the current design segment is done.

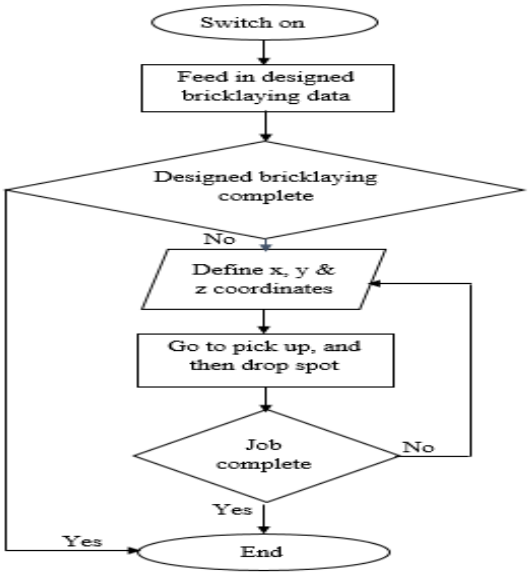

Figure 2: Flow chart showing the principle of operation of the Gantry robot

2.2 Design Consideration

The design considerations are: the robot is expected to lift a block of max. load of 100 g, a simplified control system of the joints, simplified and functional design of the joint, capturing the prototype design/geometry, material selection (e.g., speed range and power output of motor), due to cost, space and other related factors, the design is going to be a prototype, thus, a suitable multiplication scale factor must be included for enlargement to model type. Other design considerations are structure, workspace, singularities and link inference.

2.3 Material Selection

Some factors that must be considered in material selections include availability, strength, weight, ease of manufacture, damping property, etc. for stability, and system equilibrium should be observed; forces and moments should be counterbalanced [15]. Factors to consider regarding links material are strength and weight ratio since they add weight to the manipulator's actuators. Furthermore, heavy materials should be avoided as they are associated with a reduction of payload capacity. According to Meena *et al.* [16], aluminium alloy (Al 6061) is one of the materials that qualify for use because of its associated mechanical properties and hence qualify for use. Table 1 gives the properties of Al 6061.

Table 1: Mechanical and physical properties of Al 6061

Properties	Value
Density	2.70 g/cm³
Young's Modulus	68.9 GPa
Yield Strength	276 MPa
Ultimate Tensile Strength	310 MPa
Elongation at Break	12%
Hardness (Brinell)	95 HB
Thermal Conductivity	167 W/(m·K)
Melting Point	582-652°C

2.4 Manipulator Specifications

The specifications of the parallel manipulator imply the initial design specifications and conditions imposed on it and are given in Table 2. These conditions are the dimensions, constraints, work environment, the object and weight and dimensions of work, and the required performance criteria also included.

Table 2: Specification of the objective of the design

Specification	RM Range
The magnitude of each connector/joint deflection	±0.1 mm
The maximum magnitude of workload	1 N
Motion range magnitude in the X-direction	±330 mm
Motion range magnitude in the Y-direction	±360 mm
Motion range magnitude in the Z-direction	±300 mm
Rotation angle about X, Y-axes	±90°

2.5 Manipulators Dexterity Measurement

Due to space limitations or design in manipulators, joints are constrained, and an inequality of the form is used for the measurement. $q_i^L \leq q_i \leq q_i^U$ where q_i^L is the lower limit, q_i^U is the upper limit and i = 1, 2… n. Due to geometric constraints, there are conditions for manipulators shown in Table 3 and the workspace specification shown in Figure 3.

Table 3: Workspace boundary conditions of the RM

θ_i	Upper Limits	Lower Limits
1	0	π
2	2π	$\pi/2$

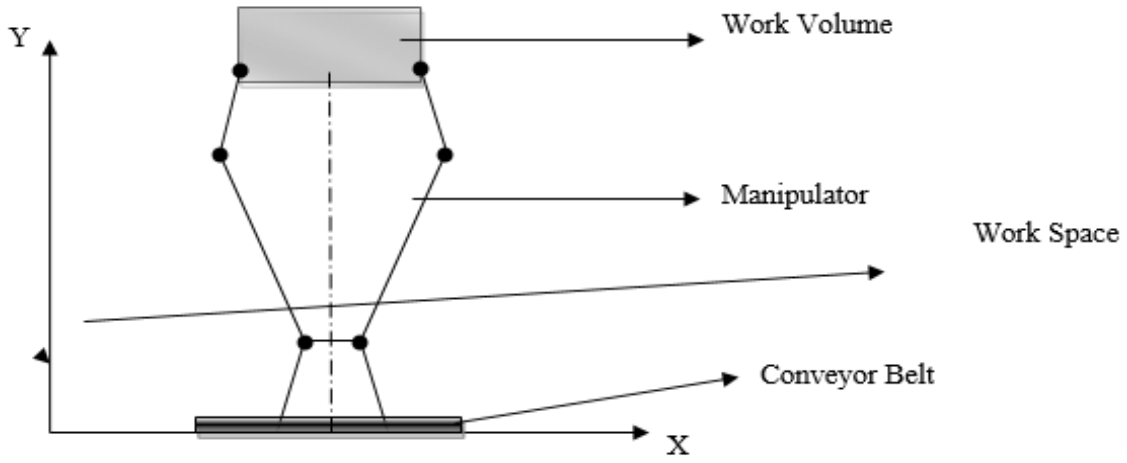

Figure 2: RM Workspace specification

2.6 Kinematic Synthesis

Typical manipulator operates in 3-D planes; this mostly requires 6-DOF. Therefore, the length of the links and actuators must be determined based on the needed workspace area and trajectory. Table 4 shows the reference.

Table 4: Specification of the length of links

Link Numbers	Lengths of Links (mm)
1	330
2	360
3	360
4	300

2.7 Robot Manipulator Mobility Analysis

The number of DOF of a robot is the number of independent parameters that must be specified for determining the position of the link relative to the body frame [17]. According to Grubler's criterion and Euler's equation, the DOF of a structure or mechanism/device can be obtained from Equations (1) and (2) [18].

$$m = \lambda(n - j - 1) + \sum_{i=1}^{j} f_i \quad (1)$$

$$L = j - n + 1 \quad (2)$$

For the considered parallel manipulator, $\lambda = 6$, $n = 14$, $j = 15$ and $f_i = 15$, therefore, $m=3$ (i.e. for motion along x, y & z coordinates).

2.8 Design of the Manipulator Mechanically

The method to be adopted for the design is that the components will be designed individually and separately, that is, the modular design method. According to Hoover *et al.* [19], a dynamic model is a significant tool for the mechanical design of a structure, the ability to choose actuators, control system determination and simulation of the motion of the parallel robot manipulator. The kinematics formulations form the general basis for deriving the manipulator's dynamics. Table 5 shows the design calculation of the robot.

Table 5: Design Calculation

Initial Data	Design Calculation	Remark
Maximum length sideways movement = 180 mm Length = 450 mm	**Design for y-axis rotating shaft (y-axis follower)** The maximum bending moment on the shaft 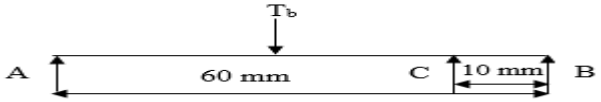 **Shaft analysis diagram** Since the pulley on the stepper motor ≡ pulley on the shaft; $$N_{sm} = \frac{V_{platform} \times 60}{\pi d_{pulley}}$$ $$N_{sm} = N_{yrr}$$ $$V_{pf} = \frac{180mm}{3s} = \frac{60mm}{s} = 0.06m/s$$ $$\theta = (180 - 2\alpha)\frac{\alpha}{180}$$ $$\alpha = sin^{-1}\left[\frac{r_{p1} - r_{p2}}{x}\right] = 0$$ Taking $\theta = \pi rad$, $\mu = 0.25$, $K_m = 2.5$, and $K_t = 2.25$ **Shear force and bending moment diagram** Obtaining shear force as well as bending moment for the shaft section, we have; 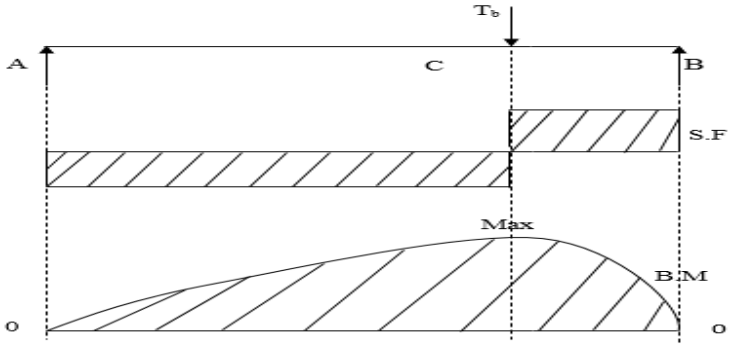 $$S_c = R_B - T_B = 58.02N$$ $S_A = R_A, S_B = R_B$ $M_C = R_B \times 0.01 = 290.11 \times 0.01 = 2.9\ Nm \Longrightarrow M_{max}$ $d_{yr,r}$ $$= \sqrt[3]{\frac{16}{\pi(56 \times 10^6)}\sqrt{(2.5 \times 2.9)^2 + (2.25 \times 0.974)^2}}$$	$r_{p1} = r_{p2}\}$ According to the ASME shaft design code, $d_{yr,r} = 8mm$

Consider nema 17, Sprocket standard pitch dia. = 55mm Assuming $\eta = 95\%$ h = 300mm Assume 2 steppers	**Effective Torque Required** $T_{hs} = 0.36Nm \;\; \eta = 95\%$ $T_{hs} = 0.36 \times 0.95$ **The maximum mass of the prototype block** $\Rightarrow \sum T_{hs} = (m + m_{bl})gh$ $\Rightarrow 2(0.342) = (1 + m_{bl}) \times 9.81 \times 0.3$ ***Force required to hold*** & ***retain the grip*** ⇒Force necessary would be thus: Assuming the efficiency of the arm is 25% $\Rightarrow \sum T_s = 0.25 \times 1.08 = 0.27Nm$ Hence $m_{bl} = \frac{\sum T_s}{gh} = \frac{0.27}{9.81 \times 0.3} \cong 0.09kg$	$T_{hs} = 0.342Nm$ $m_{bl} = 0.77kg$ $\sum T_s = 0.27Nm$ $m_{bl} = 0.09$kg
Density of MDF wood = 800kg/m3 $v_{bl} =$ $l_{bl}\, x\, b_{bl} x\, h_{bl}$	**Length of Block (modelled)** $m_{bl} = \rho_{bl} \times v_{bl}$ $0.09 = 800 \times v_{bl} \times 0.035 \times 0.016 \Rightarrow v_{bl} = 0.234mm$ $\Rightarrow v_{bl} \cong 200.89mm$ For the convenience of the grip, this length is divided in 3 $\Rightarrow size\ for\ the\ downscale \Rightarrow 65mm \times 35mm \times 16mm$	$v_{bl} = 200.89mm$
p = pitch = 6mm (chain) z = no of teeth = 28	**The speed required for the stepper motor** $v = \frac{pzn}{1000} \Rightarrow N = \frac{v \times 1000}{p \times z} = \frac{6 \times 1000}{6 \times 28}$ $\Rightarrow N \cong 35.71rpm \Rightarrow N = 40rpm$	$N = 40rpm$
$mass = density\ x\ volume$ $m_z = 2.5kg$ $h_z = 0.3mm$	**Z-axis required torque** $\Rightarrow \sum m_z = 0.15 \times 2.5 = 0.375kg$ $T_z = \sum m_z \times g \times h_z = 0.375 \times 9.81 \times 0.3$ $T_z = 110Nm$	$T_z = 110Nm$
The Z-component also added 0.375kg to the mass. Hence, 2 steppers motor would be sufficient	**X-axis required torque** Mass of x-axis members; $m_x = 0.97kg$ $\sum m_x = \mu \times\ m_x = 0.15 \times\ 0.97 = 0.15$kg Hence torque required $\Rightarrow \sum m_x \times g \times h = 0.15 \times 9.81 \times 0.3$, $T_x = 0.44Nm$ Provided 1 motor provides 0.36Nm; hence 2 motors are required for x-axis motion. $\sum T_x = (0.36 \times 2) \times \eta_b \Rightarrow 0.36 \times 2 \times 0.95 = 0.68Nm$ $\sum T_x > T_x$, hence is suficient.	$T_x = 0.68Nm$ $\sum T_x > T_x$

The X-component also added 0.15kg to the mass. Hence, 2 steppers motor would be sufficient	**Y-axis required torque** Mass of x-axis members; $m_y = 1.2kg$ $\sum m_y = \mu \times m_y = 0.15 \times 1.2 = 0.18$kg Hence torque required $\Rightarrow \sum m_y \times g \times h = 0.18 \times 9.81 \times 0.36$, $T_y = 0.64Nm$ Provided 1 motor provides 0.36Nm; hence 2 motors are required for x-axis motion. $\sum T_y = (0.36 \times 2) \times \eta_b \Rightarrow 0.36 \times 2 \times 0.95 = 0.66Nm$ $\sum T_y > T_y$, hence is suficient.	$T_y = 0.66Nm$ $\sum T_y > T_y$
Motor selection	**(viii) Motor selection criterion** From belt calc., Power req. = 7.792W Stepper motor phases = 4. Each phase draws 1.7A at 2.8V $\therefore$ I (total) = 1.7 x 4 = 6.8A, V(total) = 2.8 x 4 = 11.2V Thus, Power = I x V = 6.8 x 11.2	P = 76.16W = 0.07616KW
Total power input, used & lost	**(ix) Total power required & loss** Stepper input & used current = 5A Stepper input & used voltage = 12V & 11.2V, respectively. Servo input & used current = 50mA Servo input & used voltage = 5V & 4.8V respectively Stp. $T_{power\text{-}input}$ = 5 x 12 = 60W x 6 (6steppers) = 360W Belt $T_{power\text{-}input}$ = (7.792 x 2) + 7.792 / 2) = 19.48W Servo $T_{power\text{-}input}$ = 5 x 50mA = 0.25W $T_{power\text{-}input}$ = (360 + 19.48 + 0.25) W = 379.73W	$T_{power\text{-}input}$ = 379.73W
	Stp. $T_{power\text{-}used}$ = 5 x 11.2 56W x 6 (6steppers) = 336W Belt $T_{power\text{-}used}$ = 19.48W Servo $T_{power\text{-}used}$ = 4.8 x 50mA = 0.24W $T_{power\text{-}used}$ = (336 + 19.48 + 0.24) W = 355.72W $T_{power\text{-}loss}$ = $T_{power\text{-}input}$ - $T_{power\text{-}used}$ = 379.73 − 355.72	$T_{power\text{-}used}$ = 355.72W $T_{power\text{-}loss}$= 24.01W

2.9 Circuit Diagram Showing Motors Connection

The microcontroller used for system control was Arduino Mega. The stepper motors 1 & 2 were used for x-axis motion drive, motors 3 & 4 for y-axis motion and motors 5 & 6 for z-axis motion control. From the circuit diagram shown in Figure 4, the servo motor at the bottom of the circuit was used as the gripper for picking and dropping the bricks.

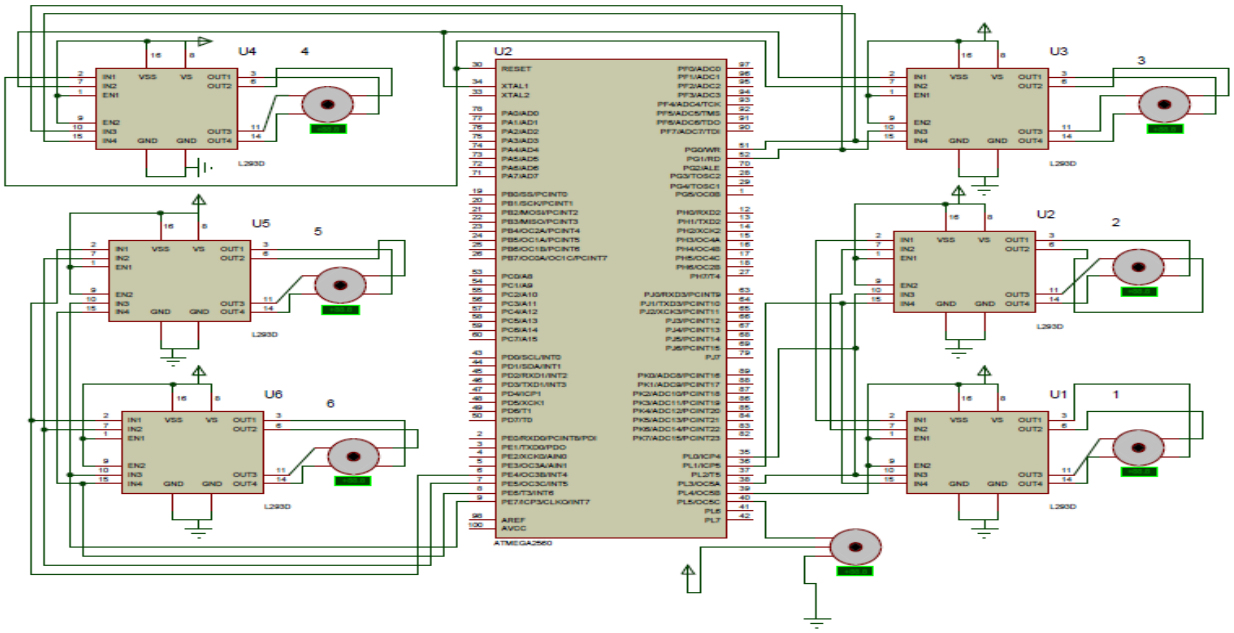

Figure 4: Circuit diagram showing motors connection

A4988 was the driver for the stepper motors, but in the proteus environment, L293D was used as a substitute. The A4988 driver requires two capacitors, 47µf, 50V and 100µf, 25V but L293D contains those capacitors embedded, so none is shown on the circuit diagram.

The power supply unit used was digital Tektronix, capable of providing the required 6A and 12V power as stated in the design calculation table (Table 5).

3. Results and discussion

3.1 Simulation Results of the Gantry Robot and Discussion

From the result obtained in Figure 5(a), (b), and (c), the constructed robot material (Al alloy) has a yield strength of 276 MPa, the Z-member maximum load produced 12.57 MPa, the X-member maximum load produced 4.814 MPa, and the robot frame maximum load produced 13.34 MPa. All the 3 members were subjected to stresses below the design yield strength of the robot material. Furthermore, for any good and acceptable design, the design yield strength should never be more than 25% of the yield strength of the material under any given condition [20]. Since the material yield strength is 276 MPa, the design yield strength is 15% of the material yield strength by conversion. Thus, the device would function effectively from a strength point of view. Thus, this result represents good and acceptable structures or members' designs mechanically.

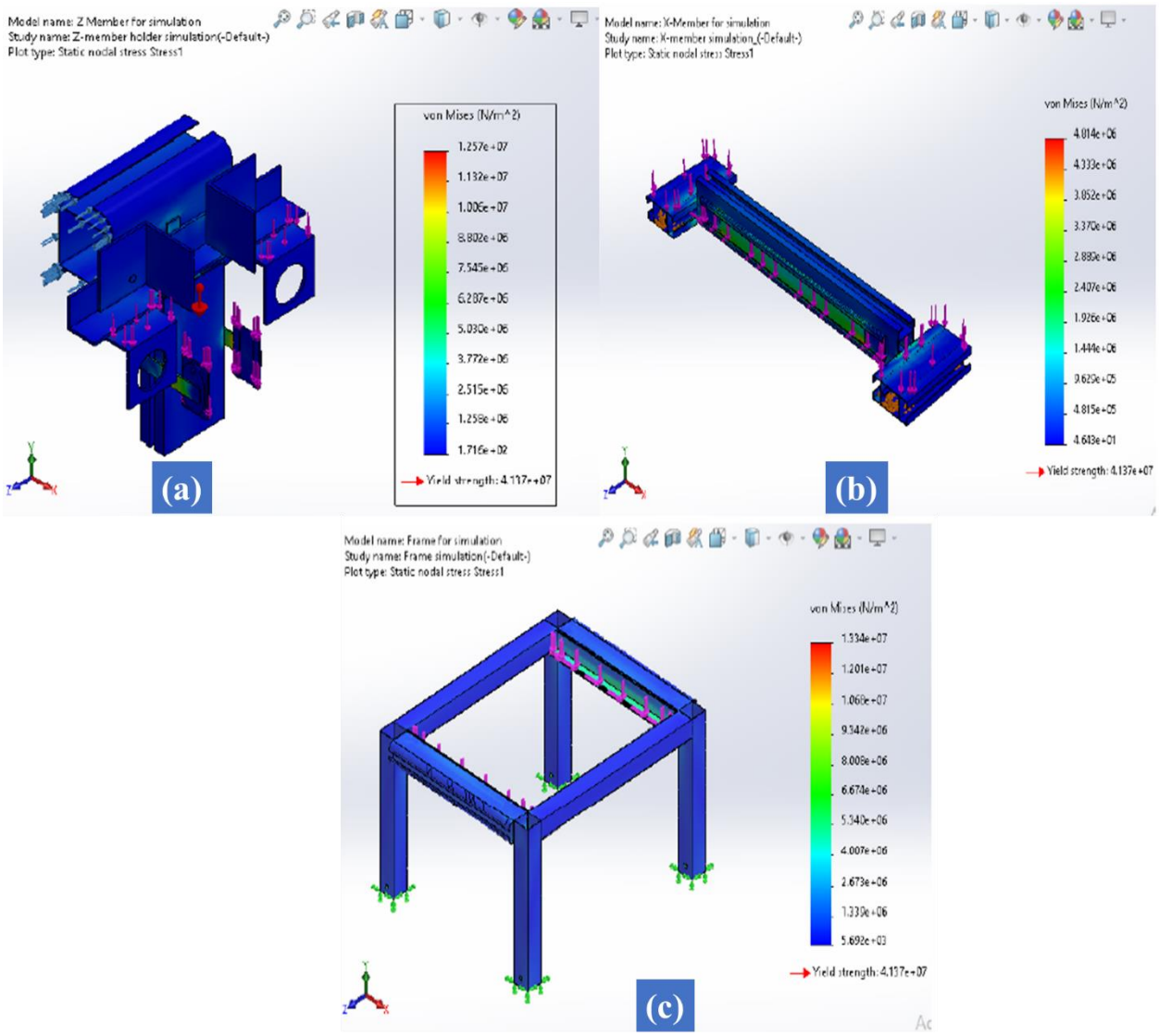

Figure 5: Stress simulation result of (a) Z-member, (b) X-member, and (c) Robot frame

3.2 Performance Efficiency Measuring Procedure of the Gantry Robot

In conducting a performance efficiency test for the device, a 2D planer map having a series of uniform rectangular boxes (i.e., x-y plane) was constructed using 2D cardboard paper, as seen in Figure 6. Hence, the gantry robot was placed on the map on the floor to such an extent that it occupied half of the planer map. These uniform rectangular boxes were the same size as the width of the scaled building blocks. Previous studies such as Zou *et al.* [21] and Sonar *et al.* [22] employed a similar approach.

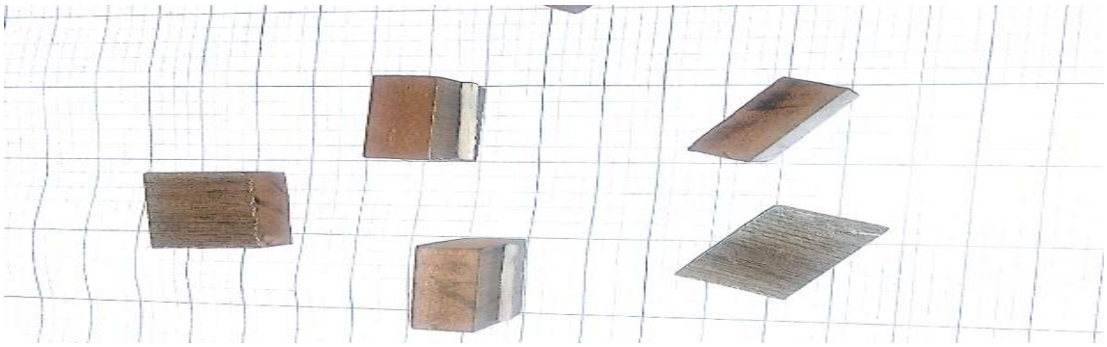

Figure 6: 2D planar map

The first approach was keeping y-values fixed on level one. Block placement graph boxes are drawn on a plain sheet titled a 2D planar map for each evaluation procedure carried out while increasing level values of x in ascending order. The boxes were numbered as follows; first box value = level 1, second box value = level 2..... n^{th} box value = level n. Figure 7 shows the obtained result. The second approach was keeping in ascending order increasing both level values of x and y exclusively and correspondingly at a time. Figure 8 illustrates the results of the procedure. Results obtained in Figures 7 and 8 showed that the best-fit lines on the x and y axes are linear.

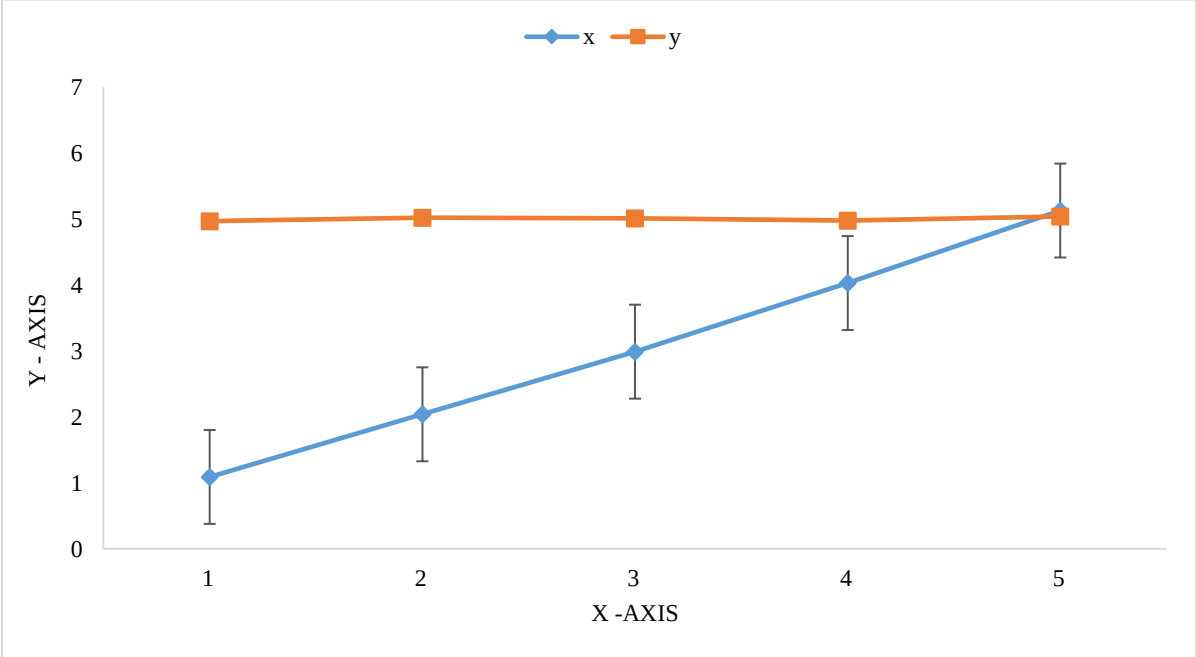

Figure 7: 1st setup of the 2D planar map of the robot under constant y-values

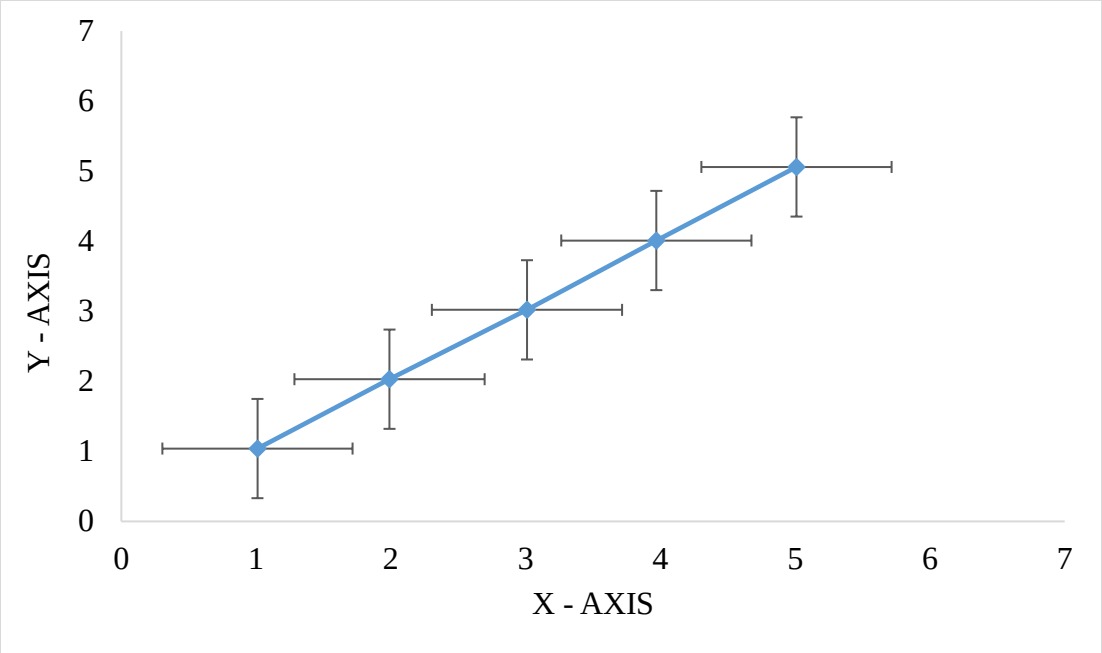

Figure 8: 2nd setup of the 2D planar map of the robot under varying x and y-values

3.3 Model Fit and Validation

Ljung [23] developed an ideology, later developed into a method called System Identification. It involves feeding a system or system joints with data (e.g., displacement, velocity, torque, etc.), then building a hypothesis by predicting the output and measuring the actual output. Hofer and D'Andrea [24] and Gale *et al.* [25] employed the same approach to improve a robotic manipulator model based on multivariate residual modelling. The validation of this model is given in Equation (3).

$$fit = 100\left[1 - \frac{\sqrt{\sum_{t=1}^{N}(y(t)-\hat{y}(t))^2}}{\sqrt{\sum_{t=1}^{N}(y(t)-\bar{y})^2}}\right] \quad (3)$$

Where from Figure 7,

$y(t)$ = measured value = 5.13mm

$\hat{y}(t)$ = predicted value = 5mm

$\bar{y}$ = mean value of $y(t)$ =3.06mm

And from Figure 8,

$y(t)$ = measured value = 5.14mm

$\hat{y}(t)$ = predicted value = 5mm

$\bar{y}$ = mean value of $y(t)$ =3.08mm

Hence, from Equation (3), for the 1st setup, fit =94%; for the 2nd setup, fit=97%. From the results obtained, it can be justified that the model is well-fitted with values of 94% and 97% from the first and second approaches, respectively. It is important to note that these approximately 3-6% fitting errors can be attributed to several factors, including measurement inaccuracies, inherent system noise, and modelling assumptions. The slight deviations between the predicted and measured values are within an acceptable range considering the complexity of the system and the inherent uncertainties involved. These results were obtained from the average of the methodology repetition as a means of cross-evaluation. Comparing this result (with an average model fit of 95.5%) with that of the cross-validation of the study by Gunnar [12], an average model fit of 95.16%, it can be observed that the developed model shows promising results of manipulator mobility; hence, it can be said to be logically and technically justified as it falls within the expected and acceptable range of literature.

4. Conclusions

In this study, a novel gantry-based parallel robot manipulator was developed and evaluated for bricklaying applications in the construction industry. The objective was to design and simulate the robot manipulator, implement a control algorithm, and evaluate its speed, accuracy, and payload capacity. The gantry-based parallel robot manipulator was designed and analyzed using appropriate design considerations, material selection, and kinematic synthesis. The robot's operational principle and design specifications were carefully defined, and the necessary calculations and simulations were performed to ensure the structural integrity and performance of the manipulator. Simulation results demonstrated that the robot design met the strength requirements, with stress values well below the yield strength of the chosen material. The performance efficiency of the robot was evaluated through a 2D planar map test, where different setups were assessed. The results indicated linear relationships and demonstrated the robot's ability to perform bricklaying tasks effectively.

Furthermore, the model fit and validation were carried out using a system identification approach. The developed model showed good fitting with measured values, achieving 94% and 97% fit for the first and second setups, respectively. These fitting errors of approximately 3-6% can be attributed to various factors but still fell within an acceptable range considering the complexity of the system and inherent uncertainties. The study successfully designed and evaluated a gantry-based parallel robot manipulator for bricklaying applications. The developed robot demonstrated enhanced mobility, workspace utilization, and promising speed, accuracy, and payload capacity results. The findings of this study contribute to the advancement of robotic systems in the construction industry, offering potential benefits in terms of efficiency, safety, and productivity.

ACKNOWLEDGEMENTS

The authors acknowledge the support offered by Engr. Awwal Isa Bello, Mallam Ibrahim and Mallam Musa Nari, as well as the Department of Mechanical Engineering staff and students, Ahmadu Bello University, Zaria, Nigeria.

Conflicts of Interests

The authors declare no competing interests

Authors' Contributions

M.H.I. is responsible for data collection, methodology, and writing of the original draft. U.A.U. is responsible for the conceptualization, supervision, methodology and writing of the original draft. M.A.O. is responsible for the conceptualization, supervision and methodology. A.N.O. is responsible for the data analysis and review of the original draft.

5.References

[1] M. Javaid, A. Haleem, R. P. Singh, and R. Suman, "Substantial capabilities of robotics in enhancing industry 4.0 implementation," *Cognitive Robotics*, vol. 1, pp. 58–75, Jan. 2021, doi: 10.1016/J.COGR.2021.06.001.

[2] S. Luhar and I. Luhar, "Additive Manufacturing in the Geopolymer Construction Technology: A Review," *The Open Construction & Building Technology Journal*, vol. 14, no. 1, pp. 150–161, Aug. 2020, doi: 10.2174/1874836802014010150.

[3] O. Adepoju, "Robotic Construction Technology," *Springer Tracts in Civil Engineering*, pp. 141–169, 2022, doi: 10.1007/978-3-030-85973-2_7/COVER.

[4] T. Bruckmann, H. Mattern, A. Spengler, C. Reichert, A. Malkwitz, and M. König, "Automated Construction of Masonry Buildings using Cable-Driven Parallel Robots".

[5] F. P. Bos *et al.*, "The realities of additively manufactured concrete structures in practice," *Cem Concr Res*, vol. 156, p. 106746, Jun. 2022, doi: 10.1016/J.CEMCONRES.2022.106746.

[6] C. Y. Lai, D. E. Villacis Chavez, and S. Ding, "Transformable parallel-serial manipulator for robotic machining," *International Journal of Advanced Manufacturing Technology*, vol. 97, no. 5–8, pp. 2987–2996, Jul. 2018, doi: 10.1007/S00170-018-2170-Z/METRICS.

[7] C. Yang, W. Ye, and Q. Li, "Review of the performance optimization of parallel manipulators," *Mech Mach Theory*, vol. 170, p. 104725, Apr. 2022, doi: 10.1016/j.mechmachtheory.2022.104725.

[8] R. Simoni, P. R. Rodriguez, P. Cieslak, L. Weihmann, and A. P. Carboni, "Design and kinematic analysis of a 6-DOF foldable/deployable Delta parallel manipulator with spherical wrist for an I-AUV," *OCEANS 2019 - Marseille, OCEANS Marseille 2019*, vol. 2019-June, Jun. 2019, doi: 10.1109/OCEANSE.2019.8867496.

[9] M. O. Afolayan, D. S. Yawas, C. O. Folayan, and S. Y. Aku, "Mechanical Description of a Hyper-Redundant Robot Joint Mechanism Used for a Design of a Biomimetic Robotic Fish," *Journal of Robotics*, vol. 2012, pp. 1–16, 2012, doi: 10.1155/2012/826364.

[10] Z. A. Karam and M. A. Neamah, "Design, Implementation, Interfacing and Control of Internet of Robot Things for Assisting Robot," *International Journal of Computing and Digital Systems*, vol. 11, no. 1, pp. 387–399, 2022, doi: 10.12785/IJCDS/110132.

[11] B. K. Panda, S. S. Panigrahi, G. Mishra, and V. Kumar, "Robotics for general material handling machines in food plants," *Transporting Operations of Food Materials within Food Factories: Unit Operations and Processing Equipment in the Food Industry*, pp. 341–372, Jan. 2023, doi: 10.1016/B978-0-12-818585-8.00005-2.

[12] J. Gunnar, "Dynamical Analysis and System Identification of the Gantry-Tau Parallel Manipulator," 2005, Accessed: May 13, 2023. [Online]. Available: https://urn.kb.se/resolve?urn=urn:nbn:se:liu:diva-5322

[13] "Robotic gantry with end effector for product lifting," Nov. 2018.

[14] C. Ye, N. Chen, L. Chen, and C. Jiang, "A variable-scale modular 3D printing robot of building interior wall," *Proceedings of 2018 IEEE International Conference on Mechatronics and Automation, ICMA 2018*, pp. 1818–1822, Oct. 2018, doi: 10.1109/ICMA.2018.8484433.

[15] A. N. Oyedeji, U. A. Umar, L. S. Kuburi, A. A. Edet, and Y. Mukhtar, "Development and performance evaluation of an oil palm harvesting robot for the elimination of ergonomic risks associated with oil palm harvesting," *Journal of Agricultural Engineering*, vol. 53, no. 3, Sep. 2022, doi: 10.4081/JAE.2022.1388.

[16] J. Meena, T. K. Sunil Kumar, and T. R. Amal, "Design and Implementation of a Multi-purpose End-effector Tool for Industrial Robot," *2021 International Symposium of Asian Control Association on Intelligent Robotics and Industrial Automation, IRIA 2021*, pp. 70–76, Sep. 2021, doi: 10.1109/IRIA53009.2021.9588746.

[17] K. Mohamed, H. Elgamal, and A. Elsharkawy, "Dynamic analysis with optimum trajectory planning of multiple degree-of-freedom surgical micro-robot," *Alexandria Engineering Journal*, vol. 57, no. 4, pp. 4103–4112, Dec. 2018, doi: 10.1016/J.AEJ.2018.10.011.

[18] E. V. Gaponenko, D. I. Malyshev, and L. Behera, "Approximation of the parallel robot working area using the method of nonuniform covering," *J Phys Conf Ser*, vol. 1333, no. 5, p. 052005, Oct. 2019, doi: 10.1088/1742-6596/1333/5/052005.

[19] A. M. Hoover, E. Steltz, and R. S. Fearing, "RoACH: An autonomous 2.4g crawling hexapod robot," *2008 IEEE/RSJ International Conference on Intelligent Robots and Systems, IROS*, pp. 26–33, 2008, doi: 10.1109/IROS.2008.4651149.

[20] R. V. Martinez *et al.*, "Robotic Tentacles with Three-Dimensional Mobility Based on Flexible Elastomers," *Advanced Materials*, vol. 25, no. 2, pp. 205–212, Jan. 2013, doi: 10.1002/ADMA.201203002.

[21] Z. Zou *et al.*, "Real-time Full-stack Traffic Scene Perception for Autonomous Driving with Roadside Cameras," *Proc IEEE Int Conf Robot Autom*, pp. 890–896, 2022, doi: 10.1109/ICRA46639.2022.9812137.

[22] H. A. Sonar, J.-L. Huang, and J. Paik, "Soft Touch using Soft Pneumatic Actuator–Skin as a Wearable Haptic Feedback Device," *Advanced Intelligent Systems*, vol. 3, no. 3, p. 2000168, Mar. 2021, doi: 10.1002/AISY.202000168.

[23] L. Ljung, "System Identification," pp. 163–173, 1998, doi: 10.1007/978-1-4612-1768-8_11.

[24] M. Hofer and R. D'Andrea, "Design, Modeling and Control of a Soft Robotic Arm," *IEEE International Conference on Intelligent Robots and Systems*, pp. 1456–1463, Dec. 2018, doi: 10.1109/IROS.2018.8594221.

[25] S. Gale, H. Rahmati, J. T. Gravdahl, and H. Martens, "Improvement of a Robotic Manipulator Model Based on Multivariate Residual Modeling," *Front Robot AI*, vol. 4, p. 28, Jul. 2017, doi: 10.3389/FROBT.2017.00028/BIBTEX.

Towards Hajj and Umrah Digital Transformation Using Smartwatches

Hashim K. Sawadi[1*], Ibrahim O. Al-Zahrani[1*], Ahmad F. Al-Ghoraibi[1*], Abdullah M. Al-Ghamdi[1*], Ghassan F. Bati[1*2]

[1] Computer Engineering Dept., Umm Al-Qura University, KSA

[2] gfbati@uqu.edu.sa
[*]Equal contribution

Abstract: Many of us now rely on smartwatches as an integral part of our lives. The smartwatch market has become one of the world's most popular and best-selling markets. They have been used in various fields like health and sports. They have valuable features that assist people in their daily lives. With Hajj and Umrah undergoing digital transformation, smartwatches can be used to enhance pilgrims' experience during sacred rituals. NUSK is a smartwatch launched by (SDAIA) in Hajj season 1442 AH (2021) to provide several services like displaying pilgrims' information and health status, monitoring their health data, and requesting emergency medical or security assistance. It is vital to develop similar projects and build upon the success of NUSK. Hence, this work uses "Bangle.js", an open-source (sw/hw) smartwatch, to present some Hajj and Umrah applications to enhance the pilgrim's experience in the sacred journey and to help achieve our country's ambitious vision towards Hajj and Umrah digital transformation. We also propose incorporating "Bangle.js" into the labs of microprocessor courses at Saudi Computer Colleges to allow students to broaden their skills, abilities, and thinking toward real-life applications facilitating digital transformation.

Keywords: Digital Transformation, Smartwatches, Smart Hajj, Smart Umrah, Auto Tawaf.

نحو التحول الرقمي للحج والعمرة باستخدام الساعات الذكية

الملخص: يعتمد الكثير منا الآن على الساعات الذكية كجزء لا يتجزأ من حياتنا. أصبح سوق الساعات الذكية أحد الأسواق الأكثر شهرة والأكثر مبيعًا في العالم. لقد تم استخدامها في مجالات مختلفة مثل الصحة والرياضة. لديهم ميزات قيمة تساعد الناس في حياتهم اليومية. مع خضوع الحج والعمرة للتحول الرقمي ، يمكن استخدام الساعات الذكية لتعزيز تجربة الحجاج خلال الشعائر المقدسة *NUSK* .هي ساعة ذكية أطلقتها *(SDAIA)* في موسم الحج 1442 هـ (2021) لتقديم العديد من الخدمات مثل عرض معلومات الحجاج وحالتهم الصحية ، ومراقبة بياناتهم الصحية ، وطلب المساعدة الطبية أو الأمنية الطارئة. من الضروري تطوير مشاريع مماثلة والبناء على نجاح *NUSK.* ومن ثم ، يستخدم هذا العمل *"Bangle.js"*، وهي ساعة ذكية مفتوحة المصدر *(sw / hw)* ، لتقديم بعض تطبيقات الحج والعمرة لتعزيز تجربة الحجاج في الرحلة المقدسة وللمساعدة في تحقيق رؤية بلدنا الطموحة تجاه الحج والعمرة. التحول الرقمي. نقترح أيضًا دمج *"Bangle.js"* في مختبرات دورات المعالجات الدقيقة في كليات الكمبيوتر السعودية للسماح للطلاب بتوسيع مهاراتهم وقدراتهم وتفكيرهم تجاه تطبيقات واقعية تسهل التحول الرقمي.

1. Introduction

As scientific and economic studies indicate, the smartwatch market is witnessing significant and remarkable development. The global smartwatch market was valued in 2019 at $20.64 billion and is expected to reach $96.31 billion by 2027. With a compound annual growth rate (CAGR) of 19.6%, the smartwatch market has become one of the world's most popular and best-selling markets [1]–[3]. These enormous numbers indicate the heavy reliance on smartwatches at present and the extent of their growth over the next few years to include a broader range of users than it is today. Smartwatches' applications and use cases vary in many fields due to the services and features they provide, starting from the fields of sports and health to more complex fields such as personal assistants and artificial intelligence applications [4], [5]. Undoubtedly, this diversity provides a wide range of applications that can be developed to improve the worshipper's experience in Hajj and Umrah.

The Kingdom of Saudi Arabia is moving towards a comprehensive digital transformation in all governmental fields and services. The numbers indicate that it has made great leaps and gains. The Kingdom is the seventh globally in financing technical development. Also, it is the ninth in the development of technology and digital transformation, as mentioned in the annual report on global competitiveness (IMD) [6]. Undoubtedly, the Hajj and Umrah sectors have always gained significant attention from the Saudi government. They are cornerstones in the process of digital transformation for the Kingdom, as it aims to employ digital transformation to maximize the services provided to the pilgrims [7]–[9].

Digital transformation in Hajj and Umrah requires a thorough procedure for updating the vision and strategy of all agencies working in the Hajj and Umrah sectors by replacing traditional procedures with digital and automated ones [10]. This paper uses "Bangle.js", an open-source (hardware/software) smartwatch, to provide applications and services to pilgrims. The Hajj and Umrah include many services that smartwatches can enhance and facilitate to expedite the desired digital transformation and enhance the pilgrims' experience. To the best of our knowledge, no previous work has explored and paved the way for using smartwatches in Hajj and Umrah digital transformation besides "NUSK" and this work.

2. Related Work

The smartwatch market is relatively new, as Microsoft launched the first smartwatch, "SPOT," in 2004 [11]. The Google Trends website also shows that the term "smartwatch" is relatively new and has gained much attention recently, as shown in Figure 1 [12].

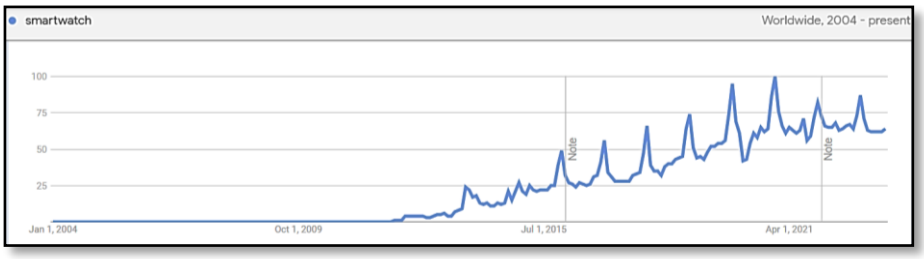

Figure 1. The trend of the keyword "Smartwatch" in Google Search over time [12].

Thus, the first real experience of using smartwatches in Hajj, as far as we know, was in the Hajj season of 1442 AH (2021) when the Saudi Authority for Data and Artificial Intelligence, in cooperation with the Doyof Al Rahman Program, and STC, launched the smartwatch "NUSK" in its trial version, with about 5,000 smartwatches distributed to pilgrims [13], [14]. "NUSK" provides various services, including the pilgrim's personal information, immunity status, and health data monitoring by measuring blood oxygen and heartbeat. Furthermore, it allows the pilgrim to request assistance from the camp supervisor and provide medical emergency or security assistance from official government agencies to accelerate access to their location and rescue operations. The smartwatch sends awareness messages and alerts to pilgrims [15]–[17]. This paper uses "Bangle.js" smartwatch to mimic "NUSK", build upon its success, and suggest new directions in Hajj and Umrah digital transformation using smartwatches.

3. Current Applications

As far as we know, this section shows all mobile applications used in Hajj and Umrah that can be implemented in smartwatches. These apps cover several fields, like health and navigation.1

a. Health Applications

"Aseifni" is a mobile application that provides multiple services, including reporting a health condition and making emergency calls. The application is capable of tracking emergency cases using the mobile's GPS. It also provides first aid instructions and other services, such as locating the nearest pharmacies or hospitals [18], [19].

b. Navigation Applications:

"Tarwiyah" is a mobile application that provides a map of Al-Mashaer (Holy sites) showing drinking water fountains, toilets, camps, and sacred locations. The map also shows the distributors of Zamzam water in Makkah, Madinah, and Jeddah [18].

c. Hybrid Applications:

This subsection presents various applications that provide miscellaneous services that cannot be categorized in one section like the abovementioned two. "Manasikana" is an official application introduced by the Ministry of Hajj and Umrah. The application provides many services in many languages, such as supplications, prayer timings, Qibla direction, weather, navigation, currency conversion, and notifications. This application helps pilgrims find their lost peers using the navigation capability [18].
"Al-Haramain" is an official application introduced by the Ministry of Hajj and Umrah. The application answers the worshipper's questions live via audio and video in different languages and shows if the Holy Mosques are crowded or not. The worshipper can also request a wheelchair. It also provides the usual services like Hajj and Umrah rituals guide, supplications, prayer times, and navigation [18].

d. Suggested Applications:

This section shows suggested applications that could be useful in Hajj and Umrah, especially if developed for smartwatches. These proposed applications can benefit and assist pilgrims, camps, and organizations [18], [20].

Pilgrims & Camps.

One of the ideas that can be used to help the pilgrims or camp leaders is location tracking via the smartwatch's GPS. For example, it is possible to monitor the pilgrim while offering their rituals inside the two holy mosques, providing a solution for camp leaders to quickly find lost pilgrims and direct them to the nearest gathering center.
Pilgrims also need to determine the direction of Qibla, indoor or outdoor, to pray in the right direction. Determining the Qibla outdoors is usually highly accurate. However, determining it indoors is still an open challenge.

Organizations.

One of the practical applications that can be used in Hajj and Umrah is Big Data analytics. If distributed at a large scale, the smartwatch could be a great source of data collection that could help various organizations managing Hajj and Umrah make better decisions and predict future patterns and scenarios, besides the fact that it would be a memorable souvenir documenting the sacred journey for the pilgrim. For example, if smartwatches were used in Tawaf (circumambulation around Kaaba), they would help the decision-maker count the number of worshippers and predict future Tawaf patterns throughout the year.

4. Implementation

As mentioned previously, many applications can be developed using smartwatches to help in Hajj and Umrah. We will showcase four applications using "Bangle.js", an open-source (hardware/software) smartwatch released in 2019. It has a 64 MHz ARM Cortex-M4 processor with Bluetooth LE, 64 KB RAM, 512 KB on-chip flash, and 4 MB external flash. In addition, it has several sensors like a heart rate monitor sensor, a GPS receiver, and an accelerometer.
Moreover, various open-source applications can be installed from the smartwatch website, while new applications could be developed from scratch using JavaScript or Blockly languages [21].

The first step to developing an app and uploading it to "Bangle.js" is writing the code in the "Espruino" Web IDE [22] or the emulator using JavaScript, as shown in Figure 2.

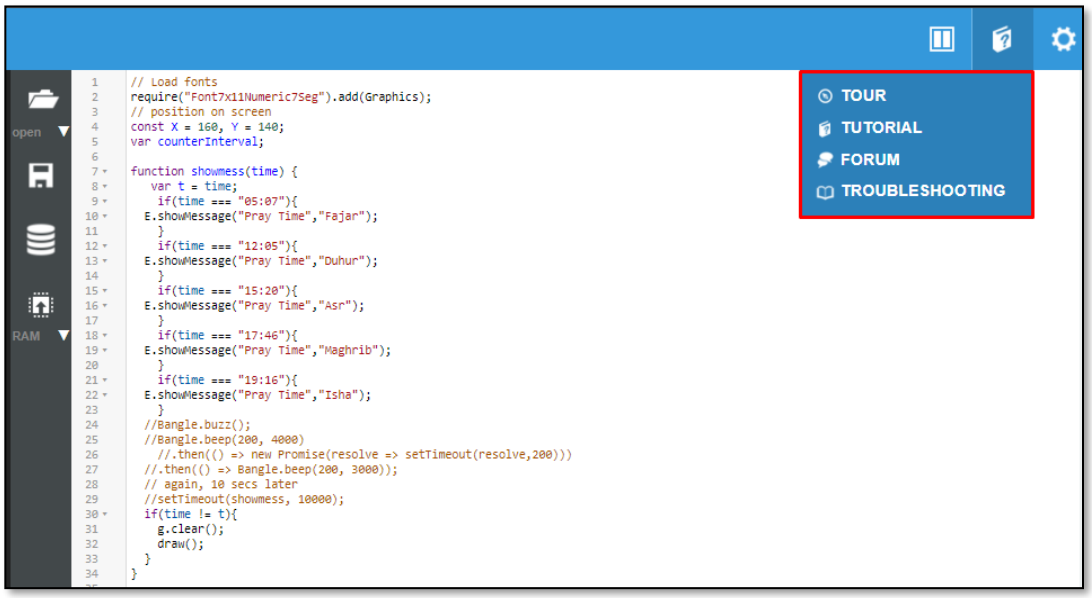

Figure 2. A screenshot of a code written in the "Espruino" Web IDE.

After writing the app in the "Espruino" Web IDE, the app must be uploaded to the app loader by forking the existing "Bangle.js App Loader" and enabling GitHub pages, as shown in Figure 3.

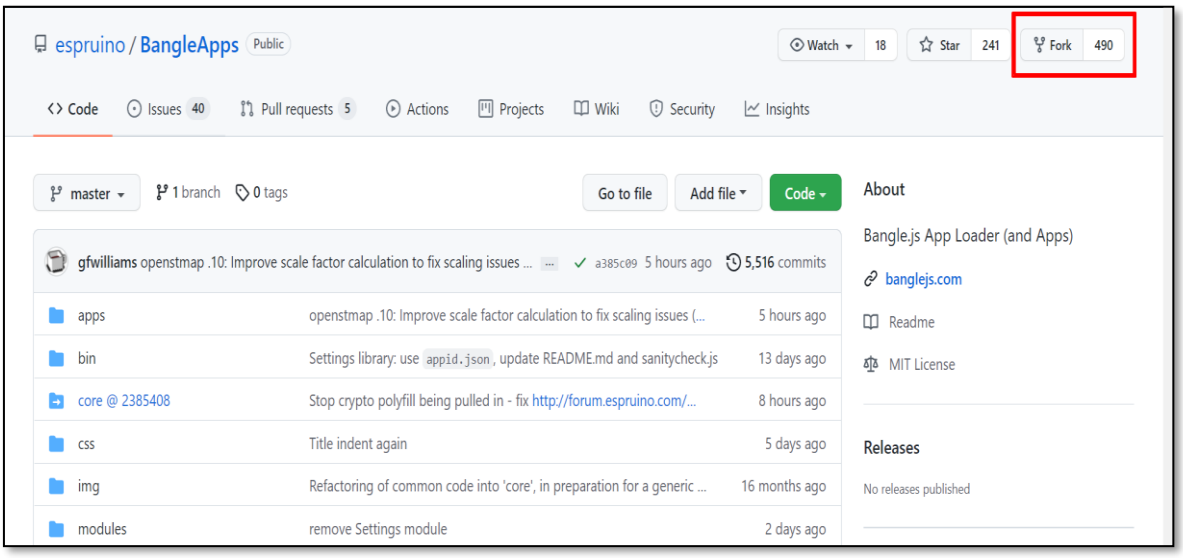

Figure 3. Forking "Bangle.js" apps on GitHub.

Finally, after uploading the files to GitHub, the app is added to the app loader as an object in an "apps.json" file on GitHub, as shown in Figure 4.

```
},
{ "id": "timer",
  "name": "My Timer App",
  "shortName":"My Timer",
  "icon": "app.png",
  "version":"0.01",
  "description": "This is a description of my awesome timer app",
  "tags": "",
  "storage": [
    {"name":"timer.app.js","url":"app.js"},
    {"name":"timer.img","url":"app-icon.js","evaluate":true}
  ]
}
]
```

Figure 4. A screenshot of an app's json file.

For research reproducibility and educational purposes, we shared the codes of the following four applications on GitHub "Daqiqah SmartWatch" repository [23] and made an Arabic video on YouTube explaining how to use the smartwatch and develop apps on it briefly [24].

a. First Application: (Watch Interface & Prayer Time Alarm)

There is no doubt that many applications can determine prayer times. However, most of them are available on mobile applications only, unsuitable for working in smartwatches. Some of them lack accuracy in calculating the prayer time compared to Umm Al-Qura calendar, the official calendar of the Kingdom of Saudi Arabia. We developed a smartwatch application to generate prayer times identical to Umm Al-Qura calendar. At first, we searched the Internet for the calculation method used in Umm Al-Qura calendar for prayer times. Unfortunately, we did not find the correct calculating method identical to the one adopted by Umm Al-Qura calendar. We have found some sources that provide Umm Al-Qura calculation method, but when tested, we found that they are not identical.

Since the primary goal of this application is that the prayer times should be 100% identical to Umm Al-Qura calendar, and in the absence of an exact and correct Umm Al-Qura calculating method code or API, we have used the lookup table method. We chose the city of Makkah and created a lookup table that includes the five daily prayer times and sunrise times from the beginning of 2022 to the end of 2025. Figure 5 shows screenshots of the application's interface.

Figure 5. Screenshots of "Bangle.js" showing the Prayer Times interfaces.

We got the official prayer times and the Hijri dates from the official Umm Al-Qura calendar website [25]. Then we divided the collected data into four tables, each year having its own table. Each table starts from the first day of that year to the last day of the same year. Thus, we have four tables with ten columns: the Gregorian day of the year, five daily prayer times, sunrise times, and corresponding Hijri dates (day, month, and year). Figure 6 presents a sample of the 2023 lookup table for Makkah prayer times. Figure 7 shows the flowchart of the app. The code is here [26].

```
function  lookupTable2023(x)  {

      day= {
1  : " 05:38 06:58 12:25 03:29 05:50 07:20 8 06 1444 " ,
2  : " 05:38 06:58 12:25 03:30 05:51 07:21 9 06 1444 " ,
3  : " 05:38 06:59 12:26 03:30 05:52 07:22 10 06 1444 " ,
4  : " 05:39 06:59 12:26 03:31 05:52 07:22 11 06 1444 " ,
5  : " 05:39 06:59 12:26 03:32 05:53 07:23 12 06 1444 " ,
6  : " 05:39 06:59 12:27 03:32 05:54 07:24 13 06 1444 " ,
7  : " 05:39 07:00 12:27 03:33 05:54 07:24 14 06 1444 " ,
8  : " 05:40 07:00 12:28 03:34 05:55 07:25 15 06 1444 " ,
9  : " 05:40 07:00 12:28 03:34 05:56 07:26 16 06 1444 " ,
10  : " 05:40 07:00 12:29 03:35 05:56 07:26 17 06 1444 " ,
```

Figure 6. A snippet of the lookup table code for Makkah Prayer Times in 2023.

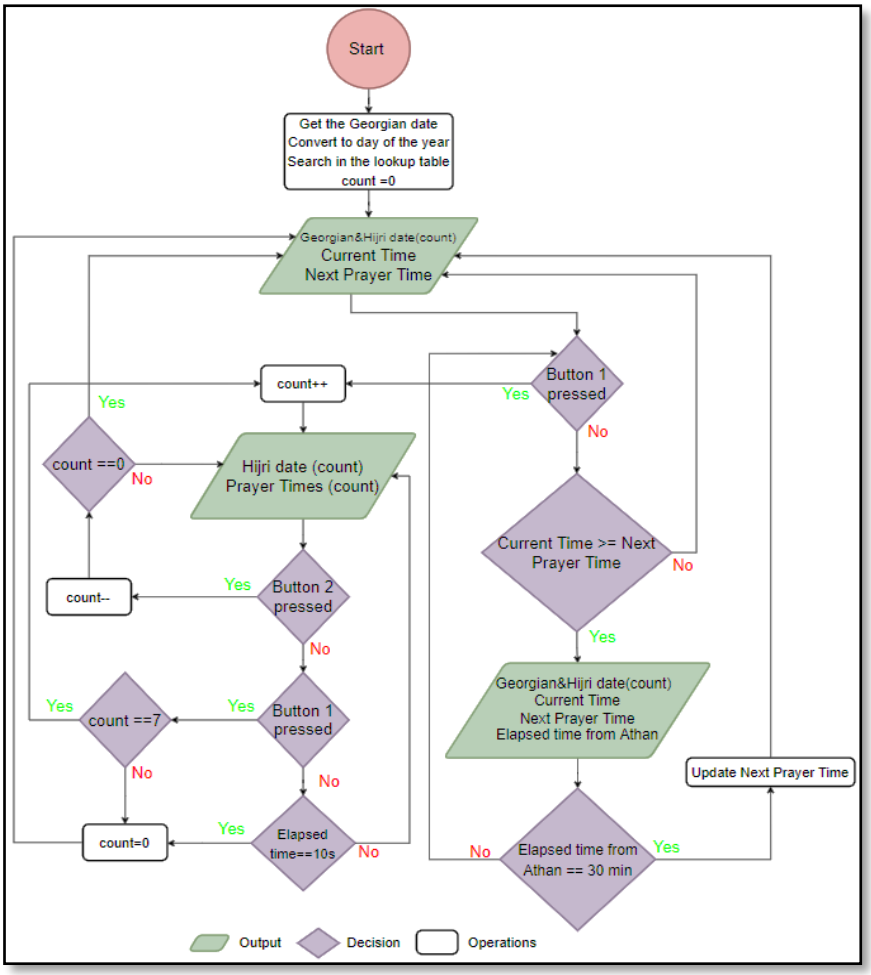

Figure 7. The flowchart of the Athan app.

b. Second Application: (Tawaf Counter)

Tawaf (circumambulation around Kaaba) counter is an application that automatically counts the number of rounds using the smartwatch's GPS sensor. The worshipper will start the Tawaf by setting the starting point. The center of the screen displays the number of rounds, it also displays how far the worshipper is from the starting point. After completing the seven rounds, the app will display "Taqabal Allah" (May Allah accept), indicating the end of Tawaf. As far as we know, no previous work has implemented an automatic Tawaf counter. Figure 8 displays a screenshot of the application's interface when tested in the Holy Mosque.

Figure 8. Screenshots of "Bangle.js" showing the Tawaf counter's interface before and after a round.

In addition, the app can also guide the worshipper to reach known sacred places like Mina, Muzdalifa, and Arafat and inform the worshipper if they are within their sacred boundaries or not. Figure 9 shows how the Tawaf counter works. The green line indicates the starting point, "beginning of Tawaf", which the worshipper determines by pressing the middle button. The grey circle is the range in which the round is incremented on the smartwatch screen automatically every round. It is a circle because the worshipper might reach the end of the Tawaf round from any direction or point as far as they are within less than 30m. The app saves the previous and present destinations to prevent false incrementing while still in the grey circle. Figure 10 displays the app's flowchart. The code is here [27].

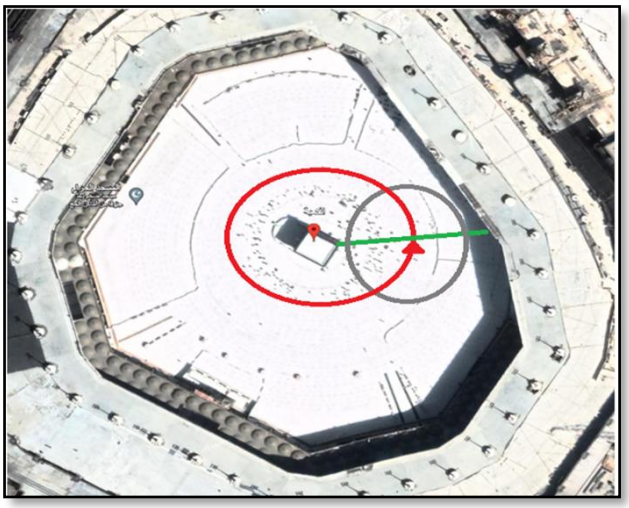

Figure 9. Tawaf counter mechanism.

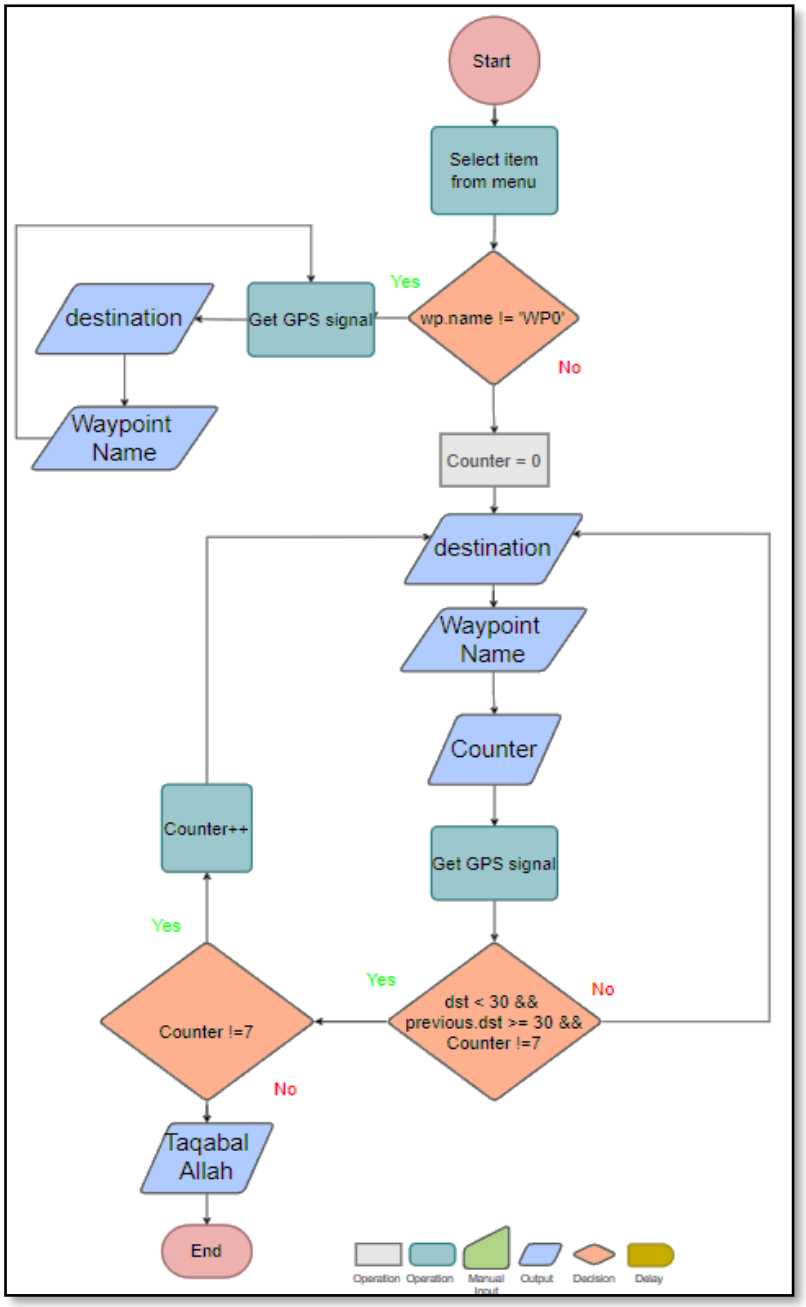

Figure 10. The flowchart of the Tawaf app.

c. Third Application: (Heartbeat Monitor)

The heart rate monitor is another helpful app for the smartwatch, as it allows the heart rate to be read, and a widget record the rates in the background, which helps to determine the health status of the pilgrims and to analyze health indicators based on them, we develop and modify an existing application form “Bangle.js” community app-loader [28]. Figure 11 shows a screenshot of the edited code and the application interface.

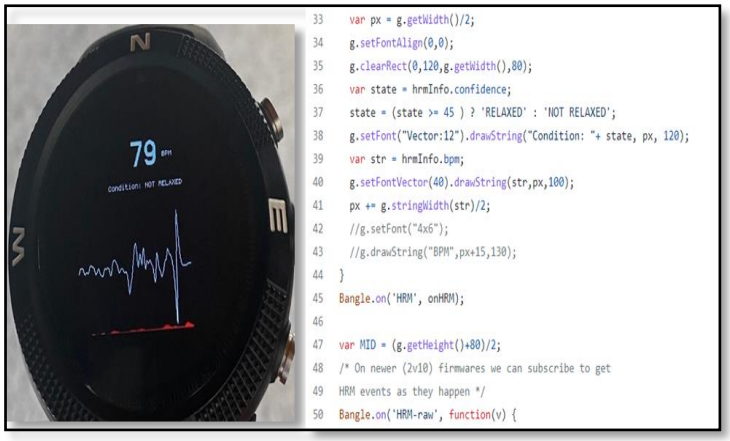

Figure 11. A snippet of the code and the application interface of the Heartbeat Monitor app.

Future work might consider using machine learning to detect whether the pilgrim has a heart attack based on the recorded heart rates in the application and then send an emergency signal to authorities to rescue them as soon as possible. Figure 12 displays the flowchart of the app. The code is here [29].

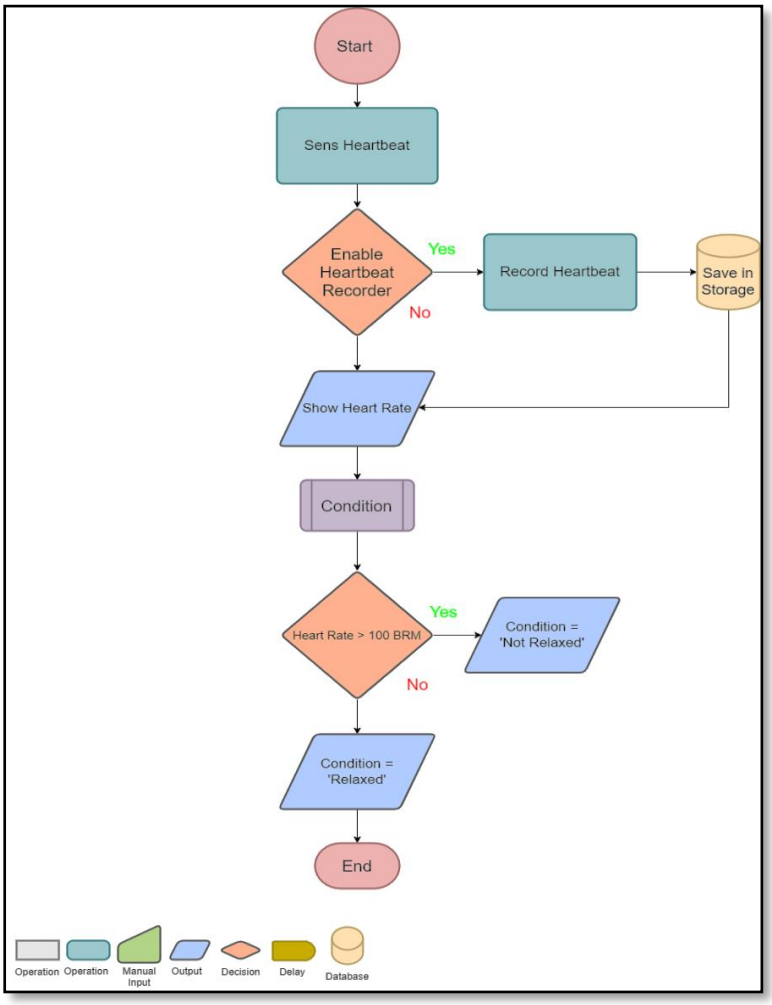

Figure 12. The flowchart of the Heartbeat Monitor app.

d. Fourth Application: (Misbahah)

Misbaha is an application to help the worshipper with Tasbeeh, which resembles the actual dhikr beads. Every 33 counts, the watch beeps to alert the user. Figures 13 and 14 show a snippet of the application code and its flowchart. The code is available here [30].

```
setWatch(() => {
  g.clear();

  counter += 1;
  if(counter==33){
Bangle.buzz(200, 1);


  }
  if(counter==66){
Bangle.buzz(200, 1);


  }
  if(counter==99){
Bangle.buzz(200, 1);



  }


  if(counter==101){

    counter=0;
  }
  updateScreen();
}, BTN1, {repeat:true});
```

Figure 13. A snippet of the code of the Misbahah app.

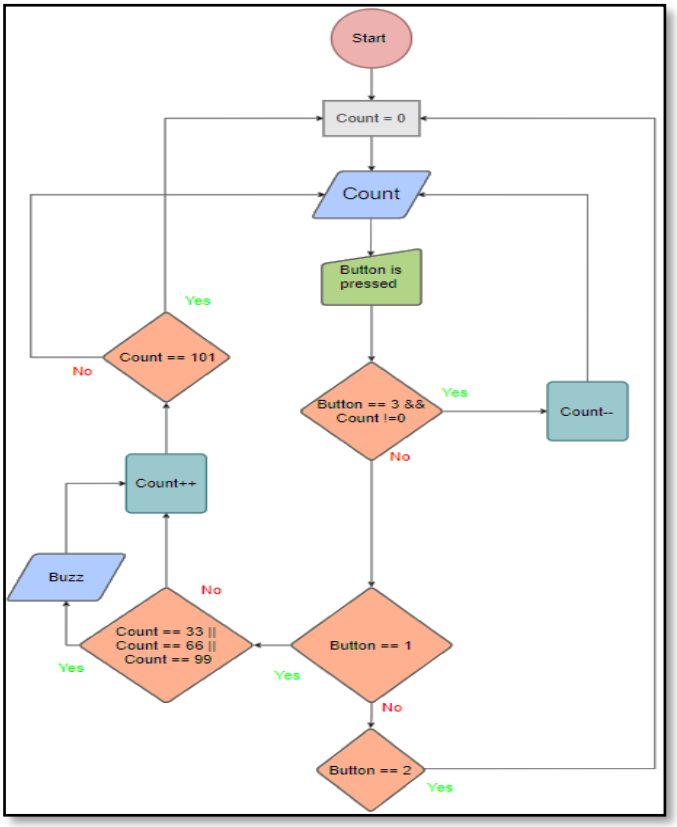

Figure 14. The flowchart of the Misbahah app.

5. Conclusion & Future Work

This paper presented the importance of using smartwatches in Hajj and Umrah. In addition, we mentioned and presented various smartwatches applications, many features, and capabilities that smartwatches could provide in Hajj and Umrah to enhance the pilgrim's experience and facilitate attaining the vision of our country towards digital transformation in Hajj and Umrah. Except for "NUSK" and this effort, no previous work has studied and opened the ground for adopting smartwatches in Hajj and Umrah digital transformation. Although this paper showcases some smartwatch applications, many could be developed dramatically. For example, adding multiple languages to the smartwatch is vital for future work. In addition, updating the prayer times based on the current location automatically is another potential future work.

Regardless of the type and service of the developed applications, smartwatches and internet-of-things gadgets would not only be an accelerator towards digital transformation and enhancing the pilgrims' experience at the Sacred Sites; they would also be a great source of data collection that could help countless organizations managing Hajj and Umrah to make smarter decisions and predict future patterns provided the glory of artificial intelligence and machine learning in particular [31], [32].

This work is part of our capstone project (graduation project) requirement in the Computer Engineering Department at Umm Al-Qura University. We believe that using open-source smartwatches such as "Bangle.js" in microprocessor courses will significantly broaden students' perceptions, skills, and abilities towards creating and developing real-life applications that would put our academic knowledge into practice while enabling a future generation capable of attaining the Saudi Vision 2030 and the fourth industrial revolution.

6. References

[1] "Gartner Forecasts Global Spending on Wearable Devices to Total $81.5 Billion in 2021," *Gartner*. https:// er.com/en/newsroom/press-releases/2021-01-11-gartner-forecasts-global-spending-on-wearable-devices-to-total-81-5-billion-in-2021 (accessed Jul. 15, 2023).

[2] "Smartwatch Market Size, Share & Industry Growth | Analysis - 2027," *Allied Market Research*. https://www.alliedmarketresearch.com/smartwatch-market (accessed Jul. 15, 2023).

[3] "Smartwatch Market Grows 24% YoY in 2021, Records Highest Ever Quarterly Shipments in Q4," *Counterpoint Research*, Mar. 14, 2022. https://www.counterpointresearch.com/global-smartwatch-market-2021/ (accessed Jul. 15, 2023).

[4] "Personal Transformation: Smartwatches | Digital Transformation." https://www.worldscientific.com/doi/epdf/10.1142/9789811214639_0010 (accessed Jul. 15, 2023).

[5] P. C. Verhoef *et al.*, "Digital transformation: A multidisciplinary reflection and research agenda," *J. Bus. Res.*, vol. 122, pp. 889–901, Jan. 2021, doi: 10.1016/j.jbusres.2019.09.022.

[6] "Saudi Arabi: Leadership of Digital Economy in the Middle East." Accessed: Jul. 15, 2023. [Online]. Available: https://www.mcit.gov.sa/sites/default/files/2023-03/MCIT_DEC_23_En_V7.pdf
[7] Falhamid2@, "Employing digital transformation to maximize Hajj services: Automation of decision-making and risk governance," *Okaz*, Aug. 15, 2021. https://www.okaz.com.sa/news/local/2078781 (accessed Jul. 15, 2023).
[8] "Hajj-report.pdf." Accessed: Jul. 15, 2023. [Online]. Available: https://ndu.gov.sa/sites/default/files/2021-09/Hajj-report.pdf
[9] "Pilgrim Experience Program," *Vision 2030*. https://www.vision2030.gov.sa/v2030/vrps/pep/ (accessed Jul. 15, 2023).
[10] A. Aljuwaiber and A. K. Elnagar, "Predicting Pilgrim and Visitor Satisfaction Through Using Smartphone Applications at Holy Sites During Covid-19," *Virtual Econ.*, vol. 5, no. 3, Art. no. 3, Nov. 2022, doi: 10.34021/ve.2022.05.03(5).
[11] "Smartwatch | Fitness Tracking, Wearable Tech & Health Monitoring | Britannica," Jun. 06, 2023. https://www.britannica.com/technology/smartwatch (accessed Jul. 15, 2023).
[12] "Google Trends," *Google Trends*. https://trends.google.com/trends/explore?date=all&q=smartwatch (accessed Jul. 15, 2023).
[13] "SDAIA, DARP & STC Launch Pilgrim's Smart Bracelet (NUSK) The official Saudi Press Agency." https://sp.spa.gov.sa/viewfullstory.php?lang=en&newsid=2259982 (accessed Jul. 15, 2023).
[14] S. M. Alghamdi, A. S. Alsulayyim, J. S. Alqahtani, and A. M. Aldhahir, "Digital Health Platforms in Saudi Arabia: Determinants from the COVID-19 Pandemic Experience," *Healthcare*, vol. 9, no. 11, Art. no. 11, Nov. 2021, doi: 10.3390/healthcare9111517.
[15] "Hajj \ Artificial intelligence applications and technologies make it easier for pilgrims to perform their rituals." https://www.spa.gov.sa/viewfullstory.php?lang=ar&newsid=2262638 (accessed Jul. 15, 2023).
[16] SDAIA [@SDAIA_SA], "سوار الحاج الذكي (نُسك).. خدمة تقنية فريدة؛ لتحسين رحلة الحاج. #سدايا #سوار_الحاج_الذكي #بسلام_آمنين https://t.co/CswwoDxzRw," *Twitter*, Jul. 14, 2021. https://twitter.com/SDAIA_SA/status/1415297816033890309 (accessed Jul. 15, 2023).
[17] إمارة منطقة مكة المكرمة [@makkahregion], "انفوجرافيك تعرّف على #سوار_الحاج_الذكي (نُسك).. # ▼ أحد الخدمات الجديدة التي طورتها #سدايا بالتعاون مع وزارة الحج والعمرة وبرنامج خدمة ضيوف الرحمن https://t.co/4izFTDHEEw," *Twitter*, Jul. 14, 2021. https://twitter.com/makkahregion/status/1415360510036434948 (accessed Jul. 15, 2023).
[18] E. A. Felemban *et al.*, "Digital Revolution for Hajj Crowd Management: A Technology Survey," *IEEE Access*, vol. 8, pp. 208583–208609, 2020, doi: 10.1109/ACCESS.2020.3037396.
[19] A. Aljohani, S. Nejaim, M. Khayyat, and O. Aboulola, "E-government and logistical health services during Hajj season," *Bull. Natl. Res. Cent.*, vol. 46, no. 1, p. 112, Apr. 2022, doi: 10.1186/s42269-022-00801-4.

[20] A. J. Showail, "Solving Hajj and Umrah Challenges Using Information and Communication Technology: A Survey," *IEEE Access*, vol. 10, pp. 75404–75427, 2022, doi: 10.1109/ACCESS.2022.3190853.
[21] "Bangle.js - Espruino." https://www.espruino.com/Bangle.js (accessed Jul. 15, 2023).
[22] "Espruino Web IDE." https://www.espruino.com/ide/ (accessed Jul. 15, 2023).
[23] DaqiqahSW, "Bangle.js App Loader (and Apps)." May 21, 2022. Accessed: Jul. 15, 2023. [Online]. Available: https://github.com/DaqiqahSW/BangleApps
[24] *كيفية استخدام الساعة الذكية #Bangle.js*, (May 28, 2022). Accessed: Jul. 15, 2023. [Online Video]. Available: https://www.youtube.com/watch?v=DfcM5CErpng
[25] "Prayer Times for a city Mecca, 1444." https://www.ummulqura.org.sa/yearprayer.aspx?l=39.83&m=21.42&t=3.00&year=1444&day=27&city=Mecca (accessed Jul. 15, 2023).
[26] "BangleApps/apps/athan at master · DaqiqahSW/BangleApps · GitHub." https://github.com/DaqiqahSW/BangleApps/tree/master/apps/athan (accessed Jul. 15, 2023).
[27] "BangleApps/apps/mguide at master · DaqiqahSW/BangleApps," *GitHub*. https://github.com/DaqiqahSW/BangleApps/tree/master/apps/mguide (accessed Jul. 15, 2023).
[28] "BangleApps/apps/hrm at master · espruino/BangleApps · GitHub." https://github.com/espruino/BangleApps/tree/master/apps/hrm (accessed Jul. 15, 2023).
[29] "BangleApps/apps/hbm at master · DaqiqahSW/BangleApps," *GitHub*. https://github.com/DaqiqahSW/BangleApps/tree/master/apps/hbm (accessed Jul. 15, 2023).
[30] "BangleApps/apps/misbaha at master · DaqiqahSW/BangleApps," *GitHub*. https://github.com/DaqiqahSW/BangleApps/tree/master/apps/misbaha (accessed Jul. 15, 2023).
[31] M. K. Shambour and A. Gutub, "Progress of IoT Research Technologies and Applications Serving Hajj and Umrah," *Arab. J. Sci. Eng.*, vol. 47, no. 2, pp. 1253–1273, Feb. 2022, doi: 10.1007/s13369-021-05838-7.
[32] M. Binsawad and M. Albahar, "A Technology Survey on IoT Applications Serving Umrah and Hajj," *Appl. Comput. Intell. Soft Comput.*, vol. 2022, p. e1919152, Aug. 2022, doi: 10.1155/2022/1919152.

An overview of Utilization of Rice Husk Ash for Sustainable Concrete Manufacturing

Abdul Qadir Bhatti[1*], Muhammad Jahanzaib Khalil[2], Muhammad Aslam[2], Sajjad Ahmad[3]

[1] Department of Civil Engineering, Faculty of Engineering Islamic University of Madinah, Kingdom of Saudi Arabia,
[2] Department of Civil Engineering, School of Engineering & Technology, Institute of Southern Punjab, 60000 Multan, Pakistan
[3] Department of Building & Architectural Engineering, Bahauddin Zakariya University, 60000 Multan, Pakistan

*Corresponding author: Email: draqbhatti@iu.edu.sa Tel: +966530650087

Abstract: The concrete is one of the most important material due to growing construction industry. Due to green building and sustainability requirement and scarcity of natural products, the researchers are investigating the innovative solutions to replace the cement partially with the economical methods. Rice Husk Ash (RHA) which shows an important role during the hydration process of cement which results as: (1) amount of silica in RHA effects the incineration method, time and grinding time; (2) only RHA produced to be as amorphous, generally achieved at burning temperature of between 600-700 ^{o}C; and (3) by applying proper incineration technique RHA can be a partially cement replacement in concrete because of pozzolanic properties of RHA.

Keywords: Mechanism of RHA, Sustainable Concrete, Chemical Composition of RHA, RHA Concrete Mechanical Properties

نظرة عامة على استخدام أرز قشر الرماد لتصنيع الخرسانة المستدام

الملخص: الخرسانة هي واحدة من أهم المواد بسبب صناعة البناء المتنامية. نظرًا لمتطلبات البناء الأخضر والاستدامة وندرة المنتجات الطبيعية ، يبحث الباحثون في الحلول المبتكرة لاستبدال الأسمنت جزئيًا بالطرق الاقتصادية. رماد قشر الأرز (RHA) الذي يظهر دورًا مهمًا أثناء عملية ترطيب الأسمنت والذي ينتج عنه: (1) كمية السيليكا في RHA تؤثر على طريقة الحرق والوقت ووقت الطحن ؛ (2) يتم إنتاج RHA فقط ليكون غير متبلور ، ويتم تحقيقه بشكل عام عند درجة حرارة الاحتراق بين 600-700 درجة مئوية ؛ و (3) بتطبيق تقنية الحرق المناسبة يمكن أن يكون RHA بديلاً جزئيًا للأسمنت في الخرسانة بسبب الخصائص البوزولانية لـ.RHA

1.Introduction

The extensively use of concrete is now a days common material for construction [1]. The advancement in concrete technology are introducing new material for sustainability [2]. The concrete can be manufactured in any shape and using economical solution [3, 4]. The concrete production based on the common materials as cement, fine and coarse aggregates [5]. The concrete is one of the largest contributed construction material in the world [6], It is estimated by different researchers that the construction industry is annually utilizing 9 billion tons aggregates with 1.5 billion tons cement [7]. It is assumed that the cement is most important material then to water and is been used as binding material in huge amount annually [8, 9]. It is approximated that the annually production of greenhouse gas is about 1.35 billion tons from only cement or around 7% of overall gas emissions for environment [10, 11, 12]. Carbon dioxide gas emitted from three main sources during the production of cement [13]. Furthermore, it is reported that approximately, 1.6 ton of natural resources needed to make only 1 ton of cement [14].

The supplementary cementitious material concept is introduced to minimize this problem. The fly ash (FA), RHA, wood ash, bagasse and olive oil ash are agricultural and industrial waste ash which possess pozzolanic properties [15, 16]. Concrete is produced using cementitious material which is started to lower the cost and the rate of production of cement, overcome the adverse effects of OPC and utilize the industrial and agriculture waste materials which were providing injurious to atmosphere [17]. The various concrete properties and mortar such as resistance to cracks, strength, durability, workability and permeability is improved with use of cementitious material. Further, the adding industrial waste resulted in the producing concrete high-performance [17]. These products can be potential to increase concrete performance because of their reaction with pozzolanic and micro filler [18]. Different concrete mixes are improved with the replacement of different pozzolanic admixtures, which increase various concrete properties as microstructure and results in the reduction of calcium hydroxide concentration through a pozzolanic reaction [19].

This paper is arranged in sections in which section two defines origin of RHA and the different temperature effect on the structural RHA characteristics. Section three and four describes the physical and chemical RHA characteristics. Section five presents reaction RHA mechanism. Section 6 summarizes on fresh concrete at various level of Rice Husk Ash. Section seven summarizes RHA utilization as cement ingredient for various concrete types such as ultra high performance concrete (UHPC), high and normal strength concrete. Additionally, it is considered that realistic mathematical expression obtained by using all the possible testing results of RHA in the mixes to provide ease for obtaining the hardened concrete properties without performing any tests. The review on various RHA concrete characteristics as modulus of elasticity and absorption water in section 8, 9 and 10. A roadmap to use RHA and recommended further research regarding the usage of RHA are presented. Recent breakthroughs in low-cost materials developed using waste products that can be used to develop carbon captured concrete is also shows that RHA is one of the cement replacement constituent material [122, 123].

2.Origin of RHA

The agricultural waste such as rice husk material which comprises about 20% rice mass. It includes 15-20% of silica, 50% cellulose, 25-30% lignin [20]. There are most important three biomasses come from rice, bran, straw and shell [21]. Rice Husk (RH) is cover of white seed having large silica [21]. Incineration process of rice husk produced from open air incineration on the ground (about 1970s) to ignition applying liquidized layers technique (around 1990s) [22]. Silica content in the ash is found to be increases with higher the burning temperature [23]. It may also improve the fresh state characteristics of concrete such as workability, slow done the hydration process, increase strength at longer ages and reduce permeability [24]. Furthermore, the use of RHA reduces the cement requirement in the civil construction engineering work, decreases charges for production of concrete and minimize negative impact on environment which produced due to CO_2 emissions through the cement production [25, 26]. It is approximated that 200 kg Rice Husk produce from 1 ton of rice grain and about 40 kg Rice Husk or 20 percent RHA when rice husk is burnt at specific temperature [27]. As per food and agriculture organization (FAO) of UN (2018), the annual world rice production for 2017 was estimated by 759.6 million tons (503.9 million tones, milled basis) [28], and rice husk contribute around 20% of it [29]. The disposal of rice husk has been very challenging universally because of huge amount of residual ash resulting from improper burning [30]. As RHA have pozzolanic nature, so utility of this waste may provide safe environment easy disposal of RHA. Due to its potential ability to enhance the concrete properties through their pozzolanic and filling ability RHA will be recommended to use it in concrete [31].

The chemical composition of RH is depending on different factors such as climate, geographical conditions and variances in the paddy type [29]. The samples of RHA and RH are shown in Fig. 1.

Fig. 1. a) Rice Husk [32], b) Burnt RHA [33] and c) burning of husk at about 700°C for 6 hours and wet grinding for 80 minutes [34]

2.1. Combustion of Rice Husk

Rice Husk Ash is a ash obtained by incineration of RH either controlled or open field incineration in which burning time and temperature is controlled. On the field incineration method produces weak quality RHA. Furthermore, open field burning of RH always leads to the production of silica ash, which differs from gray color to black

depending on unburned carbon content and inorganic impurities [34]. By uncontrolled incineration less than 500°C temp- the burning of rice husk is not completed and consequences of this the specific content of unburnt carbon is left in developing ash [35], excessive amount of carbon which negatively affect concrete performance and also form crystalline silica that is of minimal reactivity [36]. Dolage et al. [37] described that when carbon content is more than 30% was expected to minimize the RHA pozzolanic reactivity, rice husk ash quality is adjusted by ignition treatment to produce amorphous silica that is important for concrete structure [38]. Ignition rice husk using adjusted incineration below 800 °C temperature will return silica in ash [39, 40].

In addition, the pozzolanic reactivity is linked to area of ash's particles [41]. Mehta and Nair et al. [42, 43] also said ash is produced at burning temp of 550 to 800 °C and variation appears from amorphous to crystalline shape at about 800 to 900 °C temperature. Other researchers revealed that duration is important factor for burning the rice husk to make suitable ash [44, 45]. Nair et al. [43] described that lower temp- long period or higher temp- short duration will result in the production of amorphous ash. Therefore, it is mandatory to confirm that silica inside rice husk ash is amorphous form which is produced via adjusted burning process.

Different researchers worked to determine the burning temp- effects on specific surface area and structure of the RHA as checked from Mercury Intrusion Porosimetry, Scanning Electron Microscopy (SEM), X-Ray Diffraction, and Back-scattered Electron Image (BSE), values are mentioned in Table 1. [46, 47, 48]

Table 1. Burning Temperature Effect on the Structure of Rice Husk Ash [25, 36, 49, 50]

Temperature	Structure of RHA	Specific Surface Area (m^2/g)
Till 500 °C	Particles are spherical, globular form or with porous shape	0.5 – 2.1
500 – 600 °C	Particles are partially non-crystalline and crystalline	76 – 122
600 – 700 °C	Particles are amorphous, and diameter of pores is maximum	100 – 150 at low temperature
700 – 800 °C	Partly crystalline	6 – 10
800 – 900 °C	Crystalline	< 5
900 -1000 °C	The development of coral formed crystals increased, gradually finer & melted significantly.	-

3.Chemical Properties

The chemical characteristics of RHA to ensure that when it replaced with cement in concrete using it behaves properly. Hardened concrete rest on many factors such as chemical composition of material, water-cement ratio, cement content, type of cement, ,

quality of filler material and control of quality for the period of production of concrete etc. Based on an assessment of the chemical compositions shown in Table 2. The CaO content of ordinary Portland cement and RHA is within range of about 59 to 66% and 0.08 to 1.58%. Therefore the OPC have higher amount of calcium oxide as compared with mineral admixtures. Note that the proportion of SiO_2 in RHA is 67.30-95.04 %, the reaction of RHA is assessed by SiO_2 content in RHA. It is concluded that silica is the compound that may responsible for the strength development in RHA concrete [43]. If RHA is used during the production of concrete, which have the ability to participate the strength process. It is noted that the sum of SiO_2 + Fe_2O_3 + Al_2O_3 go beyond 70% for all the RHA cases and summarized that the RHA has similar composition as fly ash of Class F (ASTM C 618) with great pozzolanic reactivity [51, 52, 53, 54].

Table 2. RHA and Ordinary Portland Cement Chemical Characteristics

Elements		**OPC**	**RHA**
Calcium oxide	CaO	58.51-66.28	0.08-1.58
Silica dioxide	SiO_2	19.80-23.50	67.30-95.04
Ferric oxide	Fe_2O_3	2.50-11.38	0.16-2.86
Sulphur trioxide	SO_3	1.40-3.30	0.01-1.21
Graphite	-	-	4.77
Aluminum oxide	Al_2O_3	4.51-6.90	0.15-4.90
Magnesium oxide	MgO	0.22-3.13	0.21-1.81
Phosphorous pentoxide	P_2O_5	0.05-0.26	0.25-60
Potassium oxide	K_2O	0.22-1.10	0-3.68
Manganese trioxide	Mn_2O_3	0.17	-
Natrium oxide	Na_2O	0.10-2.72	0.05-3.56
Titanium dioxide	TiO_2	-	0.01-0.15
Manganese oxide	MnO_2	-	0.14-0.16
Chloride	Cl	0.06	-
LOI	-	0.51-5.68	0.51-18.25
References		[27, 29, 55-66]	[20, 29, 56, 57, 59-77]

4.Physical properties

The comparison of OPC and RHA mentioned in Table 3 [78, 79, 80]. The color of RHA is grey, black or dark grey. Color variations have directly linked with the completeness of the incineration process as well as unburned carbon and silica content in ash [35, 82, 83].

Table 3. Physical RHA characteristics and OPC

Physical properties	OPC	RHA
Color	Grey	Grey, Black dark grey
Particle size	22.5	7 – 42
Shape of Particle	-	Not regular
Sp Gravity	2.9 – 3.15	2 – 2.4
Fineness passing 45 microns	93%	70 – 99%
Loose Bulk density (g/cm^3)	1.16	0.40
Compacted Bulk density (g/cm^3)	1.56	0.49
Specific surface area Blaine (m^2/kg)	309 – 373	376 - 1620
Soundness (mm)	1 – 9	-
References	[24, 27, 35, 37, 42, 58-60, 67, 84-90]	[22, 24, 27, 35, 37, 42, 59, 64, 65, 67, 70, 85, 87, 90-95]

5.Reaction Mechanisms of RHA

A pozzolanic reaction starts only when aluminous/siliceous components of RHA react with $Ca(OH)_2$ (calcium hydroxide) in the presence of moisture to form compounds having good adhesive properties. OPC is made up of four principal mineralogical phases symbolically represented by C_3S, C_2S, C_4AF and C_3A. During the hydration process of cement's components (C_3S and C_2S) the CSH (gel) and CH (lime) are produced [96].

For C_3S:

$$2(3CaO.SiO_2) + 6H_2O \longrightarrow Primary\ 3CaO.2SiO_2.3H_2O + 3Ca(OH)_2 \quad (1)$$

For C_2S:

$$2(2CaO.SiO_2) + 4H_2O \longrightarrow primary 3CaO.2SiO_2.3H_2O + Ca(OH)_2 \quad (2)$$

The $3CaO.2SiO_2.3H_2O$, (C-S-H) is known as gel, is the main strengthening ingredients that produced during the hydration of C_3S and C_2S component as can be seen in equations (1) and (2). C-S-H is a glue that binds the filling particles together and provides concrete its strength, while $Ca(OH)_2$ causes small contribution to the strength development [97]. Furthermore, the Pozzolanic activity of RHA be governed by silica content, silica in amorphous or crystalline phase, surface area and size of the particles [98]. The Reactions that occur during the production of RHA concrete are; first the Silicon incinerated in the presence of oxygen produce silica [27].

$$Si + O_2 \longrightarrow SiO_2$$

The secondary reaction starts only when this silica gets in touch with $Ca(OH)_2$ which released during the hydration of cement, resulting in the production of calcium silicate hydrate.

$$SiO_2 + Ca(OH)_2 + H_2O \longrightarrow Secondary\ CaO.SiO_2.H_2O$$

This reaction decreases the $Ca(OH)_2$ content in the concrete. The weak calcium hydroxide does not participate to strength [27]. The pozzolanic reaction, fills the pores in concrete making the microstructure of the concrete denser and improves the interfacial bond among filler and binder materials and thus the durability, strength and transport properties of the concrete are enhanced [99].

where:

$2CaO.2SiO_2$	=	C_2S, Dicalcium silicate
$3CaO.2SiO_2$	=	C_3S, Tricalcium silicate
$3CaO.2SiO_2.3H_2O$	=	(C-S-H gel), Calcium silicate hydrate

6.Fresh Properties of Concrete

6.1. Compaction Factor (C.F)

The compaction factor results for the different concretes having RHA as cement replacement are shown in Table 4. The workability of concrete usually evaluates the behavior of concrete in the fresh form from mixing up to the compaction. The terms transportability, mix-ability, mould ability and compact-ability mutually indicate the workability of concrete. Various researchers had performed different tests to examined the workability of concrete and also studied the effects of RHA on fresh properties of concrete [6]. Kishore, Bhishma [27] in their studies concluded that the bulk density decreases as the amount RHA increases. Therefore, value of compaction factor is minimum at higher amount of replacement. Krishna, Sandeep [80] in their studies about use of RHA as cement replacement, revealed that the compaction factor reduces as the amount of RHA increases. Abhijith, Anjali [100] also assessed the influence of RHA on the properties of concrete prepared at various %age replacement of RHA with cement. The results demonstrated that the C.F values get reduced with the increasing of rice husk ash ratios. Authors reported that the compacting factor values decreased from 0.91- 0.79 as the percentage replacement of RHA increased from 0% - 25%. Kachwala, Pamnani [101] in their studies reported the same as the previous authors that the compacting factor values become reduced with the increasing of rice husk ash content. Further they described that the its values decreased from 0.92 - 0.88 with 5% - 25% RHA content. They concluded that presence of RHA causes to decrease the workability of concrete. Hence higher amount of water or super-plasticizing admixture is needed to get more workability.

Obilade [102] have evaluated the properties of RHAC. The results demonstrated that the bulk density of concrete get decreased at higher replacement levels of RHA. This might be recognized to the increase in air voids in the concrete specimens as the amount of rice husk ash increases.

Table 4. Compaction factor of Rice Husk Ash concrete

RHA %	**Compaction Factor**					
0	0.87	0.87	0.882	0.91	0.92	0.91
5	0.86	0.83	0.866	0.85	0.91	0.91
10	0.82	0.81	0.782	0.84	0.90	0.90
15	0.80	0.80	0.661	0.83	0.89	0.90
20	-	-	0.601	0.82	0.88	0.89
25	-	-	-	0.79	0.88	0.88
Mix Proportions	1:0.83:2.53	1:0.78:2.36	1:1.64:3.41	1:1.34:3.16	M20	1:2:4
w/b	0.36	0.35	0.55	0.50	-	-
References	[27]		[80]	[16]	[101]	[102]

6.2. Workability

The RHA effect on workability is shown in Table 5 [79, 18, 103]. Gaesan, Rajagopal [35] have examined the RHA as cement replacement. In their study 5-35% RHA is substituted by cement weight. Authors concluded that slum increases up to 10% RHA replacement further the percentage of RHA increases, the workability reduces.

Padhi, Patra [86] experimented the influence of RHA on the concrete workability. The results showed that the presence of RHA reduced the workability of the concrete. This decrease in slump values increased as RHA amount increased. Madandoust, Ranjbar [24] have analyzed the effects of RHA as cement replacement (5%, 10%, 15%, 20% and 25%) on concrete properties. Authors revealed that the slump value of concrete decreases with the replacement of RHA by cement. Abhijith, Anjali [100] explored the influence of RHA as cement replacement on workability 0%, 5%, 10%, 15%, 20%, and 25% RHA replaced with cement. Results showed that the slump value decreased from control mix to 25% addition of RHA. Krishna, Sandeep [80] have carried out research on RHA concrete.in their study they substituted up to 20% of cement by RHA. The authors described that the addition of RHA in concrete caused to a decrease in workability, which rest on the RHA amount. Further they revealed that this reduce in slump value is due to the absorption of water by admixture particles.

Kishore, Bhishma [27] experimented on the effects of RHA replacement by cement on concrete workability. It was observed that the concrete workability decreases by 27% when the amount of RHA increases. Aleem, Istehsan-ur-Rahim [31] carried the experimental work on the properties of concrete containing RHA as partial replacement of cement. The RHA replaced with cement at the rate of 5 - 15%. They performed the slump test to check the concrete workability, results showed that the slump value of concrete is 72 mm at 20% replacement and the normal concrete workability is 76 mm.

Table 5. Slump of RHA Concrete

RHA %	**Slump (mm)**

0	98	73	65	112	65	40	35	76
5	106	70	60	98	55	37	32	80
10	115	64	55	95	32	35	29	75
15	91	58	55	92	14	32	27	72
20	81	54	56	86	6	-	-	-
25	74	50	50	82	-	-	-	-
30	64	46	45	-	-	-	-	-
35	41	42	-	-	-	-	-	-
40	-	-	-	-	-	-	-	-
Mix Proportions	1:1.50:3.00	1:1.51:2.93	1:2.13:2.40	1:1.34:3.16	1:1.64:3.41	M40 1:0.83:2.53	M50 1:0.78:2.36	-
W/b	0.53	0.45	0.53	0.50	0.55	0.36	0.35	-
References	[35]	[86]	[24]	[100]	[80]	[27]		[31]

6.3. Density

Mass per unit volume of concrete is known as density. It is a main factor in the evaluation of porosity, determination of strength and durability [81]. The influence of different percentage of RHA are shown in Table 6. Padhi, Patra [86] performed the experiment on the Risk Husk Ash concrete. They substituted up to 35% cement by RHA. The results demonstrated that the density of control mix is 2420 kg/m^3 which reduces to 2190 kg/m^3 with the 35% RHA replacement. Madandoust, Ranjbar [24] examined the effect of different percentage of replacement of cement by RHA on density of concrete. The concrete made with several content of RHA (0-30%) as cement replacement. The authors reported that there is no significant variation in density is observed when compared with normal concrete.

Further investigation by Kachwala, Pamnani [101] described that the bulk density of concrete decreased when amount of RHA increased. Obilade [102] Made concrete containing up to 25% of RHA. They revealed that the density of normal concrete mix is 2430 kg/m^3 which decreases to 2280 kg/m^3 with 25% of RHA.

Table 6. RHA Concrete Density

RHA (%)	Density (kg/m³)			
Mix Proportions	1:1.5:2.9	1:2.1:2.4	M20	1:2:4
Water to cement ratio	0.45	0.53	-	-
0	2418	2346	2430	2430
5	2410	2345	2330	2330
10	2390	2345	2300	2300
15	2370	2346	2300	2300
20	2320	2342	2280	2290
25	2280	2342	2270	2280
30	2140	2345	-	-
35	2190	-	-	-
References	[86]	[24]	[101]	[102]

7.Concrete Mix proportion

7.1. Normal Strength Concrete (20-45 MPa) Using RHA

Paramveer et al. [84] investigated on RHA concrete. In their study the RHA used to substitute the cement by weight at the rate of 5-20%. The results showed that Compressive strength increased by 2.1% at 5% replacement as compared with referral mix for M40 concrete grade and then decreased with the increment of RHA percentage.

Akeke et al. [104] have evaluated the influence of RHA as cement replacement on the strength of concrete. The RHA was replaced by cement at the rate of 10%, 20% and 25%. Authors concluded that 25% replacement gave the maximum compressive strength. Anwara et al. [105] directed the investigational work on RHA concrete. 10-20% RHA used as cement replacement. The test results demonstrated that the compressive strength of the concrete decreased by the influence of RHA. Kishore et al. [27] have investigated to study the influence of RHA on the concrete strength for M40 and M50 concrete grade. In their study the RHA replaced with cement (on the mass basis) at the rate of 0%, 5%, 10% and 15% [80]. In their work 0 to 20% RHA has been introduced as cement replacement, result showed that the 28-days strength increased from 27MPa to 29.3MPa with addition of 10% RHA. It is also detected that the compressive strength increased gradually, up to nearly 10% replacement and then reduced. Siddika et al. [91] experimented the influence of RHA as cement replacement on the hardened properties of concrete. 0%, 10% and 15% RHA is used as a replacement of cement. W/B was kept 0.4, 0.5 and 0.6. From their investigation, concluded that compressive strength of the concrete decreases by the influence of RHA.

7.2. High Strength Concrete (45-85 MPa) Using Rice Husk Ash

Padhi et al. [86] researched the individual effect of RHA replacement on the strength of concrete. The cement was changed by RHA at rate of 0% (control mix), 5%, 10%, 15%, 20%, 25%, 30% and 35% (by weight) in concrete. The authors concluded the same as previous authors that the percentage of RHA increases the strength of the concrete decreases. Bhushan et al. [92] evaluated the best replacement of RHA for M20 concrete. Results showed that the compression strength of the concrete mix increases with the

replacement of RHA up to 10% afterward the gradually reduce in strength is noted. Kirti et al. [32] substituted up to 20% of RHA by cement weight. The test results described that the maximum 28 days compressive strength observed at 5% RHA.

Gaesan et al. [35] have worked to examined the optimum replacement of RHA as cement replacement for M25 concrete grade. The cement was substituted by RHA at rate of 0% (control mix), 5%, 10%, 15%, 20%, 25%, 30% and 35% (by weight) in concrete. The test results demonstrated that the 20% replacement is an optimum replacement for M25 mix and at 30% RHA, the strength of RHAC with 30% RHA replacement attained values more than to the referral concrete specimens. Tashima et al. [88] have experimented the effect of utilization of RHA as cement replacement on the concrete strength. in their study up to 15% RHA is substituted by cement weight. The results demonstrated that the optimum strength was attained at 5% replacement. Madandoust et al. [24] assessed the impact of different proportion of RHA by cement on compressive strength of concrete. The RHA was replaced by cement at the rate of 5%, 10%, 15%, 20%, 25% and 30%, results demonstrated that at early age testing, the compressive strength of referral mix is higher than other concrete mixes having different percentage of RHA.

Abhijith et al. [100] examined suitability of RHA replacement on the concrete strength. The cement is replaced by RHA at rate of 0% (control mix), 5%, 10%, 15%, 20% and 25% (by weight) in concrete. The experimental results described that the maximum compressive strength attained at 20% replacement and the compressive strength at 25% replacement is more than the referral mix. Abalaka et al. [30] assessed the hardened RHA characteristics concrete prepared with different replacement of RHA at different water cement ratios of 0.35 and 0.3. A partial replacement of 5%, 10%, 15% and 20% RHA by cement were studied. The Experimental results describes the maximum 28days compressive strength observed at 5% replacement is 55.5MPa and 59.9 MPa at water to binder ratios 0.35 and 0.3 respectively. Therefore, 5% RHA seems to be the optimal limit. Zareei et al. [106] made concretes containing up to 25% RHA. The results demonstrated that although the best percentage of replacement is 20%, the concrete with 25% RHA has a more compressive strength to the referral one.

Sensale et al. [87] researched the hardened of concrete in which the RHA was replaced 10-20% by weight of cement and three different water-cement ratios (0.32, 0.40, 0.50), were used. Based on results, 10% RHA is observed as optimum percentage replacement at both waters to binding ratios of 0.5 and 0.4. and 20% RHA is observed as optimum replacement at 0.32 water to binding material ratio. Zhang et al. [81] demonstrated that the concrete strength at 10% RHA content is greater than the referral concrete mix. Suman et al. [23] investigated to examine the optimum replacement of RHA for M20 concrete grade mix. A partial replacement of 5%, 10%, 15% and 20% by cement were studied. Authors reported that 15% is an optimum replacement for M20 concrete grade. Giaccio et al. [89] assessed the properties of concrete at 10% replacement of RHA by cement and four different water to binder ratios (0.28, 0.32, 0.4, 0.5), were used. The

authors reported the same as previous authors, in that 10% RHA content contributed the maximum compressive strength.

Nirubha et al. [93] concentrated to produce an economic concrete by substituting the cement with RHA at the rate of 10% - 20%. The authors expected that the optimum utilization of RHA for M60 concrete grade is as 10%. Bawankule et al. [1] made concretes containing up to 15% of RHA. Authors reported the same as previous authors that the compressive strength of the concrete decreases by the influence of RHA. Ephraim et al. [107] investigated to assess the compressive strength of RHA concrete. 0- 25% RHA is used as cement replacement.

The results demonstrated that the compressive strength of the concrete at 28days of curing is 38.4 MPa, 36.5 MPa and 33.0 MPa with 10%, 20% and 25% replacement respectively. The strength of the referral concrete mix is 37 MPa. The authors concluded that 10% replacement gave the maximum compressive strength.

Rambabu et al. [108] investigated to analyze the optimum replacement of RHA for M35 concrete grade mix. A partial replacement of 5%, 6%, 7%, 8%, 9% and 10% RHA by cement were studied. The authors suggested that the 6% is an optimum replacement for M35 concrete grade. Bangwar et al. [109] examined the individual effect of RHA replacement on the strength of concrete. In their research 0%, 2.5%, 5%, 7.5% 10%, 12.5% and 15% of RHA has been used as cement Replacement. Mahmud et al. [110] conducted research to produce M80 grade concrete in which RHA is replaced with 15% of weight of cement. The compressive strength with 10% Rice Husk Ash content is greater with all the mixes. The authors suggested that it is efficient to use 10% RHA for Mega structures. Kumar et al. [111] employed up to 30% cement by RHA at variuos w/c ratios. The author suggested same as previous authors that the %age replacement of cement by RHA enhance will result in the decreases of concrete strength.

Obilade [102] examined the individual effect of RHA on concrete strength. This study cement is replaced with 5%-25% RHA. From the test results the compressive strengths of concrete reduces with RHA content. Sundararaman et al. [112] explored the use of various %age of replacement RHA by cement in concrete. In their study RHA replaced in the with 25%, 20%, 15%, 10% and 5% with weight of cement and 10% silica fume for M20 concrete. Authors reported similar as other authors, in which 10% RHA content contributed with highest compressive strength, beyond 10% replacement reduce in strength is observed. Naveen et al. [113] have assessed the effect of RHA as cement substitute of concrete compressive strength. RHA was partially replaced at different percentage (20%, 15%, 10%, 5% 0%) by cement weight.

The authors expected that the optimum utilization of RHA for M30 and M60 concrete grade is as 10%. Investigation results performed by various researchers are given in Table 7.

7.3. UHPC using Rice Hush Ash

Van Breugel, K. and Y. Guang. [118] examined produce UHPC using RHA. It was specified that RHA contributes highly to long term development of UHPC compressive strength after 28 days [114, 115, 116, 117]. It was reported that the compressive strength of UHPC enhanced to 12 % and 18% at 28 and 91 days respectively, as the percentage RHA replacement to 20%. Van Tuan et al. [119] examined the flexibility to produce UHPC using RHA. Results described that the UHPC compressive strength containing RHA, could achieve more than 150 MPa with normal curing method. Additionally, this achievement was even greater than samples with silica fume (SF). Furthermore, investigation conducted by ößler, C., D.-D. Bui and H.-M. Ludwig., [120], revealed that the sample containing 10% of SF and 10% RHA substituted with cement showed better compressive strength than control sample. The RHA with higher average particle size attains lesser compressive strength than the minimum mean particle size. Nguyen [121] have suggested the mean particle size of RHA to be used in UHPC vary between 3.6µm-9µm which will be combined with cement. However, Van Tuan, N., et al. [119] studied that the packing density of UHPC with particle sizes of RHA ranging from 3.6µm-5.6µm at 20% replacement of OPC give the best results in comparison to the UHPC containing SF. Nguyen V [121]

Table 7. Different Replacement levels of RHA for Hardened Properties of Concrete

`RHA (%)	Mix proportion	w/b ratio	SP (%)	Compressive strength (MPa)		28-day splitting tensile strength (MPa)	28-day flexural strength (MPa)	References		RHA (%)	Mix proportion	w/b ratio	SP (%)	Compressive strength (MPa)		28-day splitting tensile strength (MPa)	28-day flexural strength (MPa)	References
				28 days	90 days									28 days	90 days			
0	M40 1:1.82:2.77	0.4	0.5	47.4	-	3.2	4.9	[84]		10	1:1.5:3.0	-	-	22.0	-	1.9	3.0	[104]
5			0.5	48.5	-	3.3	5.5			20			-	20.0	-	1.2	2.5	
10			1.0	46.8	-	2.7	4.7			25			-	29.0	-	0.9	2.5	
15			1.0	40.5	-	2.6	3.9			0	M20 1:1.59:2.075	0.4	-	30.30	-	3.91	-	[112]
20			1.0	33.8	-	2.2	3.1			5			-	31.50	-	3.12	-	
0	1:2.41:2.44	0.6	-	31.1	33.4	3.1	4.8	[105]		10			-	34.20	-	3.32	-	
10			-	24.6	30.6	2.8	4.4			15			-	23.00	-	2.83	-	
20			-	20.5	27.0	3.4	4.4			20			-	20.20	-	2.78	-	
0	M40 1:0.83:2.53	0.36	-	50.8	51.7	4.2	4.9	[27]		0	1:1.64:3.41	0.55	-	27.0	-	2.2	2.1	[80]
5			-	48.2	49.1	4.0	4.4			5			-	24.8	-	2.3	2.5	
10			-	44.7	47.0	4.0	4.3			10			-	29.3	-	2.5	1.9	
15			-	43.1	45.0	4.0	4.1			15			-	17.6	-	2.1	-	
0	M50 1:0.78:2.36	0.35	-	59.4	62.5	4.2	5.3			20			-	16.0	-	2.0	-	
5			-	56.4	58.3	4.6	4.9			0	1:1.51:2.93	0.45	0.90	41.0	-	2.9	4.1	[86]
10			-	53.4	56.4	4.2	4.7			5				39.5	-	2.8	4.0	
15			-	50.5	52.5	4.2	4.7			10				38.7	-	2.6	3.9	
0	1:1.6:2.61	0.4	-	35.6	-	4.8	5.2	[91]		15				37.1	-	2.5	3.8	
10			-	35.0	-	4.5	4.9			20				32.3	-	2.2	3.5	
15			-	31.0	-	4.2	3.9			25				28.9	-	2.1	3.3	
0	1:1.65:3.40	0.5	-	31.7	-	4.7	5.1			30				25.6	-	1.9	3.1	
10			-	30.9	-	4.2	4.7			35				21.2	-	1.6	2.7	
15			-	28.6	-	3.9	3.9			0	M20	0.50	-	34.5	-	2.9	4.5	[92]
0	1:2.028:4.19	0.6	-	29.4	-	4.4	5.0			5			-	36.2	-	3.4	4.6	
10			-	28.8	-	4.0	4.1			10			-	34.8	-	3.0	4.5	
15			-	26.0	-	3.5	3.6			15			-	27.2	-	2.4	3.5	
0	1:1.33:2.27	0.42	-	48.10	58.3	5.37	-	[88]		20			-	19.2	-	2.0	2.2	
5			-	60.40	62.00	5.79	-			25			-	14.5	-	1.9	1.8	

10			-	54.20	60.90	5.78	-			-	-	-	-	-	-	-	-	-
0	1:1.51:3.06	0.50	-	30.6	-	4.0	-	[32]		0	M25 1:1.5:3.0	0.53	-	37.1	38.3	4.5	-	[35]
5			-	31.5	-	4.1	-			5			-	40.0	43.3	4.7	-	
7.5			-	31.1	-	3.6	-			10			-	41.3	44.8	4.8	-	
10			-	30.7	-	3.3	-			15			-	41.8	45.7	5.0	-	
12.5			-	30.1	-	3.0	-			20			-	42.5	46.0	5.1	-	
15			-	25.3	-	2.0	-			25			-	38.8	43.0	4.7	-	
0	1:2.13:2.40	0.53	0	35.4	-	3.3	-	[24]		30			-	37.6	38.7	4.5	-	
5			0.95	33.6	-	-	-			35			-	35.1	37.2	-	-	
10			0.98	32.4	-	-	-			0	1:1.34:3.16	0.50	-	22.2	-	3.2	-	[100]
15			1.04	32.1	-	-	-			5			-	24.3	-	3.3	-	
20			1.07	30.8	-	3.0	-			10			-	28.6	-	3.4	-	
25			1.11	29.7	-	-	-			15			-	29.6	-	3.6	-	
30			1.15	26.6	-	-	-			20			-	33.5	-	3.9	-	
0	1:0.864:2.46	0.30	1.57	49.5	50.0	-	-	[30]		25			-	29.9	-	3.5	-	
5			1.26	55.5	59.0	-	-			0	1:1.875:2.1	0.4	3.75	83.4	-	5.83	-	[106]
10			1.32	53.0	60.0	-	-			5				85.1	-	5.95	-	
15			1.38	54.3	57.7	-	-			10				86.9	-	6.1	-	
20			1.32	48.3	51.2	-	-			15				92.5	-	6.47	-	
0		0.35	1.26	52.7	61.7	-	-			20				93.3	-	6.52	-	
5			1.26	60.0	66.5	-	-			25				89.1	-	6.23	-	
10			1.23	52.0	56.4	-	-			0	1: 1.75: 2.86	0.4	0.77	36.4	-	2.70	6.30	[81]
15			0.94	50.4	55.9	-	-			10			1.40	38.6	-	3.50	6.80	
20			0.94	38.2	40.6	-	-			0	1:1.40:1.96	0.28	2.00	63.10	-	-	7.60	[89]
0	1:1.29:1.97	0.32	0.40	55.5	60.60	3.63	-	[87]		10			2.05	63.60	-	-	7.60	
10			0.20	60.4	64.30	3.57	-			0	1:1.71:2.24	0.32	1.20	54.60	-	-	5.80	
20			0.20	54.8	62.70	3.34	-			10			1.88	56.60	-	-	6.10	
0	1:1.875:2.10	0.4	0.10	42.3	45.60	-	-			0	1:2.00:2.48	0.40	0.90	46.20	-	-	5.10	
10			0.20	50.4	54.90	-	-			10			0.91	49.70	-	-	5.00	
20			0.40	40.7	51.40	-	-			0	1:2.49:2.92	0.50	0.00	36.40	-	-	4.00	
0	1:1.86:2.41	0.5	0	32.9	35.90	2.85	-			10			0.00	38.40	-	-	4.50	
10			0	31.5	35.50	2.32	-			-	-	-	-	-	-	-	-	-

20			0	34.9	37.90	2.63	-			-	-	-	-	-	-	-	-	-
0	M20	Not Given	-	31.04	-	-	3.06	[23]		0	1:1.5:3	Not Given	-	28.12	-	-	-	[1]
5			-	31.52	-	-	3.12			2.5			-	26.13	-	-	-	
10			-	31.89	-	-	3.04			5			-	24.96	-	-	-	
15			-	32.06	-	-	2.53			7.5			-	23.04	-	-	-	
20			-	25.33	-	-	2.46			10			-	21.09	-	-	-	
0	M60	Not Given	-	60.00	-	-	-	[93]		12.5			-	18.39	-	-	-	
5			-	64.50	-	-	-			15			-	16.49	-	-	-	
10			-	68.50	-	-	-			0	M35 1:1.16:2.73	0.42	-	44.80	-	-	-	[108]
15			-	61.50	-	-	-			5			-	47.08	-	-	-	
20			-	61.00	-	-	-			6			-	48.39	-	-	-	
0	1:1.5:3	Not Given	-	37.00	-	-	-	[107]		7			-	47.25	-	-	-	
10			-	38.40	-	-	-			8			-	46.10	-	-	-	
20			-	36.50	-	-	-			9			-	45.12	-	-	-	
25			-	33.00	-	-	-			10			-	47.41	-	-	-	
0	1:2:3	0.55	-	22.69	-	-	-	[109]		0	1:0.985:1.98	0.31	1.2	81.80	86.20	-	-	[110]
2.5		0.56	-	23.20	-	-	-			5			1.8	88.50	90.00	-	-	
5.0		0.57	-	23.32	-	-	-			10			1.7	87.30	92.00	-	-	
7.5		0.58	-	23.50	-	-	-			0	1:2:4	0.56	-	29.24	-	-	-	[111]
10.0		0.60	-	23.64	-	-	-			10			-	22.99	-	-	-	
12.5		0.61	-	17.26	-	-	-			20			-	19.42	-	-	-	
15		0.62	-	13.71	-	-	-			30			-	15.49	-	-	-	
0	1:2:4	Not Given	-	29.15	-	-	-	[102]		0	1:2:4	0.58	-	27.14	-	-	-	
5			-	27.68	-	-	-			10			-	23.26	-	-	-	
10			-	20.88	-	-	-			20			-	19.48	-	-	-	
15			-	18.70	-	-	-			30			-	15.51	-	-	-	
20			-	18.59	-	-	-			0	1:2:4	0.60	-	27.26	-	-	-	
25			-	13.29	-	-	-			10			-	23.48	-	-	-	
0	M30 1:1.48:2.64	0.43	-	44.50	-	-	-	[113]		20			-	19.60	-	-	-	
5			-	46.00	-	-	-			30			-	15.83	-	-	-	
10			-	47.50	-	-	-			0	1:2:4	0.62	-	24.36	-	-	-	
15			-	38.50	-	-	-			10			-	21.26	-	-	-	
20			-	36.50	-	-	-			20			-	19.50	-	-	-	
-	-	-	-	-	-	-	-	-		30			-	16.15	-	-	-	
0	M60 1:1.34:2.35	0.35	-	61.50	-	-	-	[113]		-	-	-	-	-	-	-	-	-
5			-	64.50	-	-	-			-			-	-	-	-	-	
10			-	65.50	-	-	-			-			-	-	-	-	-	
15			-	62.00	-	-	-			-			-	-	-	-	-	
20			-	58.00	-	-	-			-			-	-	-	-	-	

7.4. Rice Husk Ash Splitting Tensile Strength

Table 7 listed splitting tensile strength. Paramveer et al. [84] investigated on RHA concrete. The cement is partially substituted with RHA up to 20% by cement weight. The splitting tensile strength improved from 3% to 5% RHA replacement. But decrease afterward approximately 31.25% to the control mixes at 20% replacement. Some Researchers [35, 100, 105, 106] investigated RHA concrete. Splitting tensile strength increased at different water to cement ratios of 0.6, 0.53, 0.5 and 0.4 (as compared to referral mix) with the addition of 20% RHA by cement weight. Krishna et al. [80] suggested that at 10% replacement of cement by RHA Exhibits good splitting tensile strength. Numerous researchers [27, 86, 87, 91, 104, 112] investigated to examine the hardened properties of M20 concrete. The authors stated that the splitting tensile strength decreases with the addition of RHA in concrete. Bhushan et al. [92] evaluated the hardened properties for M20 concrete grade. Results showed that the 14.7% splitting tensile strength increased as compared to referral mix at 5% RHA. Kirti et al. [32] reported that the 5% replacement gave the maximum splitting tensile strength. Further investigation by [88] showed that 7.25% splitting tensile strength increased at 5% RHA replacement level.

7.5. Rice Husk Ash Flexural Strength

Flexural strength is shown in Table 7. Some researchers [23, 80, 84, 92] assessed the flexural strength of concrete at 0-25% replacement of RHA by cement weight and four different water-binder ratios (0.4, 0.55 and 0.5), were used. The authors concluded that the flexural strength at 5% replacement is higher as compared to control mix and the flexural strength at 10% replacement is equivalent to the referral mix. Further investigation by [81, 91] revealed that flexural strength improved with the increase in RHA up to 10%. Some researchers [27, 86, 91, 104, 105], also assessed the RHA concrete flexural strength. Flexural strength of RHA concretes decreased with increase in RHA content.

7. Elastic Modulus (EM)

The EM results for the concrete containing various RHA amount is listed in Table 8. The objective of this computation, tensile stress of test specimens shall be determined by dividing load to the test samples area. The output is presented in gigapascals (GPa) [48]. Padhi et al. [86] in their laboratory study on different properties of concrete prepared with various %age RHA as cement replacement. The authors revealed that the E-value of RHA concrete is not enhanced when matched with control specimens. Zareei et al. [106] performed the investigational work to studied the RHA characteristics of concrete. The authors described that the maximum E- value observed at 5% replacement level and the modulus of elasticity with 25% RHA is also greater to normal concrete. Kishore et al. [27] have experimented the influence of RHA as cement replacement in concrete. The results showed that the MOE attained with different percentage of RHA is satisfied with the design values for all percentage replacements. Tashima et al. [88] have worked to determine the optimum replacement of RHA in concrete. They revealed that all samples have approximately similar results in elasticity module at different percentages of RHA.

Table 8. RHA as partial replacement of OPC on the E-value of Concrete [27, 86, 88, 106]

RHA %	Modulus of Elasticity (GPa)				
0	32.2	39.3	47.3	50.7	40.9
5	32.1	49.3	44.6	47.2	40.7
10	32.1	40.1	39.5	43.5	40.2
15	31.5	41.6	35.6	38.9	-
20	31.1	41.9	-	-	-
25	30.4	40.9	-	-	-
30	29.7	-	-	-	-
35	29.3	-	-	-	-
Mix Proportions	1:1.51:2.93	1:1.875:2.10	M40 1:0.83:2.53	M50 1:0.78:2.36	1:1.33:2.27
W/b	0.45	0.40	0.36	0.35	0.42

8.Water Absorption

The effect of RHA as a supplementary cementitious on the water absorption of concrete mixes is shown in Table 9. Padhi et al. [86] have investigated the influence of RHA as cement replacement in concrete.in their investigational work the RHA is substituted up to 35%. The results showed that the water absorption of the referral mix is 5.55% and further increased up to 7.21% when RHA percentage increased from 5%-35%. The authors summarized that the water absorption of RHA concrete increased due to increase in water absorption of RHA particles. Further they described that this increment in water absorption shows the concrete that prepared with RHA is lesser durable than control mixes. Gaesan et al. [35] have worked to investigate the influence of RHA as cement replacement for M25 concrete grade. The RHA is substituted up to 35%.

The authors described the same as previous authors that the percentage of water absorption increases with the addition of RHA up to 35% at 28days of curing. The reason behind is that the RHA particles are finer than cement particles. Zareei et al. [106] investigated to study the RHA characteristic of concrete. 0-25% RHA used as cement replacement. It is concluded that water absorption of normal concrete mix is 4.12% and %age of water absorption decreases by increasing the RHA amount, at 25% RHA the water absorption is 3.05%.

Krishna et al. [80] have evaluated the effect of RHA on the water absorption of concrete. The water absorption of control mix is lower; from the results it is concluded that the water absorption of the concrete increases by increasing the amount of RHA. Further the authors described this increase in water absorption is due to the fact that the RHA is more porous material, water occupies these pores which rise the rate of water absorption. Tashima et al. [88] revealed that higher replacement amounts result in lesser water absorption values, this happens due to the RHA particles are finer than cement. The results showed that 38.7% reduction in water absorption is noted at 10% RHA replacement when compared to the referral mix. Siddika et al. [91] have worked to investigate the influence of RHA as cement replacement on the water absorption of

concrete. W/B were kept 0.4, 0.5 and 0.6. The authors described that the rate of water absorption is varies with water-binder ratio if taking all the other contents same. Further they described that the concrete with different percentage of RHA has more water absorption as compared to referral mix. The results showed that the rate of water absorption varies about 10 - 28%. This phenomenon take place because of RHA concrete is more porous than referral mix. Furthermore, it is also reported that the concrete porosity increases with the increase in water-binder ratio.

Table 9. Water absorption of concrete for RHA replacement

RHA %	Water Absorption %							
0	5.55	4.71	4.12	-	1.80	4	3.60	3.40
5	5.65	4.83	3.95	1.28	1.65	-	-	-
10	5.68	5.02	3.70	1.49	1.40	4.40	4.00	3.60
15	6.00	5.58	3.46	1.64	-	5.00	4.70	4.00
20	6.30	5.81	3.23	1.85	-	-	-	-
25	6.70	6.09	3.05	-	-	-	-	-
30	6.90	6.35	-	-	-	-	-	-
35	7.21	6.92	-	-	-	-	-	-
Mix Proportions	1:1.51:2.93	1:1.50:3.00	1:1.875:2.10	1:1.64:3.41	1:1.33:2.27	1:2.028:4.19	1:1.65:3.40	1:1.26:2.61
W/b	0.45	0.53	0.40	0.55	0.42	0.60	0.50	0.40
References	[86]	[35]	[18]	[80]	[88]	[91]		

9.Sorptivity

Gaesan et al. [35] have worked to examine the influence of various RHA amount as cement substitute on concrete sorptivity. The sorptivity gradually reduces up to 25% RHA content and further increase in sorptivity is observed at 30-35% RHA content. The sorptivity value at 35% RHA is relatively lower to the referral specimens. The authors reported that long curing starts for reducing pore size. Abalaka et al. [30] have investigated RHA for cement replacement to concrete sorptivity. They performed sorptivity test at cured and uncured concrete specimens. The results showed that, sorptivity gradually enhance with the enhancement in RHA amount and value of sorptivity inf uncured specimen is higher than the water cured specimen at the same RHA content. In the other words, the water cured samples had dense microstructure as compared to the uncured samples. Furthermore, the authors also demonstrated that the concrete which prepared at lower water to cement ratios have better dense microstructure as compared to higher water cement ratio mixes.

10.Conclusions

To obtain RHAC is analyzed by available materials for RHA replacement as cement. The RHA physical and chemical characteristics were studied with OPC. The following results are achieved.

1. The replacement of RHA requires more water to obtain the similar workability and compaction factor.
2. RHAC Density is in between 2190 – 2430 kg/m^3 which lies as semi-lightweight and normal concretes, and therefore considered as the conventional RHA concrete which is the general purposes.
3. The RHA replacement for normal concrete between 5 to 10% showed the excellent durability and mechanical properties.
4. The RHA addition in the conventional concrete even enhance elastic modulus from 29.3 to 49.3 GPa, which is more than the normal and conventional concrete strength whose values vary in the range of 14 to 41 GPa Aslam et al. [72].
5. The RHA replacement in the conventional concrete enhances absorption of water up to 7%, that shows less that 10% for good concrete [95].
6. The RHA addition reduces the loss of ignition compared to the conventional cement concrete.

11.References

[1] Bawankule, S.P., P.D. Hiwase, and M.S. Balwani, *Effect of Partial Replacement of Cement by Rice Husk Ash in Concrete*. International Journal of Research in Engineering, Science and Technologies, 2015. **1**(8): p. 310-313.

[2] Hosseini, P., et al., *Use of nanoSiO2 to improve microstructure and compressive strength of recycled aggregate concretes*. In: Proceeding, nanotechnology in construction (NICOM3), 2009: p. 215-222.

[3] Calkins, M., *A Complete Guide to the Evaluation, Selection, and Use of Sustainable Construction Materials*. Materials for Sustainable Sites John Wiley, New York, 2009.

[4] Gopi, N. and P. Sruthi, *An Experimental Study On The Strength Of Concrete with Partial Replacement of Cement by Rice Husk Ash*. International Conference on Emerging trends in Engineering, Science and Sustainable Technology, 2017: p. 9-12.

[5] Ghosal, S. and S. Moulik, *Use of Rice Husk Ash as Partial Replacement with Cement In Concrete- A Review*. International Journal of Engineering Research, 2015. **4**(9): p. 506-509.

[6] Karri, S.K., G.V.R. Rao, and P.M. Raju, *Strength and Durability Studies on GGBS Concrete*. SSRG International Journal of Civil Engineering (SSRG-IJCE), 2015. **2**(10): p. 34-41.

[7] Mehta, P.K. and P.J.M. Monteiro, *Concrete: microstructure, properties, and materials*. 3rd ed. New York: McGraw-Hill, 2006.

[8] Altwair, N. and S. Kabir, *Green concrete structures by replacing cement with pozzolanic materials to reduce greenhouse gas emissions for sustainable environment. In*. American society of civil engineers, 6th international engineering and construction conference (IECC'6), June 28–30, Cairo, Egypt, 2010.

[9] Alex, J., J. Dhanalakshmi, and B. Ambedkar, *Experimental investigation on rice husk ash as cement replacement on concrete production*. Construction and Building Materials, 2016. **127**: p. 353-362.
[10] Bayasi, et al., *Properties of Silica Fume Concrete and Mortar*. ACI Materials Journal, 1993. **90**(4): p. 349-356.
[11] Cleetus, et al., *ANALYSIS AND STUDY OF THE EFFECT OF GGBFS ON CONCRETE STRUCTURES*. International Research Journal of Engineering and Technology (IRJET), 2018. **5**(3): p. 3033-3037.
[12] Coutinho, S., et al., *The combine benefit of CPF and RHA in improving the durability of concrete structures*. Cement and Concrete Composites, 2003. **25**(1).
[13] Özbay, E., M. Erdemir, and H.I. Durmus, *Utilization and efficiency of ground granulated blast furnace slag on concrete properties – A review*. Construction and Building Materials, 2016. **105**: p. 423-434.
[14] Muga, H., et al., *Development of Appropriate and Sustainable Construction Materials*. Sustainable Futures Institute, 2005: p. 17.
[15] Owaid, H.M., et al., *A Review of Sustainable Supplementary Cementitious Materials as an Alternative to All Portland Cement Mortar and Concrete*. Australian Journal of Basic and Applied Sciences, 2012. **6**(9): p. 2887-303.
[16] Gurunaathan, K. and G.S. Thirugnanam, *Effect of mineral admixtures on durability properties of concrete*. International Journal of Advance Structures and Geotechnical Engineering, 2014. **03**(01).
[17] Srivastava, V., et al., *Effect of Silica Fume in Concrete*. International Journal ofInnovative Research in Science, Engineering and Technology, 2014. **3**(4): p. 254-259.
[18] Johari, M.A.M., et al., *Influence of supplementary cementitious materials on engineering properties of high strength concrete*. Construction and Building Materials, 2011. **25**: p. 2639-2648.
[19] MADHANASREE, R.M., A.J. PAULSON, and R.A. PRABHAVATHY, *STUDY ON SILICA FUME REPLACED CONCRETE WITH SUPER PLASTICIZER*. Int. J. Chem. Sci, 2016. **14**(S1): p. 359-366.
[20] Bakar, B.H.A., R. Putrajaya, and H. Abdulaziz, *Malaysian Rice Husk Ash – Improving the Durability and Corrosion Resistance of Concrete: Pre-review*. Concrete Research Letters, 2010. **1**(1): p. 6-13.
[21] Rashid, M.H., M.A.M. Keramat, and T.U. Ahmed, *Durability of Mortar in Presence of Rice Husk Ash*. International Journal of Civil, Environmental, Structural, Construction and Architectural Engineering 2010. **4**(7): p. 176-179.
[22] Zain, M.F.M., et al., *Production of rice husk ash for use in concrete as a supplementary cementitious material*. Construction and Building Materials, 2011. **25**: p. 798-805.
[23] Suman, A.K., A.K. Saxena, and T.R. Arora, *Assessment of Concrete Strength using Partial Replacement of Cement for Rise Husk Ash*. International Journal of Soft Computing and Engineering (IJSCE), 2015. **4**(6): p. 131-133.
[24] Madandoust, R., et al., *Mechanical properties and durability assessment of rice husk ash concrete*. Biosystems Engineering, 2011. **110**: p. 144-152.
[25] Hwang, C.L. and D.S. Wu, *Properties of cement paste containing rice husk ash*. In V. M. Malhotra (Ed.), Proceedings of the third CANMET/ACI international

conference on fly ash silica fume, slag and natural pozzolans in concrete 1989: p. 733-762.
[26] Bui, D.D., J. Hu, and P. Stroeven, *Particle size effect on the strength of rice husk ash blended gap-graded Portland cement concrete*. Cement and Concrete Composites, 2005. **27**: p. 357-366.
[27] Kishore, R., V. Bhishma, and P.J. Prakash, *Study on Strength Characteristics of High Strength Rice Husk Ash Concrete*. Procedia Engineering, 2011. **14**: p. 2666-2672.
[28] *Rice Market Monitor*. Food and Agriculture Organization of the United Nations, 2018. **XXI**(I).
[29] Habeeb, G.A. and M.M. Fayyadh, *Rice Husk Ash Concrete: the Effect of RHA Average Particle Size on Mechanical Properties and Drying Shrinkage*. Australian Journal of Basic and Applied Sciences, 2009. **3**(3): p. 1616-1622.
[30] Abalaka, A.E. and O.G. Okoli, *Strength Development and Durability Properties of Concrete Containing Pre-Soaked Rice Husk Ash*. Construction Science, 2013/2014: p. 4-12.
[31] Aleem, M., et al., *Incorporation of Rice Husk Ash as Cement Replacement*. IOSR Journal of Engineering, 2015. **05**(07): p. 25-30.
[32] Kirti, C., et al., *Experimental Study of RHA Concrete*. International Journal for Research in Applied Science & Engineering Technology (IJRASET), 2015. **3**(11): p. 77-82.
[33] Della, V.P., I. Ku¨hn, and D. Hotza, *Rice husk ash as an alternate source for active silica production*. Materials Letters, 2002. **57**: p. 818-821.
[34] Krishnarao, R.V., et al., 2011. **21**: p. PP.
[35] Gaesan, K., K. Rajagopal, and K. Thangavel, *Rice Husk Ash Blended Cement: Assessment of Optimal Level of Replacement for Strength and Permeability Properties of Concrete*. Journal of Construction and Building Materials, 2008. **22**: p. 1675-1683.
[36] Hwang, C.L. and S. Chandra, *The Use of Rice Husk Ash in Concrete*. 2016.
[37] Dolage, D.A.R., et al., *Use of Rice Husk Ash Blended Cement to Produce Cemnet Sand Blocks: Optimal Level of Cement Replacement for Compressive Strength*. ENGINEER, 2011. **XXXXIV**(02): p. 11-19.
[38] Fapohunda, C., B. Akinbile, and A. Shittu, *Structure and properties of mortar and concrete with rice husk ash as partial replacement of ordinary Portland cement—a review*. Int J Sustain Built Environ, 2017.
[39] Chandrasekhar, S., et al., *Review processing, properties and applications of reactive silica from rice husk—an overview*. Journal of Materials Science (Norwell). **38**(15): p. 3159-3168.
[40] Zhang, M. and V. Malhotra, *High-performance concrete incorporating rice husk ash as a supplementary cementing materials*. ACI Materials Journal (Detroit), 1996. **93**(6): p. 629-636.
[41] James, J. and S.M. Rao, *Reactivity of rice husk ash*. Cement Concrete Res 1986. **16**: p. 296-302.
[42] Mehta, P.K., *Rice Husk Ash - A unique supplementary cementing material Proceeding*. International Symposium on Advances in Concrete Technology. Editor. Malhotra,V.M. Athens, Greece, 1992: p. 407- 430.

[43] Nair, D.G., et al., *A Structural Investigation Relating to the Pozzolanic Activity of Rice Husk Ashes*. Cement and Concrete Research Letters, 2008. **38**: p. 861-869.
[44] Boating, A. and D. Skeete, *Incineration of rice hull for use as a cementitious materials; the Guyana experience*. Cement Concrete Res, 1990. **20**: p. 795–802.
[45] James, J. and S.M. Rao, *Silica from rice husk through thermal decomposition*. Thermochim Acta, Elsevier Science, Amsterdam, 1986(97): p. 329–336.
[46] Zhang, M.H., R. Lastra, and V.M. Malhotra, *Rice husk ash paste and concrete: some aspects of hydration and the microstructure of the interfacial zone between the aggregate and paste*. Cem Concr Res 1996. **26**(6): p. 963-977.
[47] Farooque, K.N., et al., *Characterization and utilization of rice husk ash (RHA) from rice mill of Bangladesh*. Bangladesh J Sci Ind Res, 2009. **44**(2): p. 157-162.
[48] Circuits, P.E. and O.T. Group, *Ipc-tm-650 test methods manual 1.0*. Deposited Dielectric Task Group (C-13a), 2009. **2**: p. 4-6.
[49] Yuzer, N., et al., *Influence of raw rice husk addition on structure and properties of Concrete*. Construction and Building Materials, 2013. **44**: p. 54-62.
[50] 50. Shodhganga, *Production Methodologies And Properties of RHA - A Review*. 2016.
[51] *ASTM Standard Specification for Coal Fly Ash and Raw or Calcined Natural Pozzolan for Use in Concrete*. Designation: C 618 – 05, 2005.
[52] Chusilp, N., C. Jaturapitakkul, and K. Kiattikomol, *Effects of LOI of ground bagasse ash on the compressive strength and sulfate resistance of mortars*. Construction and Building Materials, 2009. **23**: p. 3523-3531.
[53] Qing Xu, Q., et al., *Characteristics and Applications of Sugar Cane Bagasse Ash Waste in Cementitious Materials*. Materials, 2019. **12**(39).
[54] Siddique, R., *Utilization of wood ash in concrete*. Resour. Conserv. Recycl., 2012. **67**: p. 27-33.
[55] Sadrmomtazi, A., et al., *Properties of multi-strength grade EPS concrete containing silica fume and rice husk ash*. Construction and Building Materials, 2012. **35**: p. 211-219.
[56] Rawaid, K., et al., *Reduction in environmental problems using rice-husk ash in concrete*. Construction and Building Materials, 2012. **30**: p. 360-365.
[57] Dabai, M.U., et al., *Studies on the Effect of Rice Husk Ash as Cement Admixture*. Nigerian Journal of Basic and Applied Science, 2009. **17**(2): p. 252-256.
[58] Ismail, M.S. and A.M. Waliuddint, *Effect of rice husk ash on high strength concrete*. Construction and Building Materials, 1996. **10**(7): p. 521-526.
[59] Habeeb, G.A. and H.B. Mahmud, *Study on Properties of Rice Husk Ash and Its Use as Cement Replacement Material*. Materials Research, 2010. **13**(2): p. 185-190.
[60] Zhang, M.H., R. Lastra, and V.M. Malhotra, *Rice-Husk Ash Paste and Concrete: Some Aspects of Hydration and the Microstructure of the Interfacial Zone Between the Aggregate and Paste*. Cement and Concrete Research, 1996. **26**(6): p. 963-977.

[61] Parande, A.K., et al., *Utilization of Agroresidual Waste in Effective Blending in Portland Cement*. ISRN Civil Engineering, 2011: p. 1-12.
[62] Zerbino, R., G. Giaccio, and G.C. Isaia, *Concrete incorporating rice-husk ash without processing*. Construction and Building Materials, 2011. **25**: p. 371-378.
[63] Jongpradist, P., et al., *Efficiency of Rice Husk Ash as Cementitious Material in High-Strength Cement-Admixed Clay*. Advances in Civil Engineering, 2018: p. 1-11.
[64] Binyamien, I., et al., *The Effect of Rice Husk Ash on the Strength and Durability of Concrete at High Replacement Ratio*. Mechanics, Materials Science & Engineering, 2017.
[65] Ramezanianpour, A.K., M. Balapour, and E. Hajibandeh, *Effect of nano rice husk ash against penetration of chloride ions in mortars*. 5th National and 1st Iternational Conference on Modern Materials and Structures in Civil Engineering, October 26-27, 2016.
[66] Chatveera, B. and P. Lertwattanaruk, *Durability of conventional concretes containin g black rice husk ash*. Journal of Environmental Management, 2011. **92**: p. 59-66.
[67] Hwang, C.L., B.A.T. Le, and C.T. Chen, *Effect of rice husk ash on the strength and durability characteristics of concrete*. Construction and Building Materials, 2011. **25**: p. 3768-3772.
[68] Banjare, V., et al., *An Experimental Study on Tensile Strength Behavior of Advance Concrete using Rice Husk Ash and Core Fiber*. International Journal for Innovative Research in Science & Technology, 2017. **4**(2): p. 149-154.
[69] Prasad, D.S. and D.A.R. Krishna, *Production and Mechanical Properties of A356.2 /RHA Composites*. International Journal of Advanced Science and Technology, 2011. **33**: p. 51-58.
[70] Tang, L.V., et al., *Effect of Rice Husk Ash and Fly Ash on the workability of concrete mixture in the High-Rise Construction*. E3S Web of Conferences, 2018. **33**(02029): p. 1-12.
[71] Givi, A.N., et al., *Contribution of Rice Husk Ash to the Properties of Mortar and Concrete: A Review*. Journal of American Science, 2010. **6**(3): p. 155-165.
[72] Oyetola, E.B. and M. Abdullahi, *The Use of Rice Husk Ash in Low - Cost Sandcrete Block Production*. Leonardo Electronic Journal of Practices and Technologies, 2006(8): p. 58-70.
[73] Rashid, M.H., *Strength Behavior of Cement Mortar Assimilating Rice Husk Ash*. Int'l Journal of Advances in Agricultural & Environmental Engg. (IJAAEE) 2016. **3**(2): p. 288-292.
[74] Karim, M.R., et al., *Strength of Mortar and Concrete as Influenced by Rice Husk Ash: A Review*. World Applied Sciences Journal, 2012. **19**(10): p. 1501-1513.
[75] Qamruddin, M. and P.L.G. Kalurkar, *EFFECT OF UNPROCESSED RICE HUSK ASH AS A CEMENTITIOUS MATERIAL IN CONCRETE (A COMPARISON WITH SILICA FUME)*. International Journal of Civil Engineering and Technology (IJCIET), 2013. **4**(2): p. 240-245.
[76] Yu, Q., et al., *The reaction between rice husk ash and Ca(OH)2 solution and the nature of its product*. Cement and Concrete Research, 1999. **29**: p. 37-43.

[77] Sarkar, B. and S. Hazari, *Behavior of Concrete Made with Rice Husk Ash as Mineral additives*. National Level Conference on Engineering Problems and Application of Mathematics, 2016: p. 1-6.
[78] Aslam, M., P. Shafigh, and M.Z. Jumaat, *Oil-palm by-products as Lightweight Aggregate in Concrete Mixture: A Review*. Journal of Cleaner Production, 2016. **126**: p. 56-73.
[79] Fapohunda, et al., *Structure and Properties of Mortar and Concrete with Rice Husk Ash as Partial Replacement of Ordinary Portland cement – A Review*. International Journal of Sustainable Built Environment, 2017.
[80] Krishna, N.K., S. Sandeep, and K.M. Mini, *Study on concrete with partial replacement of cement by rice husk ash*. Materials Science and Engineering 2016. **149**: p. 1-11.
[81] Zhang, M.H. and V.M. Malhotra, *High-Performance Concrete Incorporating Rice Husk Ash as a Supplementary Cementing Material*. ACI Materials Journal, 1996: p. 629-636.
[82] Nehdi, M., J. Duquette, and E. Damatty, *Performance of rice husk ash produced using a new technology as a mineral admixture in concrete*. Cem Concr Res, 2003. **33**(8): p. 1203–1210.
[83] Fapohunda, e.a., *Structure and Properties of Mortar and Concrete with Rice Husk Ash as Partial Replacement of Ordinary Portland cement – A Review* International Journal of Sustainable Built Environment, 2017.
[84] Paramveer, S., S. Tarunbir, and S. Gurpreet, *To Study Strength Characteristics of Concrete with Rice Husk Ash*. Indian Journal of Science and Technology, 2016. **9**(47): p. 1-5.
[85] Ahmed, M., S. Brijbhushan, and P.D. Maneeth, *Strength Characteristics of M25 Grade Concrete by Partially Replacing Cement with Rice Husk Ash and Fine Aggregate with Copper Slag*. IJSRD - International Journal for Scientific Research & Development, 2017. **5**(06): p. 743-746.
[86] Padhi, R.S., et al., *Influence of incorporation of rice husk ash and coarse recycled concrete aggregates on properties of concrete*. Construction and Building Materials, 2018. **173**(2018): p. 289-297.
[87] Sensale, G.R., *Strength development of concrete with rice-husk ash*. Cement & Concrete Composites 2006. **28**: p. 158-160.
[88] Tashima, M.M., et al., *Influence of Rice Husk Ash in Mechanical Characteristics of Concrete*. IV INTERNATIONAL ACI/CANMET CONFERENCE ON QUALITY OF CONCRETE STRUCTURES AND RECENT ADVANCES IN CONCRETE MATERIALS AND TESTING, Advancing Concrete Knowledge: p. 780-790.
[89] Giaccio, G., G.R.D. Sensale, and R. Zerbino, *Failure mechanism of normal and high-strength concrete with rice-husk ash*. Cement & Concrete Composites, 2007. **29**: p. 566-574.
[90] Ikpong, A.A. and D.C. Okpala, *Strength characteristics of medium workability ordinary Portland cement-rice husk ash concrete*. Building and Environment, 1992 **27**(1): p. 105-111.
[91] Siddika, A., M.A.A. Mamun, and M.H. Ali, *Study on concrete with rice husk ash*. nnovative Infrastructure Solutions, 2018: p. 1-9.

[92] Bhushan, E.R., et al., *Partial Replacement of Cement by Rice Husk Ash*. International Research Journal of Engineering and Technology (IRJET), 2017. **04**(10): p. 251-256.
[93] Nirubha, E. and V. Ponmalar, *Effect of Rice Husk Ash in Concrete*. Civil Engineering Systems and Sustainable Innovations: p. 191-194.
[94] Chatveera, B. and P. Lertwattanaruk, *Evaluation f Sulfate Resistance of Cement Mortars Containing Black Rice Husk Ash*. Journal of Environtal Management, 2009. **90**(3): p. 1435-1441.
[95] Chindaprasirt, P. and S. Rukzon, *Strength, Porosity and Corrosion Resistance of Ternary Blend Portland Cement, Rice Husk Ash and Fly Ash Mortar*. Construction and Building Materials, 2008. **22**(8): p. 1601-1606.
[96] Omotosoa, O.E., D.G. Ivey, and R. Mikulab, *Characterization of chromium doped tricalcium silicate using SEM/EDS, XRD and FTIR*. Journal of Hazardous Materials, 1995. **42**(1): p. 87-102.
[97] Sabir, B.B., *High-strength condensed silica fume concrete*. Magazine of Concrete Research, 1995. **47**(172): p. 219-226.
[98] Kulkarni, M., et al., *Effct of rice husk ash on properties of concrete*. Journal of Civil Engineering and Environmental Technology, 2014. **1**(1): p. 26-29.
[99] Singh, J. and H. Singh, *A REVIEW ON UTILIZATION OF RICE HUSK ASH IN CONCRETE*. INTERNATIONAL JOURNAL OF INNOVATIONS IN ENGINEERING RESEARCH AND TECHNOLOGY [IJIERT], 2015. **2**(11): p. 1-8.
[100] Abhijith, C., S, et al., *Partial Replacement of Binder Material With Rice Husk Ash (RHA) In Concrete*. International Journal of Scientific & Engineering Research, 2016. **7**(4): p. 200-204.
[101] Kachwala, A., A. Pamnani, and A. Raval, *Effect of Rice Husk Ash as a Partial Replacement of Ordinary Portland cement in Concrete*. International Research Journal of Engineering and Technology (IRJET), 2015. **2**(5): p. 175-177.
[102] Obilade, I.O., *USE OF RICE HUSK ASH AS PARTIAL REPLACEMENT FOR CEMENT IN CONCRETE*. International Journal of Engineering and Applied Sciences, 2014. **5**(4): p. 11-16.
[103] Neville, A.M., *Properties of Concrete*. Fourteenth Ed. CTP-VVP, Malaysia, 2008.
[104] Akeke, G.A., et al., *STRUCTURAL PROPERTIES OF RICE HUSK ASH CONCRETE*. International Journal of Engineering and Applied Sciences, 2013. **3**(3): p. 57-62.
[105] Anwara, M., T. Miyagawab, and M. Gaweesh, *Using of Rice Husk Ash as a Cement Replacement Material in Concerete*. WasteMaterialsin Construction: p. 671-684.
[106] Zareei, S.A., et al., *Rice husk ash as a partial replacement of cement in high strength concrete containing micro silica: Evaluating durability and mechanical properties*. Case Studies in Construction Materials, 2017.
[107] Ephraim, M.E., G.A. Akeke, and J.O. Ukpata, *Compressive strength of concrete with rice husk ash as partial replacement of ordinary Portland cement*. Scholarly Journal of Engineering Research, 2012. **1**(2): p. 32-36.
[108] Rambabu, P.V., V.C. Varm, and G.V. Ramarao, *Experimental Study on Rice Husk Ash for Optimum Level of Replacement of Cement in Concrete*.

International Journal of Engineering Research & Technology (IJETRT) 2015. **4**(10): p. 354-359.

[109] Bangwar, D.K. and M.A. Keerio, *Improvement of Mechanical Properties of Concrete with Rice Husk Ash*. International Journal of Scientific & Engineering Research, 2017. **8**(3): p. 1254-1260.

[110] Mahmud, H.B., N.A.A. Hamid, and K.Y. Chin, *Production of high strength concrete incorporating an agricultural waste - rice husk ash*. 2nd International Confeence on Chemical, Biological and Environmental Engineering (ICBEE 2010), 2010: p. 106-109.

[111] Kumar, P.R.S., *Experimental study on the properties of concrete made with alternate construction materials*. International Journal of Modern Engineering Research (IJMER), 2012. **2**(5): p. 3006-3012.

[112] Sundararaman, S. and S. Azhagarsamy, *A Study on Performance of Concrete by Partial Replacement of Cement with Rice Husk Ash and Silica Fume*. European Journal of Advances in Engineering and Technology, 2015. **2**(11): p. 69-72.

[113] Naveen, S. Bansal, and Y. Antil, *Effect of Rice Husk on Compressive Strength of Concrete*. International Journal on Emerging Technologies, 2015. **6**(1): p. 144-150.

[114] Van Tuan, N., G. Ye, and K. van Breugel, *Effect of rice husk ash on autogenous shrinkage of ultra high performance concrete*. In Proceedings of International RILEM Conference on Advances in Construction Materials Through Science and Engineering, Hong-Kong. , 2010.

[115] Mosaberpanah, M.A.a.O.E., *Statistical models for mechanical properties of UHPC using response surface methodology*. COMPUTERS AND CONCRETE, 2017. **19**(6): p. 667-675.

[116] Wang, D., et al.,, *A review on ultra high performance concrete: Part II. Hydration, microstructure and properties*. Construction and Building Materials, 2015. **96**: p. 368-377.

[117] Courtial, M., et al.,, *Effect of polycarboxylate and crushed quartz in UHPC: microstructural investigation*. Construction and Building Materials, 2013. **44**: p. 699-705.

[118] van Breugel, K.a.Y.G., *Analyses of hydration processes and microstructural development of UHPC through numerical simulation*. in Proceedings of the International Symposium on Ultra-High Performance Concrete, Kassel, Germany, Sept. 13. 2004.

[119] Van Breugel, K.a.N.V.T., *Ultra high performance concrete made with rice husk ash for reduced autogenous shrinkage*. in Proceedings of the 4th International FIB Congress, Mumbai, India Authors version. 2014. Universities Press, 10-14 February 2014.

[120] ößler, C., D.-D. Bui and H.-M. Ludwig, *Rice husk ash as both pozzolanic admixture and internal curing agent in ultra-high performance concrete*. Cement and Concrete Composites, 2014. **53**: p. 270-278.

[121] V. Nguyen, *Rice husk ash as a mineral admixture for ultra high performance concrete*. 2011.

[122] Mukarram, et. al., (2022), "Cellulose nanocrystals from office paper waste for green concrete: Process optimization modeling, characterization, and mechanical testing", *Arabian Journal for Science and Engineering*, Vol. 1, No. 1, pp. 1-17. DOI: https://doi.org/10.1007/s13369-022-06609-8

[123] Aziz, et. al., (2023), "Destructive, Nondestructive and Thermal Testing of Biochar-Mortar composite", *Biomass Conversion and Biorefinery*, pp. 1-14. DOI: https://doi.org/10.1007/s13399-023-03838-1

Multi-Model Deep Learning Ensemble Approach for Detection of Malicious Executables

Mohammad Eid Alzahrani
Department of Engineering and Computer Science,
Faculty of Computer Science & Information Technology
AlBaha University, AlBaha, Saudi Arabia
meid@bu.edu.sa

Abstract: Due to the growing significance of the Internet in many facets of our lives, the World Wide Web, which end-users access via web browsers, is evolving into the next platform for those who want to engage in illegal activity for either their own or another person's financial or personal benefit. Among the reported types of attacks, attacks through malicious executables files are still one of the prevalent challenges. Different static and dynamic analysis approaches have been proposed to detect such executables. The challenge with these approaches is that they failed to detect novel attack types in malicious executables. With the dawn of Machine learning, the detection of novel attacks in malicious executables was possible to detect with high accuracy. Deep learning, which is a part of machine learning that works similarly to human neurons, provides a way to achieve much greater accuracy compared to machine learning. In this study, we propose a stacking-based ensemble approach combining CNN, LSTM, and GRU models to detect malicious executables. The experiment results demonstrate that an accuracy of 99.02% was achieved, which is very high compared to individual deep-learning models.

Keywords: Cybersecurity, Malware Detction, Malacious Executables, Deep Learining.

نهج مجموعة التعلم العميق متعدد النماذج للكشف عن العناصر التنفيذية الضارة

الملخص: نظرًا للأهمية المتزايدة للإنترنت في العديد من جوانب حياتنا ، فإن شبكة الويب العالمية ، التي يصل إليها المستخدمون النهائيون عبر متصفحات الويب ، تتطور إلى النظام الأساسي التالي لأولئك الذين يرغبون في الانخراط في نشاط غير قانوني لأيٍّ منهما. أو المنفعة المالية أو الشخصية لشخص آخر. من بين أنواع الهجمات المبلغ عنها ، لا تزال الهجمات من خلال الملفات التنفيذية الضارة أحد التحديات السائدة. تم اقتراح مناهج تحليل ثابتة وديناميكية مختلفة لاكتشاف مثل هذه الملفات التنفيذية. التحدي في هذه الأساليب هو أنها فشلت في اكتشاف أنواع الهجمات الجديدة في الملفات التنفيذية الضارة. مع فجر التعلم الآلي ، أصبح من الممكن اكتشاف هجمات جديدة في ملفات تنفيذية ضارة بدقة عالية. يوفر التعلم العميق ، وهو جزء من التعلم الآلي الذي يعمل بشكل مشابه للخلايا العصبية البشرية ، وسيلة لتحقيق دقة أكبر بكثير مقارنة بالتعلم الآلي. في هذه الدراسة ، نقترح نهجًا جماعيًا قائمًا على التكديس يجمع بين نماذج CNN و LSTM و GRU لاكتشاف الملفات التنفيذية الضارة. أظهرت نتائج التجربة أنه تم تحقيق دقة 99.02٪ ، وهي نسبة عالية جدًا مقارنة بنماذج التعلم العميق الفردية.

1.Introduction

Computer programs known as "malware" have harmful intentions and are designed to steal personal information, impair the user's network, and harm the operating system [1]. In cyber security, malware detection and mitigation are still works in progress [2]. While many researchers have focused on improving the accuracy and time efficiency of malware detection, not much effort has been placed into developing systems that automatically identify the presence of malware at compile time and avoid further execution. Traditional and paid market antivirus programs (AV) typically use a signature-matching approach. The database must keep a local signature on file to match known malware patterns. Malware may be uniquely identified using signatures, which are brief byte sequences (hashes) with low error rates [3]. However, although malware identification is possible at the compile-time, it could lead to false positives if the application is infected by a polymorphic virus or an unknown malicious program [4].

Malicious PE files are a type of executable file that has the ability to harm computer system. Malicious PE files are commonly used for malware distribution, and some malware creators use them in their attacks [5]. Malicious PE files can be created by programmers who want to make an executable file with malicious intent or by hackers who wish to distribute malware through different channels. Malware that is commonly associated with the malicious PE file includes Trojans, spyware, adware, and rootkits. Malicious file types of malware from Windows Software Development Kit (SDK)When using the Microsoft software development kit (SDK), the file types that can be created are executable files (.exe), libraries (.lib), and plugins (.dll) [6].

The two primary methods for detecting malware are static analysis and dynamic analysis [7]. The static analysis uses portable executable (PE) files to extract certain characteristics without running the code. Using static analysis poses no risk to the user's system, making it a secure option. It is less resistant to malicious executables that are compressed and encrypted Dynamic analysis is more vulnerable to malicious executables that are compressed and encrypted, as it generates features while the executable runs within a sandbox or controlled environment. Dynamic analysis shows the actual nature of the code and is better suited for real-time detection. However, analysis takes longer since the execution route is always the same from run to run. The scientific and anti-malware communities have observed that machine learning and deep learning models offer increased resilience against code modifications in systems used for malware detection[8].

The focus of this study is to create a ensemble of machine-learning models that work together to identify malicious executable files. The approach involves utilizing hybrid features derived from both static and dynamic analysis. The CNN, LSTM, and GRU models will be trained separately to recognize the structural characteristics of malware within the dataset. Finally, an ensemble of these models will be employed to detect malicious executable files.

The paper is structured as follows: Section 2 presents the related work, Section 3 explains the proposed approach, Section 4 describes the experimental setup, and Section 5 provides the conclusion.

2.Related Work

Researchers and experts have utilized domain-level expertise to detect malicious PE files. Feature selection is considered one of the crucial steps in malware detection using machine learning to achieve high detection accuracy. In the process of using Machine and deep learning models for malware detection, the selection of features plays a crucial role. The authors of this study propose a data mining approach [9] to analyze static features, namely PE head, string sequence, and byte sequence, in order to identify malware. Another study [10] introduces a taxonomy for malware detection using machine learning algorithms, describing feature categories, feature selection methods, and ensemble algorithms employed in this research. Additionally, a different approach [11] focuses on malware detection based on automated behavior, utilizing the Anubis online dynamic analysis tool to track collected samples. Classification tasks were performed using machine learning classifiers such as Naive Bayes, decision trees, and k-nearest neighbors. Furthermore, authors [12] present a novel paradigm to classify malware variants into distinct families. The author's prioritized methods for feature extraction and selection. The suggested approach will function on packed and obfuscated samples since the features were retrieved from the content and sample structure. Malware behavior characteristics were used to categorize the data, and fusion was carried out using a per-class weighting paradigm.
Authors [13] discovered that opcode frequency is a distinguishing characteristic of PE files. They used Random Forest as a baseline model and compared it with other deep learning models. To improve performance, [9] proposed a hybrid malware detection method that combines features derived from opcode frequency with dynamic features. This approach outperformed using each set of features individually. Additionally, the process of identifying malware can be viewed as an image recognition problem by converting the binary data into grayscale images and employing various vision-based techniques. In a separate study, [14] utilized high-level gist descriptors and kNNs for malware classification, presenting one of the initial attempts to classify malware using image processing without relying on gist descriptors. A study by [15] demonstrations that the deep Learning (DL) technique produced marginally better results. To illustrate the higher performance, they contrasted DL approaches with feature-based traditional methods like kNN [16]. A general CNN architecture for classifying malware was put out by researchers [17, 18] and tested on well-known benchmark datasets to achieve high accuracy. Instead of focusing on detection, these efforts primarily concentrate on family classification.

Numerous studies have been done on the dynamically acquired opcode sequences from PE files. The lengthy execution time of this approach was its main flaw. An RNN-based method that uses run-time API calls as features was proposed by [19]. Using opcode sequences from the assembly code, an opcode vocabulary is first generated using an LSTM-based technique that was described in [20]. Following that, CBOW embeddings [21] were produced using this and passed through a two-stage LSTM model. By using several parallelization strategies, they decreased the prediction time. Accounting for large opcode sequences of varying lengths created, which results in information loss and the ensuing delay in obtaining them and training, is one issue with these systems [22].

The contribution of the study is to propose a stacking-based ensemble approach that combines CNN, and GRU models to detect malicious executables. The researchers address the challenge of detecting novel attack types in malicious executables by leveraging the power of deep learning, specifically deep neural networks.

3.Proposed Ensemble Model

3.1 Dataset

The dataset used in this study was downloaded from Kaggle.com [23], and prepared by UCI. Features from both malicious and non-malicious Windows executable files are included in the dataset. The dataset contains 373 samples which include 301 malicious and 72 non-malicious files. There are 531 features in this dataset.

3.2 Feature Selection

In this study, a dataset consisting of 531 features was utilized, necessitating the need for feature selection to obtain the most optimal feature set. The Chi-Square feature selection method was employed for this purpose. Chi-Square feature selection is a statistical technique used to identify the most relevant features within a given dataset. It is also known as the chi-square test for independence [24]. This method helps determine the subset of features that are most predictive for the target variable while eliminating those that are less predictive or irrelevant. The tool used for performing chi-square feature selection in this study was WEKA, a Java-based machine learning software suite developed at the University of Waikato in New Zealand [25]. WEKA provides a range of tools for pre-processing, including classification, regression, clustering, association rules, and feature selection. Two scenarios were examined during the feature experiments in this study: the first scenario utilized all the available features in the dataset, while the second scenario employed the selected features obtained from the chi-square test.

3.3 Ensemble Approach

The ensemble of deep learning models is a group of neural networks that work together to improve the detection accuracy of malware attacks. This means using multiple models instead of just one. The advantage of this approach is that it can help to improve accuracy by combining the strengths of different models. The models are developed by training them on different datasets and then combining their predictions. In a wide range of tasks such as image classification, object detection, and text classification, ensembles of deep learning models have demonstrated superior performance compared to conventional machine learning approaches. This can be accomplished by training one model using random data, called a "holdout dataset." Then the model is evaluated against the holdout dataset. This process can be repeated with other models to generate a consensus among the different models. The architecture of the proposed ensemble approach is shown in Fig. 1.

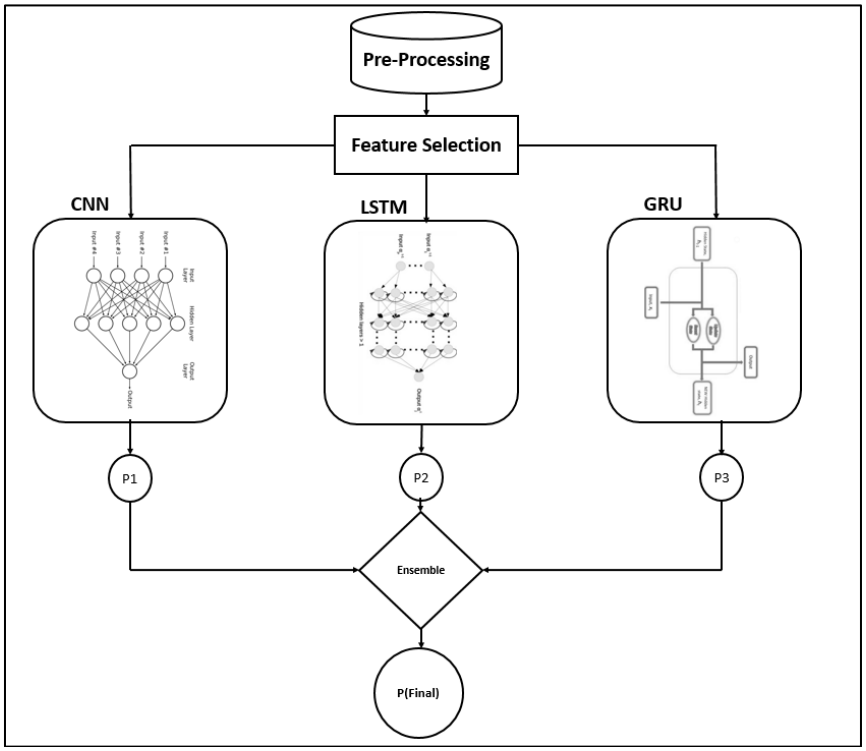

Figure 1: Architecture of the Proposed Approach

3.3.1 CNN

Convolutional neural networks (CNNs) are deep learning architectures primarily designed to recognize patterns. A CNN comprises five layers: the input layer, the convolutional layer, the subsampling layer, the fully connected layer, and finally, the output layer [26], as shown in Fig 2 [27]. The input layer is where all of our data comes.

The convolutional and subsampling layers process this data by performing convolutions and subsamples on it. The fully connected layer then takes all of these processed images and combines them into a single output image using many different combinations of weights. Finally, we have our output layer responsible for taking this final combination of weighted outputs and making predictions about what each one means. Equation 1-3 shows the working of CNN.

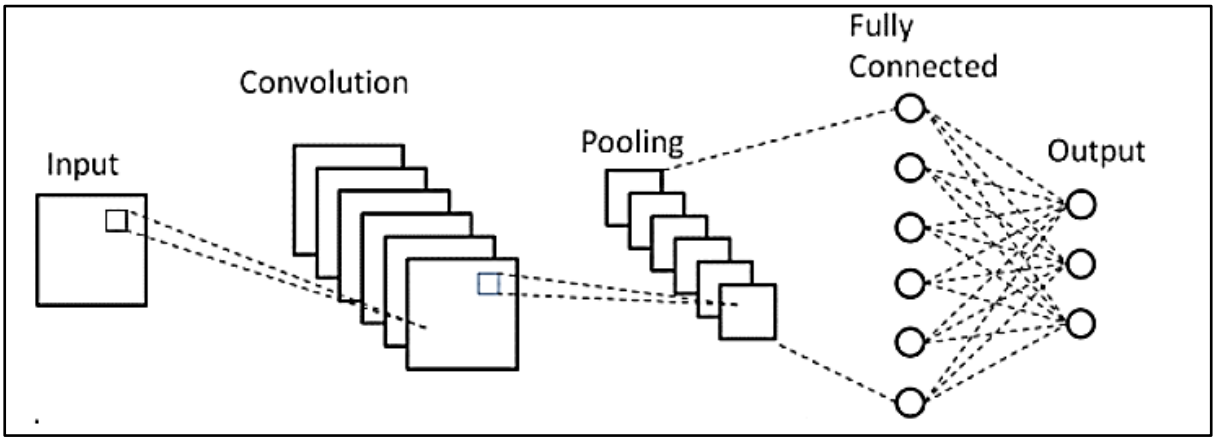

Figure 2: Architecture of CNN

$$x_j = pW_{jxj-1} \quad (1)$$

// x represents the input signal, while as x_j is a subsequent layer, W_j=convolution, p = rectifier or sigmoid

$$x_j(u, k_j) = p\left(\sum_k (x_{j-1}(., k) * W_{j,kj}(., k))(u)\right) \quad (2)$$

$$(f * g)(x) = \sum_{u=-\infty}^{\infty} f(u)g(x-u) \quad (3)$$

3.3.2 LSTM

LSTM networks, a form of recurrent neural networks, possess the ability to acquire knowledge of data sequences and retain them [28]. LSTMs are often used in natural language processing because they can learn to predict words given the context. The LSTM is a type of recurrent neural network or RNN. An RNN is designed to take in a sequence of inputs and produce a sequence of outputs by mathematically modeling the dependencies between inputs and outputs. The LSTM is an enhanced version of the traditional RNN that has improved learning capabilities for long sequences. In order to understand what LSTMs are, it is necessary first to understand the basic difference between RNNs and feed-forward networks. A feed-forward network consists of an input layer, an output layer, and no hidden layers in between.

In a traditional RNN (not the LSTM), there is one hidden layer at the top of a network that receives all inputs as well as one for each output [29]. An LSTM instead has multiple hidden layers at the top— one for each output. There is no input layer, so the only inputs to an LSTM are the previous outputs. The mathematics behind the operation of LSTM is given in Equations 4 to 8. The basic structure of LSTM is shown in Fig. 3 [30].

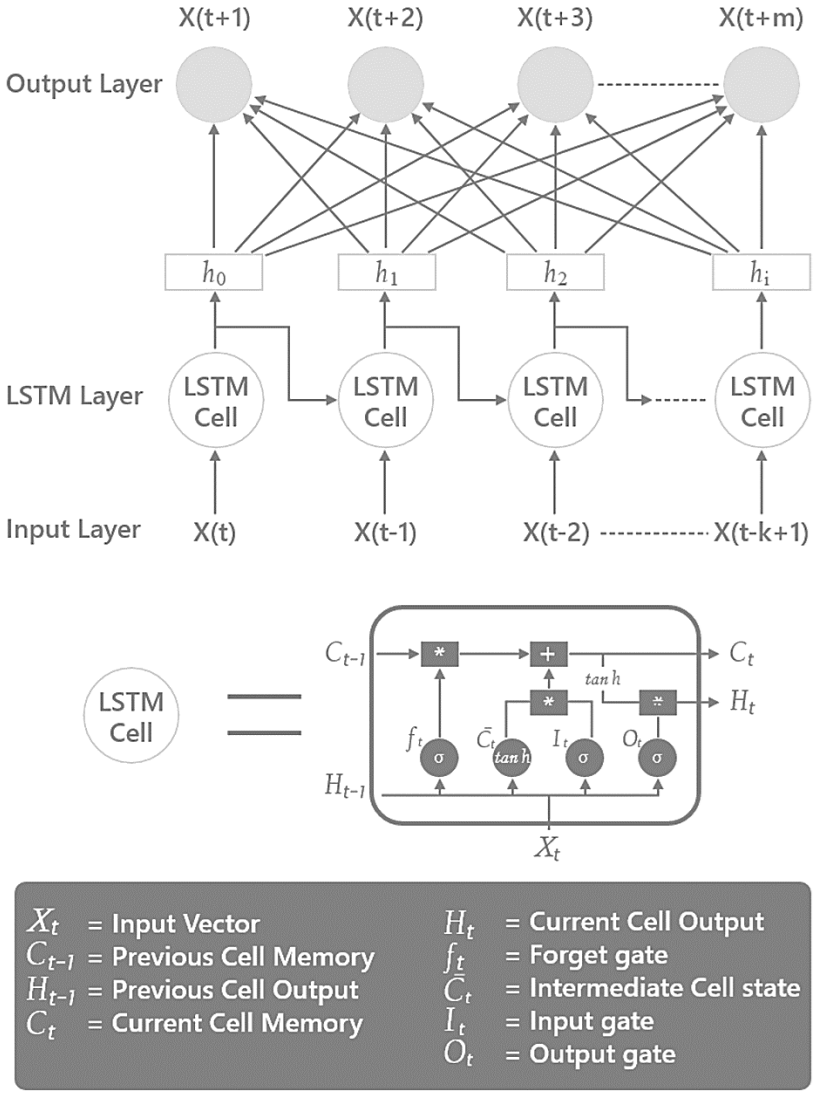

Figure 3: Structure of LSTM

$$h_t = \sigma(W_i.[h_{t-1}, x_t] + b_i) \quad (4)$$

$$h_t = \sigma(W_f.[h_{t-1}, x_t] + b_f) \quad (5)$$

$$o_t = \sigma(W_0.[h_{t-1}, x_t] + b_0) \quad (6)$$

$$\tilde{C}_t = \tanh(W_c.[h_{t-1}, x_t] + b_c \quad (7)$$

$$C_t = f_t * C_{t-1} + i_t * \tilde{C}_t \quad (8)$$

3.3.3 GRU

The Gated Recurrent Unit (GRU) in deep learning is a type of neural network capable of learning from sequential data [31]. The GRU is more accurate than other types of networks, such as the LSTM [32]. The GRU can learn from sequential data, which makes it more accurate than other types of networks, such as the LSTM. GRU can learn representations that are more abstract than those learned by LSTM networks and is utilized as a basic foundation for more complicated networks. The Gated Recurrent Unit (GRU) in deep learning is a type of neural network that is capable of learning from sequential data, as shown in figure 4 [33]. The GRU is more accurate than other types of networks, such as the LSTM. The GRU can learn from sequential data, which makes it more accurate than other types of networks, such as the LSTM.

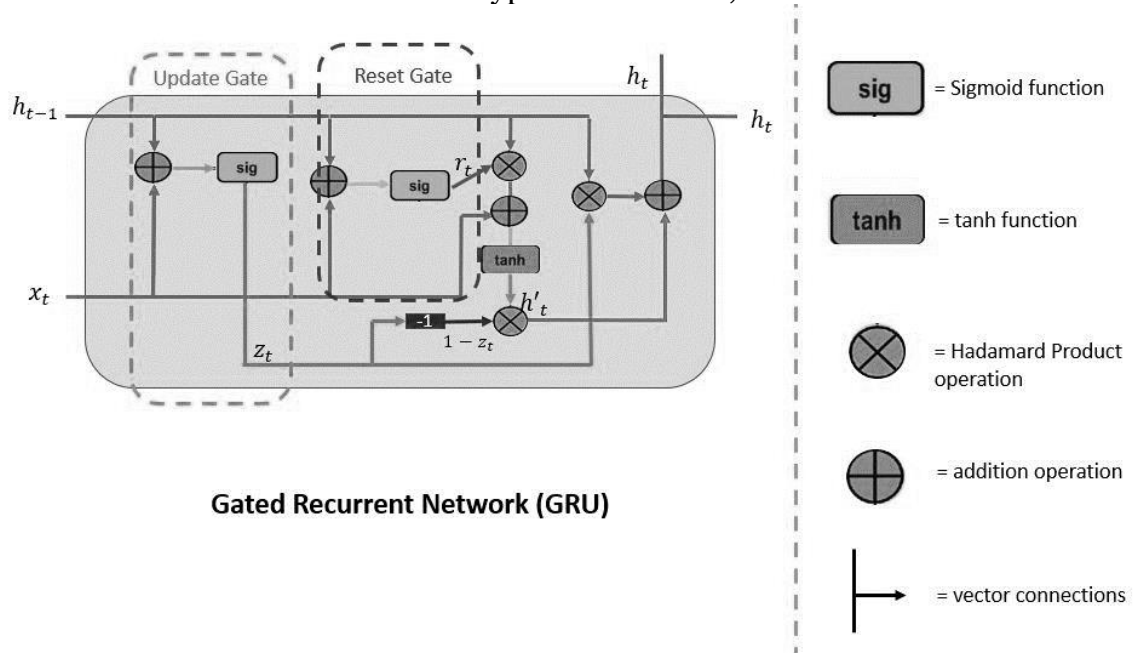

Figure 4: Gate Recurrent Network

Equations 9-12 are used to compute the output from GRU model.

$$z_t = \sigma(W_{xz}x_t + W_{xz}h_{t-1} + b_z) \quad (9)$$

$$r_t = \sigma(W_{xr}x_t + W_{hr}h_{t-1} + b_r \quad (10)$$

$$\tilde{h}_t = \tanh(W_{xr}x_t + W_{hh}(r_t \odot h_{t-1}) + b_h \quad (11)$$

$$\tilde{h}_t = z_t \odot h_{t-1} + (1 - z_t) \odot \tilde{h}_t \quad (12)$$

3.4 Stacking Ensemble

Stacking ensemble is a technique used in machine learining and deep learning combine the predictions of different deep neural networks to produce more accurate predictions [34]. The idea behind stacking ensemble is that when using a deep neural network, the error typically increases as the number of layers increases. The idea behind stacking an ensemble is that combining different models can get better results than with one model alone [35]. A deep neural network is a series of layered nodes that

takes an input and then transforms it into an output. The nodes are stacked on top of one another, with each layer transforming the input data into something more complex. A stacking ensemble combines different DL models with different architectures to produce even better results than any single model could on its own [36]. The key advantage of a stacking ensemble is that it may protect a variety of effective models' ability to address classification and regression issues [37].
Stacking, also known as stacked generalization, is an enhanced iteration of the Model averaging ensemble technique. In this approach, sub-models make equal contributions based on their performance weights to construct a new model that generates more precise predictions. This newly formed model, which incorporates the insights from the previous models, is metaphorically referred to as stacking since it builds upon the foundation laid by the older models. To combine the results generated by individual models, a meta-learner is used. The term "meta-learning" in machine learning describes learning algorithms that take inspiration from one another [38]. In the context of ensemble learning, this most frequently refers to the application of machine learning algorithms that discover the most effective way to combine predictions from different machine learning algorithms. In the meta-learning algorithm, at each iteration of its learning process, it utilizes some additional source of knowledge to predict the desired output [39]. This is particularly useful when the task to be learned is very complex and requires significantly more training data than available to achieve good performance. In our case, we used a multi-model such as CNN, LSTM and GRU to create an ensemble based on stacking methodology to get the final classification results.

3.5 Evaluation Matrix

The evaluation and performance evaluation metrics used to evaluate individuals, and the proposed approach are given in Table 1.

Table 1: Evaluation Matrix

Metrics	Formula
Accuracy	Accuracy = $\frac{TP+TN}{TP+TN+FP+FN}$
Precision	Precision=$\frac{TP}{TP+FP}$
Recall	Recall=$\frac{TP}{TP+FN}$
F1-Score	F1-Score =$\frac{2\ X\ (Precision*Recall}{Precision+Recall}$

4.Experimental Setup and Results

The experiments for this study were conducted on a PC with an i7, 3.5 GHz processor, 16 GB of RAM, and NVIDIA's RTX 3090 graphics processor. In the first step, the data set was checked for correctness. Then the dataset was shuffled to increase accuracy, and the data was split into 80–20% subsets for training and testing. Then chi-square feature selection was used to get the optimal feature set. Only 165 features out of 531 are used in this experiment when the Chi-square value falls in this given error region using the threshold (alpha from 0 to 0.05). The three models, CNN, LSTM, and GRU,

were first used individually to generate the results based on evaluation matrices, then an ensemble of these models was tested. The experiment was also performed without using the optimal feature set from the feature selection method. The experimental results are depicted in Table 2 without using feature selection, and the result obtained when applying feature selection is in Table 3.

Table 2: Results Obtained without using Feature Selection Method

Model	**Accuracy**	**Precision**	**Recall**	**F1-Score**
CNN	96.32	94.46	95.88	0.96
LSTM	97.61	98.25	97.32	0.97
GRU	96.53	98.84	97.93	0.98
Ensemble	98.84	98.32	98.64	0.99

Table 3: Results Obtained using Feature Selection Method

Model	**Accuracy**	**Precision**	**Recall**	**F1-Score**
CNN	97.94	95.62	96.48	0.97
LSTM	98.12	99.51	98.52	0.98
GRU	97.39	98.99	98.56	0.97
Ensemble	99.02	99.32	99.68	0.99

The experimental results show that in both cases when the ensemble approached performed better and achieved 98.84% and 99.02% accuracy, respectively, in detecting malicious executables. The selection of activation function and other parameters plays an important role. In this study, the activation function used for CNN was SIGMOID, while for LSTM and GRU tanh activation function was used. The activation function is a node positioned either in the middle or at the end of neural networks. They influence whether or not the neuron fires. Activation functions are the thresholds that change the network's output and are a set of rules that can be applied to a node within the neural network and alter its values. The batch size in training must be greater than or equal to one and smaller than or equal to the total number of samples in the training dataset. It is crucial to select an integer value for the number of epochs that falls within the range of one to infinity. If a neural network model is trained with excessive epochs, it tends to learn specific patterns unique to the training data, resulting in poor performance when applied to new datasets. While such a model may perform well on the training set (sample data), it fails to generalize effectively and performs poorly on the test set. This phenomenon is known as overfitting, where the model loses its ability to generalize beyond the training data. The number of complete passes over the training dataset is referred to as the number of epochs.

In this particular study, the epoch sizes were set at 100 for CNN, 50 for LSTM, and 120 for GRU. Compared to the studies [10-12] our proposed approach perfomed better. This study offers advantages such as high detection accuracy and the ability to detect novel attacks.

5.Conclusion

It is well-recognized that different machine learning and deep learning models have different prediction performances. An ensemble learning approach outperforms a single base classifier by combining numerous separate learning algorithms. As a result, it has become a widely used and successful approach. There are two main problems to be resolved for the ensemble learning methodologies. How to combine is the first problem. base-classifiers that are "fair and distinct." The second is to provide each base -classifier taken into account by the ensemble learning appropriate parameters. We suggest a stack-based ensemble method to detect malicious executables.

The proposed ensemble approach outperformed the individual deep-learning models and achieved an accuracy of 99.02%. Future work of this study include exploring real-time detection, expanding the dataset, addressing evolving attack types, benchmarking against other models, generalizing to other domains, and improving interpretability and explainability of the ensemble approach.

6.References

[1] Patil, B. P., Kharade, K. G., & Kamat, R. K. (2020). Investigation on data security threats & solutions. *International Journal of Innovative Science and Research Technology*, *5*(1), 79-83.

[2] Kapoor, A., Gupta, A., Gupta, R., Tanwar, S., Sharma, G., & Davidson, I. E. (2021). Ransomware detection, avoidance, and mitigation scheme: a review and future directions. *Sustainability*, *14*(1), 8.

[3] Khan, N., Abdullah, J., & Khan, A. S. (2017). Defending malicious script attacks using machine learning classifiers. Wireless Communications and Mobile Computing, 2017.Thambi-Rajah, T., & Jahankhani, H. (2021). The Role of Deep Neural Network in the Detection of Malware and APTs. In *Challenges in the IoT and Smart Environments* (pp. 161-188). Springer, Cham.

[4] Khan, N., Johari, A., & Adnan, S. (2017). A Taxonomy Study of XSS Vulnerabilities. Asian J. Inf. Technol, 16, 169-177.

[5] Case, A., Jalalzai, M. M., Firoz-Ul-Amin, M., Maggio, R. D., Ali-Gombe, A., Sun, M., & Richard III, G. G. (2019). HookTracer: A system for automated and accessible API hooks analysis. Digital Investigation, 29, S104-S112.

[6] Khan, N., Abdullah, J., & Khan, A. S. (2015, August). Towards vulnerability prevention model for web browser using interceptor approach. In 2015 9th International Conference on IT in Asia (CITA) (pp. 1-5). IEEE.

[7] Rathore, H., Sahay, S. K., Nikam, P., & Sewak, M. (2021). Robust android malware detection system against adversarial attacks using q-learning. *Information Systems Frontiers*, *23*(4), 867-882.

[8] Schultz M, Eskin E, Zadok F, Stolfo S. Data mining methods for detection of new malicious executables. In: Proceedings of the IEEE computer society symposium on research in security and privacy; 2001, pp. 38–49.

[9] Shabtai A, Moskovitch R, Elovici Y, Glezer C. Detection of malicious code by applying machine learning classifiers on static features: A state-of-the-art survey. Inf Secur Tech Rep. 2009;14(1):16–29.

[10] Firdausi I, lim C, Erwin A, Nugroho AS. Analysis of machine learning techniques used in behavior-based malware detection. In: Second international conference on advances in computing, control, and telecommunication technologies, Jakarta; 2010, pp. 201–203.

[11] Ahmadi, M., Ulyanov, D., Semenov, S., Trofimov, M., & Giacinto, G. (2016, March). Novel feature extraction, selection and fusion for effective malware family classification. In Proceedings of the sixth ACM conference on data and application security and privacy (pp. 183-194).

[12] Rathore, H., Agarwal, S., Sahay, S. K., & Sewak, M. (2018, December). Malware detection using machine learning and deep learning. In International Conference on Big Data Analytics (pp. 402-411). Springer, Cham.

[13] Nataraj, L., Karthikeyan, S., Jacob, G., & Manjunath, B. S. (2011, July). Malware images: visualization and automatic classification. In *Proceedings of the 8th international symposium on visualization for cyber security* (pp. 1-7).

[14] Yajamanam, S., Selvin, V. R. S., Di Troia, F., & Stamp, M. (2018, January). Deep Learning versus Gist Descriptors for Image-based Malware Classification. In *Icissp* (pp. 553-561).

[15] Bhodia, N., Prajapati, P., Di Troia, F., & Stamp, M. (2019). Transfer learning for image-based malware classification. *arXiv preprint arXiv:1903.11551*.

[16] Kalash, M., Rochan, M., Mohammed, N., Bruce, N. D., Wang, Y., & Iqbal, F. (2018, February). Malware classification with deep convolutional neural networks. In *2018 9th IFIP international conference on new technologies, mobility and security (NTMS)* (pp. 1-5). IEEE.

[17] Choi, S., Jang, S., Kim, Y., & Kim, J. (2017, October). Malware detection using malware image and deep learning. In *2017 International Conference on Information and Communication Technology Convergence (ICTC)* (pp. 1193-1195). IEEE.

[18] Pascanu, R., Stokes, J. W., Sanossian, H., Marinescu, M., & Thomas, A. (2015, April). Malware classification with recurrent networks. In *2015 IEEE International Conference on Acoustics, Speech and Signal Processing (ICASSP)* (pp. 1916-1920). IEEE.

[19] Lu, R. (2019). Malware detection with lstm using opcode language. *arXiv preprint arXiv:1906.04593*.

[20] Mikolov, T., Chen, K., Corrado, G., & Dean, J. (2013). Efficient estimation of word representations in vector space. arXiv preprint arXiv:1301.3781.

[21] Yan, J., Qi, Y., & Rao, Q. (2018). Detecting malware with an ensemble method based on deep neural network. *Security and Communication Networks*, *2018*.

[22] https://www.kaggle.com/datasets/piyushrumao/malware-executable-detection

[23] Sharpe, D. (2015). Chi-square test is statistically significant: Now what?. *Practical Assessment, Research, and Evaluation*, *20*(1), 8.

[24] Weka 3: Machine Learning Software in Java: https://www.cs.waikato.ac.nz/ml/weka/

[25] Abiyev, R. H., & Ma'aitaH, M. K. S. (2018). Deep convolutional neural networks for chest diseases detection. Journal of healthcare engineering, 2018.
[26] MK Gurucharan, Basic CNN Architecture: Explaining 5 Layers of Convolutional Neural Network Available at: https://www.upgrad.com/blog/basic-cnn-architecture/
[27] Sak, H., Senior, A. W., & Beaufays, F. (2014). Long short-term memory recurrent neural network architectures for large scale acoustic modeling.
[28] Fan, B., Wang, L., Soong, F. K., & Xie, L. (2015, April). Photo-real talking head with deep bidirectional LSTM. In *2015 IEEE International Conference on Acoustics, Speech and Signal Processing (ICASSP)* (pp. 4884-4888). IEEE.
[29] Chandra, R., Jain, A., & Singh Chauhan, D. (2022). Deep learning via LSTM models for COVID-19 infection forecasting in India. *PloS one*, *17*(1), e0262708.
[30] Patil, S. A., Raj, L. A., & Singh, B. K. (2021). Prediction of IoT traffic using the gated recurrent unit neural network-(GRU-NN-) based predictive model. *Security and Communication Networks*, *2021*.
[31] Hamayel, M. J., & Owda, A. Y. (2021). A Novel Cryptocurrency Price Prediction Model Using GRU, LSTM and bi-LSTM Machine Learning Algorithms. *AI*, *2*(4), 477-496.
[32] Gaurav Singhal, LSTM versus GRU Units in RNN, Available at: https://www.pluralsight.com/guides/lstm-versus-gru-units-in-rnn
[33] Ganaie, M. A., & Hu, M. (2021). Ensemble deep learning: A review. *arXiv preprint arXiv:2104.02395*.
[34] Wang, Y., Pan, Z., Yuan, X., Yang, C., & Gui, W. (2020). A novel deep learning based fault diagnosis approach for chemical process with extended deep belief network. *ISA transactions*, *96*, 457-467.
[35] Ko, J., Baldassano, S. N., Loh, P. L., Kording, K., Litt, B., & Issadore, D. (2018). Machine learning to detect signatures of disease in liquid biopsies–a user's guide. *Lab on a Chip*, *18*(3), 395-405.
[36] Sesmero, M. P., Ledezma, A. I., & Sanchis, A. (2015). Generating ensembles of heterogeneous classifiers using stacked generalization. *Wiley interdisciplinary reviews: data mining and knowledge discovery*, *5*(1), 21-34.
[37] Pfahringer, B., Bensusan, H., & Giraud-Carrier, C. G. (2000, June). Meta-Learning by Landmarking Various Learning Algorithms. In *ICML* (pp. 743-750).
[38] Yao, H., Liu, Y., Wei, Y., Tang, X., & Li, Z. (2019, May). Learning from multiple cities: A meta-learning approach for spatial-temporal prediction. In *The World Wide Web Conference* (pp. 2181-2191).

Preparation and Evaluation of *Terminalia catappa* Shell-Based Activated Carbon for Methylene Blue Dye Removal

Muktar Abdulazeez Abdullahi[1*], Aminu Dikko Mahmud[1*], Gazali Tanimu[2*], Nuhu Umar Hussaini[1*], Dahiru Abdulmalik Kona[1*]

[1] Department of Chemical Engineering, Ahmadu Bello University, Nigeria
[2] Center for Refining and Advanced Chemicals, King Fahd University of Petroleum and Minerals, Saudi Arabia

[*]Corresponding authors: abdulazeezbinmuktar@gmail.com, admahmud@abu.edu.ng, **gtu4ever@yahoo.com,** ask4umarhussayn@gmail.com, abdulmaleekkona@gmail.com

Abstract: Tropical almond (*Terminalia catappa*) is a large tree that is widely distributed in coastal environments throughout the tropics. In this study the feasibility of using *Terminalia catappa* shells as a cheap adsorbent for removing methylene blue dye in aqueous solutions was investigated. Two separate samples of activated carbon were prepared from the fruit shells of *Terminalia catappa* via physical and chemical activation, respectively. The specific surface area of the activated carbon prepared using physical activation was found to be 1095 m^2/g, while that prepared via chemical activation was 1613.4 m^2/g. The changes were due to different contact times and the dosage of the adsorbent in the adsorption process were investigated for both samples. The results showed that for both samples, increasing the contact time and adsorbent dosage resulted in a greater percentage of methylene blue dye being removed.
The highest percentage removal was achieved using the chemically activated carbon, which showed an exponential increase from 68.25% to 87.41% at 0 to 40 minutes and a small increment from 89.00% to 90.12% in the last 20 minutes. Similarly, the percentage removal also rose with an increase in the adsorbent dosage from 59.65% to 90.69% at 0.1 to 0.6g of the adsorbent. These findings suggest that *Terminalia catappa* shells is an efficient and cheap adsorbent that be used for the removal of methylene blue dye from aqueous solutions.

Keywords: Terminalia catappa, activated carbon, methylene blue, adsorption, specific surface area, contact time.

إعداد وتقييم الكربون المنشط المستند إلى غلاف *Terminalia catappa* لإزالة صبغة الميثيلين الزرقاء

الملخص: اللوز الاستوائي (*Terminalia catappa*) عبارة عن شجرة كبيرة يتم توزيعها على نطاق واسع في البيئات الساحلية في جميع أنحاء المناطق المدارية. في هذه الدراسة تم دراسة جدوى استخدام قذائف *Terminalia catappa* كمادة ماصة رخيصة لإزالة صبغة الميثيلين الزرقاء في المحاليل المائية. تم تحضير عينتين منفصلتين من الكربون المنشط من قشور ثمار *Terminalia catappa* عن طريق التنشيط الفيزيائي والكيميائي على التوالي. تم العثور على مساحة السطح المحددة للكربون المنشط المحضر باستخدام التنشيط الفيزيائي لتكون 1095 م 2 / جم ، في حين أن المساحة المحضرة عن طريق التنشيط الكيميائي كانت 1613.4 م 2 / جم. كانت التغييرات بسبب أوقات التلامس المختلفة وتم فحص جرعة المادة الماصة في عملية الامتزاز لكلتا العينتين. أظهرت النتائج أنه لكلتا العينتين ، أدى زيادة وقت التلامس وجرعة الممتزات إلى إزالة نسبة مئوية أكبر من صبغة الميثيلين الزرقاء.

تم تحقيق أعلى نسبة إزالة باستخدام الكربون المنشط كيميائيًا ، والتي أظهرت زيادة أسية من 68.25٪ إلى 87.41٪ في 0 إلى 40 دقيقة وزيادة صغيرة من 89.00٪ إلى 90.12٪ في آخر 20 دقيقة. وبالمثل ، ارتفعت نسبة الإزالة أيضًا مع زيادة جرعة الممتزات من 59.65٪ إلى 90.69٪ عند 0.1 إلى 0.6 جم من المادة الممتزة. تشير هذه النتائج إلى أن قذائف *Terminalia catappa* هي مادة ماصة فعالة ورخيصة يمكن استخدامها لإزالة صبغة الميثيلين الزرقاء من المحاليل المائية.

1. Introduction

Due to its significant inter-particulate surface area and a high degree of porosity, activated carbon is a commonly utilized adsorbent. There are several different kinds of activated carbon available, including granular, powdered, spherical, fibrous, and textile forms (Roop and Meenakshi, 2005). In contrast to the powdered form, which has reduced internal surface area and higher pore sizes, the granular form has a large internal surface area and few pores. In comparison, carbon fabric and fibrous activated carbons include a higher percentage of bigger pores and have a larger surface area (Roop and Meenakshi, 2005). (Meena et al., 2022) addresses the value of activated carbon in several environmental applications, including the cleaning of water and air, as well as its part in reducing climate change.

However, the steep price of activated carbon prevents its widespread use. Commercial activated carbon is produced using a variety of carbonaceous sources, including turf, lignite, nutshells, wood, and coal, to cut costs (Adinata et al., 2007). Making activated carbon from inexpensive components like agricultural byproducts could help to further cut its price. Concise research on an overview of the many agricultural waste kinds that can be utilized to create activated carbon, as well as the numerous activation techniques that can be used, has been conducted in recent years (Ahmad et al., 2021).

The article by Yan and Wang (2021) offers a thorough analysis of the uses of activated carbon for reducing air pollution. The potential of activated carbon as a useful remedy for removing several air pollutants, such as particulate matter, sulfur dioxide, nitrogen oxides, and volatile organic compounds, is examined by the authors. The article discusses the difficulties and potential future directions for the development and use of activated carbon in air pollution control and highlights the critical elements influencing the performance of activated carbon.

Research has focused on using synthetic materials to manufacture activated carbon in addition to natural materials. One such substance is *Terminalia catappa*, a big tropical tree found primarily in Asia, Africa, and Australia's tropical regions. Rich in carbon, the *plant Terminalia catappa* has been investigated to be a potential natural precursor for manufacture of activated carbon (Olatidoye et al., 2011). About 700,000 tons of this fruit are produced annually throughout the world (Olatidoye *et al.*, 2011).

Processes involving physical or chemical activation are used to create activated carbon. Using heated gases, the source material is transformed into activated carbon during the physical activation process. The gases are subsequently extinguished with the addition of air, resulting in a well screened, dedusted and fine grade of activated carbon.

(Acharya et al., 2021) offered a thorough analysis of the creation, characteristics, uses, and applications of activated carbon. Additionally, they go over the methods for the characterization of activated carbon and their uses in a variety of industries, including energy storage, wastewater treatment, and the reduction of air pollution. Production of activated carbon from inexpensive resources like agricultural waste has the potential to lower its price and make it more readily available for large-scale applications. It is encouraging that materials like *Terminalia catappa* can be used to make activated carbon.

2.0 Materials and Methods

2.1 Preparation of Adsorbents

Fruits of *Terminalia catappa* plant were gathered from within the campus of Ahmadu Bello University in Zaria. The shells were sun-dried for five days and then broken into smaller pieces. The shells were then burned for one hour in a box furnace at 300 ^{o}C. Smaller pieces of the carbonated materials were crushed. Two samples A and B were collected. Sample A was chemically activated, while sample B was physically activated. In sample A, 10 grams of KOH was dissolved in 40 mL of water to create KOH solution. The carbonized particles were then steeped in the KOH solution for 40 grams. The resulting material was put into a tube furnace and the temperature was raised to 400 ^{o}C, then steam was passed over, and Nitrogen gas to provide an inert environment for 1 h. After carbonization, sample B was physically activated in the same furnace at 600 ^{o}C with steam for a specified time of 1 hour 30 minutes without the addition of KOH.

2.2 Characterization of the adsorbents

Sear's Method for Surface Area Determination;

The Sear's technique was used to estimate the adsorbent's specific surface area (Jawad *et al.*, 2019; Ahmad *et al.*, 2013). 1.5 g of the adsorbent was weighed and acidified with dilute HCl (dropwise) using a burette until the pH was 4.0, then 30 g of NaCl was added to the solution whilst stirring, then water was used to make up the volume to 150 mL. 0.1 M NaOH was used to titrate the solution until the pH was 9. And the specific surface area S (m^2/g) was calculated using the relation;

$$S = 32 * V - 25 \quad (1)$$

Where V is the volume of NaOH needed to raise the pH of the solution to 9.

2.3 Preparation of adsorbate solutions

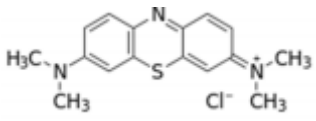

Fig. 1: The structure of Methylene Blue.

In a 1000 mL distilled water, 0.2 g of Methylene Blue was weighed and dissolved to make a 20 mg/L stock solution of Methylene Blue. A series of dilutions were performed to obtain a 10 ml volume of the diluted solution containing specific percentages of water and the original stock solution. The concentration of the new solution was obtained using the dilution formula

$$C_1 \times V_1 = C_2 \times V_2 \quad (2)$$

A UV-visible spectrophotometer was used to record and measure the absorbance of each diluted solution.

2.4 Effect of operating parameters

The influence of interaction time and dose for the adsorption process of Methylene Blue on activated carbon were examined.

2.4.1 Effect of contact time

120 mL (from the stock solution) was measured and 0.6 g of the adsorbent weighed and dissolved in the new volume at a temperature of 25 ^{o}C. The mixture was stirred constantly using a magnetic stirrer and at different time intervals of 10 min each, 20

ml of the solution was taken, then a UV-visible spectrophotometer was used to record and measure the absorbance.

2.4.2 Effect of adsorbent dose
A volume of 20 mL (from the stock solution) was measured and a contact time of 20 min was kept constant. While the adsorbent doses were varied from 0.1 g, 0.2g, up to 0.6g for each 20mL at a temperature of 25 ^{o}C, and the absorbance was measured using a UV-Visible spectrophotometer.

3.0 Results and Discussion
Calculations show that sample A has a specific area of 1613.4 m^2/g as obtained using sear's method. Similarly, it was also discovered that the specific area of sample B as found to be 1095 (m^2/g).

3.1 Adsorption of Methylene Blue
A plot of Absorbance (nm) against Concentration (mg/L) was done using Microsoft Excel to obtain the Calibration curve as shown in Figure 3.1. It shows a standard curve (calibration curve) with an R^2 = 0.9939. Since the graph shows a linear relationship between absorbance and concentration.

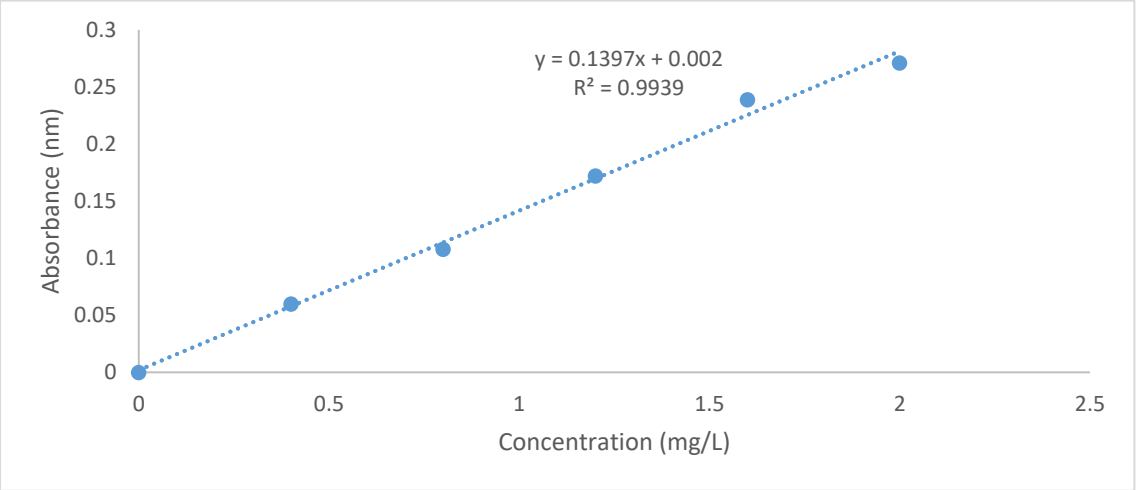

Figure 3.1: Plot showing the Calibration Curve

3.2 Effect of Contact Time on the Adsorption of Methylene Blue Using AC
The impact of contact time is depicted in Figure 3.2 and Figure 3.3, showing similar trend in this variation. It was observed that the rate at which the adsorption occurs rises as contact time increases. Initially, within the first 40 mins, an exponential increase in adsorption was reflected, and thereafter a steady state equilibrium was obtained in the last 20 mins.

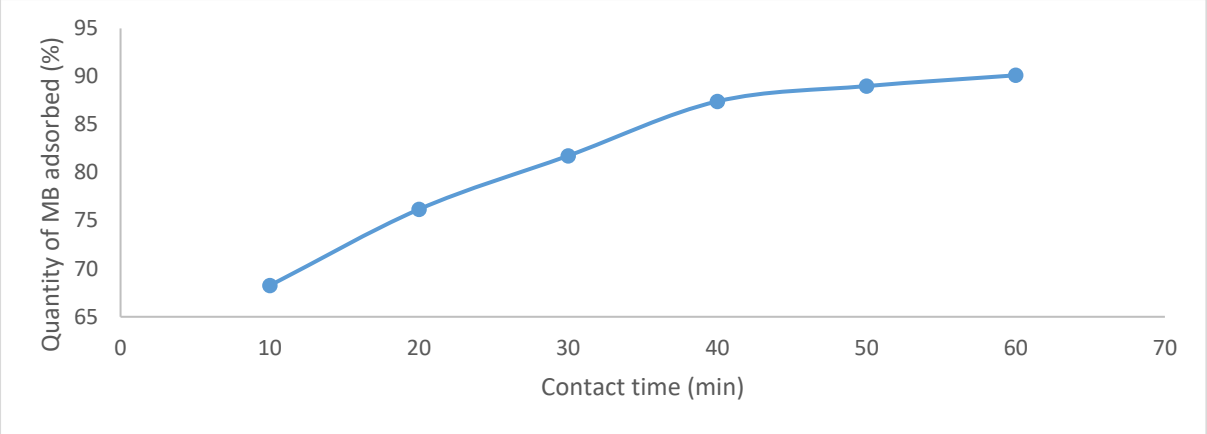

Figure 3.2: Impact of varying contact time on the adsorption process for sample A

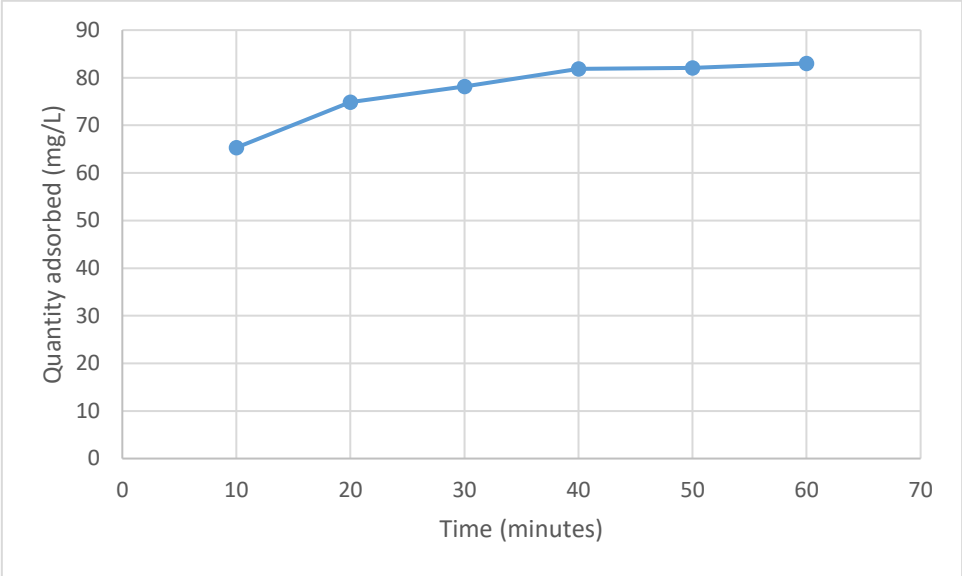

Figure 3.3: Impact of varying contact time on the adsorption process for sample B

The impact of varying contact time on Methylene Blue adsorption onto activated carbon is shown in Figure 3.3. The results show that equilibrium was reached at about 40 minutes, and that the dye elimination increased slightly increased with contact time. This phenomenon might be brought on by the earlier availability of a finite number of available sites, which over time gradually become saturated. Because there was a lot of existing and accessible surface area for the adsorption process at the beginning of the contact time, a high removal rate was seen; however, as time went on, the capacity of the adsorbent gradually became saturated. This is because the few remaining vacant surface sites became difficult to occupy due to the repulsive forces between the solute molecules in the solid and bulk phases. Various researchers have reported this trend in different literature, such as Mondal and Kar(2018).

3.3 Effect of Adsorbent Dosage

The adsorbent effect is depicted in Figure 3.3, which also displays the trend in this variation. Figure 3.3 demonstrates that from 0.1 to 0.3 g of the adsorbent, the amount

of Methylene Blue adsorbed increased quickly from 59.65 to 85.23 percent. When the dose was increased from 0.3 to 0.6 g, the amount of Methylene Blue adsorbed became practically constant. The rise in adsorbent dosages may have increased the surface area and the number of adsorption sites, which may have contributed to the rise in the percentages of Methylene Blue adsorbed. The results in Figure 3.5, however, shows how the dosage affected the adsorption of methylene blue in sample B. According to the results, increasing the adsorbent dosage from 0.1g to 0.6g rose the percent removal from 55.23% to 86.96% as a result, more accessible sites are available to bind the methylene blue from the aqueous phase. These results are findings reported by Ai *et al.* (2011) and Li *et al.* (2013).

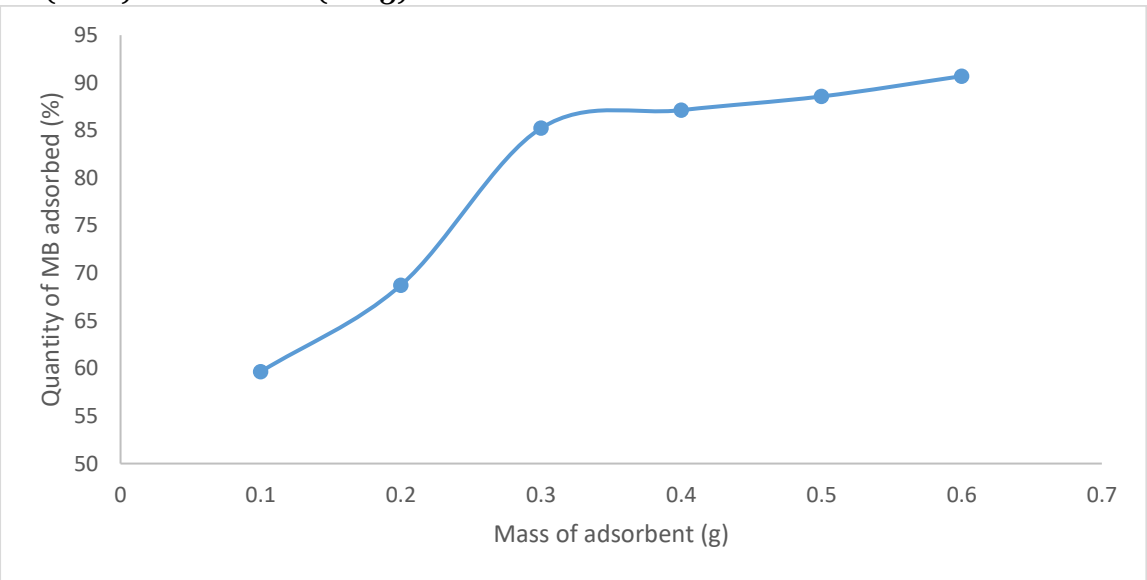

Fig 3.4: Impact of varying AC dosage on the adsorption process for sample A

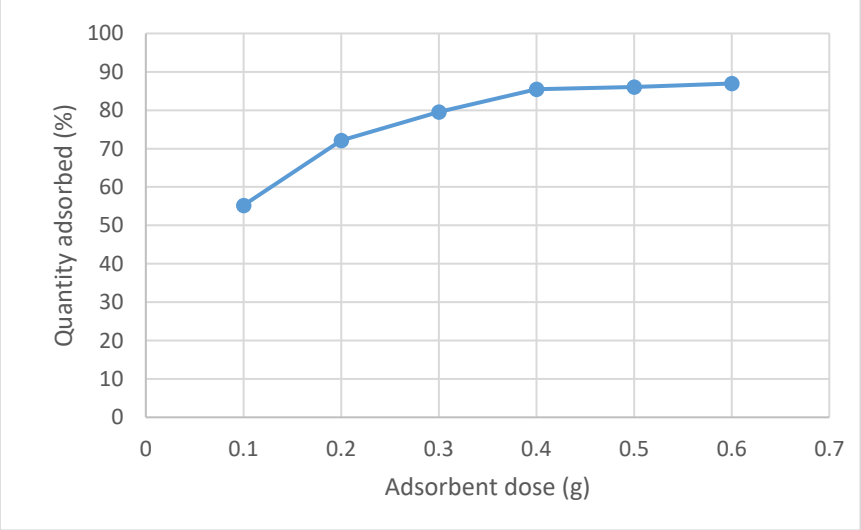

Figure 3.5: Impact of varying AC dosage on the adsorption process for sample B

4.Conclusion

The present work investigated the effectiveness of using *Terminalia catappa* shells as an activated carbon for the removal of Methylene Blue whether it is created using physical or chemical activation. The specific surface area characterization of physical

activation revealed an area of 1095 m^2/g, while the chemical activation demonstrated a specific surface area of 1613.4 m^2/g, which falls within the recommended range for adsorption (500 m^2/g to 3000 m^2/g).
Adsorption tests were performed on both the physical and chemical activated carbon to ascertain the impact of the interaction time and dosage on methylene blue elimination. The results showed that the contact duration generated an increase in removal percent from 65.32 percent to 83.01 percent, while an increase in adsorbent dosage caused an increase in removal percent from 55.23 percent to 86.96 percent.

Additionally, the quantity adsorbed by the activated carbon increased exponentially over the course of the first 40 minutes, from 68.25 percent to 87.41 percent, with a slight increment from 89.00 percent to 90.12 percent in the final 20 minutes. This pattern is explained by the rising adsorbate-adsorbent interaction with increasing contact time.

5.References

[1] H. Adejenwo, "The production of activated carbon from elemi (canarium schweinfurthii) Nutshell using chemical method, A research project, department of chemical engineering, Ahmadu Bello University, Zaria," 2006.

[2] R. H. Bradley, I. Sutherland, and E. Sheng, "Carbon surface: Area, porosity, chemistry, and energy," Journal of Colloid and Interface Science, vol. 179, no. 2, pp. 561–569, 1996, doi: 10.1006/jcis.1996.0250.

[3] J. Romanos, "Nanospace engineering of KOH activated carbon," Nanotechnology, vol. 23, no. 1, p. 015401, 2012, doi: 10.1088/0957-4484/23/1/015401.

[4] O. P. Olatidoye, S. S. Sobowale, J. V. Akinlotan, and O. O. Olorode, "Chemical composition and physicochemical characteristics of tropical almond nuts (terminalia catappia l) cultivated in southwest Nigeria," Journal of Medical and Applied Biosciences, 2011.

[5] Y. Soo, N. Chada, M. Beckner, J. Romanos, J. Burress, and P. Pfeifer, "Adsorbed Methane Film Properties in Nanoporous Carbon Monoliths," Bulletin of the American Physical Society, 2013.

[6] World Health Organization, "World Health Organization model list of essential medicines: 21st list 2019," Geneva: World Health Organization, 2019, hdl:10665/325771. WHO/MVP/EMP/IAU/2019.06.

[7] I. K. Adewumi, "Activated carbon for water treatment in Nigeria: Problems and Prospects," in Appropriate Technologies for Environmental Protection in the Developing World, E. K. Yanful, Ed. Dordrecht: Springer, 2009, doi: 10.1007/978-1-4020-9139-1_13.

[8] D. Adinata, W. M. Ashri, and M. K. Aroua, "Preparation and characterization of activated carbon from palm shell by chemical activation with K2CO3," Bioresour Technol, vol. 98, pp. 145–149, 2007.

[9] F. Ahmad, W. M. A. W. Daud, M. A. Ahmad, and R. Radzi, "The effects of acid leaching on porosity and surface functional groups of cocoa (Theobroma cacao)-shell

based activated carbon," Chemical Engineering Research and Design, vol. 91, pp. 1028–1038, 2013.

[10] L. Ai, C. Zhang, F. Liao, Y. Wang, M. Li, L. Meng, and J. Jiang, "Removal of methylene blue from aqueous solution with magnetite loaded multi-wall carbon nanotube: kinetic, isotherm and mechanism analysis," Journal of hazardous materials, vol. 198, pp. 282–290, 2011.

[11] Li Y., Du Q., Liu T., Peng X., Wang J., Sun J., Wang Y., Wu S., Wang Z., Xia Y. "Comparative study of methylene blue dye adsorption onto activated carbon, graphene oxide, and carbon nanotubes." Chemical Engineering Research and Design, vol. 91, pp. 361-368, 2013.

[12] Mondal N.K., Kar S. "Potentiality of banana peel for the removal of Congo red dye from aqueous solution: isotherm, kinetics, and thermodynamics studies." Applied Water Science, vol. 8, no. 4, p. 157, 2018.

[13] Rahmat N.A., Ali A.A., Hussain N., Muhamad M.S., Kristanti R.A., Hadibarata T. "Removal of Remazol Brilliant Blue R from aqueous solution by adsorption using pineapple leaf powder and lime peel powder." Water, Air, & Soil Pollution, vol. 227, no. 3, p. 105, 2016.

[14] Meena, A. K., Kadirvelu, K., Mishra, G., & Rajagopal, C. (2022). Activated carbon from agricultural wastes: A review on potential and challenges. Journal of Environmental Chemical Engineering, 10(1), 108482.

[15] Ahmad, M. A., Ahmad, N., & Bello, M. M. (2021). Agricultural waste-derived activated carbon as a sustainable adsorbent for wastewater treatment: A review. Journal of Cleaner Production, 306, 127834.

[16] Yan, L., & Wang, X. (2021). A review on the applications of activated carbon for air pollution control. Journal of Cleaner Production, 306, 127784.

[17] Acharya, J., Lenka, N., Rath, P., & Sahoo, B. K. (2021). A comprehensive review on activated carbon: Development, properties, characterization and applications. Journal of Environmental Chemical Engineering, 9(6), 105487.

[18] Wu, X., Gao, J., Zhang, L., Li, M., & Zhou, J. (2021). A review on the preparation and modification of activated carbon materials and their applications in environmental fields. Journal of Cleaner Production, 315, 128134.

Comparative Analysis Of Ergonomic Knowledge And Implementation Among Sofa Producers In Kano State Nigeria

Hassan Salihu Abubakar[1], Umar Ali Umar[1,*], Ayodeji Nathaniel Oyedeji[1]

[1]Department of Mechanical Engineering, Ahmadu Bello University, Zaria, 810107, Nigeria

[*]Corresponding Author: Umar Ali Umar. Email: umaraliumar@yahoo.co.uk

Abstract: Awareness of ergonomics in the manufacturing industry is necessary for survival in a highly competitive business world. For the first time, this study aims to assess the ergonomics knowledge of sofa producers and conduct a comparative analysis of the knowledge of the sofa producers and implementations of ergonomics using Kano State, Nigeria, as a case study.

Also, this study considered the factors hindering ergonomics implementation in sofa production. Using the descriptive research design, the questionnaire consisted of close-ended questions and Likert-scale type and was distributed to members of Sofa Producers' Association in Kano State. The study's result showed that only 43.61% of the respondents displayed good awareness and knowledge of ergonomics.

The study also showed that only 42.5% of the respondents always implement ergonomic knowledge in the design and production of Sofa producers. Furthermore, Spearman's correlation analysis showed a coefficient value of 0.08, implying a weak positive correlation between the level of awareness and implementation of this knowledge in the design and production among Sofa producers in Kano.

Keywords: Ergonomics, Sofa, Knowledge, Implementation, Furniture

تحليل مقارن للمعرفة الهندسية والتنفيذ بين منتجي صوفا في ولاية كانو في نيجيريا

الملخص: الوعي ببيئة العمل في الصناعة التحويلية ضروري للبقاء في عالم أعمال شديد التنافسية. لأول مرة ، تهدف هذه الدراسة إلى تقييم معرفة بيئة العمل لمنتجي الأرائك وإجراء تحليل مقارن لمعرفة منتجي الأرائك وتطبيقات بيئة العمل باستخدام ولاية كانو ، نيجيريا ، كدراسة حالة.

أخذت هذه الدراسة بعين الاعتبار العوامل التي تعيق تنفيذ بيئة العمل في إنتاج الأريكة. باستخدام تصميم البحث الوصفي ، يتكون الاستبيان من أسئلة مغلقة ونوع مقياس ليكرت وتم توزيعه على أعضاء جمعية منتجي الأرائك في ولاية كانو. أظهرت نتيجة الدراسة أن 43.61٪ فقط من المستجيبين أظهروا وعيًا ومعرفة جيدة ببيئة العمل.

أظهرت الدراسة أيضًا أن 42.5 ٪ فقط من المستجيبين يطبقون دائمًا المعرفة المريحة في تصميم وإنتاج منتجي الأرائك. علاوة على ذلك ، أظهر تحليل ارتباط سبيرمان قيمة معامل قدرها 0.08 ، مما يدل على وجود علاقة إيجابية ضعيفة بين مستوى الوعي وتنفيذ هذه المعرفة في التصميم والإنتاج بين منتجي الأرائك في كانو.

1. Introduction

In the fiercely competitive corporate world, understanding ergonomics is essential for survival in the industrial sector [1]. Ergonomics is a technique for designing safe, healthy, and comfortable work environments, with innumerable advantages for both the systems and the components of the systems [2], [3]. The entire company must be involved in creating, designing, executing, controlling, evaluating, and redesigning processes. Managers are crucial in raising ergonomic awareness since implementing a participatory ergonomics culture is a top-down approach [4]. Implementing an ergonomics culture may cause managers anxiety if they are unaware of the benefits and drawbacks [5]. According to studies, managers of a company that needs ergonomics as one of its outputs may only support the ergonomics concept at their workplaces when informed of its costs and advantages [1]–[3].

To achieve objectives like safety, health, and ergonomics management, knowledge is the primary source [6]; transferring ergonomics expertise, however, might be difficult in industrial enterprises, particularly in underdeveloped nations. Industries in these nations frequently lack the instruments essential to acquire information swiftly; therefore, knowledge providers lack the assistance needed for knowledge transfer [7]. Because of these circumstances, knowledge recipients are presumably less motivated to comprehend knowledge transfer ideas and less able to identify actual knowledge transfer challenges. Researchers contend that to implement ergonomic treatments more successfully, it is vital to use suitable tactics to facilitate information transmission and highlight its significance [8], [9].

Due to the high prevalence of stresses that lead to occupational injury and sickness, the furniture manufacturing sector must build a culture based on human factors and ergonomics [10]. Additionally, from another angle, the manual handling of numerous heavy, bulky, and uncomfortable materials and manual, labour-intensive procedures like sanding, rubbing, stapling, and spraying result in significant physical work demands for the furniture manufacturing business [11]. While ergonomics is greatly needed in furniture production, it is not utilised to its fullest potential. A few variables constrain the use of ergonomics expertise in furniture production. Stakeholder self-interest, illiteracy, employee acceptability, regulatory agency/union, material cost, and accessibility to contemporary equipment are a few of them [10].

Adedeji *et al.* [10] conducted a study evaluating the ergonomics of carpentry and furniture-making enterprises in Port Harcourt, Nigeria. The study found that while there is a growing awareness of ergonomic difficulties, there is not enough information accessible regarding the ergonomic settings of Nigerian carpentry and furniture-making (CFM) businesses. The study's findings revealed a weakly positive correlation between the heights of tables built by CFM firms and the necessary heights, indicating that a significant portion of the tables utilised were not anthropometrically matched. The CFMs regularly experienced the following occupational hazard outcomes: hand cuts, bruises, back discomfort, and infections of the nose, muscles, and eyes. Yun [12] studied integrating ergonomics in the design of contemporary kitchens and electric appliances. For monitoring the modelled systems, the study used pure numerical control charts. However, it was noted that when general data complexity and dimensionality increased, the employment of the numerical conversion approach was considered illogical.

Additionally, Gerding et al. [13] carried out a study on the ergonomic issues in the home offices of university employees sent home due to the COVID-19 pandemic. The study found that moderate to severe discomfort in the eyes, neck, head, upper back, and shoulders, and severe low and middle back pain, were all reported by more than 40% of the participants. According to the survey, less than 45% of seating arrangements were observed to have movable armrests. The study concluded that as teleworking in temporary offices grows more prevalent, poor static postures may increase the risk of considerable pain and maybe more serious musculoskeletal problems.

Previous studies have highlighted the importance of management commitment and employee participation for successfully integrating ergonomics into manufacturing processes [1], [5]. However, there is a lack of research focusing on ergonomic knowledge and implementation practices among sofa producers. Therefore, this study aims to compare ergonomic knowledge and implementation among sofa producers in Kano State, Nigeria. By examining the factors hindering ergonomics implementation in sofa production, this study seeks to contribute valuable insights into improving ergonomics practices in the furniture manufacturing industry.

2. Research methodology

A descriptive survey research method was adopted to adequately carry out the comparative analysis of ergonomic knowledge and implementation among Sofa producers in Kano State, Nigeria. This is because the survey method is suitable for collecting mass raw data from many respondents to facilitate a clear understanding of the subject matter under investigation [14]–[17]. The population of this study comprises the owners of Sofa producing businesses, managers, engineers, and technicians. As obtained from the Sofa Producers' Association in Kano State, there are about 1,250 members in Kano State. This comprises Local Government Areas (LGA) such as Kano Municipal, Dala, Gwale, Fagge, Tarauni, Nassarawa, Ungogo, Kumbotso, and others.

Using 's formula [18] given in Equation 1) for determining sample size from a large population, a sample was drawn from the population size of 1,250 members in the study comprising mostly small and medium enterprises businesses. Applying Equation (1) at a confidence level or significance level of 95% while the precision level was taken to be 5%, the sample size was obtained approximately 300 members of the Sofa Producers' Association in Kano State.

$$n = \frac{N}{1+N(e)^2} \qquad (1)$$

Where, n= sample size, N =Population size and e =Margin error/ level of precision (0.05).

Similarly, the researchers used structured questionnaires to obtain the required information from the respondents. The questionnaire items were a combination of close-ended questions and Likert-scale type questions, allowing the respondents to choose from alternatives provided by the researcher.

The questions were obtained and modified from previous literature. The researchers administered the questionnaire personally, in which this exercise took approximately four (4) days. Taking into account the research questions associated with this study, the questionnaire had 4 sections:

- **Section A:** Socio-economic/demographic information of respondents such as age group, educational qualification, number of employees in the business, work duration/years of experience, and position in the business.
- **Section B:** Knowledge-based questions on ergonomics to help assess the level of ergonomic awareness among the respondents.
- **Section C:** Implementation of the knowledge of ergonomics in the design and production of Sofa by the respondents.
- **Section D:** Identification of factors that hinder/limit the use of ergonomic knowledge in the design and production of Sofa by the respondents.

Furthermore, data obtained were analysed using descriptive statistics to facilitate a clear understanding of the subject matter under investigation. In contrast, Spearman's rank correlation statistical method was used to compare the relationship between ergonomic knowledge and implementation by the respondents. In the descriptive statistics data analysis method, data obtained were expressed in percentages and displayed in tables and charts. On the other hand, based on the mean responses of the respondents on ergonomic knowledge and implementations, the variables were ranked such that R_1 denotes the level of awareness, and R_2 denotes the level of implementation. The Spearman's rank correlation formula is given in Equation (2) [19]:

$$R = 1 - \frac{6\sum d^2}{n(n^2-n)} \qquad (2)$$

Where d= Difference in the rank of each variable and n =number of variables.

3. Results and discussion

3.1 Socio-Economic/Demographic

The socio-economic distribution of the respondents whose ergonomics knowledge was analysed in terms of age group, education qualification, number of employees under them, work duration/years of experience, and current position in the sofa industrial sub-sector, as given in Figures 1 and 2.

Figure 1(a) shows the age range of the respondents, 16% of respondents are between the ages of 18 to 20 years, 8% belong to the age range of 21 to 25, 10% are between the ages of 26 to 30 years, 26% belong to the age range of 31 to 35 while the most of the respondents (40%) are of the ages of 36 and above. This implies that most of this study's responses come from respondents with experience in the field of sofa production and the use of ergonomics while designing their output or products. Similarly, Figure 1(b) shows the educational qualifications of respondents under study, in which 26% of respondents have informal education, 25% have a primary school education, 15% have secondary school qualifications, and 34% have a tertiary education range.

This result implies that most of the respondents of this study come from sofa producers with tertiary education levels (NCE, ND, B.Sc., and others), which shows that most of the respondents are aware of the use and importance of ergonomics in sofa production.

Figure 1(c) shows the number of employees within the organisation or factory of each study area. 40% of respondents have a population within zero to nineteen in their factories, 8% have 20-49 employees, 10% have 50-99, 10% have 250-249 employees in their factories, 16% have 100-249 employees, and 16% also have above 500 employees in the factories. This result implies that the majority of the respondents of this study come from respondents with 0-19 workers or employees within their factories, which denotes a small-scale enterprise. Figure 1(d) shows how long respondents have stayed in the business of sofa production. 10% of respondents have zero-to-one-year years of experience in sofa making, 24% have 1-3 years of experience in sofa making, 26% have 4-10 years of experience in sofa making, and 40% have above 10 years of experience in sofa making. This result implies that the majority of the respondents of this study come from respondents who have stayed in the furniture-making business for over ten years, suggesting that they have gained huge experience over time.

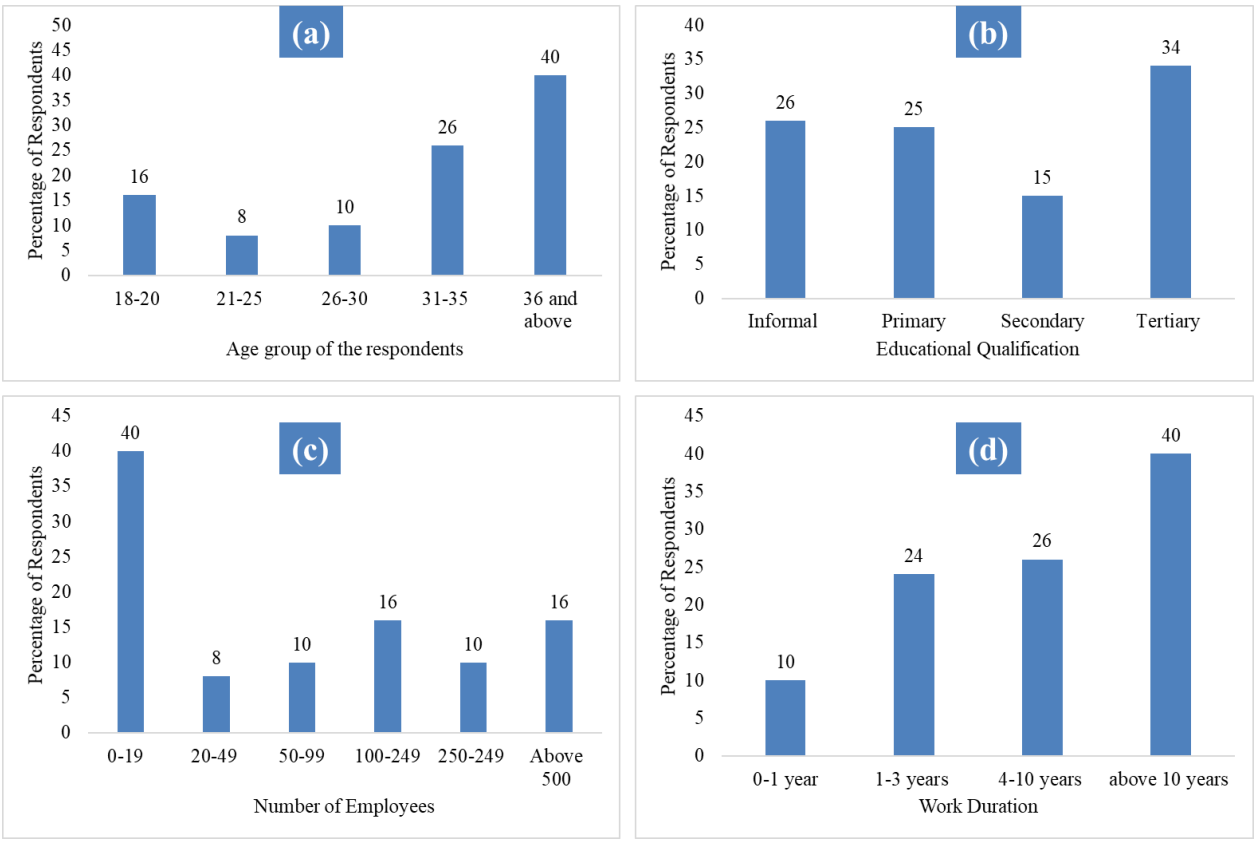

Figure 1: Distribution of the respondents by (a) age group, (b) educational qualification, (c) number of employees, and (d) work duration/years of experience

Furthermore, Figure 2 shows the current position of each respondent as it relates to the business of furniture production. 40% of respondents are the owners of the factories, 8% are Managing Directors in the business, 10% belong to the Production department and technicians, and they only determine the number of outputs to be produced, 40% are engineers and other categories in the factories. This result implies that most respondents have sufficient knowledge, exposure, and authority to implement ergonomics in sofa production.

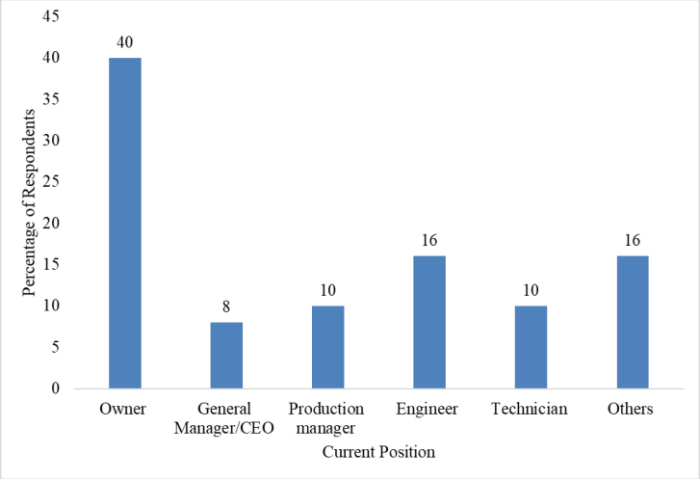

Figure 2: Current Position Distribution of Respondents

3.2 Level of Ergonomics Awareness among Sofa Producers in Kano

In accessing the level of ergonomics awareness among Sofa producers in the study area, questions with regard to ergonomics were asked. These questions were based on anthropometric data in the design and construction of sofa, the importance of posture, sofa material's comfort provision ability, workspace safety, manual material handling equipment, and the effect of lighting and temperature on the comfort of end-users. Table 1 gives the percentage response to these questions based on the Likert scale, the mean score, and the ranking of these knowledge-based questions.

From the result obtained in Table 1, it was observed that only 43.61% of the respondents displayed a good knowledge of ergonomics. The result is related to the findings of Oladeinde *et al.* [20], who carried out awareness and knowledge of ergonomics among medical laboratory scientists in Nigeria and observed that the ergonomics awareness among medical laboratory was poor among the medical laboratory scientists in the study area. Furthermore, Table 1 shows that knowledge of workstation evaluation toward the clean and safe environment, equipment and ease of movement in the workspace as it relates to workers' health and comfort is the most ranked knowledge-based awareness among the Sofa producers. This is followed by the knowledge that bad sitting posture results in bad health conditions, and then suitable manual handle equipment provision for routine activities to promote the health and comfort of workers. It was observed from the result that the use of anthropometric data for the design and construction of seating room chairs had the lowest ranking score, which denotes poor awareness among the Sofa producers in the study area. The reason for this is not farfetched from the fact that there is the inadequacy of proper anthropometric databases and societal health care system considerations in countries such as Nigeria.

Table 1: Response on the level of ergonomics awareness among Sofa producers in Kano and their rankings.

S/N	Questions	SA	A	N	D	SD	Mean Score	Ranking
1	Do you believe the use of anthropometric data in the design and construction of seating room chairs can improve users' comfort and health?	40%	30%	10%	6%	14%	3.70	6th
2	Do you believe bad sitting posture can result in any bad health condition?	48%	30%	15%	5%	2%	3.82	2nd
3	Do you believe some materials used (i.e., form, material) in seating room furniture affect users' comfort and health?	40%	28%	16%	8%	8%	3.75	5th
4	Do you believe workstation evaluation toward a clean, safe environment, equipment and ease of movement in the workspace is related to workers' health and comfort?	40%	30%	10%	6%	15%	3.87	1st
5	Do you believe that Suitable manual material handling equipment provision for routine activities can promote the health and comfort of workers?	50%	26%	6%	8%	10%	3.81	3rd
6	Do you believe good lighting and comfortable temperature affect the health and comfort of workers?	40%	30%	10%	6%	14%	3.79	4th

SA: Strongly Agreed; A: Agreed; N: Neutral; D: Disagree, SD: Strongly Disagree

3.3 Implementation of Ergonomic Knowledge

Furthermore, to evaluate the level of implementation of knowledge of ergonomics by the Sofa producers in the study area, questions about the implementation of ergonomics in Sofa production were asked. These questions were in line with the questions asked on the level of ergonomics awareness. Table 2 gives the percentage response to these questions based on the Likert scale, the mean score, and the ranking of the level of implementation of this ergonomic knowledge.

Table 2: Response on the level of implementation of ergonomic knowledge among Sofa producers in Kano and their rankings.

S/N	Questions	A	B	C	D	E	Mean Score	Ranking
1	Do you use anthropometric data to determine the optimum size, shape, and form of a product to make it easier for the people that will use your seating room chairs?	43%	35.3 %	10%	3.3%	8.3 %	4.01	3rd
2	Do you provide chairs that will give a good seating posture in your design process?	45%	28.3 %	8.3%	10%	8.3 %	3.91	4th
3	Do you ensure the safety, health and comfort of users in selecting materials for your living room chairs?	46.7%	31.7 %	10%	6.7%	5%	4.11	2nd
4	Do you continuously evaluate the level of comfort, safety and health of your workplace by getting the workers' opinions in relation to the work they perform?	35.3%	33%	10%	10.7 %	11%	4.15	1st
5	Do you have any material handling system that will reduce manual lifting and transportation of	41.7%	30%	13.3 %	8.3%	6.7 %	3.91	4th

	materials within your organisation?							
6	Do you ensure that comfortable working temperature and good lighting in your workstations?	43.3%	28.3 %	11.7 %	8.3%	8.3 %	3.90	6th

A: Use it always; B: Very often; C: Sometime; D: Really; E: Never

From Table 2, it was observed that only 42.5% of the respondents always implement the ergonomic knowledge they have to design and produce sofa. This result aligns with the findings of [21], who conducted a study on ergonomics awareness and employee performance and discovered that among employees in production organisations. However, the knowledge of ergonomics is high, and there is an inadequate implementation of this knowledge in the production process. Furthermore, Table 2 shows that the implementation of the continuous evaluation of the level of comfort, safety and health of the workplace by getting the workers' opinions in relation to the work they perform is the most ranked ergonomic knowledge that is implemented in the design and production for ergonomics by the sofa producers. This is followed by the implementation of the knowledge of ensuring the safety, health and comfort of users in selecting materials for their living room chairs and also by the use of anthropometric data for the design and construction of seating room chairs. However, observed from the result that the design of the sofa based on good working temperature and good lighting in the workstation had the least implementation.

3.4 Factors that Hinder the Use of Ergonomic Knowledge

In evaluating the factors that hinder the implementation of knowledge of ergonomics in the production of Sofa in the study area, questions on the possible factors that influence the implementation were asked. These questions were based on stakeholders' self-interest, illiteracy, acceptance by employees, regulatory agency/union, cost of materials, and modern tools were considered. Table 3 gives the percentage response to these questions based on the Likert scale, the mean score, and the ranking of the factors hindering ergonomics implementation in Sofa production.

From Table 3, it was observed that the majority of the respondents, an average of 68.05%, agreed that the highlighted factors hinder the use of ergonomic knowledge in producing Sofa. The obtained result is in line with the findings of Karuppiah *et al.* [22], who carried out a study on the role of ergonomic factors in the production of leather garments in small and medium-scale enterprises in India and discovered that outdated machinery, vibration, operational setup, fatigue, and poor ventilation and lighting are the top five factors inducing ergonomic-related problems. Similarly, Table 3 shows that the lack of modern tools and equipment is the most ranking factor that hinders the use of ergonomic knowledge in design and production among the producers of living room chairs in the study area. Inadequate acceptance by employees follow this, then illiteracy. It was, however, observed from the result that the self-interest of the stakeholder (customers, regulators and unions) had the least implementation.

Table 3: Response on the factors that hinder the use of ergonomic knowledge in producing Sofa and their rankings.

S/N	Questions	SA	A	N	D	SD	Mean Score	Ranking
1	Do you believe stakeholder (customers, regulators and unions) self-interest hinders ergonomic awareness and implementation in Kano State?	50%	26%	6%	8%	10%	3.80	6th
2	Do you believe illiteracy also contributes heavily to hindering ergonomic awareness and implementation in the seating chairs furniture industry?	40%	30%	10%	6%	14%	3.96	3rd
3	Inadequate acceptance by employees hinders the implementation of ergonomics in living room chair production.	50%	26%	6%	8%	10%	3.98	2nd
4	Do you believe the lack of a strong regulatory agency or union that can oversee activities can also hinder the use of ergonomic knowledge in design and production?	40%	30%	10%	6%	14%	3.93	4th
5	Do you believe high costs in material and equipment can hinder ergonomic implementation in the design of seating room chairs?	48%	30%	15%	5%	2%	3.86	5th
6	Lack of modern tools and equipment?	50%	26%	6%	8%	10%	4.03	1st

SA: Strongly Agreed; A: Agreed; N: Neutral; D: Disagree, SD: Strongly Disagree

3.5 Correlation between the Level of Awareness and the Implementation of Ergonomics

Based on the results obtained earlier in Table 1 and Table 2, the correlation between the level of awareness of ergonomics and the level of implementation of this knowledge in the design and production was determined by the Spearman's rank correlation given in Equation (2), based on the mean with rank R_1 denoting the level of awareness. Rank R_2 denotes the level of implementation. The obtained result of this computation is given in Table 4.

Table 4: Spearman correlation computation on the level of awareness and implementation of ergonomics by Sofa producers.

S/N	Factors of Ergonomics	LA	R_1	LI	R_2	d	d^2
1	Do you believe the use of anthropometric data in the design and construction of seating room chairs can improve users' comfort and health?	3.70	6	4.01	3	3	9
2	Do you believe bad seating posture can result in bad health conditions?	3.82	2	3.91	4.5	-2.5	6.25
3	Do you believe some materials used (i.e., form, material) in seating room furniture affect users' comfort and health?	3.75	5	4.11	2	3	9
4	Do you believe workstation evaluation toward a clean, safe environment, equipment and ease of movement in the workspace is related to workers' health and comfort?	3.87	1	34.15	1	0	0
5	Do you believe that Suitable manual material handling equipment provision for routine activities can promote the health and comfort of workers?	3.81	3	3.91	4.5	-1.5	2.25
6	Do you believe good lighting and comfortable temperature affect the health and comfort of workers?	3.79	4	3.90	5	-1	1
Total							27.5

LA: Level of awareness; LI: Level of implementation

Using Equation (2), Spearman's rank correlation is 0.08. The result implies a weak positive correlation between the level of awareness and implementation of this knowledge in the design and production among sofa producers in the study area. Though sofa producers have an idea of ergonomics, they tend not to implement these ideas in practice, probably due to factors such as a lack of modern tools and equipment due to high cost, the inadequate standard by a regulatory agency that oversees their activities, low cost of living among the end-users, and even the poor knowledge of ergonomics among the end-users.

The obtained result is in line with the findings of previous works [7], [10], [23], which indicated that there is a low level of ergonomic knowledge awareness in society, as well as poor implementation of the ergonomic knowledge that is known. In these studies, most workers or end-users operate with an extra effort of unknown stress due to inadequate ergonomic knowledge in design and production at workstations or workplaces to compensate and meet their organisation's employees' expected performance.

4. Conclusion

This study considered the comparative analysis of ergonomic knowledge and implementation among Sofa producers in Kano State, Nigeria. From the results obtained:

- Averagely, only 43.61% of the respondents displayed a good knowledge of ergonomics awareness.
- Averagely, only 42.5% of the respondents always implement ergonomic knowledge in the design and production of the sofa.
- Spearman's correlation analysis showed a coefficient value of 0.08, implying a weak positive correlation between the level of awareness and the level of implementation of this knowledge in design and production among Sofa producers in Kano.
- The lack of modern tools and equipment is the most ranking factor that hinders the use of ergonomic knowledge in design and production among the producers of Sofas in Kano state. Other significant factors are inadequate acceptance by employees and illiteracy.

Acknowledgements

The authors acknowledge the support offered by the members of the Sofa Producers' Association in Kano State, as well as the staff and students of the Department of Mechanical Engineering, Ahmadu Bello University, Zaria, Nigeria.

Conflicts of Interests

The authors declare no competing interests

Authors' Contributions

HSA is responsible for collecting data, methodology, and writing the original draft. UAU is responsible for the conceptualisation, supervision, methodology and writing of the original draft. ANO is responsible for the data analysis, formal analysis and writing of the original draft.

5.References

[1] T. A. F. Hakimi, S. A. Helmi, M. Hisjam, and A. Ali, "Ergonomic improvement in a manufacturing company," *AIP Conference Proceedings*, vol. 2217, 2020, doi: 10.1063/5.0000729.

[2] M. Noor, M. H. Hilmi, R. Ghazilla, and R. Ariffin, "Physical ergonomics awareness in an offshore processing platform among Malaysian oil and gas workers," *International Journal of Occupational Safety and Ergonomics*, vol. 26, no. 3, pp. 521–537, 2020, doi: 10.1080/10803548.2018.1480341.

[3] S. Kaup, S. Shivalli, U. Kulkarni, and C. Arunachalam, "Ergonomic practices and musculoskeletal disorders among ophthalmologists in India: An online appraisal," *European Journal of Ophthalmology*, vol. 30, no. 1, pp. 196–200, Jan. 2020, doi: 10.1177/1120672118815107.

[4] N. Abdollahpour and F. Helali, "Implementing Practical Ergonomics Knowledge Transfer Using Ergonomic Checkpoints to Support the Participatory Ergonomics Process in an Industrially Developing Country," *IISE Transactions on Occupational Ergonomics and Human Factors*, vol. 10, no. 2, pp. 59–70, 2022, doi: 10.1080/24725838.2022.2054880.

[5] V. Lamarque, E. Chin, J. Queheille, and O. Buttelli, "Multidisciplinary Approach Ergonomics and Lean: Articulation Between Performance, Health and Safety," *Lecture Notes in Networks and Systems*, vol. 221 LNNS, pp. 417–422, 2021, doi: 10.1007/978-3-030-74608-7_52.

[6] M. – E. Boatca, A. Draghici, and N. Carutasu, "A Knowledge Management Approach for Ergonomics Implementation within Organizations," *Procedia - Social and Behavioral Sciences*, vol. 238, pp. 199–206, 2018, doi: 10.1016/j.sbspro.2018.03.024.

[7] S. Adaramola, "The Promotion of Ergonomics in Nigeria," *Advances in Intelligent Systems and Computing*, vol. 825, pp. 896–899, 2019, doi: 10.1007/978-3-319-96068-5_96.

[8] I. Bolis, T. F. A. C. Sigahi, A. Thatcher, P. Saltorato, and S. N. Morioka, "Contribution of ergonomics and human factors to sustainable development: a systematic literature review," *Ergonomics*, 2022, doi: 10.1080/00140139.2022.2079729.

[9] V. Kalakoski *et al.*, "Effects of a cognitive ergonomics workplace intervention (CogErg) on cognitive strain and well-being: A cluster-randomized controlled trial. A study protocol," *BMC Psychology*, vol. 8, no. 1, Jan. 2020, doi: 10.1186/s40359-019-0349-1.

[10] G. A. Adedeji, A. A. Aiyeloja, and K. E. Yusuf, "Evaluation of the Ergonomics of Carpentry and Furniture-Making Enterprise at the Illoabuchi Cluster Sawmill/Wood Market in Port Harcourt, Nigeria," *Journal of Applied Sciences and Environmental Management*, vol. 26, no. 8, pp. 1343–1349, 2022, doi: 10.4314/jasem.v26i8.4.

[11] H. Hamdan, M. Fahmy-Abdullah, and L. W. Sieng, "Technical efficiency of Malaysian furniture manufacturing industry: A stochastic frontier analysis

approach," *International Journal of Supply Chain Management*, vol. 8, no. 6, pp. 929–937, 2019.

[12] K. Yun, "Intelligent industrial design ergonomics in the integrated design of contemporary kitchens and electric appliances," *Proceedings of the 3rd International Conference on Inventive Research in Computing Applications, ICIRCA 2021*, pp. 201–204, 2021, doi: 10.1109/ICIRCA51532.2021.9544653.

[13] T. Gerding *et al.*, "An assessment of ergonomic issues in the home offices of university employees sent home due to the COVID-19 pandemic," *Work*, vol. 68, no. 4, pp. 981–992, 2021, doi: 10.3233/WOR-205294.

[14] B. S. Terab, U. A. Umar, and A. N. Oyedeji, "Information technology in supply chain management: Perspectives from key actors in the Nigerian petroleum sector," *https://doi.org/10.1080/20421338.2023.2221876*, pp. 1–7, Jun. 2023, doi: 10.1080/20421338.2023.2221876.

[15] M. Peremobower Neminebor, A. Umar, and A. N. Oyedeji, "Feasibility Studies for a Biogas Powered Standalone Power Plant: A Case Study of Giwa Community, Kaduna State, Nigeria," *Nigerian Journal of Tropical Engineering*, vol. 16, no. 1, pp. 127–138, Dec. 2022, doi: 10.59081/NJTE.16.1.011.

[16] U. Bello, D. S. Yawas, and A. N. Oyedeji, "Assessment of Perceived Performance of Solar-Powered Borehole Projects in Nigeria," *Management Science and Business Decisions*, vol. 2, no. 2, pp. 32–43, Dec. 2022, doi: 10.52812/MSBD.47.

[17] L. S. Kuburi, U. Umar, and A. N. Oyedeji, "Risk Assessment of Petrol Filling Stations in a Metropolitical City of Kaduna State, Nigeria," *SINERGI*, vol. 27, no. 2, pp. 179–184, 2023, doi: 10.22441/SINERGI.2023.2.005.

[18] T. Yamane, "Research Methods: Determination of Sample Size," *University of Florida, IFAS Extension*, 1967.

[19] P. Sedgwick, "Spearman's rank correlation coefficient," *BMJ (Online)*, vol. 349, 2014, doi: 10.1136/bmj.g7327.

[20] B. Oladeinde, I. Ekejindu, R. Omoregie, and O. Aguh, "Awareness and knowledge of ergonomics among Medical Laboratory Scientists in Nigeria," *Annals of Medical and Health Sciences Research*, vol. 5, no. 6, p. 423, 2015, doi: 10.4103/2141-9248.177989.

[21] S. O. Olabode, A. R. Adesanya, and A. A. Bakare, "Ergonomics Awareness and Employee Performance: An Exploratory Study," *Economic and Environmental Studies*, vol. 17, no. 44, pp. 813–829, 2017, doi: 10.25167/ees.2017.44.11.

[22] K. Karuppiah, B. Sankaranarayanan, S. M. Ali, and G. Kabir, "Role of ergonomic factors affecting production of leather garment-based SMEs of India: Implications for social sustainability," *Symmetry*, vol. 12, no. 9, 2020, doi: 10.3390/SYM12091414.

[23] A. Ibrahim and Q. S. M, "Ergonomics Study of the Incidence of Musculoskeletal Disorder among the School Teachers in Egba Division of Ogun State Nigeria," *nipesjournals.org.ng*, vol. 2, no. 1, pp. 13–20, 2020.

The Effect of Boron Spraying on Some Productive and Specificcharacter of two Ecotypes of Anise (Municipal and Shami) (Pimpinella anisum L.)

Hala Mohammad[1*], Ali Somaa[1*]

[1] College of Agriculture, Tishreen University, Syria

[*]Corresponding authors: halamohammad445@gmail.com, alisomaa88@gmail.com

Abstract: The lack of studies on the anise plant contributed to increasing the importance of the research, as the research was carried out in the Salhab region, Hama Governorate, Syria, for the agricultural season 2022-2023. The aim was to study the effect of boron spraying on some characteristics of two ecotypes of anise, which are the municipal anise and the Shami anise. Four concentrations of boron (0-25-50-75) mg/L had been studied according to the" split plot design for one time only" design. Thus, boron was sprayed twice at the beginning of flowering and at the beginning of the fruiting stage. In addition, averages were recorded, and significant differences were calculated. The results showed that the municipal ecotype was superior to the Shami ecotype in productivity per hectare, as model ecotype affected productivity.
The results of the interaction of the studied ecotypes with the studied concentrations of boron showed that there were significant differences between the studied treatments and control, while the interaction of the municipal ecotype of anise with boron 25 mg / L achieved a significant superiority over the rest of the treatments and control in terms of fruit weight / plant, and achieved the highest value of (18.62). g compared to control, which achieved the lowest value (7.46) g for the municipal ecotype.

On the other hand, the results of the interaction between the studied ecotypes and concentrations of boron (0,25,50,75) mg/l for the weight of 1000 fruits showed that there were significant differences between treatments and control. The interaction of the municipal aniseed ecotype with boron at a concentration of 75 mg / L achieved a significant superiority over the rest of the treatments and control. The interaction of the Shami ecotype with boron at a concentration of 75 mg / L achieved a significant superiority over the studied treatments and control in terms of the number of fruits /inflorescences.
The interaction of the municipal ecotype with boron of a concentration of 25 mg/L achieved the highest percentage of essential oil, which was (5.60%), while the lowest value was in the Shami ecotype and at the same concentration of boron, which was (2.40%). It was observed that there were no significant differences between the studied boron concentrations and the average concentrations in each of the rows, the weight of 1000 fruits, and the percentage of essential oil.
In addition, there were no significant differences in the ecotype of the studied cultivars and each of the characteristics of the number of fruits in one flower, the weight of 1000 fruits, and the weight of the fruits/plant.

Keywords: Apiaceae, Pimpinella anisum L, Anise, Boron, weight of 1000 fruits, essential oil, productivity yield, micronutrients, Ecotype.

تأثير الرش بالبورون في بعض الصفات الإنتاجية والنوعية لطرازين من اليانسون (البلدي والشامي) (*Pimpinella anisum L.*)

الملخص: ساهمت قله الدراسات عن نبات اليانسون في زيادة اهميه البحث حيث تم تنفيذ البحث في منطقة سلحب، محافظه حماه للموسم الزراعي 2022 –2023.وذلك بهدف دراسة تأثير الرش بالبورون في بعض الصفات لطرازين من اليانسون، وهما طراز اليانسون البلدي وطراز اليانسون الشامي، حيث تمت دراسة أربع تراكيز للبورون (0–25–50–75) ملغ/ل وفق تصميم القطع المنشقة لمره واحدة فقط. وتم الرش بالبورون مرتين في بداية الإزهار وفي بداية العقد، وتم تسجيل المتوسطات، وحساب الفروق المعنوية وقد بينت النتائج تفوق الطراز البلدي على الطراز الشامي في انتاجيه الهكتار الواحد. حيث أثر نوع الطراز في الإنتاجية. وأظهرت نتائج تفاعل الطرز المدروسة مع التراكيز المدروسة للبورون وجود فروق معنوية بين المعاملات المدروسة والشاهد، حيث حقق تفاعل الطراز البلدي لليانسون مع البورون 25ملغ/ل تفوقا معنويا على باقي المعاملات والشاهد في صفه وزن الثمار/نبات، وحققت اعلى قيمه التي بلغت (18.62)غ مقارنه بالشاهد التي حققت أدنى قيمه (7.46)غ للطراز البلدي.

من جهة أخرى، بينت نتائج التفاعل بين الطرز والتراكيز المدروسة من البورون (0،25،50،75) ملغ/ل بالنسبة لصفه وزن 1000ثمرة وجود فروق معنوية بين المعاملات والشاهد. وقد حقق تفاعل الطراز البلدي لليانسون مع البورون تركيز 75ملغ/ل تفوقا معنويا على باقي المعاملات والشاهد. وحقق تفاعل الطراز الشامي مع البورون تركيز 75ملغ/ل تفوقا معنويا على المعاملات المدروسة والشاهد في صفه عدد الثمار في النورة الزهرية الواحدة.

حقق تفاعل الطراز البلدي مع البورون تركيز25ملغ/ل أعلى نسبة مئوية من الزيت العطري وبلغت (5.60%) بينما كانت أدنى قيمه عند الطراز الشامي وعند نفس تركيز البورون وهي (2.40%). وتم ملاحظة غياب الفروق المعنوية بين تراكيز البورون المدروسة ومتوسط التراكيز في كل من صفه وزن ال1000ثمرة، والنسبة المئوية للزيت العطري.

بالإضافة الى ذلك لم يكن هنالك فروق معنويه في نوع الطرز المدروسة وكل من صفة عدد الثمار في النورة الزهرية الواحدة، ووزن ال1000ثمرة، و وزن الثمار/النبات.

الكلمات المفتاحية: الفصيلة الخيمية، يانسون، بورون، وزن ال1000 ثمرة، الزيت العطري، صفات انتاجيه، مغذيات دقيقه، طراز بيئي.

1. Introduction

Herbal medicine is one of the oldest forms of health care that has been used for decades in developing and developed countries and the use of plants as medicines dates back to 60,000 years ago, according to reports from ancient Babylon. In Egypt and China, written material on herbal medicines dates back nearly 5,000 years, and in Asia Minor and Greece it dates back 2,500 years[1].

Anise (Pimpinella anisum L.) is considered one of the important medicinal and aromatic plants, and its native habitat is the Mediterranean basin. It is an annual herbaceous plant, belonging to the family Apiaceae. It has common names in different countries such as: Anis vert (France), anise seed (Japan), anise and star anise (USA), anisella (Italy), petit anise (North Africa), and anise (England)[2]. It reaches an average height of 30-50 cm, and the entire plant is covered with soft bristles. Root thin and fusiform, stem rounded, grooved and branched upwards, with umbrella-shaped clusters of small white flowers, anise cross-pollinated. The fruit is oval, pear-shaped, somewhat compressed on the side. Fruits 3–5 mm long, 1.5–2.5 mm wide, smooth (grey, green to grey, brown) [3].

Basically, the part used in the anise plant is the fruits, which are an important natural raw material that is used in several fields medically, nutritionally, and pharmaceutically, and the fruits of Pimpinella anisum contain about 2 to 6% of essential oil. In addition, anise contains antimicrobial and antifungal activities. For fungicides and insecticides[4]. Nutritionally and medicinally: Anise fruits are used as flavorings, and they have digestive and carminative benefits, and relieve gastrointestinal spasms. The consumption of anise in lactating mothers increases milk and relieves their children from digestive problems. Anise is used as a flavoring and aromatic agent for fish products, ice cream and sweets. Anise fruits are used as an analgesic in cases of migraines and also as an anticonvulsant, antiseptic, and diuretic. It can increase milk production, menstruation and urine. And secretion of sweat as well as makes the complexion good. It is also effective in polishing teeth. In some traditional texts, anise is mentioned for melancholy and nightmares as well as in the treatment of epilepsy and seizures. Anise contains 1.5–6.0% volatile oil consisting mainly of anethole, but also up to 8–11% lipids rich in fatty acids, such as palmitic and oleic acids, in addition to approximately 4% carbohydrates and 18% protein[5].

In addition, the ethanolic extract has toxic activity on human prostate cancer cells. Thus, anise can be one of the foods attributed to the prevention and treatment of cancer.

It can also be a natural source of new anti-cancer compounds with anti-proliferative properties [6].

Boron is considered one of the elements necessary for plant growth, and it promotes the formation of adenosine triphosphate ATP, and accelerates the movement of sugars to the active areas during growth throughout the stages of plant reproduction, and that the deficiency in boron causes: slow plant growth, decrease in production and deterioration of crop quality, and it was found that adding boron To some industrial crops (sesame - sunflower - safflower - rapeseed - soybeans - cotton - flax) lead to stimulating plants and accelerating the growth of these crops, and increasing their production by affecting many physiological functions that determine growth and crop yield[7].

The biological yield of plants of the family; (Apiaceae), the percentage of oil and its components of the active substance are affected by the environmental pattern, and the prevailing environmental conditions in the region during the agricultural season, in addition to agricultural treatments, such as irrigation, fertilization, density, and planting distances, so that specific characteristics and productivity are negatively or positively affected by these factors[8]. It is an essential nutrient for optimal growth, development, yield, and quality of crops. Boron deficiency in general can lead to various physiological disorders in agricultural crops[9]. Previous research has proven that this element is essential for plants, and boron plays a major role in plant metabolic activities[10].

And the application of foliar feeding has multiple benefits, but the most prominent of them include: rapid response to plant growth, and it can be beneficial and more effective than soil use of nutrients, especially when there is not enough moisture in the soil, while it can be combined with other agrochemicals such as pesticides, and stands out The importance of foliar fertilization in improving plant growth and crop quality, which can complement soil fertilization, and is a cost-effective way to improve yield, yield characteristics, and crop quality standards because usually only small amounts are needed, and nutrients penetrate the stomata or leaf epidermis, then enter the cells[11].

In a study[12] conducted in Baghdad on aniseed (Pimpinella anisum L.), foliar spraying of boron at concentrations (0_0.75 _1.50) kg/ha led to (an increase in the height and branching of the anise plant, and the number of fruits/inflorescences). (one flowerpot), and the boron treatment (1.50) kg / h gave the highest oil content compared to the control, and (Anethole) compound had the highest concentration when using: (organic fertilizer 5 tons / ha) with (foliar boron 1.50 kg / ha) compared to other treatments.

The explained[13] in their study in Iraq on the fennel plant (Foeniculum vulgare Mill) that: spraying with boron at the elongation stage with a concentration (0_40_80) mg / L achieved a significant increase in plant height, fresh and dry weight of the shoot, and the number of seeds In one flower inflorescence, and the total seed yield. It was found: a significant interaction between nitrogen and boron, where the concentration of boron (40) mg / L with (92) kg / h of nitrogen fertilizer gave the highest values for the studied traits.

in their Bengal study[14] on coriander plants observed: spraying with boron (0.05%). With zinc (0.01%), it led to: an increase in the number of primary and secondary branches of plants, and the length of carrots/plant.
Zhaoma et al [15] concluded in their research on celery plants that: when spraying with a foliar fertilizer containing boron, zinc and copper (Cu-ZnB) at concentrations: (1-1.5-2) g/l, the best concentration is (1 g/l), as it led The use of the mixture (Cu-ZnB1) to: increase the content of vitamin C, enhance the quality of plant nutrition and yield, and reduce the disease index.

The results of Mohamed and others [16]in a study conducted in Egypt on the basil plant (Ocimum basilicum L.) showed that co-treatments of (1)g/l of amino acids and boron (100ppm) led to a high significant increase in plant height, number of branches, and fresh and dry weights.

The results of a study[17] conducted by researchers on the coriander plant in Brazil showed that when foliar spraying boron at concentrations (0, 1, 1.5, 2,3) kg / ha in the form of boric acid (17%), the concentration of 3 kg / ha achieved the highest increase Significant in the shoots of the plant, while there was no significant difference in the weight of the root shoots compared with the control.

The results of researchers[18] in Egypt, in a study on coriander plant (Coriandor sativumL), of the effect of different types of fertilizers and boron and their interactions on growth, yield and essential oils, indicated that foliar spraying with boron (10) mg/L led to an increase in the number of fruits, yield, and percentage of essential oil, and the interaction between the organic matter and the foliar application of boron led to a significant increase in growth characteristics (plant height, number of branches and fruit/plant weight), and in (fruit weight/acre, oil percentage, oil content).
The results of a research study[19] conducted in Iraq on hibiscus sabdariffa L. showed that foliar spraying with (boron) in the form of boric acid at a concentration of (2) g/l and (zinc) in the form of zinc sulfate at a concentration of (1) g/l, and (Gibberellin acid) at a concentration of (200) mg/L increased the plant height up to (146 cm), the number of branches up to (25 branches/plant), and the number of leaves up to (567 leaves/plant).

A study[20] by researchers in Turkey showed that foliar spraying of flax plant (Linum usitatissimum L) with boron at a concentration of (0.3)% in the form of borax, and with zinc sulfate at a concentration of (0.5%) led to: an increase in plant height up to (55.14 cm), and the plant stand up to (216.201) cm, an increase in dry matter (3.66 g/plant), the number of capsules per plant (38.68), the number of seeds/plant (8.57), and the weight of 1000 seeds (7.64 g) and thus an increase in production.

2. Research importance and objectives:

The importance of this research stems from the scarcity of studies on local medicinal and aromatic plants treated with boron, especially aromatic plants, including anise. In addition to the fact that the anise plant is of medical, nutritional and pharmaceutical importance and has a variety of uses in addition to being an important economic crop. The research also aims to study the effect of spraying with different concentrations on the growth and development of the anise plant, and to determine the optimal rate of boron, which gives the best productivity and the highest quality of the crop.

3. Matrials and methods:

3.1 The Site:

The experiment was carried out in an agricultural land in Al-Ghab Plain, Salhab district, Hama governorate. Which rises 185 meters above sea level, during the agricultural season 2022-2023. A sample of field soil was taken from a depth of (0-30 cm) and some mechanical and chemical analyzes of the soil were performed at(Jub-Ramla) research station.

Table: (1) Shows chemical analysis of some soil components

		PMM		
Soil depth	OM%	N	P	K
0-30	2.3%	8.2	4.8	264

3.2 Ecotype used:

The use of the fruits of each of the local anise plant and the Shami anise plant, where the fruits of the Syrian local ecotypes were used. And we obtained the local anise fruits from an agricultural pharmacy in the Salhab region, and these seeds had not been stored for more than one year, while the Shami anise fruits were obtained from Damascus from an agricultural pharmacy, and it had not been stored for more than one year.

3.3 Land preparation for cultivation:

We carried out a plowing of the soil, and then we turned the soil manually, removing stones and weeds, and we applied the experiment according to the" split plot design for one time only" design.
(12) repeaters, the length of each repeater is (2m) and the width is (2m) and between each two repeaters (1m) for ease of carrying out agricultural operations and taking readings, where planting was done on lines with a distance of (35cm) between one line and the other and between each two seeds (25cm) at a rate of (3 seeds) In each hole, at a depth of (2 cm) from the soil surface.
Planting took place on 11/12/2022, and after 30 days, germination occurred.

3.4 Crop management:

All crop management work was carried out after planting, and boron was sprayed twice at the beginning of flowering and at the beginning of the fruiting stage.

3.5 Treatments:

The effect of four concentrations of boron has been studied:
1-Control (0) mg/L.
2- Boron concentration (25) mg / L.
3-Boron concentration (50) mg / L.
4-Boron concentration (75) mg / L.

3.6 Environmental conditions:

Table No. (2) shows the average temperatures, precipitation rate, and natural weather phenomena, according to the monitoring station in the search area.

Months	Average precipitation Rain/ml	Minimum temp. (°C)	Maximum temp. (°C)	natural weather phenomena
12/2021	4.43	3.71	10.87	fog
1/2022	3.9	2.1	7.9	Frost and fog
2/2022	2.35	2.35	12.12	Frost and fog
3/2022	4.75	3.42	10.37	frost
4/2022	0.0	5.8	22.0	frost
5/2022	0.5	11.1	26.8	No thing
6/2022	25.7	17.1	32.4	No thing

3.7 Parameters studied:

1-Fruit/plant weight: Ten plants were randomly selected from the center of each of them,
the experimental and collect the fruits of these plants, after which the averages are calculated.
2-The weight of 1000 fruits(g): 100 fruits were counted and weighed, then we multiplied this result by 10.
3- number of fruits in one flower: Ten plants were randomly selected from the center of each of them the experimental and We collected the fruits of each plant, then number of fruits in one flower of each plant, and counted them for each plant.
4-hectare productivity(kg/h): We calculated the weight of the fruits per plant, and determined the productivity per square meter and then per hectare.
5- Extraction and quantification of oil %: The oil was extracted using the water distillation method by Clevenger was used after extracting the oil from each environmental ecotype,
Then the quantity (ml) was measured, after which the percentage of all samples was calculated.

3. 8Experimental statistical analysis:

The obtained results were tabulated in Excel, and then the results were analysed using GenStat 12 statistical analysis software, and a complete randomized design was used to calculate the least significant difference value%.

4. Result And Discussion:

• The effect of spraying with boron on the fruit weight/plant of the two ecotypes of aniseed Municipal and Shami:

Table (3) shows the effect of spraying with boron concentrations on the characteristic of fruit/plant weight for two ecotypes of anise (Municipal and Shami), thus the averages showed (11.27, 13.76, 11.70, 14.80) grams for the studied boron concentrations (0,25,50,75) mg/l. There are significant differences between the treatments and the control, and the averages of the studied ecotypes (13.20, 12.56) g/plant showed the absence of significant differences for the studied cultivars, as the ecotype of cultivar did not affect the weight of the fruit/plant.

The results of the interaction between the ecotypes and the studied concentrations of boron (0,25,50,75) mg/l showed that there were significant differences between the studied treatments and the control. And the interaction of the municipal ecotype with a concentration of boron 25 mg / L achieved a significant superiority over the rest of the treatments and the control, and achieved the highest value (18.62) compared to the control that achieved the lowest value (7.46) for the municipal ecotype. This may be attributed to the role of boron in increasing the amount of carbohydrate synthesis, and storage inside the fruits, and thus The weight of the fruits increased on the plant, and this agreed with the results of the study of (Tania et al., 2018) in their research in Bengal on the coriander plant, where it was found that: spraying with boron (0.05%) with zinc (0.1%) led to an increase in its grade (fruit weight/ the plant).

	The studied boron concentrations (mg/L)				
Ecotypes	Control	25.00	50.00	75.00	Average ecotyps
Municipal	7.46 ^{h}	18.62 ^{a}	11.93 ^{e}	14.81 ^{c}	13.20 ^{a}
Shami	15.09 ^{b}	8.90 ^{g}	11.46 ^{f}	14.79 ^{d}	12.56 ^{a}
concentration averages	11.27 ^{d}	13.76 ^{b}	11.70 ^{c}	14.80^{a}	
L.S.d5%	**V**=1.231	**B**=0.624	**B×V**=1.022		
CV%		3.9			

Table3.the effect of boron spraying on the weight of the fruit/plant(g)

• The effect of spraying with boron on the weight of 1000 fruits of the two ecotypes of anise municipal and Shami:

The studied boron concentrations (mg/L)					
Ecotypes	Control	25.00	50.00	75.00	Average ecotyps
Municipal	3.73 [a]	3.33 [b]	3.63 [a]	3.80 [a]	3.62 [a]
Shami	3.60 [a]	3.67 [a]	3.67 [a]	3.57 [a]	3.63 [a]
concentration averages	3.67 [a]	3.50 [a]	3.65 [a]	3.68 [a]	
L.S.d5%	V=0.22	B=0.31	B×V= 0.44		
CV%		6.9			

Table 4. The effect of spraying boron on the weight of 1000 fruits (g)

Table (4) shows the effect of spraying with boron concentrations on two ecotypes of anise (municipal and Shami) in its row, the weight of 1000 fruits. The averages showed (3.67, 3.50, 3.65, 3.68) grams, for boron concentrations (0,25,50,75) mg/ For the absence of significant differences between the treatments and the control, and for the studied ecotypes, the averages (3.62, 3.63) grams also showed the absence of significant differences between them, as the ecotype of ecotype did not affect the weight of 1000 fruits. The results of the interaction of the ecotypes with boron concentrations (0,25,50,75) mg/l showed significant differences, as the interaction of the boron concentration (75) mg/l with the municipal anise variety achieved a significant superiority over the rest of the treatments and the control, and achieved the highest value (3.80 grams). Compared to the concentration (25) mg / L, which achieved the lowest value (3.33) grams for the municipal ecotype. This may be due to environmental conditions, where frost occurred in the germination stage, and also frost occurred in the flowering stage, as shown in Table No. (2), and as a result of the falling of a number of flowers, which led to a decrease in the number of fruits on the plant, and this is contrary to Jassem and Al-Jarallah. (2012) in their study in Iraq on the plant (Foeniculum vulgare), where there was no significant effect of spraying boron on the weight of 1000 fruits, but it tended to increase when compared to the control treatment.

• The effect of spraying with boron on the number the number of fruits/inflorescences of the two ecotypes of anise municipal and Shami:

Table (5) shows the effect of spraying with boron concentrations on the number of fruits/inflorescences of two ecotypes of anise (municipal and Shami), where the averages (121.80, 160.90, 158.10, 188.70) for boron concentrations (0,25,50,75) mg/l showed significant differences Between the treatments and the control, where the concentration of 75 mg/L was superior to the other concentrations studied and to the control, and achieved the highest value (188.70) of fruit/inflorescence. While there were no significant differences between the two concentrations (25.50), and the control gave the lowest value (121.80) fruit / inflorescence, and for the studied

samples, the averages (154.30, 160.50) also showed the absence of significant differences between them, as the ecotype of variety did not affect the number of fruits inflorescences. The results of the interaction of the ecotypes with the studied boron concentrations (0,25,50,75) mg/l indicated that there were significant differences between the studied treatments and the control. Where the interaction of the boron concentration (75) mg / L with the Shami ecotype of anise achieved a significant superiority over the rest of the treatments and the control, and achieved the highest value (193.70) compared to the control that achieved the lowest value (115.70) for the municipal ecotype. This result is explained by the role of boron in increasing the amount of carbohydrate synthesis and storage inside the fruits, and thus the number of fruits increased. Also, boron works on the germination of pollen grains and the growth of the pollen tube, and the improvement of fertilization and contraction because it is a chemical directive for the growth of the pollen tube through the reproductive tissues towards the ovary, which in turn increases of the final production of plants, and this is consistent with the results of the study (Jasim and Al-Jarallah, 2012) in their study on the fennel plant in Iraq, where spraying with boron at a concentration of (80-40-0) mg / L significantly increased the number of fruits in the plant, and agreed with the study of (Mhedi et al., 2017) on anise plant, where it was found that foliar spraying with boron at concentrations of (1.50) kg / gave the highest number of fruits / inflorescences, and therefore the highest production compared to the control.

Table5. The effect of boron spraying on the number of fruits/inflorescences.

Ecotypes	Control	25.00	50.00	75.00	Average ecotyps
Municipal	115.70	174.40	168.10	183.70	160.50[a]
Shami	127.80	147.50	148.10	193.70	154.30[a]
concentration averages	121.80 [c]	160.90 [b]	158.10 [b]	188.70	
L.S.d5%	V=19.53	B=16.82	B×V=22.53		
CV%		8.50			

• The effect of boron spraying on the hectare productivity of the two ecotypes of anise municipal and Shami:

Table (6) shows the effect of spraying with boron concentrations on the hectare productivity of two anise ecotypes. Where the averages (28183, 3439, 29238, 36992) kg / ha, for boron concentrations (0,25,50,75) mg / L showed that there were significant differences between the treatments and the control.

Where the concentration of boron 75 mg / L exceeded the other studied concentrations and the control, and achieved the highest value (36992) kg / ha. The control gave the lowest value (28183) kg / ha. As for the ecotypes, the averages (31392, 33010) showed significant differences between them, as the municipal ecotype was superior to the Shami ecotype, and the productivity of the municipal ecotype was (33010) kg / ha, while the Shami ecotype was (31392) kg / ha.

The results of the interaction of the ecotypes with boron concentrations (0,25,50,75) mg/l showed that there were no significant differences between the studied treatments and the control.

This may be attributed to the important role of boron inside the plant, as it works to increase the synthesis and storage of carbohydrates inside the seeds, and thus greatly increase the number of fruits and weight. Boron also enhances the growth of the pollen tube and improves fertilization and nodes that increase the final production, and this is consistent with the results of a study (Tania et al., 2018) in their research in Bengal on the coriander plant, where it was found that: spraying with boron (0.05%) with zinc (0.1%) led to an increase in the yield characteristics of coriander (fruit/plant weight, fruit/inflorescence weight, and hectare productivity).

Table6. Effect of boron spraying on hectare productivity (kg).

Ecotypes	Control	25.00	50.00	75.00	Average ecotyps
Municipal	18650	46542 [a]	29833	37017	33010 [a]
Shami	37717 [a]	22242	28642	36967	31392 [b]
concentration averages	28183 [d]	34392 [b]	29238 [c]	36992	
L.S.d5%	V=1160.3	B=1641.0	B×V=2320.7		
CV%		4.1			

• The effect of boron spraying on the percentage of essential oil of the two ecotypes of anise municipal and Shami:

Table (7) shows the effect of spraying with boron concentrations on the percentage of essential oil%, for two ecotypes of anise (municipal and Shami), as the averages showed (3.20, 4.00, 3.20, 3.80), for boron concentrations (0,25,50,75) mg/ The absence of significant differences between the transactions and the control. As for the studied ecotypes, the averages (3.75, 3.35) also showed the absence of significant differences between them, as the ecotype of ecotype did not affect the percentage of essential oil. The results of the interaction of the ecotypes with boron concentrations (0,25,50,75) mg/l indicated that there were significant differences between the studied treatments and the control. Where the concentration (25) mg / L of the anise variety achieved a significant superiority over the rest of the treatments and the control, and gave the highest value (5.60%), followed by the concentration (75) mg / L of the anise variety of the Shami, as it was significantly superior to the control, and this is explained by the indirect effect of boron By transferring the products of photosynthesis to anise fruits and storing them, which increases the content of volatile oils in anise fruits, and this is consistent with the results of a study (Mheidi et al., 2017) in a study of them on anise plants, where the oil content in the fruits increased when treated (B2).) where the oil content was (3.264%), while in the treatment (B0) the oil content was (3.007%) However, the reaction (M2B2) showed a high percentage of fruit oil amounted to (3.706%), while (M0B0) showed a low oil content of the fruits It reached (2.636%).

Table7. Effect of spraying with boron on the percentage of essential oil%.

Ecotypes	Control	25.00	50.00	75.00	Average ecotyps
Municipal	2.60 e	5.60 a	3.20 d	3.60 c	3.75 a
Shami	3.80 b	2.40	3.20 d	4.00 a	3.35 a
concentration averages	3.20 a	4.00 a	3.20 a	3.80 a	3.75 a
L.S.d5%	V= 0.856	B= 1.210	B×V=1.712		
CV%		19.8			

5. Conclusion

The municipal ecotype was superior to the Shami ecotype in terms of hectare productivity, and the ecotype of ecotype affected this characteristic. While there was no effect of the studied ecotype on each of the following characteristics (number of fruits/inflorescences, weight of 1000 fruits, weight of fruits/plant, percentage of essential oil). In addition, it was observed that there were no significant differences between all the studied concentrations and the control in each of the row, the weight of 1000 fruits, and the percentage of essential oil.

On the other hand, the interaction of the municipal ecotype with a concentration of boron 25 mg / L achieved a significant superiority over all studied treatments and the control in the row of fruits / plant weight, while the interaction of the municipal ecotype with a concentration of 75 mg / L achieved a significant superiority over all studied treatments and the control in the row of 1000 fruits.

The Shami ecotype and the concentration of boron 75 mg/L achieved a significant superiority over all studied treatments, the number of fruits/inflorescences being thecontrol. As for the percentage of essential oil, it was superior to the municipal ecotype with a concentration of 25 mg / L on all studied treatments and the control.

6. References

[1] S. Wachtel-Galor and I. F. Benzie, "Herbal medicine :An Introduction to Its History, Usage, Regulation, Current Trends, and Research Needs.," Lester Packer, Ph. D., Boca Raton (FL): CRC Press/Taylor . Francis, p. 1, 2011.

[2] W. Sun, M. H. Shahrajabian, and Q. Cheng, "Anise (Pimpinella anisum L.), a dominant spice and traditional medicinal herb for both food and medicinal purposes," Cogent Biology, vol. 5, no. 1, p. 1673688, 2019.

[3] M. Özgüven, " Aniseed," in Handbook of Herbs and Spices (Second Edition), K. V. Peter, Ed.: Woodhead Publishing, pp. 138-150. University of Cukurova.Turkey.2012.

[4] K. G. El-Rokiek, M. E. Ibrahim, S. A. S. El-Din, and S. A. El-Sawi, "Using anise (Pimpinella anisum L.) essential oils as natural herbicide," J. Mater. Environ. Sci, vol. 11, pp. 1689-98, 2020.

[5] A. Shojaii and M. Fard, "Review of pharmacological properties and chemical constituents of Pimpinella anisum. ," International Scholarly Research NetworkISRN Pharmaceutic, vol. 2012, p. 8, 2012.

[6] S. Kadan, M. Rayan, and A. Rayan, "Anticancer activity of anise (Pimpinella anisum L.) seed extract," The Open Nutraceuticals Journal, vol. 6, no. 1, 2013.

[7] W. K. Al-Juheishy, "EFFECT OF BORON ON SOME INDUSTRIAL CROPS: A REVIEW," Mesopotamia Journal of Agriculture, vol. 48, no. 4, pp. 134-145, 2020.

[8] N. Tort and B. Honermeier, "Investigations on the ratio of methylchavicol and trans-anethol components in essential oil of anis (Pimpinella anisum L.) from different regions of Turkey," Asian Journal of Chemistry, vol. 17, no. 4, pp. 2365-2370, 2005.

[9] Y. Mohamed, I. Mohamed, M. Elsadek, M. Ali, and Y. Ghatas, "Improving growth, productivity, and chemical composition of Trachyspermum ammi L. by using organic and chemical fertilization in the presence of boron," Industrial Crops Products,vol. 169, pp. 1-10, 2021.

[10] R. Abdel Aliem, H. Khaled, B. Soliman, M. Mourad, and H. Dighiesh, "Boron, the forgotten element," Frontiers in Scientific Research, vol. 2023, no. 6, pp. 20-28, 2023.

[11] M. H. Shahrajabian, W. Sun, and Q. Cheng, "Foliar application of nutrients on medicinal and aromatic plants, the sustainable approaches for higher and better production," Beni-Suef University Journal of BasicApplied Sciencesvol. 11, no. 1, pp. 1-10, 2022.

[12] U. H. Mheidi, I. M. Ali, and A. H. Abdulkafoor, "The effect of organic manure, foliar spraying with boron on growth, yield, quality and quantity of active ingredients of anise palnt (Pimpinella Anisum)," Pak. J. Biotechnol, vol. 14, no. 4, pp. 729-734, 2017.

[13] A. Jassim and K. aljarallah, "Effect of boron spray and nitrogen fertilization on growth and yield of fennel (foeniculum vulgare Mill.)," journal of kerbala university, vol. 2012, no. The second scientific conference of the Faculty of Agriculture, pp. 666-672, 2012.

[14] Tania.C, Das.R, Basanta.T, Chatterjee.R, and Chattopadhyay.K, "Assessment for growth and yield of coriander (Coriandrum sativum linn.) with micronutrients.," International Journal of Current Microbiology and Applied Sciences, vol. 7, no. 12, pp. 336-339, 2018.

[15] J.-Z. Ma et al., "Copper-based-zinc-boron foliar fertilizer improved yield, quality, physiological characteristics, and microelement concentration of celery (Apium graveolens L.)," vol. 31, no. 1, pp. 261-271, 2019.

[16] Y. Mohamed, R. Zewail, and Y. Ghatas, "The role of boron and some growth substances on growth, oil productivity and chemical characterization of volatile oils in basil (Ocimum basilicum L.) cv. Genovese," Journal of Horticultural Science Ornamental Plants, vol. 8, no. 2, pp. 108-118, 2016.

[17] J. R. de Mello Duarte, S. de Aguiar Basílio, I. C. Silva, E. G. S. Moreira, and A. Pelá, "Foliar spraying of doses of boric acid in coriander (Coriandrum sativum L.)," Revista de Agricultura Neotropical, vol. 7, no. 1, pp. 66-69, 2020.

[18]S.Mohamed,and R.Khater, Adaptation of Coriander Plants by Different Types of Fertilizers with Foliar Spraying of Boron to Improve Growth and Productivity," Middle East Journal of Agriculture,vol.10,no.4,pp. 1116-1129,2021.

[19] A. K. M. Al-Karaawi, "Effect of gibberellin GA3, boron and zinc foliar application on the growth and production of Hibiscus Sabdariffa L," in Journal of Physics: Conference Series, vol. 1294, no. 9, pp. 1-9,2019.

[20] M. P. Alam and M. Kumari, "Effect of zinc and boron on growth, yield and economics of linseed (Linum usitatissimum L.) under medium land of Jharkhand," The Pharma Innovation Journal, vol. 10, no. 4, pp. 462-466, 2021.

هيئة التحرير

الهيئة الاستشارية

قواعد النشر في المجلة

- أن يكون البحث جديدا، ولم يسبق نشره
- أن يتسم بالأصالة والجدة والابتكار والاضافة للمعرفة
- أن لا يكون مستلا من بحوث سبق نشرها للباحث/للباحثين
- أن تراعى فيه قواعد البحث العلمي الاصيل، ومنهجيته.
- أن يشتمل البحث على:
  - ✓ صفحة عنوان البحث باللغة الانجليزية.
  - ✓ مستخلص البحث باللغة الانجليزية.
  - ✓ صفحة عنوان البحث باللغة الانجليزية.
  - ✓ مستخلص البحث باللغة العربية.
  - ✓ مقدمة.
  - ✓ صلب البحث.
  - ✓ خاتمة تتضمن نتائج وتوصيات.
  - ✓ ثبت المصادر والمراجع.
  - ✓ الملاحق الملازمة(إن وجدت.)
- في حال (نشر البحث ورقا)يمنح الباحث نفسه نسخة من عدد المجلة الذي نشر بحثه بها و10 نسخ من بحثة بشكل مستقل
- في حال اعتماد نشر البحث تؤول حقوق نشره كافة للمجلة، ولها ان تعيد نشره ورقيا أو إلكترونيا، ويحق لها
- إدراجه في قواعد البيانات المحلية والعالمية- بمقابل أو بدون مقابل -وذلك دون حاجة للإذن الباحث.
- لا يحق للباحث إعادة نشر بحثه المقبول للنشر في المجلة- في أي وعاء من أوعية النشر -إلا بعد إذن
- كتابي من رئيس هيئة تحرير المجلة
- نمك التوثيق المعتمد في المجلة هو نمط IEEE

معلومات الإيداع

النسخة الورقية :

تم الإيداع في مكتبة الملك فهد الوطنية برقم 1439/8742 وتاريخ 1439/09/17 هـ

الرقم التسلسلي الدولي للدوريات **(ردمد)** 7936 – 1658

النسخة الإلكترونية:

تم الإيداع في مكتبة الملك فهد الوطنية برقم 4287 /1439 تاريخ 1439/9/17 هـ

الرقم التسلسلي الدولي للدوريات **(ردمد)** 7944- 1658

الموقع الإلكتروني للمجلة:

https://jesc.iu.edu.sa

ترسل البحوث باسم رئيس تحرير المجلة إلى البريد الإلكتروني

jesc@iu.edu.sa

الآراء الواردة في البحوث المنشورة تعرب عن وجهة نظر الباحث فقط، ولا تعرب بالضرورة عن المجلة.


بسم الله الرحمن الرحيم

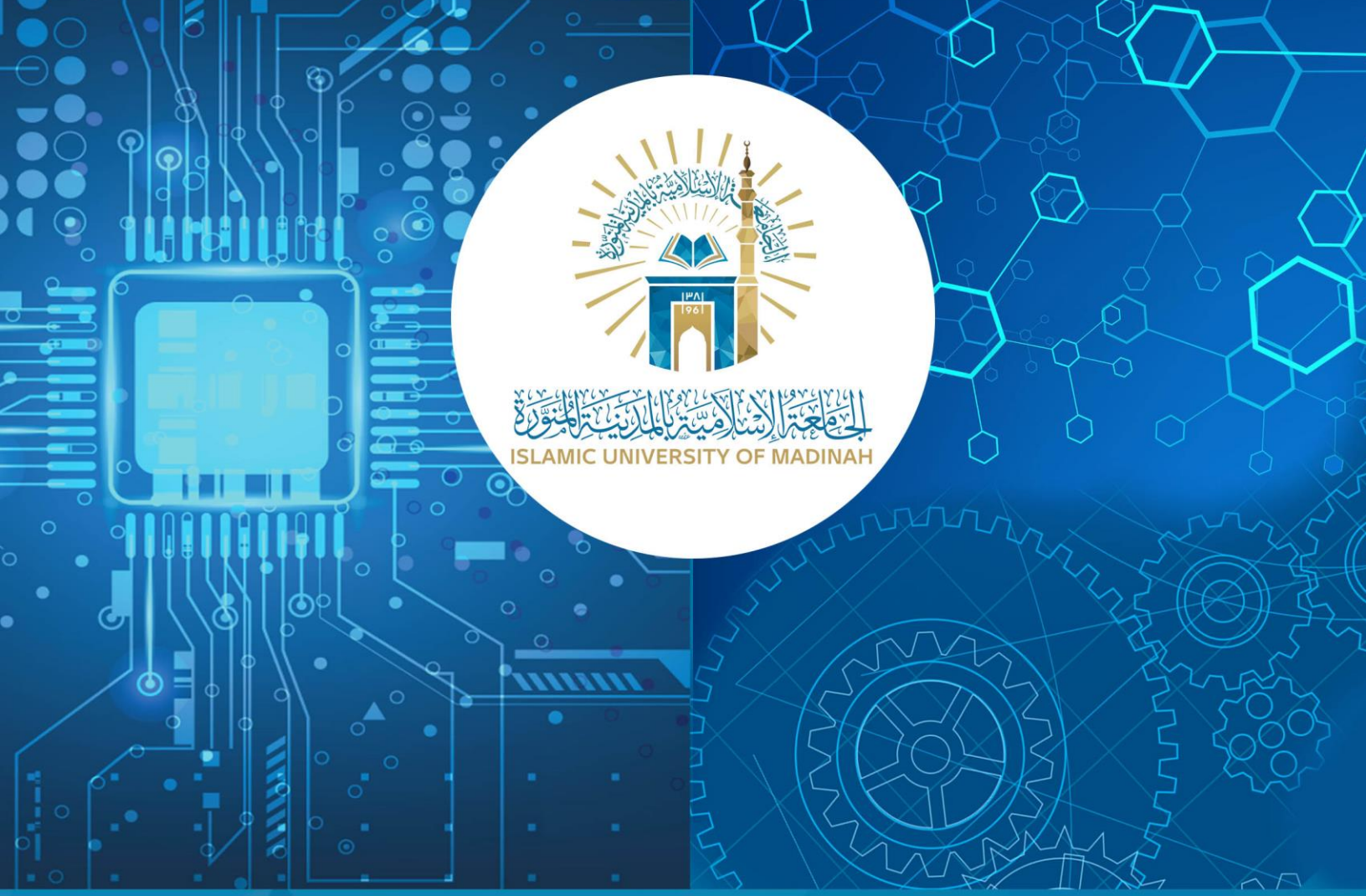

مجلة الجامعة الإسلامية

للعلوم التطبيقية

مجلة علمية دورية محكمة

العدد الأول السنة : الخامسة 1444 h